8-2003

Impacts of Environmental Factors on Flexible Pavements

Gang Zuo
University of Tennessee - Knoxville

To the Graduate Council:

I am submitting herewith a dissertation written by Gang Zuo entitled "Impacts of Environmental Factors on Flexible Pavements." I have examined the final electronic copy of this dissertation for form and content and recommend that it be accepted in partial fulfillment of the requirements for the degree of Doctor of Philosophy, with a major in Civil Engineering.

Eric C. Drumm, Major Professor

We have read this dissertation and recommend its acceptance:

Dr. Baoshan Huang, Dr. Dayakar Penumadu, Dr. Ronald E. Yoder

Accepted for the Council:

Carolyn R. Hodges

Vice Provost and Dean of the Graduate School

(Original signatures are on file with official student records.)

To the Graduate Council:

I am submitting herewith a dissertation written by Gang Zuo entitled “Impacts of Environmental Factors on Flexible Pavements.” I have examined the final electronic copy of this dissertation for form and content and recommend that it be accepted in partial fulfillment of the requirements for the degree of Doctor of Philosophy, with a major in Civil Engineering.

Eric C. Drumm, Major Professor

We have read this dissertation
and recommend its acceptance:

Dr. Baoshan Huang

Dr. Dayakar Penumadu

Dr. Ronald E. Yoder

Acceptance for the Council:

Dr. Anne Maynew
Vice Provost and Dean of
Graduate Studies

(Original signatures are on file with official student records.)

IMPACTS OF ENVIRONMENTAL FACTORS ON FLEXIBLE PAVEMENTS

A Dissertation
Presented for the
Doctor of Philosophy
Degree

The University of Tennessee, Knoxville

Gang Zuo
August 2003

DEDICATION

This Dissertation is dedicated to my mother

Haili Pan

to my sister

Hong Pan

and to the loving memory of my grandmother

Suying Xu

ACKNOWLEDGEMENTS

First, I would like to thank my advisor, Dr. Eric Drumm, for his guidance and patience throughout my studies at the University of Tennessee, who always has insightful suggestions every time I am frustrated with the research. In addition, I would like to thank Dr. Baoshan Huang for helpful discussions and recommendations. I am also very grateful to Dr. Dayakar Penumadu and Dr. Ronald Yoder for taking their precious time to serve on my committees. I would like to extend my thanks to Mr. Wesley C. Wright and Mr. N. Randy Rainwater for their assistance and constructive suggestions in laboratory testing.

I would also like to recognize Tennessee Department of Transportation, Design Division for the financial support.

My gratitude goes out to Songqing Wen and Jun Xu for being my best friends during my studies at the University of Tennessee. Without their great friendship I could not have achieved what I have. My thanks also extend to Yijia Chen, Cheng Song and other old friends for their unwavering support over the years. All these friends filled my life with happiness, and helped me to overcome the difficulties along the way.

ABSTRACT

Mechanistic-empirical pavement design methods for flexible pavements are based on the assumption that the pavement life is inversely proportional to the magnitude of the traffic-induced pavement strains. These strains vary with the stiffness of the asphalt layer and underlying base layer and subgrade. Environmental factors, such as the temperature in the asphalt concrete layer and the water content in the base layer and the subgrade, have a significant impact on the stiffness of relevant layers in pavement systems, and consequently the estimated life of flexible pavements.

A comprehensive instrumentation system was installed at four sites across the state of Tennessee to monitor long-term seasonal changes in flexible pavement response. Thermistors were used to measure the temperature at different depth of the pavement systems. Diurnal temperature variations in the asphalt concrete layer were as large as the annual variation. Multi-segment TDR probes were used to measure the volumetric water content. Because of the difference in signal strength along the probe, all segments do not provide the same level of accuracy. A series of laboratory testing were performed to study the sources of measurement error and the temperature dependence of the measurements in some segments. Water content measurements were recalibrated according to findings of this laboratory study and the measured seasonal variations in subgrade and base water content were small.

Using environmental data from instrumented pavement sites in Tennessee, the effects of asphalt concrete (AC) temperature and base and subgrade water

content variation were evaluated for three pavement profiles using the finite element method. The effect of AC temperature profile was found important to the critical strain in AC layer. Because the relationship between temperature and asphalt concrete stiffness is nonlinear, the additional pavement life consumed at higher-than-average temperatures is not offset by savings at lower-than-average temperatures. As a result, whenever average pavement temperatures are used to determine the asphalt stiffness, pavement life is overestimated. Furthermore, temperature and water content are neither completely dependent nor completely independent. Hence, the combined effects of temperature and water content variations were accounted for in the estimation of pavement life. The results of the parametric study showed that the temperature averaging period and the timing and duration of wet subgrade conditions are critical to estimated pavement life.

PREFACE

This dissertation is composed of five separate parts which are either published paper or papers to be submitted to journals, except Part V Conclusions and Recommendations. Each part is an integral part of this study on environmental impacts on flexible pavement, though it may also serve as an independent study on a specific topic of this study. Part I is a summary of the seasonal variations in flexible pavements observed at the instrumented sites, which provides the environmental data, asphalt temperature and water content in the base layer and the subgrade, for further study in later parts. Part II describes the laboratory testing for the factors affecting the determination of subgrade water content from multi-segment TDR probes. The recalibration of TDR probes made it possible to obtain usable water content data. Part III is a study of three dimensional finite element (3DFE) analysis for flexible pavement modeling. It discusses some difficulties and concerns about 3DFE analysis, such as boundary conditions, interface conditions, element type, element shape and element size. A proper FE model for further parametric study is determined in Part III. Part IV is a comprehensive study on the environmental factors on flexible pavement life using the environmental data from the instrumented sites as described in Part I and the finite element model in Part III. All the findings on environmental impacts on flexible pavements are given in Part IV.

TABLE OF CONTENTS

LIST OF TABLES

LIST OF FIGURES

Part I Impacts of Environmental Factors on Flexible Pavements I: Observed Seasonal Variations on Flexible Pavements in Moderate Climates

1.1 Abstract

A comprehensive instrumentation system was installed at four sites across the state of Tennessee to monitor long-term seasonal changes in flexible pavement response. This paper summarizes the findings after over five years of data collection. The temperature and water content of the various pavement layers were measured by thermistors and time domain reflectometry probes, respectively. Weather information was collected by a weather station at each site. Falling weight deflectometer tests were used to observe the pavement response in different seasons. All four pavement systems were new construction, and little pavement distress was observed over the study period. The impermeable surface layers were found to limit the infiltration of water through the pavement system, and the measured seasonal variations in subgrade and base water content were small. Likewise, the seasonal variations in back calculated base and subgrade modulus were small. However, significant infiltration was recorded near the longitudinal joint. As weathering takes place and the pavement systems experience additional loading cycles, it is anticipated that the infiltration rates may increase with corresponding increases in seasonal moisture variations. Diurnal temperature variations in the asphalt concrete layer were significant, and it was shown that the traditional monthly mean temperature used for design may omit significant periods of high temperature. In moderate climates, the diurnal temperature variation may be as large as the annual variation.

1.2 Introduction

Even in areas with relatively moderate climates such as Tennessee, the performance of flexible pavements is affected by environmental factors such as temperature changes in the asphalt layers and water content changes in the base and subgrade layers. Because the resilient moduli (M_R) of the base and subgrade vary with stress state, temperature induced changes in the asphalt concrete (AC) modulus results in variations of the stress magnitude transferred to the unbound base and subgrade, which in turn affects the M_R of the stress dependent unbound materials. The laboratory modulus of AC at different temperatures and the resilient modulus of the unbound materials at different volumetric water contents (VWC) have been studied by a number of researchers. It has been observed that the resilient modulus of unbound materials for a given value of dry density decreases with increasing compaction water content, and the resilient modulus of fine-grained subgrades has been found to decrease significantly with post compaction water content increases (Li and Selig, 1994; Drumm et al., 1997) . The stiffness of AC decreases considerably with increasing temperature, especially at very high temperature (Akhter and Witczak, 1985, Kim et al., 1995). To account for the seasonal variation in moisture content, the AASHTO Guide for Design of Pavement Structures (AASHTO, 1993) describes a procedure for the identification of a single subgrade resilient modulus value, "effective roadbed soil resilient modulus" for flexible pavement design, from the subgrade resilient modulus of each season. A weighted average method was proposed by Guan et al. (1998) to determine the effective subgrade resilient

modulus. These methods require the input of reliable information of the seasonal variation of the environmental data, which can only be obtained by long-term field instrumentation.

With the development of improved instrumentation and nondestructive testing technology, the effects of daily and seasonal environmental effects can be observed. Data can be logged on an hourly basis or even shorter intervals with automated instrumentation. Current instrumentation technology has made it possible to easily obtain information that was not previously available, thus allowing the incorporation of environmental factors into pavement design.

The continuous monitoring of four instrumented flexible pavement sections was started in 1996. The objectives of this research were to (1) investigate the seasonal variation of water content in the base layer and subgrade, the daily and seasonal variation of temperature in the AC layers, and the impact of these environmental effects on pavement performance; and (2) develop a mechanistic method to incorporate these environmental effects (temperature and water content changes) into the pavement design procedure. This paper summarizes the results of over five years of data collection at these four sites.

1.3 Instrumentation

The location of the four instrumented pavement sites was selected to provide the information for four representative regions of the state of Tennessee (Figure 1.1). All four pavement sections consist of an asphalt concrete surface layer, a plant-mixed asphalt stabilized base, and a base material with Tennessee DOT specification of Class A Grading D. Subgrade materials for Blount, McNairy, and

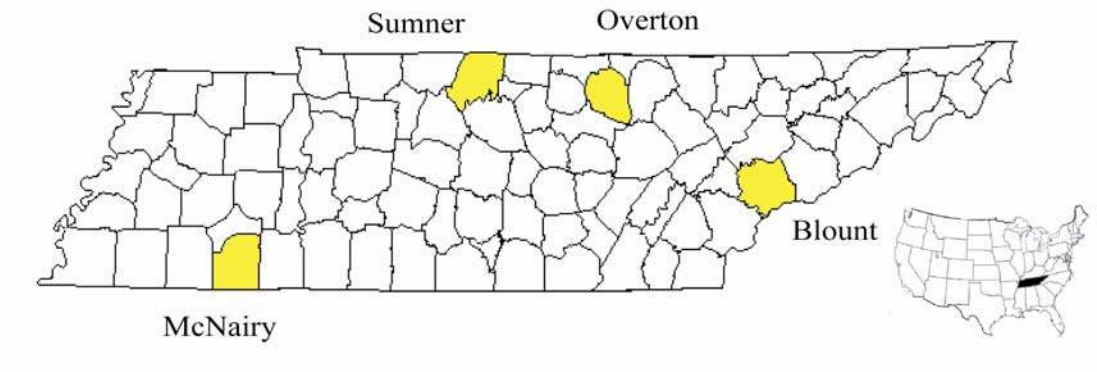

Figure 1.1 Location of the four test sites

Overton County are A-7-5(20), A-4(1), and A-7-6 (20), respectively. The top 0.15 m of the Sumner County site subgrade was lime stabilized. The pavement layers are compared in Figure 1.2.

A weather station was installed at each of the test sites. Air temperature, precipitation, relative humidity, wind speed, and solar radiation were measured every 60 seconds and an hourly average/total logged. During construction, thermistors and time domain reflectometry (TDR) probes were installed to collect temperature and water content data at different depths in the pavement system. Pan lysimeters were installed in the upper portion of the base course to collect water infiltrating into the pavement through the AC layers, with the volume of percolated water measured by tipping bucket rain gages located in an underground concrete vault. A typical roadway cross-section showing the placement of TDR probes and a pan lysimeter is given in Figure 1.3. Thermistors were installed at the same depth as the TDR probes. The entire data collection process is fully automated, with accumulated data downloaded by cellular phone to a personal computer every 24 hours. A detailed description of the

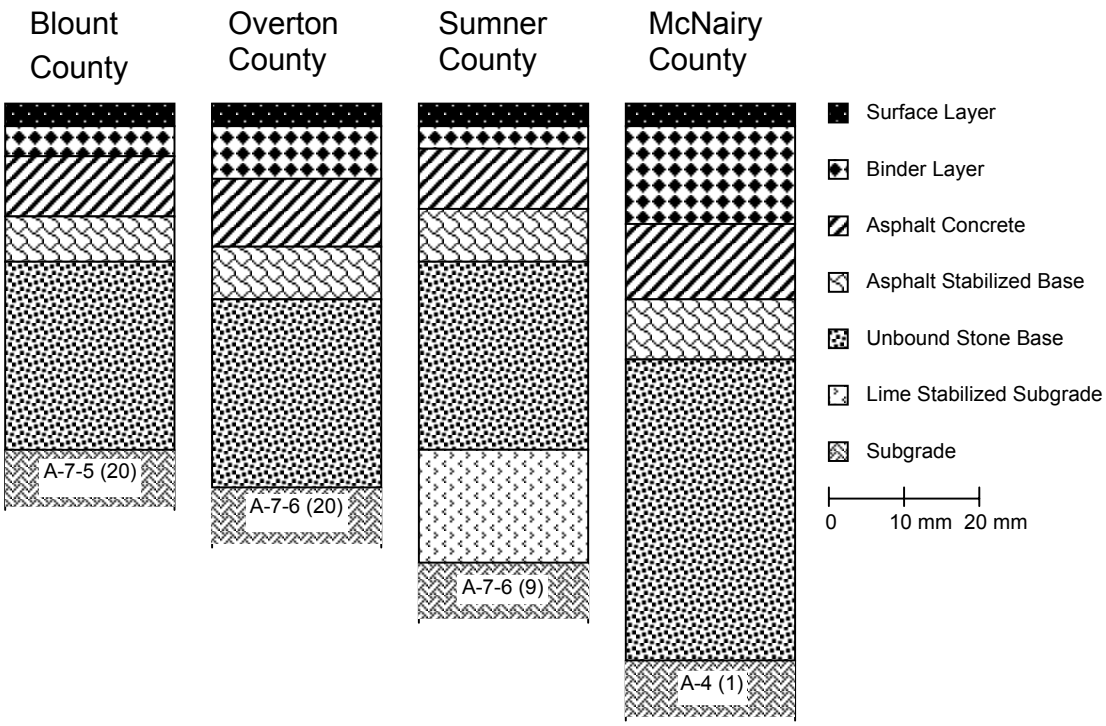

Figure 1.2 Layer thickness of the pavement sites

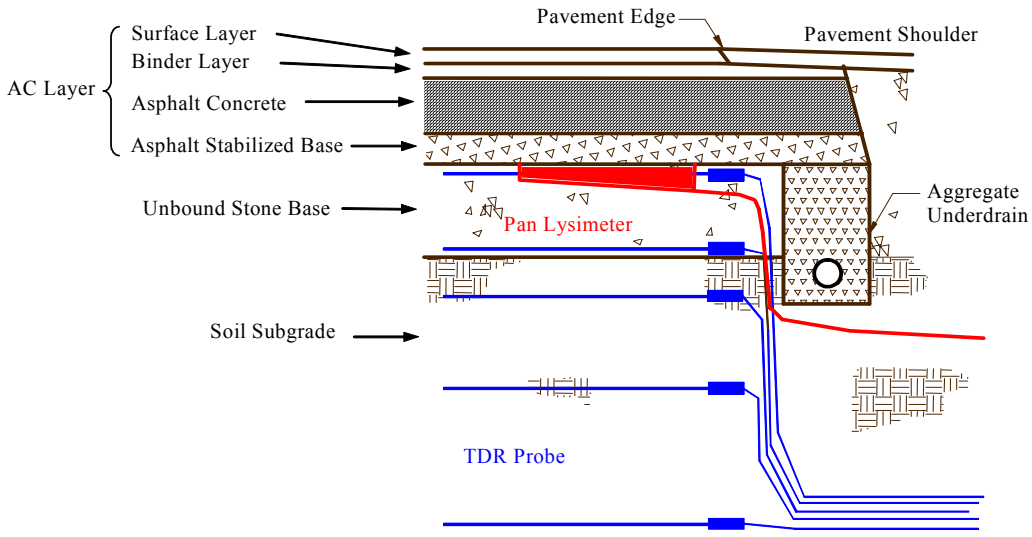

Figure 1.3 Typical cross section of the test sites (not to scale).

instrumentation system can be found in (Rainwater et al., 1999; Rainwater et al., 2001).

Along with the automated instrumentation, the pavement response was monitored seasonally by falling weight deflectometer (FWD) tests. Field work was performed regularly, during which malfunctioning instruments were replaced, soil samples were collected by coring, and pavement temperatures were verified by manual measurement using thermometers.

1.4 Results of Environmental Monitoring

1.4.1 Water Infiltration

A pair of lysimeters was installed beneath the wheel path of the outside lane at the McNairy, Overton, and Sumner County sites. The Sumner County Site also included an additional pair of lysimeters beneath the longitudinal joint in the center of the roadway. The lysimeters in each pair were placed about 2.0 m apart. Significant infiltration was recorded at the McNairy County site before the dense-graded surface layer and binder layer were installed. An empirical model was developed to predict the infiltration from rainfall intensity (Rainwater et al., 2001).

Infiltration through the longitudinal joint measured by the pan lysimeters at Sumner County showed some correlation with precipitation for the first five months after construction. Subsequent cessation of infiltration was at first believed to be the result of the compaction from traffic during the warm season, which presumably sealed the joint. It was later suspected that the drain tubes connecting the pan lysimeter and the tipping bucket were clogged. On November

3, 2000, compressed air was used in an attempt to open the pan lysimeter drain tubes. The clog in one of the pan lysimeters under the longitudinal joint was successfully removed and more than 1.5 liters of water were measured at the tipping bucket rain gage the same day. After this event, the infiltration measurement of the pan showed reasonable correlation with rainfall (Figure 1.4). The magnitude of infiltration under the longitudinal joint at the Sumner County site was greater than that measured at McNairy County site before the installation of dense-graded surface and binder layer. This confirms the belief of the Tennessee Department of Transportation engineers who had suggested that the longitudinal joint was a significant source of water infiltration in flexible pavements. To verify the function of the other pan lysimeters under the wheel path, a series of 'forced infiltration' tests were performed over the wheel path lysimeters at the three sites that include pan lysimeters. More than 1 m (3 ft) of hydraulic head was initially applied to the pavement surface. One of the pan lysimeters at the McNairy County site was tested on 10-12-01. On-site observation in head change appeared minimal to non-existent, but the data showed a marked increase in infiltration after the test. On 03-19-02, the test was performed at Overton County site, however, neither pan showed infiltration until approximately 20 days after the test. On 05-19-02, an identical test was performed on one of the wheel path pans at Sumner County site. The data did not show any infiltration resulting from the test. Hence, more infiltration is expected to be recorded as the permeability of the surface layers increases with time.

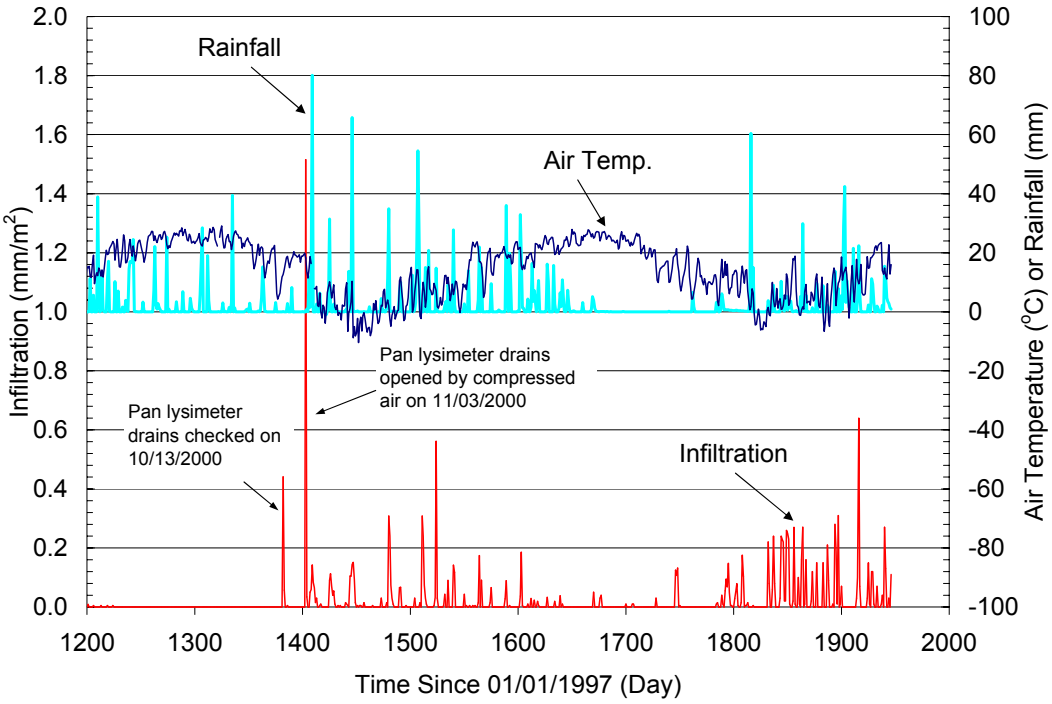

Figure 1.4 Climatic data and infiltration Measurement of a pan lysimeter beneath the longitudinal joint (Sumner County).

1.4.2 Subgrade Volumetric Water Content Variation

Time domain reflectometry (TDR) has been investigated as a means of monitoring soil water content since the 1970's (O'Connor and Dowding, 1999). TDR probes measure water content on the principle that the dielectric constant changes with water content. The velocity of a voltage pulse propagating along a waveguide is a function of the dielectric constant of the surrounding material. Multi-segment TDR probes produced by Environmental Sensors ® were used in the project to monitor the variation of volumetric water content in the base course and the subgrade. These multi-segment probes consist of five 300 mm long segments, each segment providing a distinct water content measurement. The results from some of the segments of this type of TDR probes were found to be

temperature-dependent as a result of signal attenuation (Zuo et al., 2001). The temperature variation in the base course and the subgrade is approximately 30 °C. Thus, a correction procedure was developed and applied to the data collected over a five year period. It should be noted that the measured volumetric water content results presented in Part I and Part IV are the averaged measurements from Segment 3 and Segment 4 of each probe.

Subgrade volumetric water contents measured by TDR probes for all four sites show very little variation since the beginning of the project, except for brief periods of time after heavy rainfall in winter and spring (Figure 1.5, to Figure 1.8).

Among the four sites, only the Sumner County site (top 150 mm (6 inches) of the subgrade was lime stabilized) shows some seasonal variation in subgrade

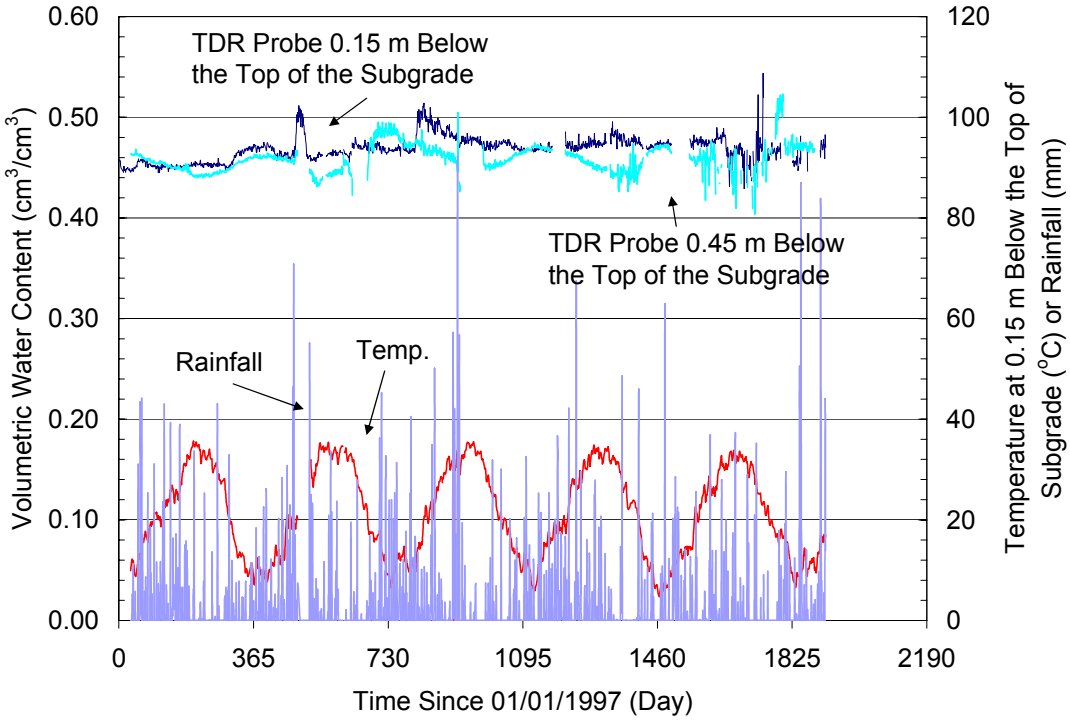

Figure 1.5 Subgrade volumetric water content variation and climatic data (Blount County).

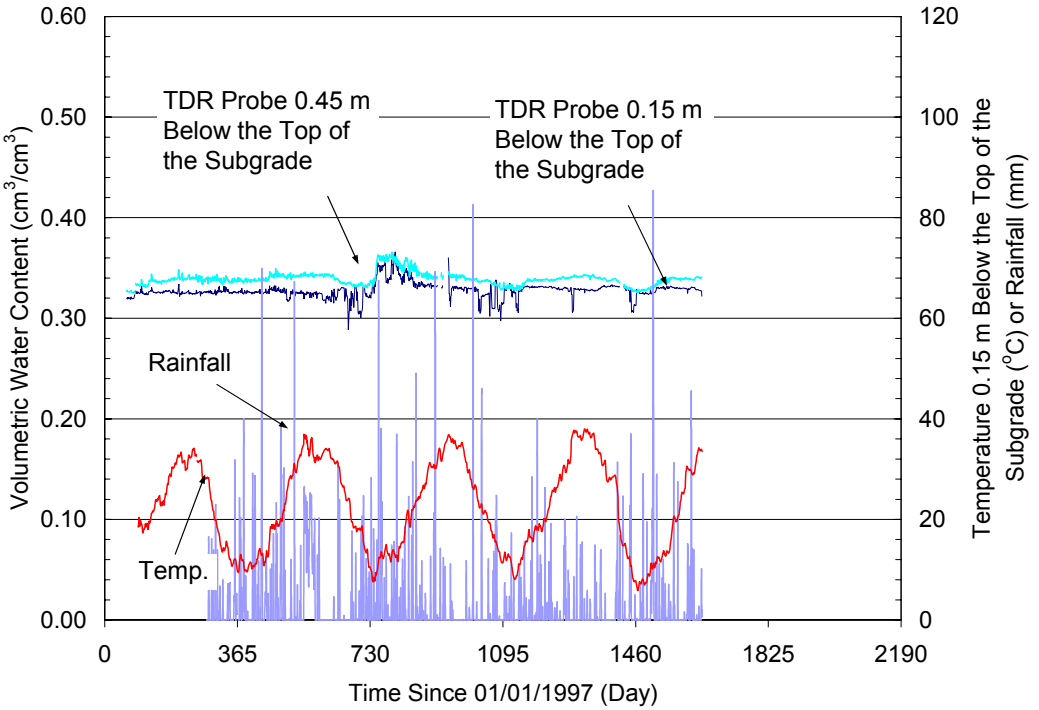

Figure 1.6 Subgrade volumetric water content variation and climatic data (McNairy County).

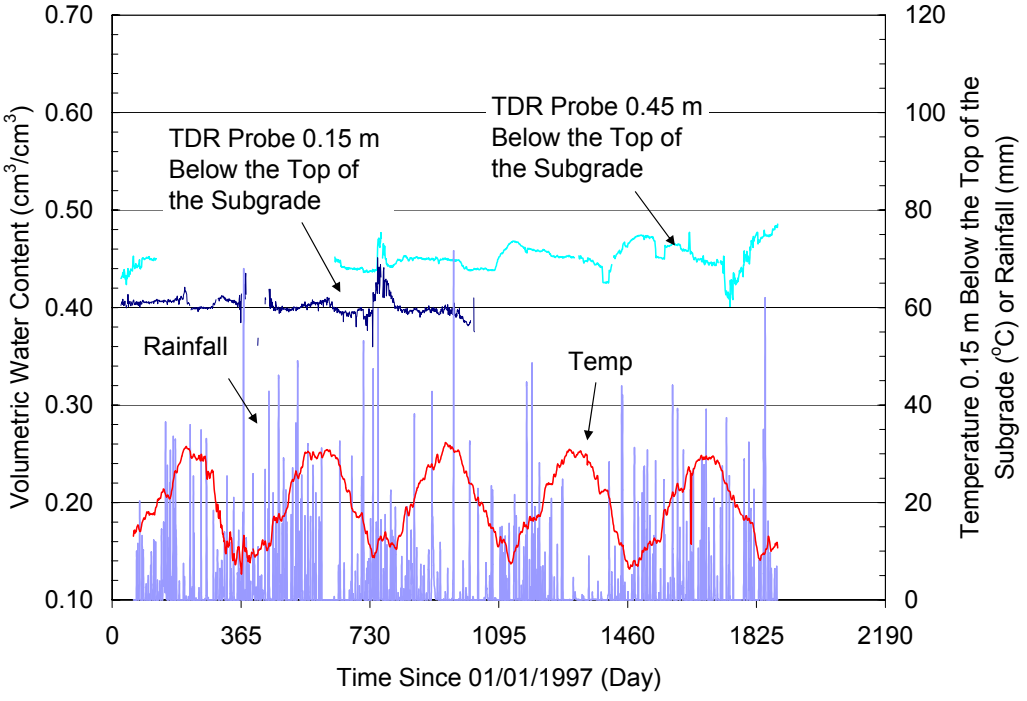

Figure 1.7 Subgrade volumetric water content variation and climatic data (Overton County).

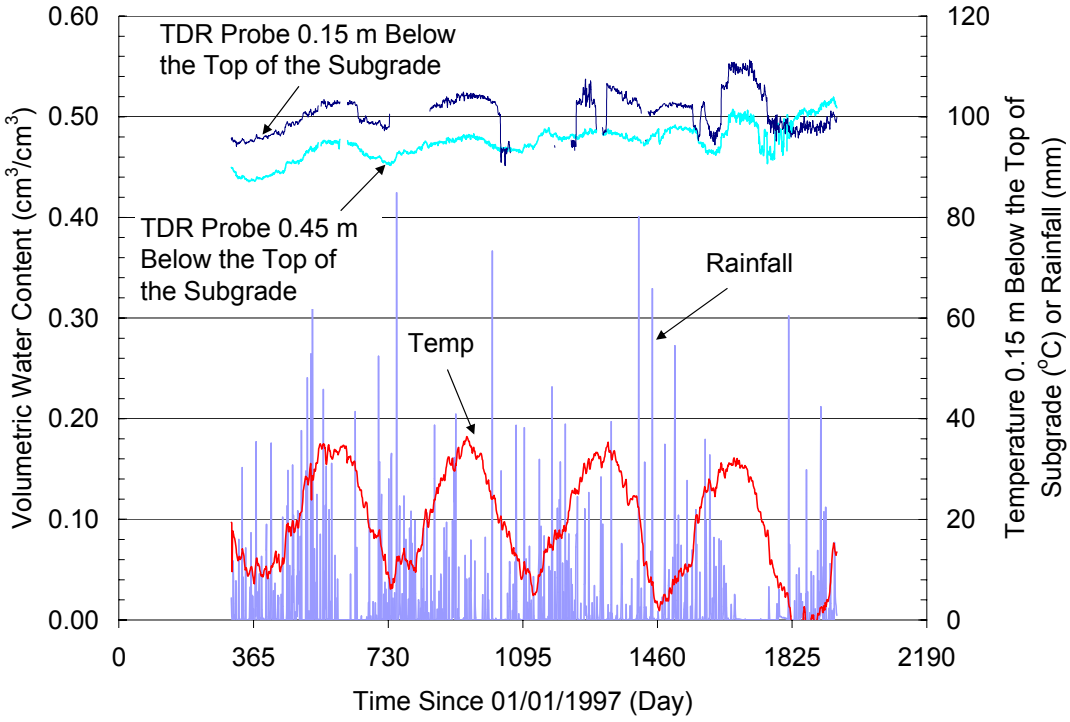

Figure 1.8 Subgrade and base course volumetric water content variation and climatic data (Sumner County).

volumetric water content (Figure 1.8). It has been suggested that elevated soil electric conductivity (EC) can result in overestimation of soil moisture (Sun and Young, 2001). Because the temperature correction of the TDR measurements was developed for subgrades that were not lime treated, an investigation of the EC of the treated and untreated material was conducted. The EC of a solution extracted from samples from the subgrades showed that lime stabilization does increase the EC of the soil solution significantly. However, EC of the soil solution decreases with increasing temperature. Therefore, according to Sun and Young (2001), soil moisture would be overestimated when the temperature is low, which contradicts the observed water content variation at the Sumner County site.

Therefore, no adjustments to the Sumner County data were made. Further study is needed on the TDR water content measurement on lime-stabilized subgrade.

1.4.3 Volumetric Water Content Variation in the Base Course

TDR probes installed at the top of the base course at all four sites showed very little seasonal variation in VWC, and the results shown in Figure 1.9, from Blount County are typical. The TDR probes installed at the bottom of the base course might be expected to exhibit the greatest seasonal variation in water content. Unfortunately, the probes at the bottom of the base course at McNairy and Overton Counties failed prematurely, and the probe at Blount County only produced results for 1.5 years. Figure 1.11 indicates measured seasonal fluctuations of about 0.05 VWC at Sumner County, while a similar variation was found during the brief operation at Blount County (Figure 1.10).

Although the TDR probe at the bottom of the base course at the Blount County site only lasted for about 500 days, it does show the same pattern as to that of the Sumner County site: volumetric water content increases rapidly in the winter and decreases gradually in summer, and as expected the water contents in the base are much lower than in the fine-grained subgrade.

The periodic drying and wetting response observed at the bottom of the base course (Figure 1.10 and Figure 1.11) is cyclic, but does not resemble the sinusoidal-like temperature cycle in the base course. In fact, the peaks of the VWC cycle in the base course lead the peaks in the temperature cycles by more than a month. The VWC at the bottom of the base rises rapidly to its maximum

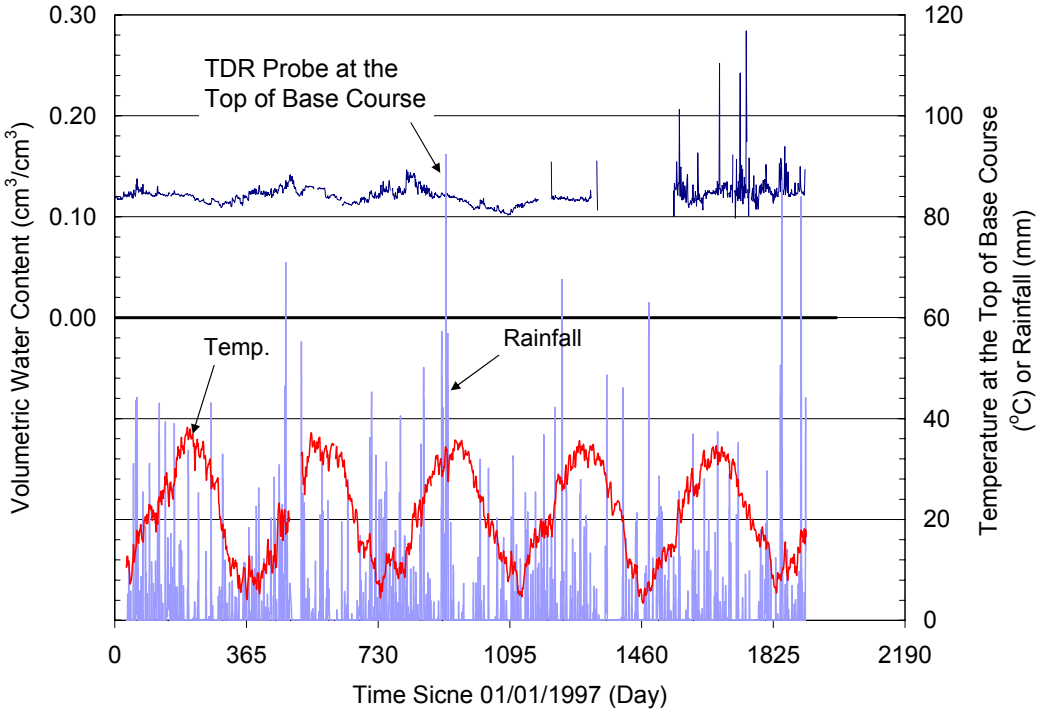

Figure 1.9 Volumetric water content variation at the top of base course and climatic data (Blount County).

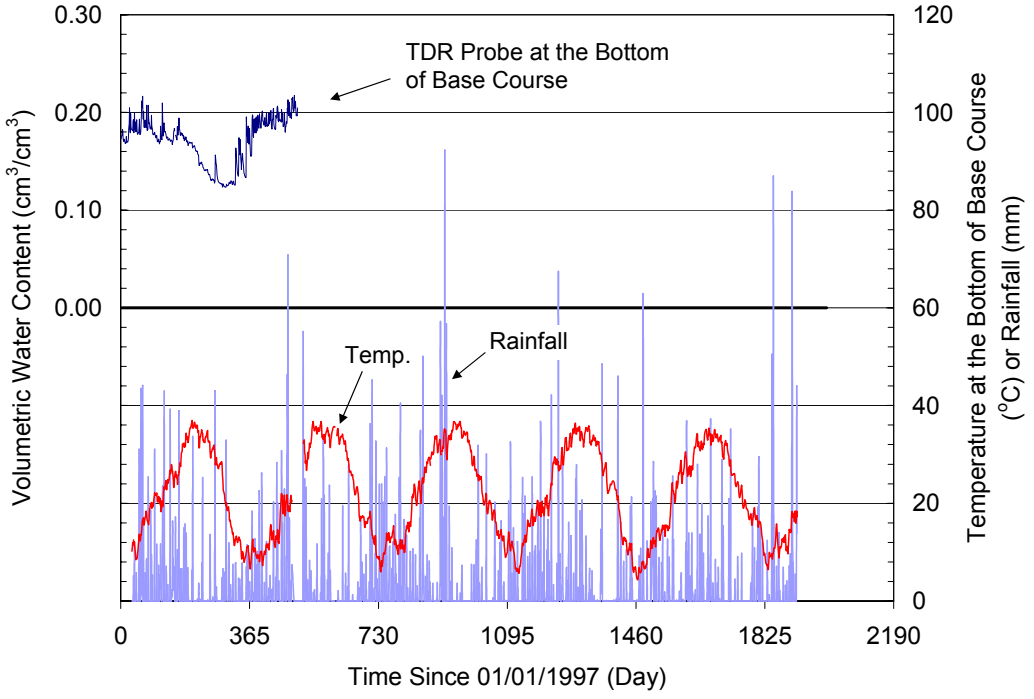

Figure 1.10 Volumetric water content variation at the bottom of the base course and climatic data (Blount County).

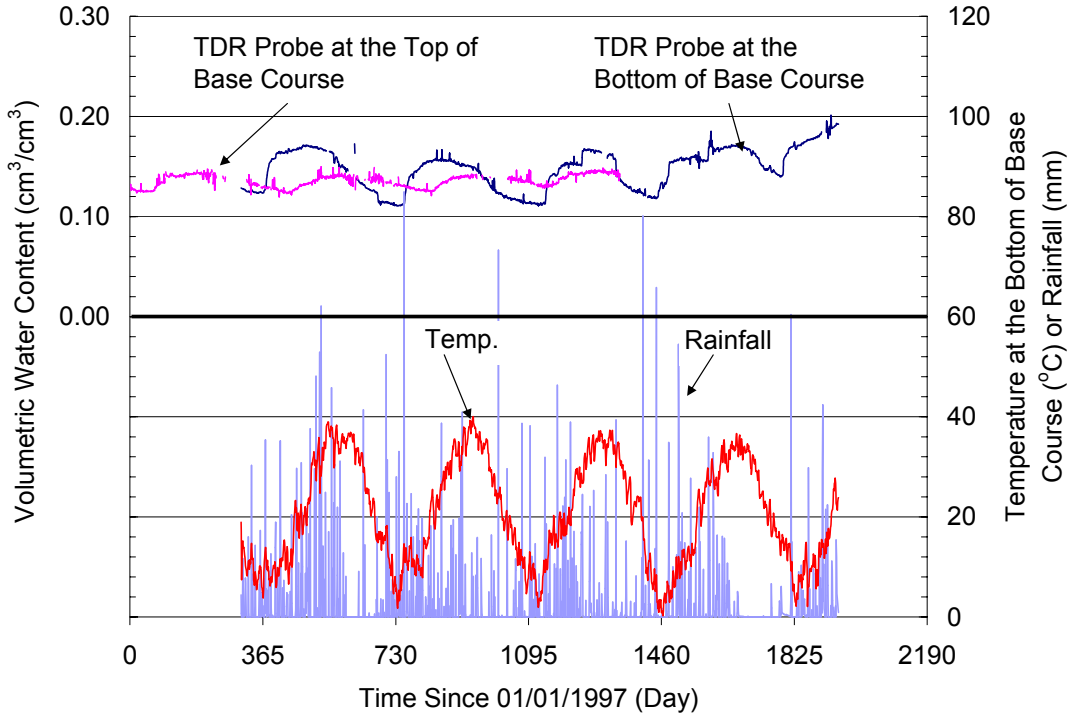

Figure 1.11 Volumetric water content variation at the bottom of the base course and climatic data (Sumner County).

while the temperature is still increasing. It is not until the temperature is highest, that the VWC gradually drops to its minimum. A possible explanation of this response is as follows. In late fall and early winter, there are more rainfall events while the temperature is low, and because of lower evaporation rates, more water infiltrates into the base. However, the base course has been drying for a long period of time and the hydraulic conductivity is low, hence, the small amount of water that percolates through the surface only wets the top of the base. The water content at the bottom of the base course does not increase until sometime later when the water content and hydraulic conductivity of the upper part of the base have increased. After a heavy rainfall, the water content of the bottom of

the base increases and the hydraulic conductivity of the entire base course is high. Water that infiltrates into the base course afterwards reaches the bottom in a very short time and the water content in the lower part of the base course increases rapidly. In summer when the pavement temperature is high, water evaporates quickly after the rainfall, and very little water reaches the bottom of the base after rainfall. In late summer and early fall when the weather is dry, the water content at the bottom of the base decreases gradually. Due to the low permeability of the subgrade, there is a lag between the base course water content variation and subgrade water content variation.

1.4.4 Asphalt Concrete Temperature

Figure 1.12 shows the temperature variation measured by a thermistor at mid-depth of the AC layer at the Overton County site, in October 2000. Diurnally, the temperature follows a nearly sinusoidal pattern. As indicated in Figure 1.12, the daily average temperature varies in a nearly sinusoidal manner over the entire year. For the month of October shown in Figure 1.12, if only the daily average temperature is considered, the difference between the maximum and minimum temperature is 13.3 °C. However, if the hourly temperature is considered, the difference is 24.5 °C. Thus, the diurnal temperature variation in hourly temperature average can be as great as the monthly variation in daily average temperatures observed over the entire year. The monthly average mid-depth AC temperature variation at the Overton County site in the year 2000 is shown in Figure 1.13. Maximum and minimum hourly and daily average temperatures of each month are also shown in the graph.

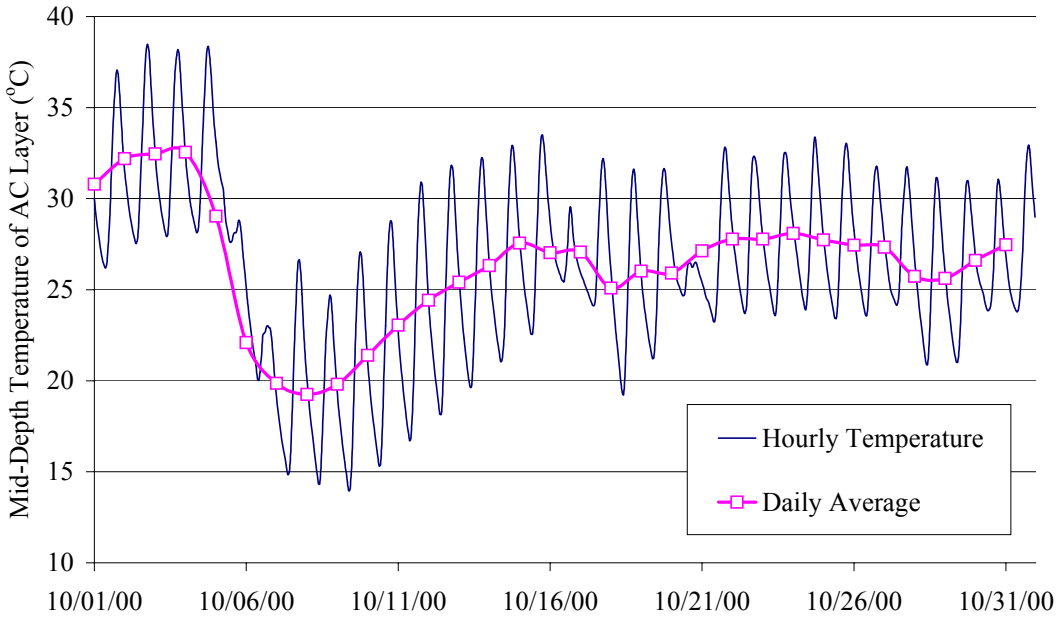

Figure 1.12 Temperature Variation of Mid-Depth AC Layer, Overton County Site, October 2000.

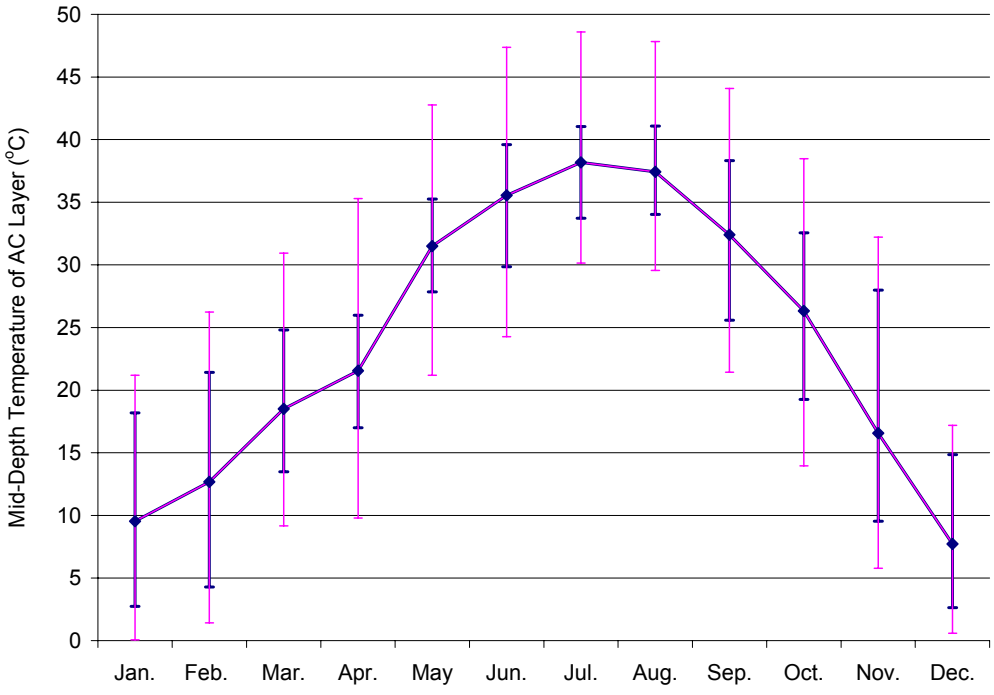

Figure 1.13 Monthly Average of Mid-Depth AC Temperature at Overton County Site in 2000 (Thick error bars show the maximum and minimum daily average and thin error bars show the maximum and minimum hourly average.)

The histogram of temperature distribution at the mid-depth of the AC layer at Overton County site using three years of data is shown in Figure 1.14. Different histograms are shown using time intervals of a month, a day, and an hour for the averaging. The significance of the temperature distribution and the time interval used for temperature averaging has been shown to have an impact on the pavement design process (Zuo et al., 2002) and will be discussed subsequently.

A bimodal distribution can be discerned in the histograms of hourly, daily and monthly temperature averages. Similar bimodal shape is found in the temperature data from the other three sites. Although a normal distribution about the average temperature might be expected, the bimodal distribution is the result of the sinusoidal type seasonal variation in temperature. For example, the frequency histogram for a perfect sinusoidal function will always be bimodal. This

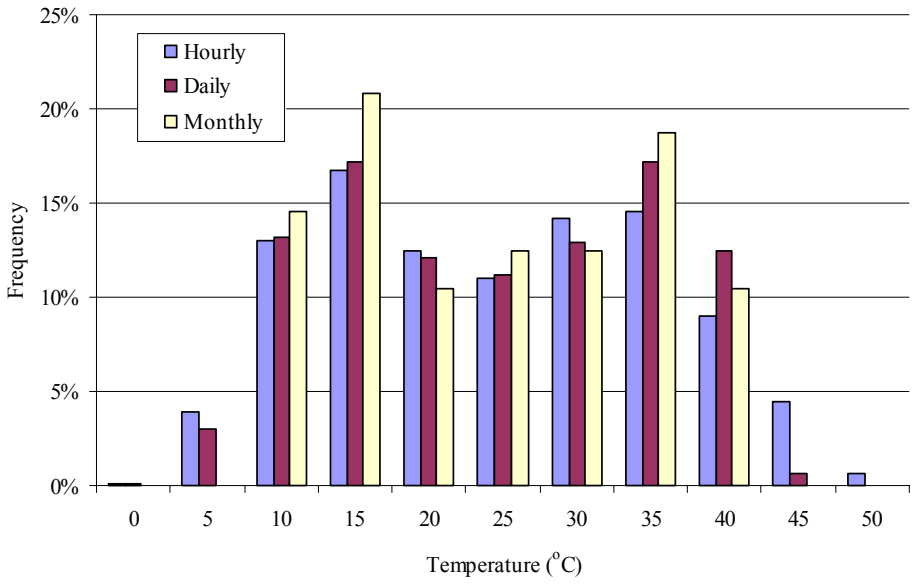

Figure 1.14 Temperature distribution for different averaging intervals (Based on three years of collected data at Overton County).

is because the slope of a sinusoidal curve is zero at the maximum and minimum values, which means that for a given sampling interval or bin size, there are more occurrences near the maximum and minimum bins. If there is some noise in the data, and/or if the time series consists of two sinusoidal components with different frequencies (such as the observed cyclic daily mean temperature on which is superimposed the cyclic hourly temperature variation) the highest frequency in the histogram will be shifted towards the middle rather than occurring exactly at the value associated with the maximum and minimum. The magnitude of the shift depends on the amplitude of the noise and/or the component with high frequency.

1.5 Pavement System Response

At all four testing sites, FWD tests were performed at five drop locations on 7.6–m (25-ft) centers in the outer wheel path. At each drop location, four replicates of FWD tests were performed using three different drop heights. MODULUS 5.0 was chosen to back-calculate pavement layer moduli from FWD test data. The pavements were modeled as three layers: subgrade, base course, and asphalt, in which the asphalt surface layer, binder layer and the asphalt stabilized base layer were considered as a single layer.

1.5.1 Asphalt Concrete Modulus

Pavement temperature has been considered one of the most critical factors that influence the structural capacity of flexible pavements. In this project, a temperature-AC modulus relationship was developed from the temperature data collected by thermistors and the back-calculated AC modulus from FWD tests.

Asphalt concrete modulus back-calculated from the FWD test was correlated to the measured mid-depth asphalt temperature. The regressed relationship between AC modulus and temperature varies from site to site due to differences in mix design and construction practices. However, when the modular ratio, the modulus divided by the modulus at 20 °C for the four sites, is used, the different temperature relationships collapse onto each other and can be modeled by a single exponential function as shown in Figure 1.15 (Marshall et al., 2001). The R-square of this relationship was 0.93. This suggests a general temperature-modulus behavior of AC concrete regardless of the slight difference in mix design or construction practices.

The relationship developed from the current study compares well with what was developed from a similar study conducted on pavements in North Carolina, which has similar latitudes as Tennessee (Kim et al., 1995). It should be noted that the binder used in North Carolina is different from what is used in Tennessee; nevertheless, almost an identical temperature-modulus relationship was obtained.

This supports Lukanen et al.'s "universal" modular ratio vs. temperature relationship that includes latitude as a surrogate measure of binder stiffness (Lukanen et al., 2000).

1.5.2 Subgrade Modulus

Subgrade modulus is typically very sensitive to water content variations. However, the instrumented sites showed little change in subgrade water content over time. Typical results of the subgrade modulus back-calculated from FWD testing are shown in Figure 1.16, which supports this observation. Similar results

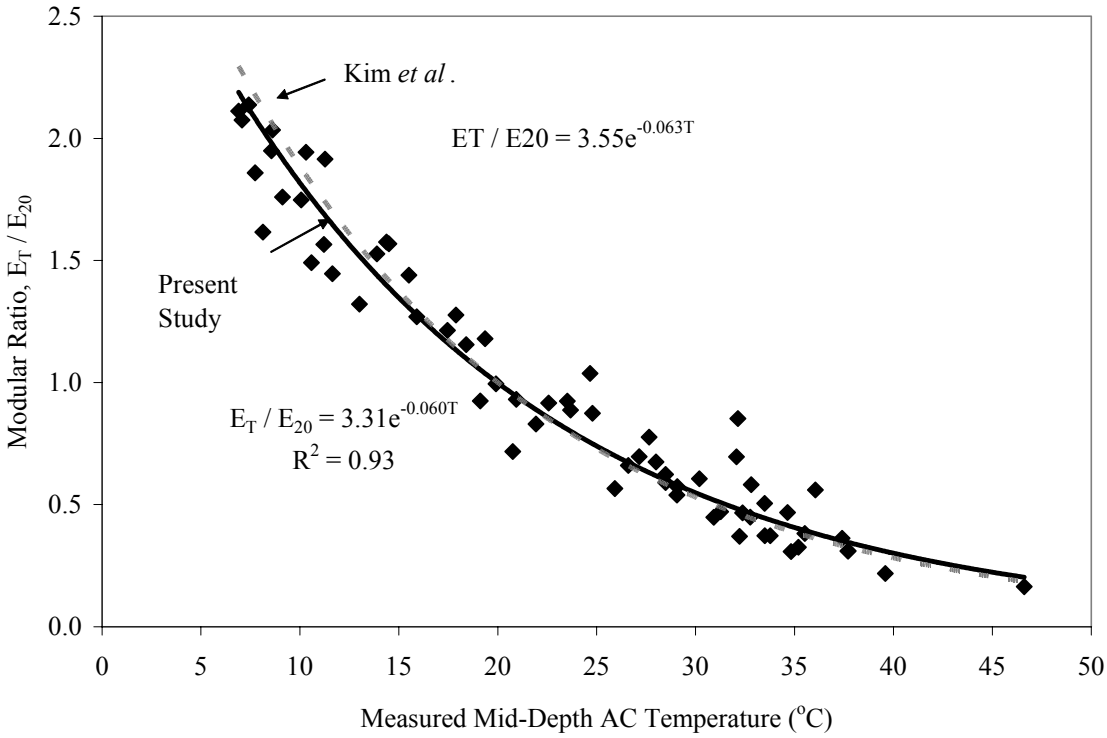

Figure 1.15 Modular ratio vs. pavement temperature (data from all four sites).

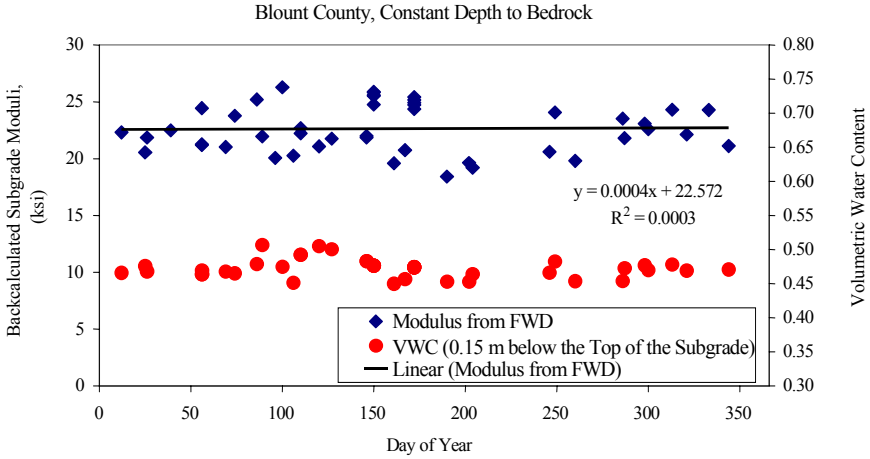

Figure 1.16 Backcalculated moduli and volumetric water content of subgrade (Blount County).

were obtained for the other sites.

1.6 Conclusions

A long-term pavement monitoring program was initiated in Tennessee, USA, to monitor seasonal changes in flexible pavement response. A comprehensive set of instrumentation equipment was installed at four sites across Tennessee, and data have been collected for over five years. Significant infiltration measured by pan lysimeters was recorded at the McNairy County site, before the dense-graded surface layer and binder layer were installed. Since all four pavement systems were new construction and lacked significant distress, very little water infiltrated from the pavement surface. As a result, the observed water content changes and corresponding changes in subgrade and base moduli in the pavement system were small. As weathering takes place and the pavement systems experience additional loading cycles, it is anticipated that the seasonal moisture changes will increase. Significant infiltration was measured underneath the longitudinal joint at the only site with joint lysimeters. However, the subgrade water content sensors were located some distance away from the longitudinal joint, so the effects of this joint infiltration on base and subgrade water content are not known.

Overall, the seasonal variation of subgrade moisture content was small, which was consistent with nearly constant FWD back-calculated subgrade moduli. Some seasonal variation in the water content at the bottom of the base course was observed, but no discernable trends were observed in the back calculated base moduli.

A relationship between mid-depth AC temperature and AC modulus relative to that at 20 °C was developed from back-calculation of FWD data. The relationship agrees well with the relationship developed by others using the data from a similar latitude, but with a different binder. Latitude of the site can be an important factor that influences the stiffness of AC layer.

1.7 Acknowledgement

The authors appreciate the support provided by the Tennessee Department of Transportation, Design Division and Materials and Tests Division.

References

AASHTO (1993) *AASHTO Guide for the Design of Pavement Structures*. American Association of State Highway Officials, p. 403.

Akhter, G. F. and M. W. Witczak (1985) Sensitivity of Flexible Pavement Performance to Bituminous Mix Properties. In *Transportation Research Record 1034*, TRB, National Research Council, Washington, D.C., pp. 70-79.

Drumm, E. C., J. S. Reeves, M. R. Madgett, and W. D. Trolinger (1997) Subgrade Resilient Modulus Correction for Saturation Effects. *Journal of Geotechnical Engineering, ASCE,* Vol. 123, No. 7, pp. 663-670.

Guan, Y., E. C. Drumm, and N. M. Jackson (1998) Weighting Factors for Seasonal Subgrade Resilient Modulus. In *Transportation Research Record 1619*, TRB, National Research Council, Washington D.C., pp. 94-100.

Kim, Y. R., B. O. Hibbs, and Y. Lee (1995) Temperature Correction of Deflections and Backcalculated Asphalt Concrete Moduli. In *Transportation Research Record 1473*, TRB, National Research Council, Washington, D. C., pp. 55-62.

Li, D. and E. T. Selig (1994) Resilient Modulus for Fine-Grained Subgrade Soils. *Journal of Geotechnical Engineering, ASCE,* Vol. 120, No. 6, pp. 939-957.

Lukanen, E. O., R. Stubstad, and R. C. Briggs (2000) *Temperature Predictions and Adjustment Factors for Asphalt Pavements*. Report FHWA-RD-98-085. Federal Highway Administration.

Marshall, C., R. W. Meier, and M. Welsh (2001) Seasonal Temperature Effects on Flexible Pavements in Tennessee. In *Transportation Research Record 1764*, TRB, National Research Council, Washington, D.C., pp. 89-96.

O'Connor, K. M. and C. H. Dowding (1999) *GeoMeasurements by Pulsing TDR Cables and Probes*. CRC Press

Rainwater, N. R., R. E. Yoder, E. C. Drumm, and G. V. Wilson (1999) Comprehensive Monitoring Systems for Measuring Subgrade Moisture Conditions. *Journal of Transportation Engineering, ASCE,* Vol. 125, No. 5, pp. 439-448.

Rainwater, N. R., G. Zuo, E. C. Drumm, W. C. Wright, and R. E. Yoder (2001) Insitu Measurement and Empirical Modeling of Base Infiltration in Highway Pavement Systems. In *Transportation Research Record 1772*, TRB, National Research Council, Washington, D.C., pp. 143-150.

Sun, Z. J. and G. D. Young. (2001) Saline Clayey Soil Moisture Measurement Using Time-Domain Reflectometry. *In* Proceedings of *Second International*

Symposium and Workshop on Time Domain Reflectometry for Geotechnical Application. Northwestern University - Evanston, IL*,* Infrastructure Technology Institute.

Zuo, G., R. W. Meier, and E. C. Drumm (2002) The Effect of Temperature Averaging on Predicted Pavement Life. In *Transportation Research Record 1809*, National Research Council, Washington D.C., pp. 119-125.

Zuo, G., N. R. Rainwater, W. C. Wright, R. E. Yoder, and E. C. Drumm. (2001) Temperature Effect on TDR Measurement of Water Content of Unbound Materials. *In* Proceedings of *Proceedings of the Second International Symposium and Workshop on Time Domain reflectometry for Geotechnical Applications.* Infrastructure Technology Institute, Northwestern University*,* Evanston, IL.

Part II Factors Affecting the Determination of Subgrade Water Content from Multi-Segment TDR Probes

This part is slightly revised from a paper with the same name published in Transportation Research Record by Gang Zuo, Wesley C. Wright, N. Randy Rainwater, Eric C. Drumm, and Ronald E. Yoder:

Zuo, G., N. Randy Rainwater, E. C. Drumm, W. C. Wright, and R. E. Yoder (2002) Factors Affecting the Determination of Subgrade Water Content from Multi-Segment TDR Probes. In *Transportation Research Record 1808*, TRB, National Research Council, Washington D.C, pp. 3-10.

My contributions to this paper include: (1) part of the literature review; (2) Laboratory temperature calibration tests; (3) Data reduction and development of calibration equations; (4) Most of the writing.

2.1 Abstract

Multi-segment TDR probes are an attractive alternative to single segment probes when used for the insitu measurement of water content changes in pavement systems. Because several independent measurements are made along the length of the multi-segment probe, these instruments offer several advantages over the more traditional TDR probes. These include the ability to obtain measurements over a greater volume of soil, the ability to install the probe into relatively undisturbed soils, and the redundancy provided by multiple measurements from the same instrument. However, because of the difference in signal strength along the probe, all segments do not provide the same level of accuracy. This paper discusses several factors that must be considered when using these probes, including the sources of measurement error and the temperature dependence of the measurements in some segments. A method is described by which the results from lower accuracy segments can be used when higher accuracy segments fail during service, taking advantage of the redundancy provided by multi-segment probes. The method is demonstrated on

data from a site from which over four years of continuous water content measurements have been obtained.

2.2 Introduction

High subgrade water content, with the resulting decrease in subgrade strength and stiffness, is detrimental to roadway pavement response. Establishing relationships between subgrade moisture variation and highway pavement response is necessary for efficient pavement design. Seasonal variations in pavement subgrade water content and the environmental factors affecting the water content have been recognized as important parameters of pavement response for at least 40 years (Guinnee, 1958; Marks and Haliburton, 1969; Russam, 1970; Vaswani, 1975; Chu et al., 1977; Rada et al., 1994; Baran, 1994; Jin et al., 1994). Early research (Guinnee, 1958) relied on extensive coring, which is time consuming and destructive, to periodically extract subgrade samples and to determine water content and density in the laboratory. Later research relied on a variety of methods including gypsum blocks, tensiometers, and neutron probes to indirectly measure soil water content or soil suction (Marks and Haliburton, 1969; Russam, 1970; Vaswani, 1975). The instruments were usually installed by coring through the pavement into the subgrade, replacing the disturbed soil around the sensors, and patching the core hole in the pavement. Soil temperature and meteorological data were usually collected along with soil water data to determine the factors influencing the subgrade moisture. The development of electronic instrumentation and automated data collection

systems has allowed less intrusive monitoring methods and higher sampling frequency.

Time domain reflectometry (TDR) has been used in the power and telecommunications industries since the 1950's to identify cable faults. A voltage pulse is propagated along a transmission line that acts as a waveguide. Changes in cable impedance are reflected in the waveform revealing cable faults. In the 1970s TDR was investigated as a means of monitoring soil water content. The velocity of the voltage pulse waveform is a function of the dielectric constant of the material surrounding the waveguide. The apparent dielectric constant (K_a), can be calculated using equation (2-1).

$$K_a = \left(\frac{cT}{2L}\right)^2 \qquad (2\text{-}1)$$

where c = velocity of light in a vacuum (3×10^8 m/s),

T = round trip propagation time of the voltage pulse along the wave guide (unit: seconds),

L = length of the wave guide (unit: meter).

In the 1980's TDR became very popular in agricultural use after G. C. Topp developed an empirical relationship between the apparent dielectric constant and soil volumetric water content, using a two-rod transmission probe (Topp and Davis, 1985; Topp et al., 1980).

TDR was introduced as a method of monitoring insitu water contents of partially frozen subgrade soils in pavement system around 1986 (Kane, 1986). As the technology improved the method became popular in pavement system

instrumentation in the early 1990's using a variety of instrumentation designs (Rada et al., 1994; Kotdwala et al., 1994; Look et al., 1994; Janoo et al., 1994; Baran, 1994; Sargand, 1994; Rainwater et al., 1999). The method has continued to gain popularity as a monitoring tool for both freeze thaw cycles and water content changes in pavement systems (Hassan and White, 1997; Benson and Bosscher, 1999; Jiang and Tayabji, 1999; Roberson and Siekmeier, 2000; FHWA, 2000; Hanek et al., 2001). Additional empirical and theoretical relationships between apparent dielectric constant and soil water content have been developed and evaluated by researchers in various calibration studies (Jacobsen and Schjonning, 1995; Klemunes, 1998; Wright et al., 2001).

Although TDR is widely used for insitu water content measurement, continued use and investigation of the method has revealed various challenges associated with collecting and interpreting the data. Research has shown contradictory trends in regard to the magnitude and direction of temperature effects on TDR measurement in soil (Verstricht et al., 1994; Halbertsma et al., 1995; Alvenas and Stenberg, 1995; Pepin et al., 1995). The effect of temperature on the dielectric properties of soil-water medium can be different for different soils, and even for the same soil the effect can be different at significantly different water contents. A comprehensive review on this topic can be found in the paper by Wraith and Or (1999), in which the contradictory effects of temperature on TDR measurement of soil water content are explained by the interplay of two competing phenomena: (1) the reduction in the dielectric constant of free water with increased temperature; and (2) the increase in the amount of released bound water with increased

temperature. Other difficulties reported include the effect of soil density (Malacki et al., 1996; Deschamps et al., 2000), soil disturbance during installation (Siddiqui et al., 2000), and the time and effort required to collect and analyze the data (Liu et al., 1999).

As part of a pavement instrumentation program conducted by the Tennessee Department of Transportation (TDOT), multi-segment TDR probes were installed to monitor the volumetric water content of subgrade soil and unbound aggregate at four sites in Tennessee. The AASHTO classification of the subgrade soils at testing sites are A-7-5, A-7-6, and A-4. To avoid significant changes to the soil structure, the probes were pushed horizontally into undisturbed subgrade from a trench beneath the shoulder. Thermistors were installed at the same depths as the TDR probes. A weather station was erected at each site to collect precipitation and air temperature. The entire data collection process is automated, with TDR data automatically collected every 6 hours, and downloaded by cellular telephone every 24 hours. The test sites and monitoring systems are described by Rainwater et al. (1999).

2.3 Multi-Segment TDR Probes

Moisture Point type III multi-segment TDR probes produced by Environmental Sensors ® were used in the project (Figure 2.1). The probe is made of two stainless steel plates approximately 12.7 mm wide by 3.2 mm thick, separated by 12.7 mm of high density plastic and epoxy. The probe consists of five 300 mm long segments, each providing a distinct water content measurement. The Moisture Point MP-917 unit is used to measure signal propagation time. A pulse

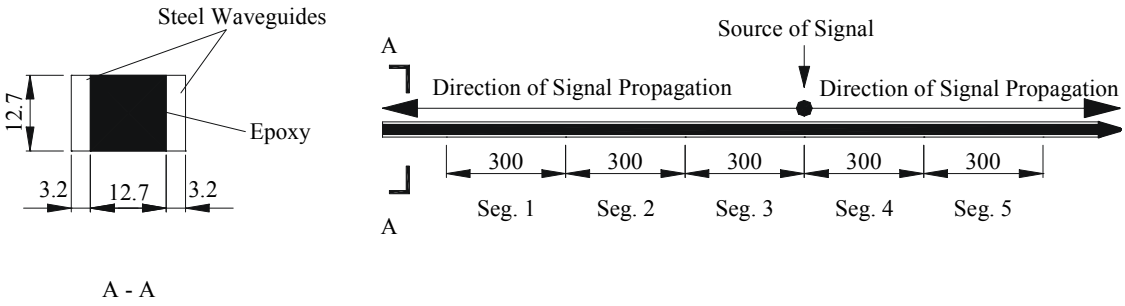

Figure 2.1 Moisture Point type III five-segment TDR probe (unit: mm).

signal is emitted at the center of the probe, between segment 3 and segment 4 (Figure 2.1). The signal then travels through segments 3 – 2 –1 in one direction, and through segments 4 – 5 in the other direction. Three multi-segment TDR probes were installed in the subgrade at each site, numbered as Probe 1, 2 and 3, with Probe 3 being nearest the subgrade surface.

Unlike typical applications in agricultural engineering where the multi-segment TDR probes are embedded in low density soil, the pavement subgrade was compacted to a high density during construction. Site-specific laboratory tests were performed to obtain the relationship between soil water content and TDR measurement for the high density soils, and twelve different calibration equations were evaluated (Wright et al., 2001). The relationship between inverse signal velocity and soil water content proposed by Herkelrath et al. (1991) was found out to be the most accurate to predict water content for all subgrade soils:

$$\theta_V = \text{Slope}(1/v) + \text{Intercept} \qquad (2\text{-}2)$$

where θ_V = volumetric water content of soil,

v = signal velocity,

Slope and Intercept = constants.

2.4 Problem Description

The multi-segment TDR probes were selected over the more common single-segment TDR probes to maximize the volume of soil measured. With a length of 1.5 m, a much larger volume of soil is monitored compared to a typical 300 mm length probe. After an initial review of the data collected over the first year, it was decided to take the mean of all 5 segments as the subgrade water content at that depth. Water content averaged over the entire length of the probe reduces the spatial variation of θ_V, which is an inevitable characteristic of soil as a heterogeneous material. However, a strong correlation between temperature and subgrade water content was noticed for all four sites. The subgrade temperature and volumetric water content measured by Probe 3 at the Blount County site is shown in Figure 2.2 for a 4 year period. An investigation of the factors affecting the determination of θ_V was initiated.

2.5 Objectives

The objective of this research is to find out the source of the temperature dependence on TDR soil water content measurement and to develop a method to remove this temperature effect from TDR measurement.

2.6 Investigation

2.6.1 Laboratory Tests of Temperature Effects

A series of laboratory tests were performed to investigate for each of the four site soils, the effect of temperature on TDR measurement of θ_V using the Moisture Point Type III five-segment TDR probe.

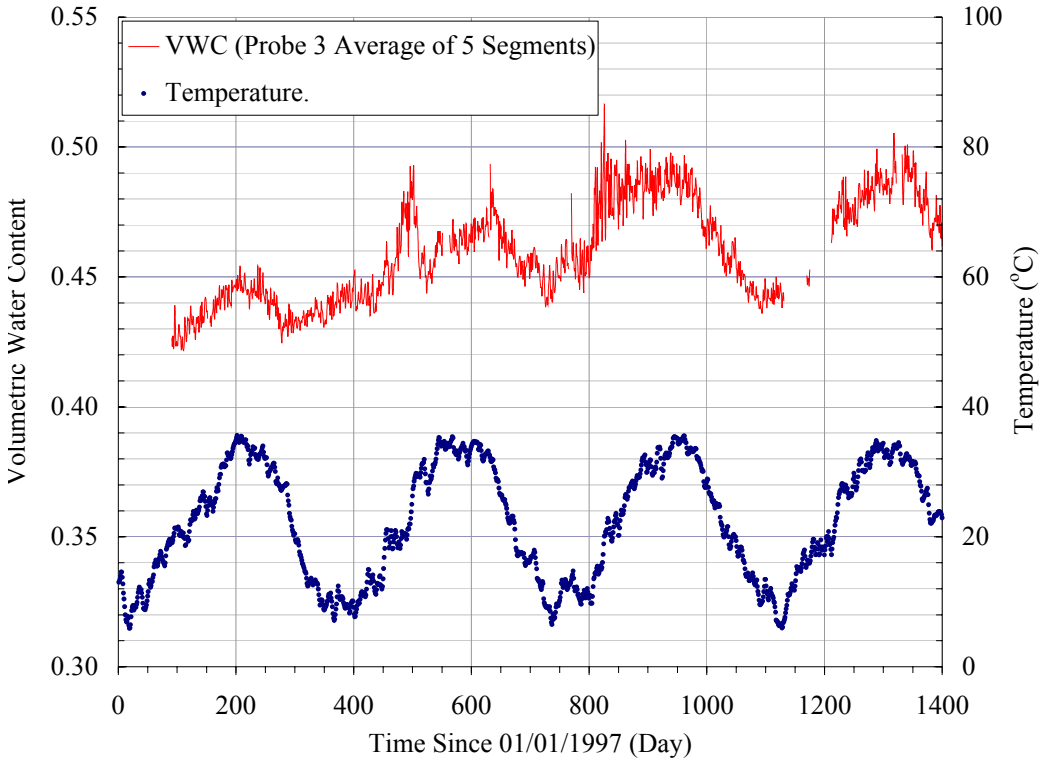

Figure 2.2 Average volumetric water content at the Blount County site, Probe 3, Average of 5 Segments.

Soil collected from the site was first mixed to a typical water content corresponding to that determined from gravimetric samples obtained by coring at the field sites. A specific mass of soil was placed into an aluminum box to achieve the same dry density as the soil samples obtained in the field. The TDR probe was placed in the middle of the soil before compressing the soil to a predetermined density. The box was then wrapped in plastic wrap to reduce moisture loss and moved into an environmental chamber where the temperature and humidity were strictly controlled. The temperature in the environmental chamber was increased by 5 °C every 24 hours ranging from 5 °C to 40 °C, the typical temperature range in the soil subgrades at the research sites. TDR

propagation time was automatically collected by the MP-917 every 30 minutes, and soil temperature, measured by thermistors, was collected simultaneously by a data logger. A detailed description of the experimental set up and laboratory test procedures is given by Zuo et al., 2001.

Three repetitions of tests were run for each soil. Due to the difficulty in the sample preparation, actual water content is slightly different for different samples. As a result, the TDR measurement at the same segment from different repetition does not coincide with each other. However, the same trend holds in all the three repetitions. A typical result of the laboratory tests is shown in Figure 2.3. Measurements by Segment 3 and 4 show little variation with changing temperature. Segments 2 and 5 show a significant increase both in the mean

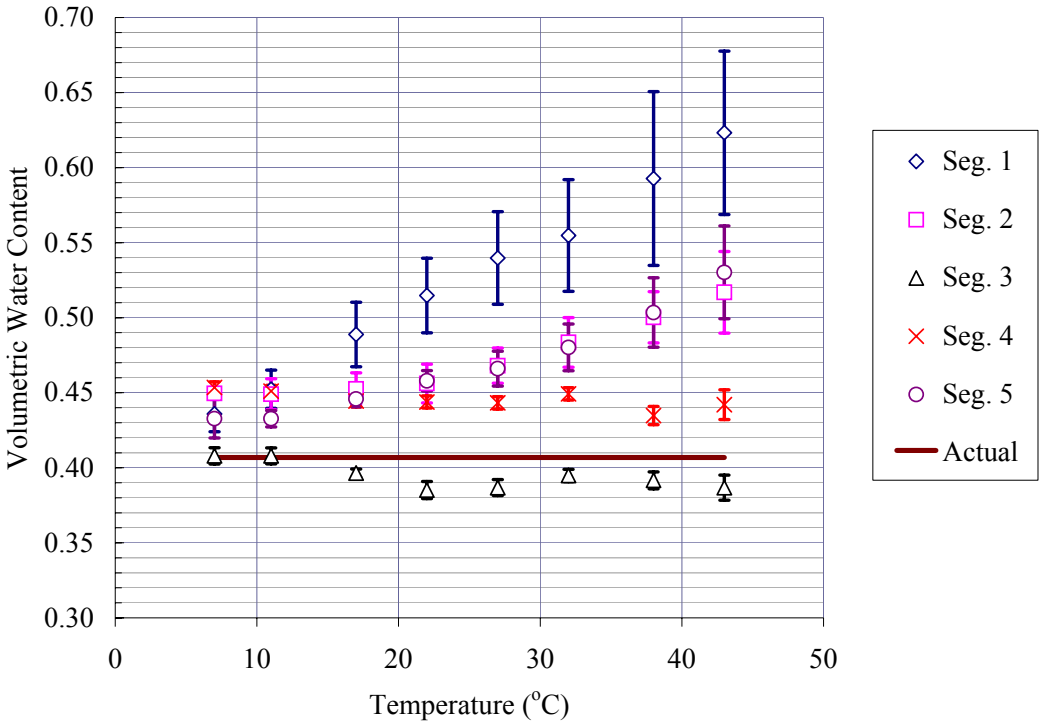

Figure 2.3 Mean and standard deviation of volumetric water content measured by different segments.

value and the standard deviation of the measured volumetric water content at each temperature step as the temperature increases. Segment 1 shows even greater dependence and deviation with temperature. The laboratory calibration led to the correction equation, Equation (2-3), to correct the temperature–dependent TDR measurement to the relevant measurement at 20 °C. Although site-specific temperature corrections were developed for each segment, these findings led to further investigation of the application of the multi-segment TDR probes.

$$\theta_{VC} = \theta_{VM} - a \cdot (T - 20) \qquad (2\text{-}3)$$

where θ_{VC} = corrected volumetric water content,

θ_{VM} = measured volumetric water content,

T = temperature at the same depth as the probe, °C.

a = constant (a = 0.005 for Segment 1; a = 0.002 for Segments 2 and 5).

2.6.2 Signal Attenuation in the Multi-Segment Probe

A remote diode shorting technique (Hook et al., 1992) is used in the Moisture Point multi-segment TDR probe design to increase the effective amplitude of reflections and significantly reduce background noise. The probes are fabricated using a switching diode at the beginning and end of each segment. When the diode acts as a open circuit, the electromagnetic pulse is unaffected and continues to propagate down the transmission line. The reflected waveform obtained with the diode shorted is identical to that obtained with the diode open

until the time that reflection from the shorted diode reaches the TDR instrument. The waveform is recorded with the diodes open, then each diode is shorted one at a time (Figure 2.4a) and the waveform is subtracted from the waveform recorded with the diodes open (Figure 2. 4b). The propagation time between the diodes of a segment can then be determined as shown in Figure 2.4b. The first horizontal portion of the waveform is used to determine a baseline value. The rising edge of the later part of the data is fitted to a straight line. The x value of the intersection of the fitted straight line and the baseline is defined as the Xover value. The difference of the two Xover values for each segment determines the round trip propagation time. Figure 2.5 shows a typical waveform obtained from a raw log file of probe scans at one of the instrumented sites. The figure contains ten signals: five segments each with two diodes (one for each diode at the end of the segment).

The amplitude of the signal at the start end of the segment decreases with increasing distance from the source of the signal, which is located between Segment 3 and 4. In Figure 2.5, the amplitudes of Segment 4-Diode 1 and Segment 3-Diode1 are identical, because Diode 1 of Segment 4 and Diode 1 of Segment 3 are actually at the same location. Similarly, amplitudes of the following pairs are almost identical:
Segment 4-Diode 2 and Segment 5-Diode 1, Segment 3-Diode 2 and Segment 2-Diode 1, and Segment 2-Diode 2 and Segment 1-Diode 1.

The decrease in signal amplitude results in a decrease in the slope of the fitted straight line of the rising edge, even if the rising time for all the segments is the

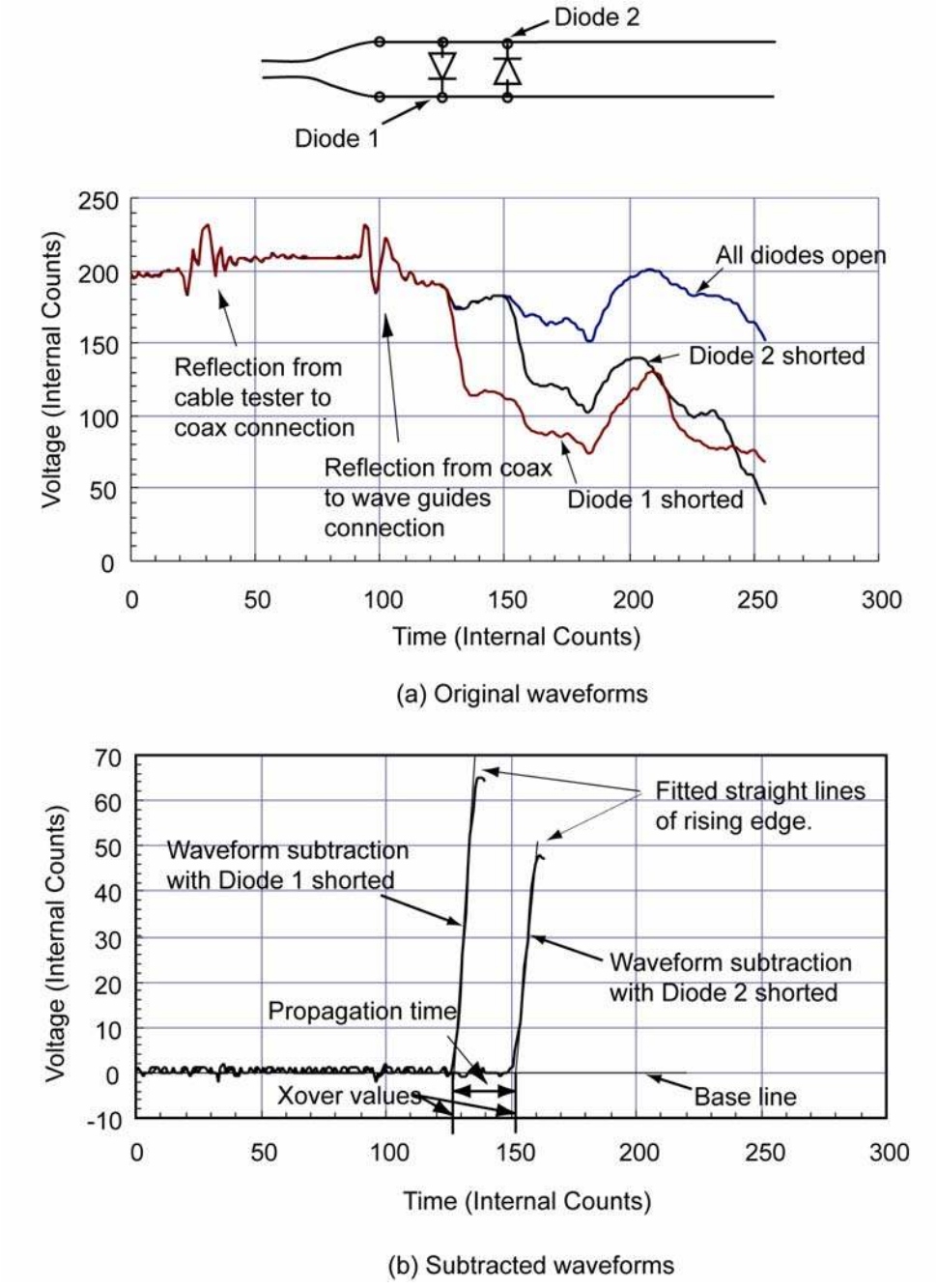

Figure 2.4 Schematic of remote diode shorting technique.

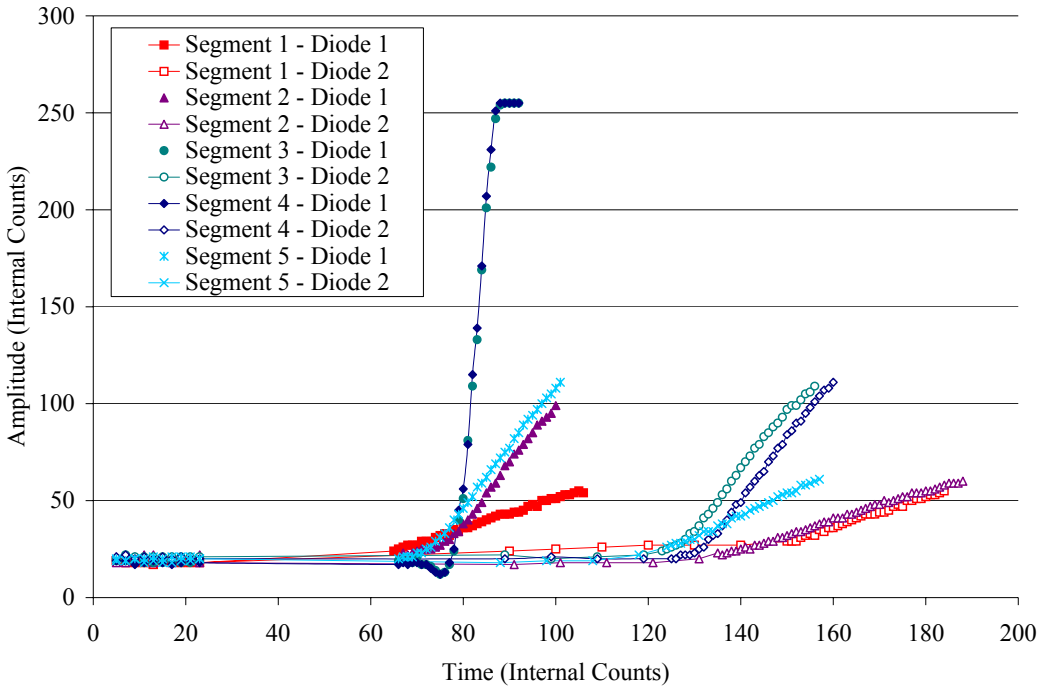

Figure 2.5 Typical waveforms of a TDR probe.

same. However, the rising time also increases with distance from the signal source. Both the decrease in amplitude and the increase in rising time reduce the slope of the fitted straight line of the rising edge.

As the slope of the rising edge decreases due to signal attenuation, it becomes more difficult to distinguish the starting points of the linear part of the rising edge. This also leads to more error in the determination of the Xover times and the calculation of water content. The signals in Segment 3 and 4 are the strongest, since the signal enters the probe at these segments. The signal at Segment 2 and 5 will be weaker, and that at Segment 1 weaker still. This explains why the results in Segment 2 and 5 are more variable than those from Segments 3 and 4, and why the results from Segment 1 are the least reliable, as

demonstrated in the laboratory test results shown in Figure 2.3. The temperature dependence is also attributed to the signal attenuation.

2.6.3 Correction for Loss of Signal Strength in Segment 2 and 5

Based on the results from laboratory tests on the effect of temperature on the TDR measurement of θ_V, Segment 3 and 4 were found to be not significantly affected by temperature, thus it was decided that the average of these two segments would be taken as the θ_V measured by that probe. However, at some of the sites, there were probes for which the data from Segment 3 and/or 4 were not available after a few months of operation. The θ_V measured by other segments (such as Segment 2 and 5) can be used instead of Segment 3 and 4 provided the temperature effects are removed using correction equations such as those developed from the site-specific calibration (Zuo et al., 2001).

An alternative way to predict θ_V measurement of the average of Segment 3 and 4 from the measurement of another segment is to perform linear regression using the field data. For Probe 3 at the Blount County site, the following equation was obtained to predict the average θ_V of Segment 3 and 4 from the data from Segment 5 and the temperature at the same depth:

$$\theta_{34} = 0.474\theta_5 - 0.00910T + 0.2777 \qquad (2\text{-}4)$$

where θ_{34} = average volumetric water content measurement of Segment 3 and 4;

θ_5 = volumetric water content measurement of Segment 5

T = temperature measured at the same depth of Probe 3, $^\circ C$.

Equation (4) can be rearranged to yield Equation (2-5),

$$\theta_{34} = 0.474 \cdot \left[\theta_5 - 0.0019 \cdot (T - 20)\right] + 0.260 \qquad (2\text{-}5)$$

Equation (2-5) suggests that in order to get the θ_V measurement close to that of the average of Segment 3 and 4, the measurement of Segment 5 should be scaled and shifted, in addition to applying the temperature correction. It should be noted that the temperature correction factor in Equation (2-5), 0.0019, is consistent with constant a in Equation (2-3). The scale factor, 0.474, indicates that in the field, Segment 5 is about twice as sensitive to the change in θ_V as Segment 3 and 4, but in the lab this scale factor was not needed.

2.7 Measured Variation in Water Content - Application of the Correction for Loss of Signal Strength

Because the data from Segments 3 and 4 were found to be stable and reliable over a range of temperatures, it was decided to use the data from only these segments to reflect the water content corresponding to a given depth of probe. However, in cases where the data from Segments 3 and/or 4 were not available, the data from Segments 2 and 5 were corrected as described above. This empirical correction appears to be more reliable than the site-specific temperature calibrations (Zuo et al., 2001) that were developed previously, because of the signal noise or inaccuracies that exist from the signal attenuation problems.

Figure 2.6a compares the average of Segments 3 and 4 with the results from Segment 5. The erratic cyclic variations shown in the Segment 5 data are similar

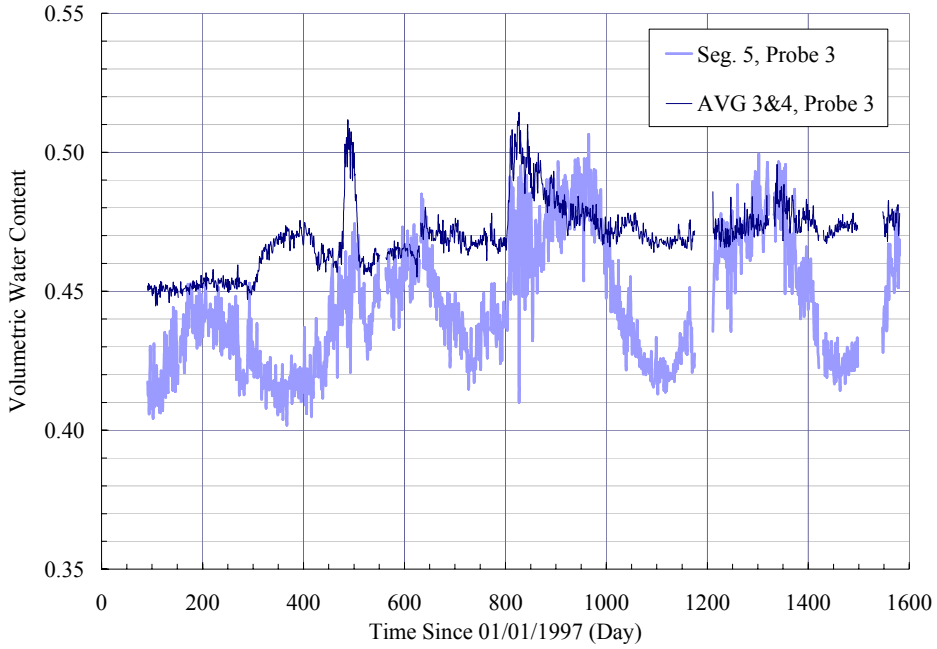

(a) Segment 5 and the average of segment 3 & 4.

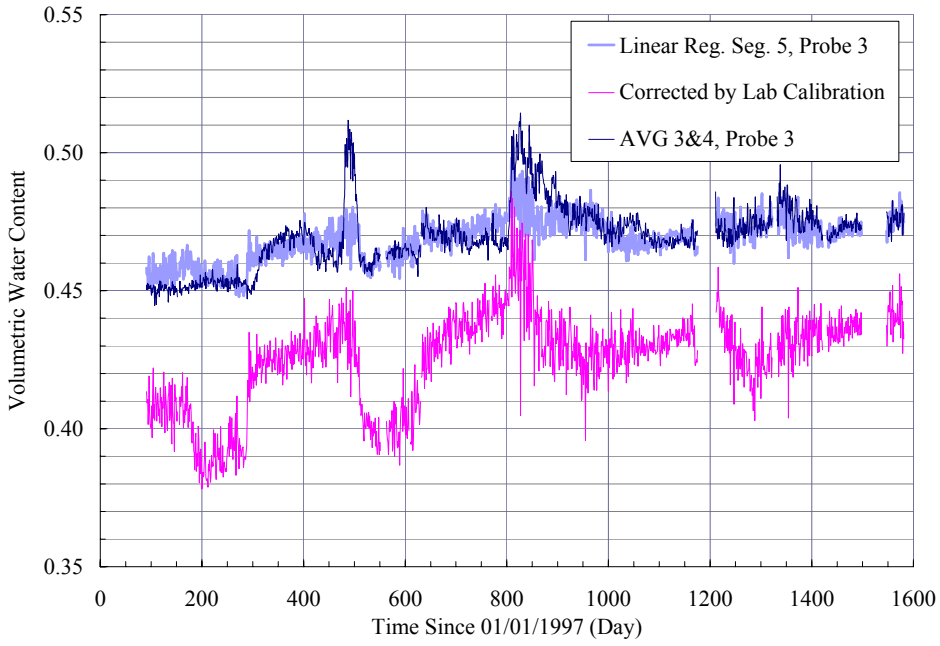

(b) Corrected water content from Segment 5 compared with average of Segments 3 and 4.

Figure 2.6 Prediction of the Average of volumetric water content from measurement at seg. 5 using linear regression (Blount County).

to those shown in Figure 2.2, when the average of all segments was plotted. In Figure 2.6b, both the proposed empirical correction method and the correction method using the results of laboratory calibration were applied to the Segment 5 data. With the exception of a few excursions, the corrected data using empirical correction method follows the average of Segment 3 and 4 very well; the one using the results from laboratory calibration shows more variation, besides the shift which may be caused by the spatial variation in the soil water content along the probe. This suggests that in cases where Segment 3 and or 4 fails during service, a correction can be developed from the less reliable and more temperature–dependent Segment 2 or 5 data. Even though site-specific temperature corrections were developed for each of the segments, it was decided not to use data from Segment 1 in any of the probes, due to the high variability of this data and very strong temperature dependence.

2.8 Conclusions

Multi-segment TDR probes provide several independent measurements of water content along the length of the probe, and offer several advantages over the more traditional TDR probes. However, because of the difference in signal strength caused by attenuation over the distance from the point where the signal enters the probe, the more extreme segments include more noise in the signal resulting in a less reliable measurement of water content. In addition, the segments with low signal strength appear to be more susceptible to temperature changes. A method was described by which the results from lower accuracy/more temperature dependent segments can be used when higher

accuracy segments fail during service. This takes advantage of the redundancy provided by multi-segment probes. It should be noted that site specific constants should be obtained for both the laboratory calibration equation (3) and linear regression of the field data (4) before they can be used to do any correction. The correction method was demonstrated on data from a site from where four years of continuous water content measurements have been collected. When the average of all five segments was used, the measured water content followed the temperature variations very closely. The corrected results from one of the extreme segments were shown to correspond well with those from the more stable, temperature independent center segments. By using the less temperature dependent segments, or the corrected temperature-dependent data, the seasonal trends in water content are still apparent, yet of more reasonable magnitude.

References

Alvenas, G. and M. Stenberg. (1995) Problems in Estimating Soil Water Content by TDR Measurements. Foulum, Denmark, pp. 121-123.

Baran, E. (1994) Use of time domain reflectometry for monitoring moisture changes in crushed rock pavements. In Proceedings of Proceedings of Symposium and Workshop on Time Domain Reflectometry in Environmental, Infrastructure, and Mining Applications. US Bureau of Mines, Infrastructure Technology Institute at Northwestern University, Los Alamos National Laboratory, pp. 349-356.

Benson, C. H. and P. J. Bosscher (1999) Remote Field Methods to Measure Frost Depth. Field Instrumentation for Soil and Rock. *ASCE STP* Vol. 1358, pp. 267-284.

Chu, T. Y., W. K Humphries, R. L. Stewart, S. S. Guram, and S. N. Chen (1977) Soil moisture as a factor in subgrade evaluation. *Transportation Engineering Journal, ASCE,* Vol. 103, No. TE1, pp. 87-102.

Deschamps, R. J., V. P. Drnevich, W. Feng, and C. P. Lin (2000) Time Domain Reflectometry for Compaction Quality Control. ASCE, Reston VA, pp. 15-34.

FHWA (2000) Computed Parameters: Moisture Content for Unbound Materials at Seasonal Monitoring Program Sites. Report FHWA-RD-00-077. FHWA, U. S. Department of Transportation.

Guinnee, J. W. (1958) Field Studies on Subgrade Moisture Conditions. In *HRB Special Report 40*, Highway Research Board, Washington D. C., pp. 253-267.

Halbertsma, J., E van den Elsen, H. Bohl, and W. Skierucha. (1995) Temperature Effects on TDR Determinated Soil Water Content. *In* Proceedings of *Proceedings of the Symposium: Time-Domain reflectometry Applications in Soil Science, SP Report 11. Foulum, Denmeark,* pp. 35-47.

Hanek, G. L., M. A. Truebe, and M. A. Kestler. (Jan.2001) Evaluating Moisture Sensors and Monitoring Seasonal Moisture Variation In Low Volume Roads. *In* Proceedings of *Proceedings 80th Annual Meeting of the Transportation Research board (PREPRINT CD-ROM).* National Research Council, Washington D.C.,

Hassan, H. F. and T. D. White (1997) Laboratory and Field Moisture Conditions for Flexible Pavement. In *Transportation Research Record 1568*, TRB, National Research Council, Washington D.C., Washington, D. C., pp. 96-105.

Herkelrath, W. N., S. P. Hamburg, and F. Murphy (1991) Automatic, Real-Time Monitoring in a Remote Field Area with Time Domain Reflectometry. *Water Resources Research* Vol. 27, No. 5, pp. 857-864.

Hook, W. R., N. J. Livingston, Z. J. Sun, and P. B. Hook (1992) Remote Diode Shorting Improves Measurement of Soil Water by Time Domain Reflectometry. *Soil Science Society American Journal* Vol. 56, pp. 1384-1391.

Jacobsen, O. H. and P. Schjonning. (1995) Comparison of TDR Calibration Functions for Soil Water Determination. *In* Proceedings of *Time-Domain Reflectometry Applications in Soil Science, SP Report 11.* Foulum, Denmark, pp. 25-33.

Janoo, V., R. L. Berg, E. Simonsen, and A. Harrison. (1994) Seasonal changes in moisture content in airport and highway pavements. *In* Proceedings of *Proceedings of Symposium and Workshop on Time Domain Reflectometry in Environmental, Infrastructure, and Mining Applications.* US Bureau of Mines, Infrastructure Technology Institute at Northwestern University, Los Alamos National Laboratory, pp. 357-363.

Jiang, Y. J. and S. D. Tayabji (1999) Analysis of Time Domain Reflectometry Data From LTPP Seasonal Monitoring Program Test Sections. Report C6B, Final Report. Report FHWA-RD-99-115. FHWA, U.S. Department of Transportation.

Jin, M. S., K. W. Lee, and W. D. Kovacs (1994) Seasonal Variation of Resilient Modulus of Subgrade Soils. *Journal of Transportation Engineering, ASCE,* Vol. 120, No. 4, pp. 603-616.

Kane, D. L. (1986) *Soil Moisture Monitoring Under Pavement Structures Using Time Domain Reflectometry*. Report FHWA-AK-RD-87-08. FHWA, U.S. Department of Transportation.

Klemunes, J. A. (1998) *Determining Soil Volumetric Moisture Content Using Time Domain Reflectometry*. Report FHWA-RD-97-139. FHWA, U.S. Department of Transportation.

Kotdwala, S. J., M. Hossain, and A. J. Gisi. (1994) Monitoring of moisture changes in pavement subgrades using time-domain reflectometry (TDR). *In* Proceedings of *Proceedings of Symposium and Workshop on Time Domain Reflectometry in Environmental, Infrastructure, and Mining Applications.* US Bureau of Mines, Infrastructure Technology Institute at Northwestern University, Los Alamos National Laboratory, pp. 364-373.

Liu, R., X. Chen, R. He, W. Ma, and H. Wu (1999) *Establishment of Reliagble Methodologies to Determine In-situ Moisture Content of Base and Subgrade Soils*. Report 3935-S,TX-00/3935-S. Texas Department of Transportation, Austin.

Look, B. G., I. N. Reeves, and D. J. Williams. (1994) Field experiences using time domain reflectometry for monitoring moisture changes in road embankments and pavements. *In* Proceedings of *Proceedings of Symposium and Workshop on Time Domain Reflectometry in Environmental, Infrastructure, and Mining Applications.* US Bureau of Mines, Infrastructure Technology Institute at Northwestern University, Los Alamos National Laboratory*,* pp. 374-385.

Malacki, M. A., R. Plagge, and C. H. Roth (1996) Improving the Calibration of Dielectric TDR Soil Moisture Determination Taking in to Account the Solid Soil. *European Journal of Soil Science* Vol. 47, pp. 357-366.

Marks, B. D. III and A. Haliburton (1969) Subgrade Moisture Variations Studied with Nuclear Depth Gages. In *Highway Research Record 276*, Highway Research Board, Washington D.C., pp. 14-24.

Pepin, S., N. J. Livingston, and W. R. Hook (1995) Temperature-Dependent Measurement Errors in Time Domain Reflectometry Determinations of Soil Water. *Soil Science Society of America Journal* Vol. 59, pp. 38-43.

Rada, G. R., Jr. A. Lopez, and G. E. Elkins. (1994) Monitoring of subsurface moisture in pavements using time-domain reflectometry. *In* Proceedings of *Proceedings of Symposium and Workshop on Time Domain Reflectometry in Environmental, Infrastructure, and Mining Applications.* US Bureau of Mines, Infrastructure Technology Institute at Northwestern University, Los Alamos National Laboratory*,* pp. 422-433.

Rainwater, N. R., R. E. Yoder, E. C. Drumm, and G. V. Wilson (1999) Comprehensive Monitoring Systems for Measuring Subgrade Moisture Conditions. *Journal of Transportation Engineering, ASCE,* Vol. 125, No. 5, pp. 439-448.

Roberson, R. L. and J. Siekmeier (2000) Using a Multisegment Time Domain Reflectometry Probe to Determine Frost Depth in Pavement Systems. In *Transportation Research Record 1709*, TRB, National Research Council, Washington, D.C., Washington, D. C., pp. 108-113.

Russam, K. (1970) Subgrade Moisture Studies by the British Road Research Laboratory. In *Highway Research Record 301*, Highway Research Board, Washington D.C., pp. 5-17.

Sargand, S. (1994) *Development of an Instrumentation Plan for The Ohio SPS Test Pavement . Final Report*. Report (DEL-23-17.48), Job No. 14573(0). Ohio Department of Transportation and Federal Highway Administration. Ohio University, Athens, OH.

Siddiqui, S. I., V. P. Drnevich, and R. J. Deschamps (2000) Time Domain Reflectomtry Development for us in Geotechnical Engineering. *Geotechnical Testing Journal* Vol. 23, No. 1, pp. 9-20.

Topp, G. C. and J. L. Davis (1985) Time-domain reflectometry (TDR) and its application to irrigation scheduling. Academic Press, New York, pp. 107-126.

Topp, G. C., J. L. Davis, and A. P. Annan (1980) Electromagnetic determination of soil water content: measurements in coaxial transmission lines. *Water Resources Research* Vol. 16, No. 3, pp. 574-582.

Vaswani, N. K. (1975) Case Studies of Variations in Subgrade Moisture and Temperature under Road Pavements in Virginia. In *Transportation Research Record 532*, TRB, National Research Council, Washington, D. C., pp. 30-42.

Verstricht, J., B. Neerdael, and G. Volckaert. (1994) Clay Moisture Measurements in Radioactive Waste Disposal Research. *In* Proceedings of *Proceedings of Symposium and Workshop on Time Domain Reflectometry in Environmental, Infrastructure, and Mining Applications.* US Bureau of Mines, Infrastructure Technology Institute at Northwestern University, Los Alamos National Laboratory*,* pp. 337-348.

Wraith, J. M. and D. Or (1999) Temperature Effects on Soil Bulk Dielectric Permittivity Measured by Time Domain Reflectometry: Experimental Evidence and Hypothesis Development. *Water Resources Research* Vol. 35, No. 2, pp. 361-369.

Wright, W. C., R. E. Yoder, N. R. Rainwater, and E. C. Drumm (2001) Calibration of Five-Segment Time Domain Reflectometry Probes for Water Content Measurement in High Density Materials. *ASTM Geotechnical Testing Journal, GTJODJ* Vol. 24, No. 2, 172-184.

Zuo, G., N. R. Rainwater, W. C. Wright, R. E. Yoder, and E. C. Drumm. (2001) Temperature Effect on TDR Measurement of Water Content of Unbound Materials. *In* Proceedings of *Proceedings of the Second International Symposium and Workshop on Time Domain reflectometry for Geotechnical Applications.* Infrastructure Technology Institute, Northwestern University, Evanston, IL.

Part III Three Dimensional Finite Element Analysis of Flexible Pavement

3.1 Abstract

A three dimensional finite element (3DFE) code was used to analyze flexible pavement under a single axle dual-wheel load. The differences between 3D analysis and two dimensional axisymmetric analysis were investigated, and typical results were compared. Some difficulties and concerns about 3DFE analysis, such as boundary conditions, interface conditions, element type, element shape and element size, were also discussed. It was found that the 3DFE idealization reduced the maximum tensile strain at the bottom of the asphalt layer by 20%, in comparison to 2D axisymmetric analysis; the smooth interface between the asphalt and base produced similar results as the frictional interface, yet was more reasonable than the fully bonded condition; the extension of the pavement shoulder to 8m from the center of the wheel path does not significantly affect the critical stresses in the pavement.

3.2 Introduction

Three dimensional finite element (FE) codes have become widely used for pavement stress, strain and displacement analysis. The FE method has been used to investigate the effect of nonlinear subgrades and foundation layers (Schwartz, 2000; Hjelmstad and Taciroglu, 2000), dynamic and moving loads (Zaghloul and White, 1993, Zaghloul et al., 1994), multiple loads (Kim et al., 1997), surface cracking and wheel interaction (Bensalem et al., 2000), doweled joints in concrete pavements (Davids, 2001), and curling and warping of Portland cement concrete slabs due to temperature (William and Shoukry, 2001). Three dimensional finite element (3DFE) analysis of pavement can be used to

account for more realistic loading and boundary conditions than traditional layered elastic methods or two dimensional finite element analyses. A parametric study was conducted to investigate the effect of element type, element size and shape, boundary condition, layer interface condition, load area, and 2D versus 3D idealizations.

3.3 Uzan's Resilient Modulus Model and ABAQUS Implementation

One of the advantages of the FE method over the layered elastic method is the ability to implement advanced material models. Uzan's (1985) resilient modulus model can account for the stress-dependent behavior of the unbound materials, as shown in Equation (3-1)

$$M_R = K\theta^n \tau_{oct}^m \qquad (3\text{-}1)$$

where M_R = resilient Modulus,

θ = Bulk stress = Sum of principal stresses = $\sigma_1 + \sigma_2 + \sigma_3$,

τ_{oct} = Octahedral shear stress = $\sqrt{\frac{1}{3}\left[(\sigma_1 - \sigma_2)^2 + (\sigma_2 - \sigma_3)^2 + (\sigma_3 - \sigma_1)^2\right]}$,

K, n and m = Material constants.

A fixed point iteration algorithm has been commonly used to implement Uzan's model into various computer programs. However, the fixed-point iteration is eventually bound to diverge if the load level is too high. Even if the fixed-point iteration converges, the performance of the algorithm is bound to degrade with increased load level (Hjelmstad and Taciroglu, 2000). Hjelmstad and Taciroglu

(2000) proposed an algorithm to implement Uzan's model, in which the resilient modulus is updated based on the strains of the last iteration, as shown in Equation (3-2), rather than the previous stresses as in the fixed point iteration algorithm.

$$M_R = (1+\nu)\left(\frac{K}{1+\nu}\left(\frac{\nu}{1-2\nu}+\frac{1}{3}\right)^n\right)^{\mu} \rho^{\mu n}\gamma^{\mu m} \qquad (3\text{-}2)$$

where ν = Poisson's ratio,

$\mu = \frac{1}{1-n-m}$,

ρ = Bulk strain = Sum of principal strains = $|\varepsilon_1+\varepsilon_2+\varepsilon_3|$,

γ = Octahedral shear strain = $\sqrt{\frac{1}{3}\left[(\varepsilon_1-\varepsilon_2)^2+(\varepsilon_2-\varepsilon_3)^2+(\varepsilon_3-\varepsilon_1)^2\right]}$,

K, n and m = Same material constants as in Equation (3-1).

The implementation of Hjelmstad and Taciroglu (2000) is theoretically sound and the model proposed by Uzan (1985) should work well for both coarse-grained and fine-grained materials, although the implementation was demonstrated for a coarse-grained material.

Some minor changes have to be made to the model before it can be applied to fine materials. The power of the octahedral shear strain, m, is negative for fine materials. An overflow error would occur if the octahedral shear strain is very small, which is common for small loading steps when the computed strains are very small. Uzan's (1985) resilient modulus model can be incorporated into the analysis using user material via user subroutine UMAT in ABAQUS 6.2-1 (2001).

Therefore, in the user subroutine, a lower limit of the octahedral strain should be used to prevent this overflow. The lower limit used in this research was arbitrarily chosen to be 1 micron (1E-06). The effect of this assumed lower limit was investigated and found to have negligible effect on the final solution.

3.4 Analysis Description

Two flexible pavements with different layer thickness were analyzed, and are termed “A” and “B” pavement systems for simplicity. The thickness of the asphalt concrete (AC) layer and base layer for each model is listed in Table 3.1.

3.4.1 Material Properties

Linear elastic material properties were assumed for the AC layer and the pavement response was investigated for constant temperature. Uzan’s (1985) resilient modulus model was adopted for the unbound base and subgrade. The material properties for different layers in the pavement system used in the FE analyses are listed in Table 3.2.

It should be noted that for simplicity, all the asphalt-bound layers, i.e., surface layer, binder layer, asphalt concrete and asphalt stabilized base, were assumed to be combined into one layer with constant material properties.

Table 3.1 Layer Thickness for Different Pavement Models

	AC Layer (mm)	Base Layer (mm)
Pavement A	216	255
Pavement B	360	425

Table 3.2 Material Properties Used in the Analysis

Material Property		Asphalt Concrete	Base Course	Subgrade
Density	ρ (Mg/m^3)	2400	2200	1700
Poisson's Ratio	υ	0.32	0.35	0.45
Young's Modulus	E (Pa)	1.38E+09	-	-
Parameters in Uzan's Model	K (Pa)	-	5.87E+05	1.60E+08
	n	-	0.45	0.26
	m	-	0.00	-0.31

3.4.2 Model Setup

Flexible pavement is a layered system, so it is desirable that the model be divided into separate layers or parts in the analysis, so that the contact condition on the interfaces between layers can be modeled properly. In addition, using parts facilitates the development of the FE mesh and assignment of material properties. The thickness of each pavement layer can be easily modified by adding or removing some sublayers which are created as parts. The mesh of different parts for a pavement model is shown in Figure 3.1, where the AC and base are each divided into 3 parts or sublayers.

3.4.3 Element Size, Shape and Type

Two meshes with similar element shape but different element size were considered to study the effect of element size. A coarse mesh of the entire model is shown in Figure 3.2. For the model with the fine mesh, the size of the element in each dimension is half of that of the coarse mesh.

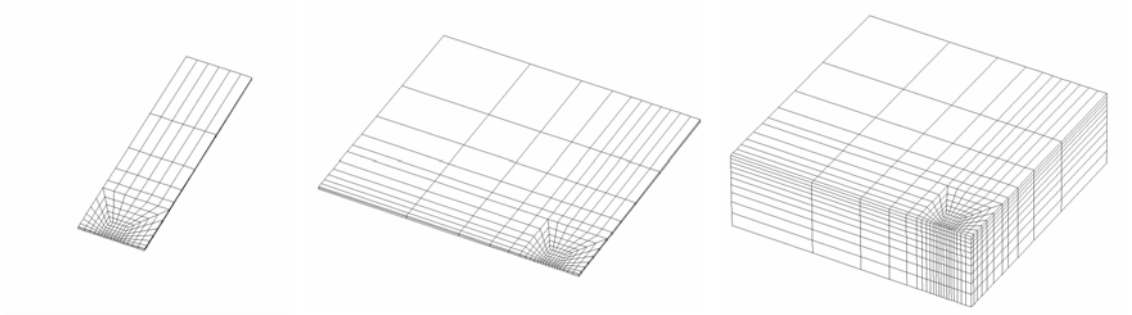

AC Layer 1 Base Layer 1 Subgrade Layer 1

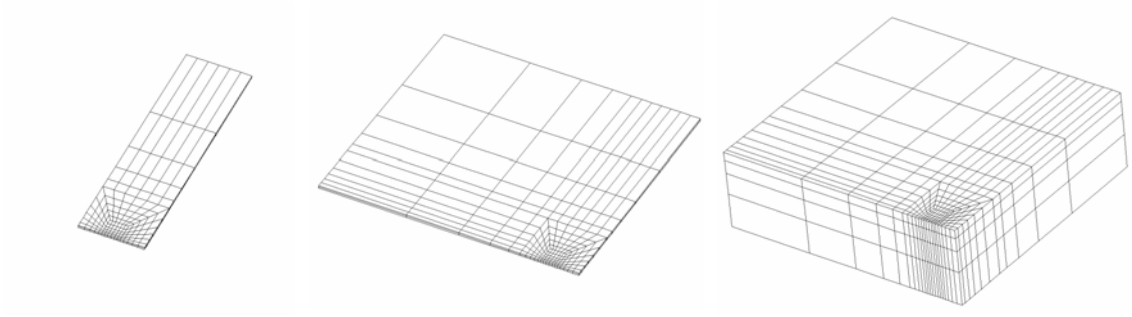

AC Layer 2 Base Layer 2 Subgrade Layer 2

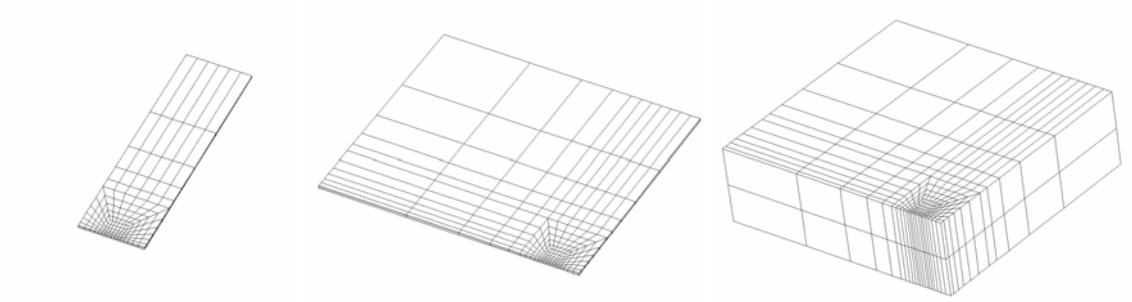

AC Layer 3 Base Layer 3 Subgrade Layer 3

Figure 3.1 Mesh of Unassembled Parts

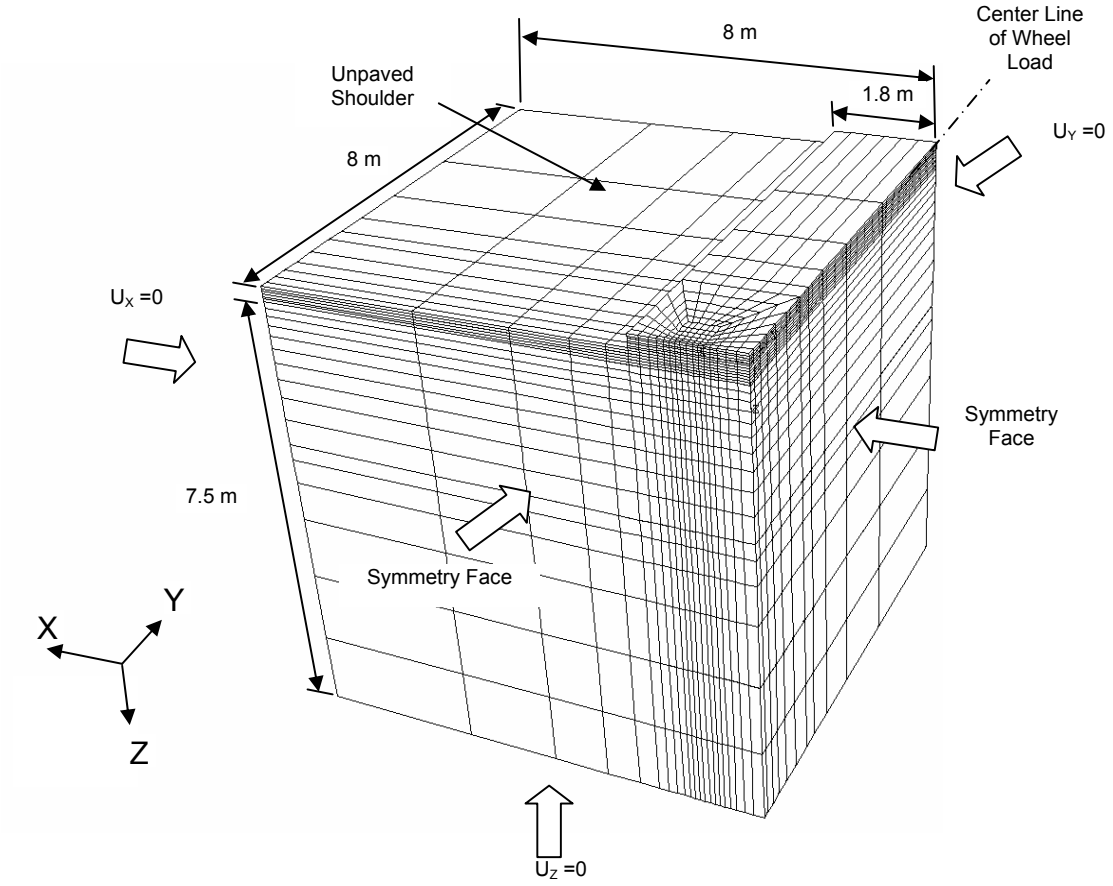

Figure 3.2 Mesh of an Assembled 3D Pavement Model and Boundary Conditions

According to Hjelmstad and Taciroglu (2000), as long as the Poisson's ratio is between -1 and 0.5, and the problem of zero volumetric and octahedral shear strains have been taken care of in the UMAT, the material stability is guaranteed. However, the 3D pavement models in this study consist 9 to 13 parts which are either tied or in contact with each other through some frictional contact. These interface constraints and interactions complicate the problem, slow down convergence, and sometimes even result in convergence problems. The convergence of the analysis also turned out to be dependent upon the shape of elements. Transitional elements in the vertical direction were attempted to reduce the large aspect ratio, but tended to produce convergence problem.

Three different element types were considered in the study, i.e. linear element, quadratic element, and quadratic element with reduced integration. Quadratic element with reduced integration is supposed to be the best for stress-displacement analysis to account for shear locking (Bathe, 1996).

3.4.4 Load

The load is applied in two steps, first a gravitational load is applied followed by wheel load.

3.4.4.1 GRAVITATIONAL LOAD

Although the magnitude of the gravitational load is small in comparison to the wheel load, the gravitational loading is necessary to import the initial geostatic stresses. Without the gravitational load, the elements at the top of the base layer

that are not close to the wheel load have zero stress, which can cause convergence problem.

3.4.4.2 WHEEL LOAD

The nonuniform contact pressure produced by a real tire can result in higher tensile strains at the bottom of the AC layer than when a uniform contact pressure is assumed, but for pavements with thick AC layer, the difference is not pronounced (Tielking and Roberts, 1987). The thickness of the AC layer considered in this analysis is above 200 mm, which is much higher than the maximum thickness considered in (Tielking and Roberts, 1987). Therefore, uniform tire contact pressure was used in this analysis.

The pavement system was subjected to a loading representative of a 80 kN (18 kips) single axle loading with a pair of dual wheels, the standard load known as equivalent single axle load (ESAL) recommended by AASHTO (1993). Different approximations of the shape of the tire contact areas are shown in Figure 3.3, in which (a) is the most realistic shape of the tire prints for the duals; (b) is double rectangular area which is typically used in 3D finite element analysis; (c) is double circular area which is used in layered system program; and (d) is single circular area used in two dimensional (2D) axisymmetric finite element analysis.

In this paper, the double rectangular area as shown in Figure 3.3 (b) was used in the 3DFE analyses, while the single circular area as shown in Figure 3.3 (d) was used for the 2D axisymmetric and relevant 3D finite element analyses. The

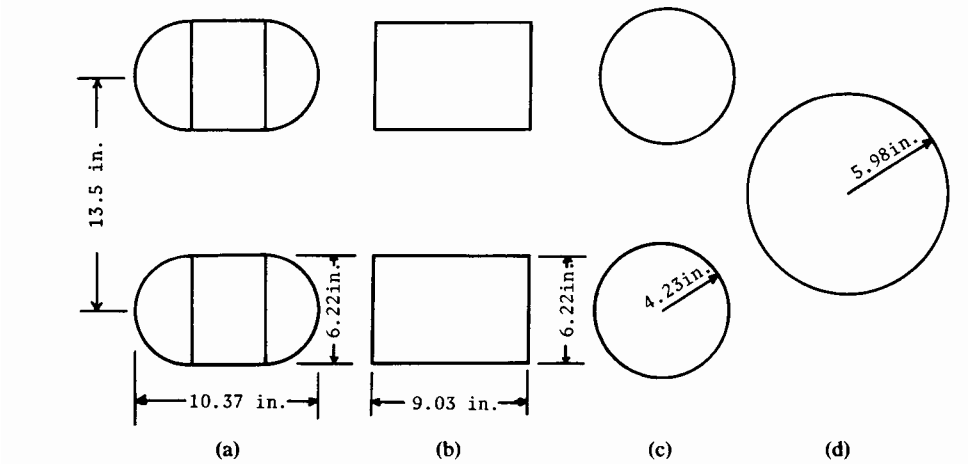

Figure 3.3 Typical Contact Areas for Single Axle Dual Wheel Loads (Huang, 1993) (1in. = 25.4 mm)

double rectangular contact area applied to the 3D mesh is shown in Figure 3.4.

3.4.5 Boundary Conditions

In this analysis, the pavement was assumed to be a one-lane pavement. Although this assumption is not very realistic, it is the worst case. Due to the symmetry of this problem, only a quarter of the model was analyzed. The Y-direction was taken as the longitudinal or traffic direction and the X-direction as the transverse direction (Figure 3.2). In the plan view, the geometry of AC layer is 1.8 m in width, which is approximately half of the single lane width without shoulder, and 8 m in length; the geometry of the base layer and the subgrade is 8 m by 8 m. Normal displacements at all four vertical surfaces and the bottom of the subgrade are constrained (Figure 3.2). The side of the AC layer (1.8 m from the center line of the wheel load) is free of any constraint, representing the condition where there is no shoulder.

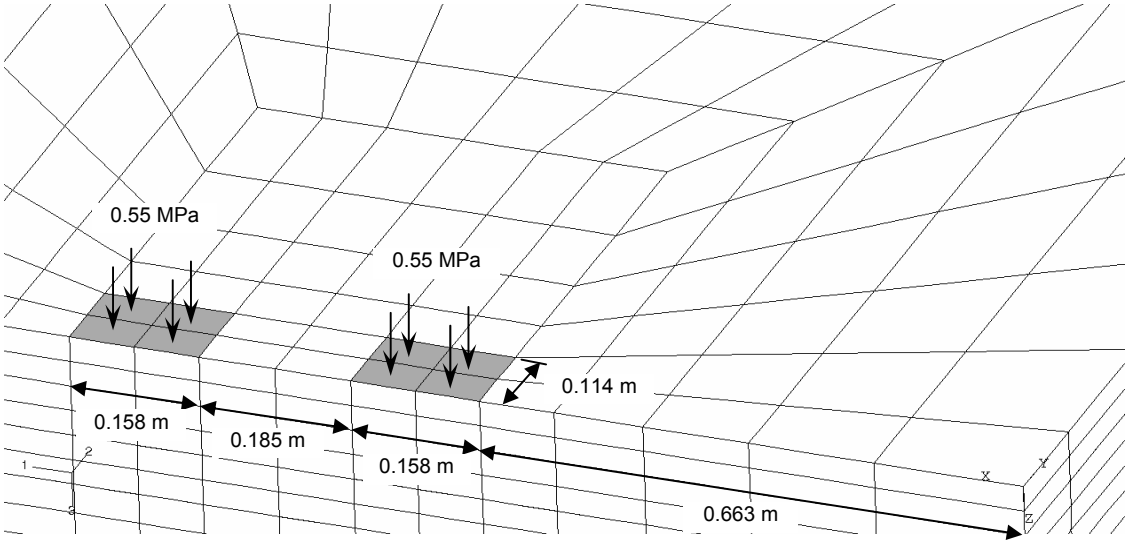

Figure 3.4 Layout of Tire Prints for a Dual Wheel Load

3.4.6 Interface Conditions

Completely bonded and completely unbonded interface conditions for the contacts between pavement layers are the two extreme conditions, which do not accurately model the real situation in the pavement. According to elastic layer theory, the stress and strain distributions are highly affected by the interface condition between asphalt layers (Uzan et al., 1978). A similar conclusion was drawn by Romanoschi and Metcalf (2001) via finite element analyses.

In 3D pavement analysis, the interface between the AC layer and the base layer is usually considered as completely bonded, which may result in underestimation of critical stresses and strains. In this research, all interfaces are assumed to be fully bonded (or tied) with the exception of the interface between the bottom of the AC layer and the top of the base layer. This interface condition was treated as either fully bonded (tied), frictionless or frictional contact with a friction of 1.0.

3.5 Results and Discussions

Models with different combinations of pavement layer thickness (Pavement A or B), AC/base interface condition (different friction coefficient), element size, and element type (linear or quadratic, with or without reduced integration) were analyzed. Not all the models resulted in successful convergence. A summary of the successfulness the analyses is listed as follows:

- When linear elements were used in the analysis, models with both contact and tied interface conditions converged successfully.
- When quadratic elements and tied interface conditions were used, the analysis of Pavement A converged successfully, but the analysis of the Pavement B failed to converge.
- When quadratic elements and contact interface condition were used, an unknown error occurred and the program terminated before the completion of the first iteration.

Layered elastic analysis or two dimensional axisymmetric models are the most common idealizations of pavement systems. Three dimensional finite element analysis is not commonly used, due to its complexity and the requirement for more computation time. However, the 2D axisymmetric analysis requires some significant assumptions, such as the shape of the contact area between the tire and pavement, and the lateral geometry of the pavement. These issues will be investigated below by comparison of results from 2D and 3D analysis. It should be noted that only one interface condition, the fully-bonded condition between the AC layer and the base layer, is considered in this comparison.

3.5.1 Contact Area

In 2D axisymmetric analysis, the dual wheel load is applied as over a single circular area (Huang, 1993). Analyses using layered system showed that using a single circular area (Figure 3.3 (d)) to represent the contact area rather than using two small circular areas (Figure 3.3 (c)) usually resulted in a more conservative design, except for very thin (25 mm thick) AC layers (Huang, 1993).

In this study, four different approximations to the actual dual wheel loading areas were considered: (1) a single circle representing dual wheels for 2D axisymmetric analysis (Figure 3.5(a)) investigated with both 2D and 3D models; (2) 3D analysis of a single circle representing the full dual wheel axle load considering the existence of the wheels at the other end of the axle (Figure 3.5(b)); (3) 3D analysis of two rectangles representing the full dual wheel axle load on a pavement without shoulder (Figure 3.5(c)); (4) 3D analysis of two rectangles representing the full dual wheel axle load on a pavement with shoulder extended to 8 m from the center line of the wheel path (Figure 3.5(d)). The results of this comparison are shown in Figure 3.6 for Pavement A and Figure 3.7 for Pavement B in terms of the strains at the bottom of AC layer in both longitudinal and transverse directions. The 2D axisymmetric analyses and the relevant 3D analyses with the circular load produce similar results. The stress field under the wheel load is not significantly affected by the stress field caused by the wheel load at the other end of the axle. The application of a circular load produced equal strains in the longitudinal and transverse directions, and these are not distinguished in the 2D axisymmetric analysis. However, there is large

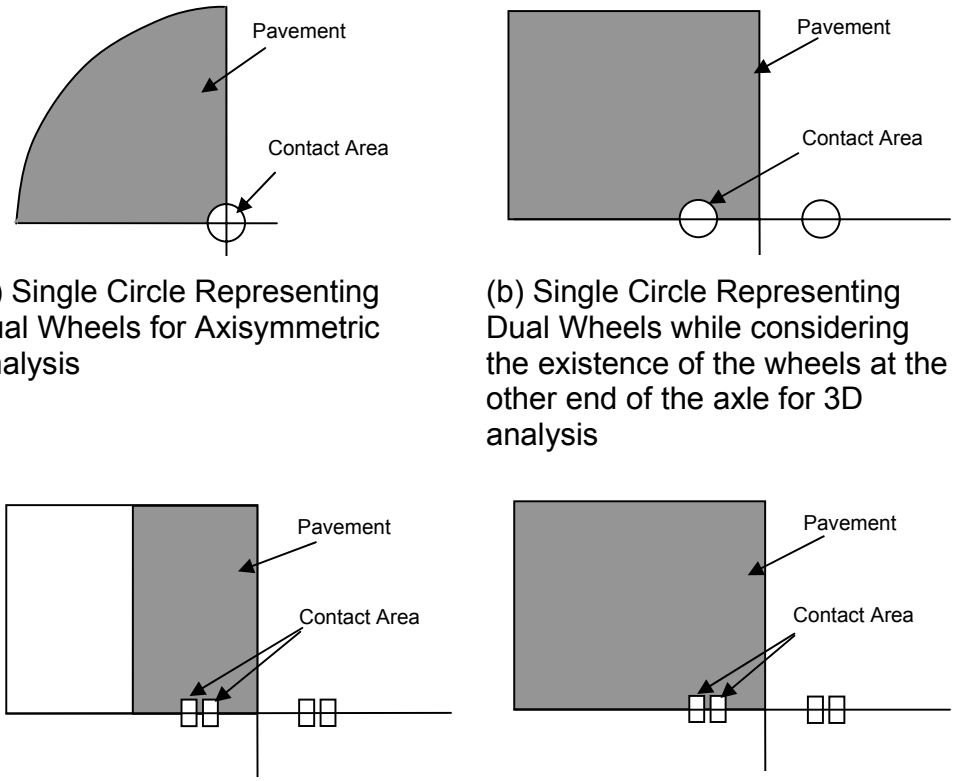

(a) Single Circle Representing Dual Wheels for Axisymmetric Analysis

(b) Single Circle Representing Dual Wheels while considering the existence of the wheels at the other end of the axle for 3D analysis

(c) Two Rectangles Representing Dual Wheels while considering the existence of the wheels at the other end of the axle on a pavement without shoulder

(d) Two Rectangles Representing Dual Wheels while considering the existence of the wheels at the other end of the axle on a pavement with shoulder extended to 8 m from the center line of the wheel path

Figure 3.5 Plan View of Different Idealization of Wheel Load Contact Area Model (Not to scale)

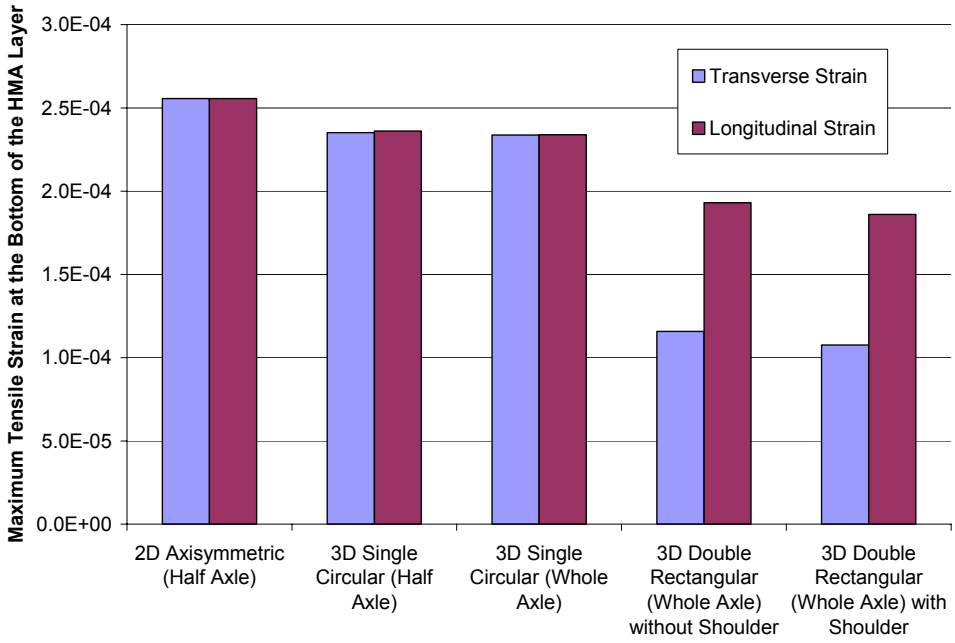

Figure 3.6 Comparison of Maximum Tensile Strain at the Bottom of the AC Layer for Pavement A with 2D and 3D Analyses

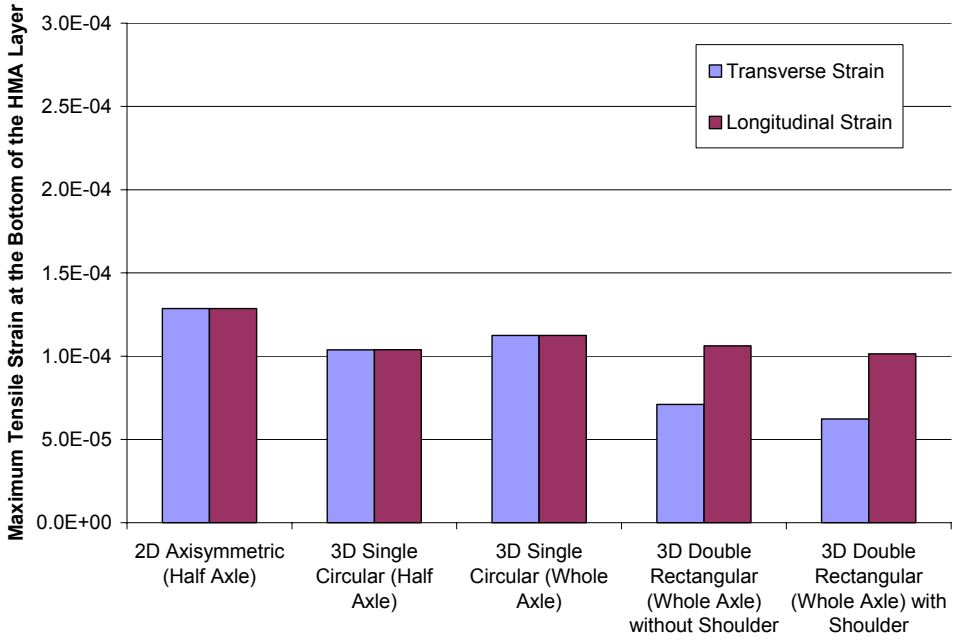

Figure 3.7 Comparison of Maximum Tensile Strain at the Bottom of the AC Layer for Pavement B with 2D and 3D Analyses

difference when the wheel load is applied over a double rectangular contact area, with significant higher tensile strain in the longitudinal direction than in the transverse direction. For Pavement A, the maximum tensile strain in the transverse direction for the double rectangular contact area is only about 40% of that of the single circular contact area. But the longitudinal strains are within 80% of the tensile strain obtained with the 2D axisymmetric model.

To investigate the effect of the shape of the contact area, a finite element model was set up purposefully for applying load at different locations on the pavement surface while keeping the total contact area constant. In this way, the differences of the shape of the contact area can be investigated using the models which are identical except for the location of the load. The pavement model for this comparison is similar to the thin pavement model shown in Figure 3.2. A plan view of the location of the contact area for three different cases is shown in Figure 3.8.

The meshes used in this comparison deviate slightly from the geometry of the typical approximations of the contact area for single axle duals as shown in Figure 3.3 (b). The possible loading area was divided into small squares with the size of 0.05m x 0.05 m. The contact area for single axle duals is approximated by 12 small squares as the shaded areas in Figure 3.8. It should be noted that single rectangular area Figure 3.8(b) is not a realistic contact area, but serves as a transition between the comparison of double rectangular area (Figure 3.8(a)) and the approximated single circular area (Figure 3.8(c)).

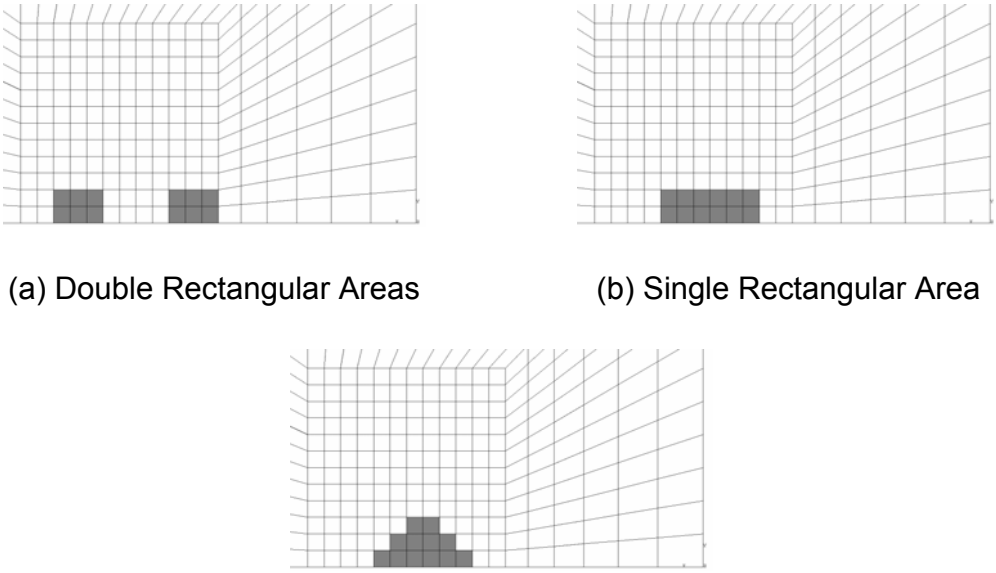

(a) Double Rectangular Areas (b) Single Rectangular Area

(c) Approximated Single Circular Area

Figure 3.8 Different Approximations of a Single Axle Dual Wheel Loading with the Same Contact Area

The maximum tensile strains at the bottom of the AC layer for the approximated single circular area are greater than those of the double rectangular model (Figure 3.9), which validates the results from the models with different shape of contact area and different mesh as shown in Figure 3.6 and Figure 3.7.

This comparison indicates that for the same pavement model, the shape of contact area of wheel load alone can significantly affect the tensile strains in the pavement analyses. The double rectangular area as a more realistic approximation of the shape of contact area yields much lower tensile strain than the single circular contact area which is commonly used in the 2D axisymmetric analysis in the transverse direction. Fortunately, in the longitudinal direction, the

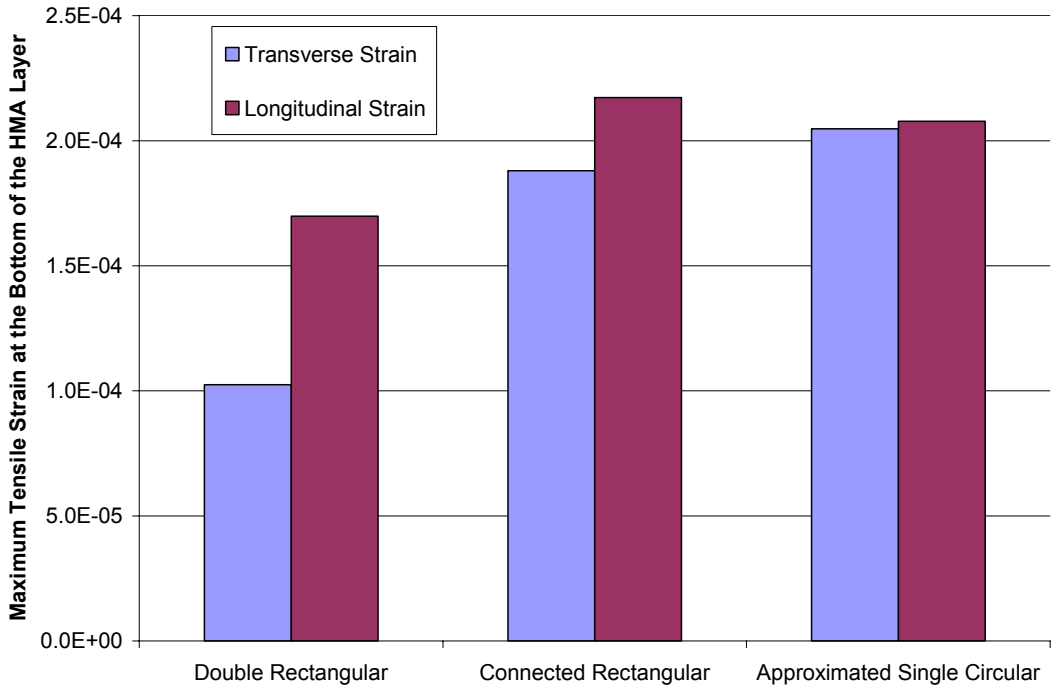

Figure 3.9 Comparison of Maximum Tensile Strain at the Bottom of the AC Layer for Three Pavement Models with Different Shape of Contact Area

direction of the maximum tensile strain, the difference between these two contact area models is not as pronounced as that in the transverse direction. However, in comparison to the double rectangular contact area, the approximated single circular contact area still overestimates the maximum longitudinal tensile strain by 22% in Figure 3.9. From a pavement design perspective, it is the maximum tensile strain that is important. This 22% of overestimation in the maximum tensile strain in the AC is sure to affect the expected pavement life.

3.5.2 Interface Condition

Three different interface conditions between the AC layer and the base layer were investigated:

- Smooth Interface – Friction Coefficient is 0;
- Frictional Interface – Friction Coefficient is 1, which corresponds to an internal friction angle of 45°, about the upper bound expected for most material in contact with the granular base;
- Tied Interface – Friction Coefficient is infinite, i.e., no slip is allowed along the interface.

The effect of interface condition for the thin pavement model is shown in Table 3.3. Similar results for the thick pavement model are shown in Table 3.4

Quadratic elements with reduced integration, which are often assumed to be the best element type for stress analysis, only produced convergent solution for the Pavement A. For the coarse mesh, interface conditions varying from smooth to tied can result in as much as 15% difference in maximum tensile strain at the bottom of AC layer. However, the maximum tensile strains change less than 2% when the interface condition changes from smooth to frictional. The frictional interface is perhaps the "best" or most realistic approximation, but similar results

Table 3.3 Tensile Strain at the Bottom of the AC Layer (Pavement A)

	Interface Condition	Transverse	Longitudinal
Fine Mesh	Smooth	1.55E-04	2.35E-04
	Tied	1.30E-04	1.96E-04
Coarse Mesh	Smooth	1.34E-04	2.20E-04
	Frictional	1.33E-04	2.18E-04
	Tied	1.16E-04	1.93E-04
	Tied (Quadratic Reduced Integration)	1.38E-04	2.01E-04

Table 3.4 Tensile Strain at the Bottom of the AC Layer (Pavement B)

	Interface Condition	Transverse	Longitudinal
Fine Mesh	Smooth	8.72E-05	1.28E-04
	Tied	7.19E-05	1.13E-04
Coarse Mesh	Smooth	8.33E-05	1.19E-04
	Frictional	8.19E-05	1.18E-04
	Tied	7.11E-05	1.06E-04

are obtained with smooth interface, which is easier to model. Therefore, it is reasonable to assume that the interface condition between AC layer and base layer to be frictionless. For the two extreme interface conditions, when models with fine meshes are used, the maximum tensile strains at the bottom of AC layer only differ for less than 16%, while the computation time increases from minutes to hours. It should be noted that the effect of interface conditions may differ for pavements with thinner AC layers.

3.5.3 Lateral Geometry of the Pavement

For 2D axisymmetric analysis, the AC layer is always assumed to be extended to a distance much greater than the width of a typical pavement. In this study, the results of two different models of lateral geometry were compared: (1) the AC layer extended 1.8 m from the centerline of the pavement as shown in Figure 3.2; (2) the AC layer extended 8.0 m to cover the entire surface of the base layer in the model. In both cases, the load was applied over the double rectangular area.

The difference in the maximum tensile strain in the longitudinal direction at the bottom of the AC layer between different lateral geometry of the pavement is small for all three different AC-Base interface conditions for both Pavement A

(Figure 3.10) and Pavement B (Figure 3.11). The difference is slightly more significant when the pavement is thick. However, the maximum difference in the maximum tensile strain at the bottom of the AC layer between two lateral geometry of the pavement is only 5%.

It should be noted that all the above conclusions about lateral geometry were drawn based on the comparison of the maximum tensile strain at the bottom of the AC layer. As indicated by Zaghloul and White (1993), pavement shoulder has significant effect on reducing surface deflection. The removal of pavement shoulder resulted in 8% increase in the surface deflection for Pavement A, and a drastic 52% increase for Pavement B. However, for simplicity, only the maximum tensile strain in the AC layer was considered.

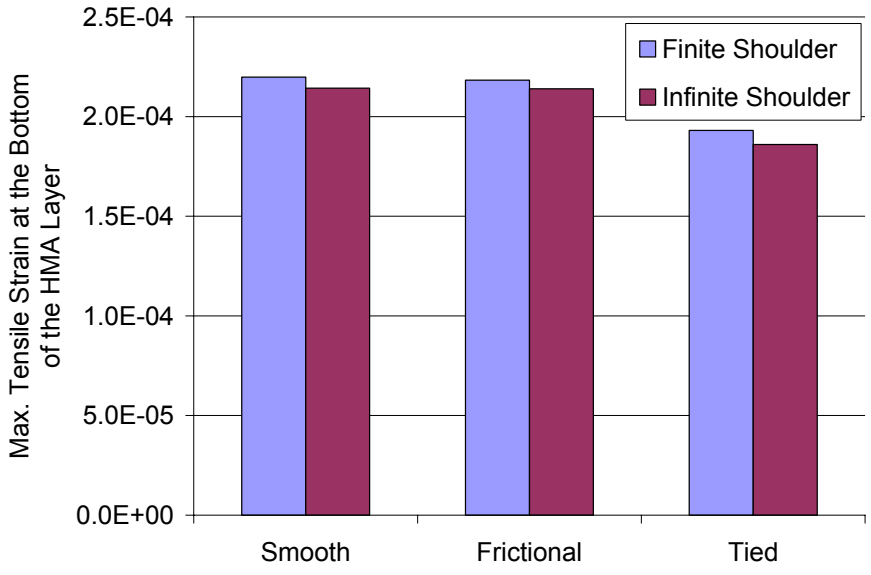

Figure 3.10 Maximum Tensile Strain in the Longitudinal Direction at the Bottom of the Thin Pavement for Different Lateral Pavement Geometry under Different AC-Base Interface Condition

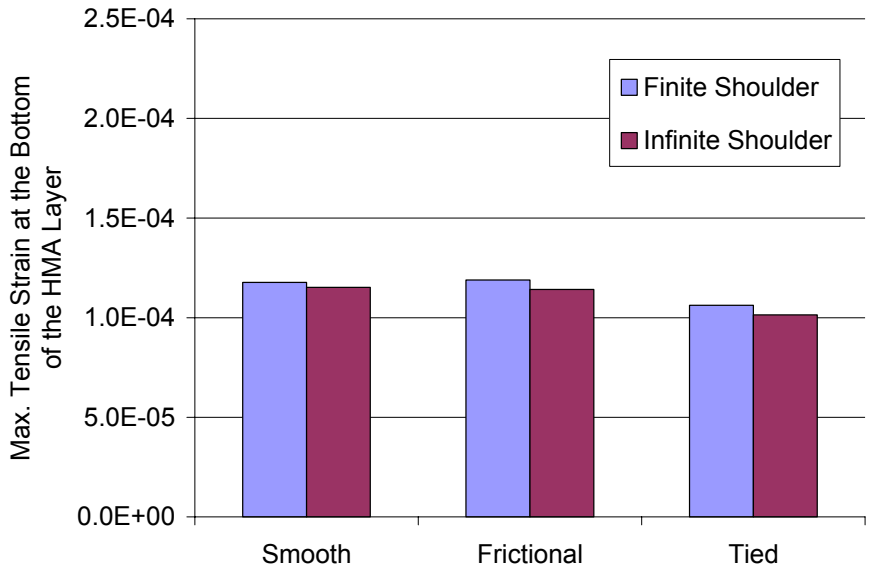

Figure 3.11 Maximum Tensile Strain in the Longitudinal Direction at the Bottom of the Thick Pavement for Different Lateral Pavement Geometry under Different AC-Base Interface Condition

3.6 Conclusions

A series of 3D finite element analyses on flexible pavements were performed using ABAQUS. This paper reviews some common assumptions employed in the analysis of flexible pavement systems. The main objective of this paper is to determine a proper model for further study. Different conditions, such as material model, element size, shape, boundary condition, interface conditions, and load, were considered in this study. Uzan's resilient modulus model was implemented into the analysis to account for the stress-dependent behavior of the both coarse-grained and fine-grained unbound materials.

In comparison to the 2D axisymmetric analysis, the application of the wheel load over dual wheels approximated by double rectangular areas in 3D analysis

produced more realistic loading condition and it lowered the computed maximum tensile strain at the bottom of the AC layer by about 20%. While frictional interface condition is the most realistic, the results obtained with smooth interface are within 5% of the frictional interface, and about 15% larger than what is obtained when the AC layer is assumed to be fully tied to the base layer. The extension of pavement shoulder to 8 m from the center line of the wheel path only causes 5% reduction in the maximum tensile strain at the bottom of the AC layer.

References

AASHTO (1993) *AASHTO Guide for the Design of Pavement Structures*. American Association of State Highway Officials, p. 403.

ABAQUS 6.2-1 (2001) Habbitt, Karlsson & Sorensen, Inc., Rhode Island.

Bathe, K. (1996) *Finite Element Procedures*. Prentice Hall, p1037.

Bensalem, A., A. J. Brown, M. E. Nunn, D. B. Merrill, and W. G. Lloyd. (2000) Finite Element Modelling of Fully Flelxible Pavements: Surface Cracking and Wheel Interaction. *In* Proceedings of *the Second International Symposium on 3D Finite Element for Pavement Analysis, Design, and Research. Charleston, West Virginia,* pp. 103-121.

Davids, W. (2001) 3D Finite Element Study on Load Trasffer at Doweled Joints in Flat and Curled Rigid Pavements. *International Journal of Geomechanics* Vol. 1, No. 3, pp. 309-324.

Hjelmstad, K. D. and E. Taciroglu (2000) Analysis and Implementation of Resilient Modulus Models for Granular Solids. *Journal of Engineering Mechanics* Vol. 126, No. 8, pp. 821-830.

Huang, Y. H. (1993) *Pavement Analysis and Design*. Prentice Hall, p 784.

Kim, J, K. D. Hjelmstad, and Q. H. Zuo. (1997) Three Dimensional Finite Element Study of Wheel Load Interaction. *In* Proceedings of *Aircraft/Pavement Technology In the Midst of Change. Seattle, Washington,* pp. 138-150.

Romanoschi, S. A. and J. B Metcalf (2001) Effects of Interface Condition and Horizontal Wheel Loads on the Life of Flexible Pavement Structures. In *Transportation Research Record* , TRB, National Research Council, Washington D.C., pp. 123-131.

Schwartz, C. W. (2000) Effect of Stress-Dependent Base Layer on the superposition of Flexible Pavement Solution. *In* Proceedings of *Proceedings of the Second International Symposium on 3D Finite Element for Pavement Analysis, Design, and Research. Charleston, West Virginia,* pp. 329-354.

Tielking, J. T. and F. L. Roberts (1987) Tire Contact Pressure and Its Effect on Pavement Strain. *Journal of Transportation Engineering* Vol. 113, No. 1, pp. 56-71.

Uzan, J. (1985) Characterization of Granular Material. In *Transportation Research Record 1022*, TRB, National Research Council, Washington D. C., pp. 52-59.

Uzan, J., M Livneh, and Y. Eshed (1978) Investigation of Adhesion Properties Between Asphaltic-Concrete Layers. *Asphalt Paving Technology* Vol. 47, pp. 495-521.

William, G. W. and S. N. Shoukry (2001) 3D Finite Element Analysis of Temperature-Induced Stresses in Dowel Jointed Concrete Pavements. *International Journal of Geomechanics* Vol. 1, No. 3, 291-308.

Zaghloul, S. and T. White (1993) Use of a Three-Dimensional, Dynamic Finite Element Program for Analysis of Flexible Pavement. In *Transportation Research Record 1388*, TRB, National Research Council, Washington D.C., pp. 60-69.

Zaghloul, S. M., T. D. White, V. P. Drnevich, and B. Coree (1994) Dynamic Analysis of FWD Loading and Pavement Response Using a Three-Dimensional Dynamic Finite Element Program. *Nondestructive Testing of Pavements and Backcalculation of Moduli (Second Volume), ASTM STP 1198*, Von Quintas, H. L., Bush III, A J., and Baladi, G. Y, Eds., American Society for Testing and Materials, Philadelphia, pp. 125-138.

Part IV Impacts of Environmental Factors on Flexible Pavements II: Effects of Temperature Averaging and Water Content Variations on Estimated Pavement Life

4.1 Abstract

Mechanistic-empirical pavement design methods for flexible pavements are based on the assumption that the pavement life is inversely proportional to the magnitude of the traffic-induced pavement strains. These strains vary with the stiffness of the asphalt layer and underlying base layer and subgrade. The stiffness of the asphalt layer varies with temperature and the stiffness of the unbound base layer and subgrade varies with water content. Because these relationships are nonlinear, the additional pavement life consumed at higher-than-average temperatures or water contents is not offset by savings at lower-than-average temperatures or water contents. Since the variation in temperature and water content can take place at different times, the effects can not simply be considered separately and the results superimposed. Hence, the combined effects of temperature and water content variations should be accounted for in the estimation of pavement life, particularly in moderate to warm climates where high temperature and high water content periods may coincide.

Using environmental data from instrumented pavement sites in Tennessee, the effects of asphalt concrete (AC) temperature and base and subgrade water content variation were evaluated for three typical pavement profiles using the finite element method. While often neglected, the effect of AC temperature profile turned out to be important to the computed critical strain in AC layer. The results of the parametric study show that the temperature averaging period and the timing and duration of wet subgrade conditions are critical to estimated pavement life.

4.2 Introduction

Temperature of the asphalt concrete (AC) and water content in the base layer and the subgrade are the most critical factors that influence flexible pavement performance. A change in the pavement temperature directly affects the stiffness of the asphalt-bound layers, which alters the stress state throughout the pavement. This change in stress state can, in turn, affect the stiffness of the underlying unbound layers since they usually exhibit stress dependence. The structural capacity of the entire pavement system is thus affected by changes in pavement temperature. Likewise, moisture induced change in the base and subgrade may cause increased strains in the AC layer.

Mechanistic-empirical pavement design methods for flexible pavements typically assume two competing failure mechanisms related to the design of the pavement cross-section: fatigue of the bound pavement layers and accumulated permanent deformations in the subgrade. Based on observations that the number of load repetitions needed to fail an asphalt concrete beam in flexure is inversely proportional to the tensile strains at the bottom of the beam, the expected life of a pavement with respect to fatigue cracking should be inversely proportional to the traffic-induced tensile strains at the bottom of the asphalt-bound pavement layers. Based on observations that cyclically loaded soil specimens accumulate plastic (non-recoverable) strains with each loading cycle, the expected life of a pavement with respect to subgrade accumulated permanent deformations should be inversely proportional to the traffic-induced compressive strains at the top of the subgrade.

The traffic-induced strains in the pavement and subgrade are substantially affected by the stiffness of the asphalt-bound layers, which affects the stress distribution throughout the pavement. The stiffness of the asphalt-bound layers is, in turn, a nonlinear function of the asphalt temperature. Because of this highly nonlinear temperature dependence, the additional pavement life consumed at higher-than-average temperatures is not offset by savings at lower-than-average temperatures. As a result, whenever average pavement temperatures are used to determine the asphalt stiffness, pavement life is overestimated.

The degree to which pavement life is overestimated depends on the extent to which the high and low temperatures are “smoothed” in the averaging process. Figure 4.1 shows histograms of hourly, daily, and monthly average mid-depth pavement temperatures based on the temperature data collected at an instrumented pavement site in Blount County, Tennessee in 2000 and 2001. Note that the breadth of the histograms changes as the averaging interval changes. This data set contains hourly average temperatures above 50 ºC while the daily average temperatures barely exceed 45 ºC and the monthly average temperatures never exceed 40 ºC. Zuo et al. (2002) showed that a disproportionate amount of damage is done at these high temperatures, so differences in pavement life can be expected depending on the distribution of temperature used in the pavement life calculations. The temperature in the AC layer varies with depth; therefore, a better way to study the effect of temperature averaging interval on estimated pavement life is to account for temperature profile, rather than only the mid-depth temperature.

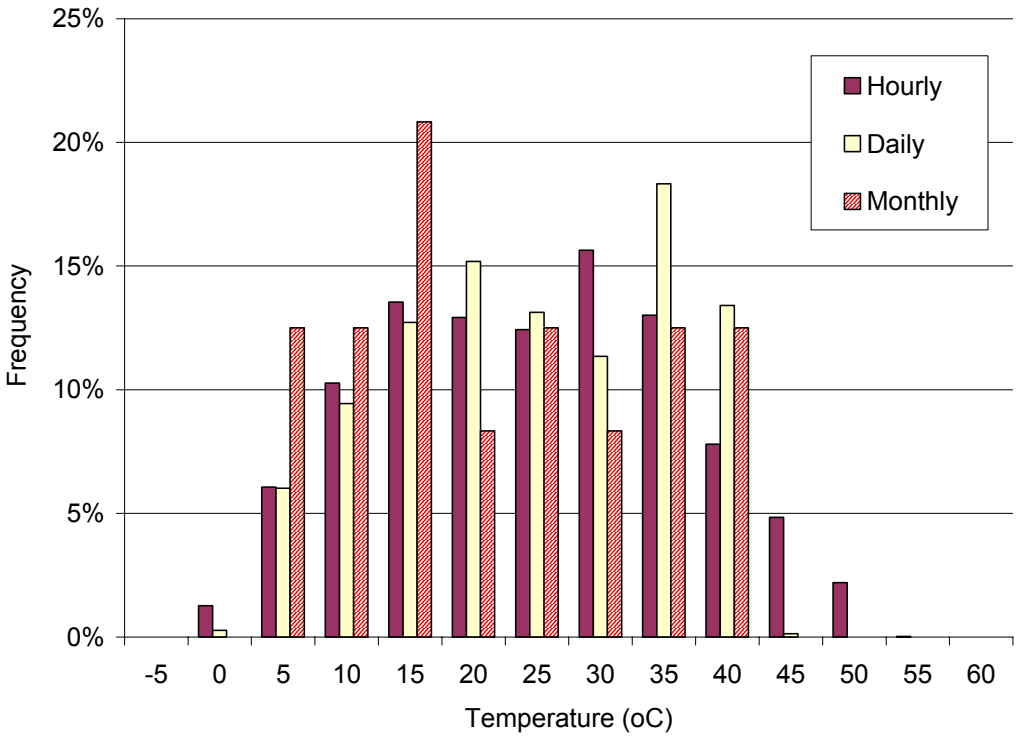

Figure 4.1 Mid-Depth Temperature Distribution for Different Averaging Intervals (Blount County)

The resilient modulus of the unbound base and subgrade soil is affected by both water content and stress state. Researchers have reported significant decreases in resilient modulus with increasing water content for both laboratory and field conditions, but the behavior can be different for different material (Cumberledge et al., 1974; Rada and Witczak, 1981; Carmichael III and Stuart, 1985; Raad et al., 1992; Jin et al., 1994; Drumm et al., 1997; Tian et al., 1998). Matter and Farouki (1994) indicated that the moisture content and temperature effects might reach their peak impacts at different times or seasons and the effects of one factor may be offset by the effects of the other. Regardless, temperature and water content are inseparable in pavement life estimation. It is

impossible to consider the reduction in pavement life as a result of temperature variation or water content variation in two independent steps.

The objective of this study is to quantify the changes in predicted pavement life that accrue from differences in temperature distribution and water content variation.

4.3 Methodology

A diagram is given in Figure 4.2 to illustrate the methodology used to predict pavement life when accounting for the impact of environmental factors. Existing models from the literature were used to describe the temperature-dependent stiffness of the asphalt-bound layers (AASHTO, 1993), and the stress-dependent stiffness of the base (Rada and Witczak, 1981) and the subgrade soils (Uzan et al., 1992). The traffic-induced strains in the pavement were calculated using ABAQUS 6.2-1 (2001), a general purpose finite element software package. A damage factor for each load repetition under different environmental conditions was calculated based on transfer functions (Asphalt Institute, 1982). The damage factors and the probabilities of occurrence for the different environmental conditions were combined using Miner's hypothesis to obtain the strain-dependent life expectancy of the pavement.

4.3.1 Finite Element Analyses

4.3.1.1 Finite Element Model

A parametric study was performed on three idealized pavement systems termed Pavement 1, Pavement 2 and Pavement 2 (Table 4.1), where Pavement 1

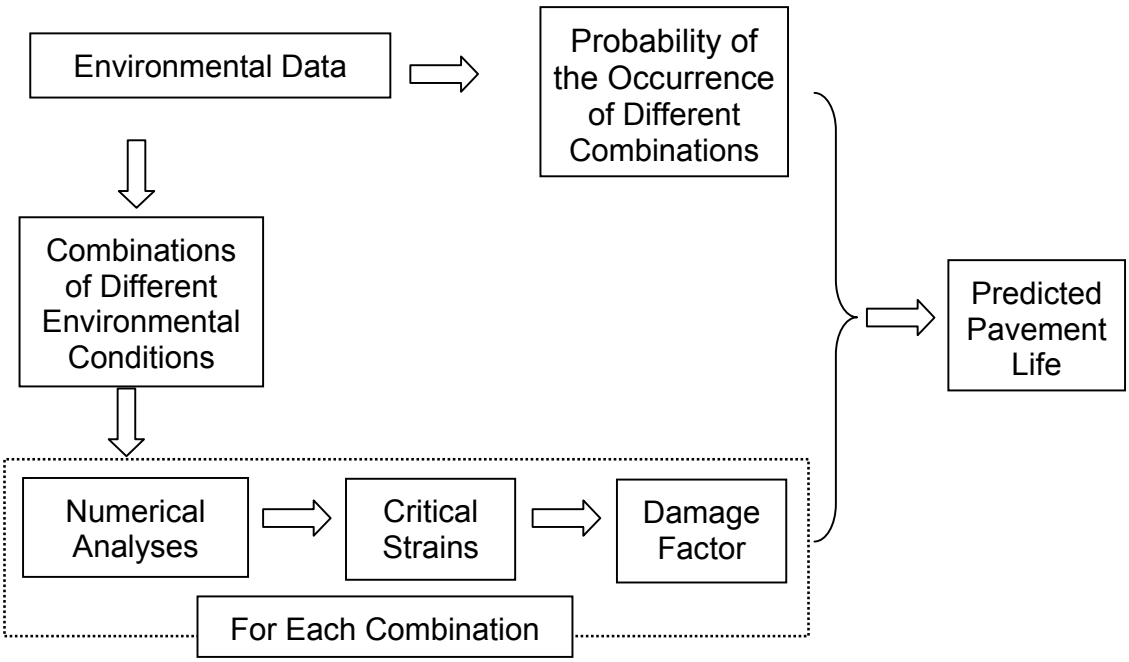

Figure 4.2 Schematic of the Calculation of Pavement life

Table 4.1 Pavement Systems Modeled in the Parametric Study

Idealized Pavement System	AC Layer		Base Layer	
	Thickness (mm)	Number of Sublayers in FE Model	Thickness (mm)	Number of Sublayers in FE Model
Pavement 1	200	4	150	3
Pavement 2	200	4	250	5
Pavement 3	300	6	250	5

consists of a moderate AC layer and a moderate base layer, Pavement 2 consists of a moderate AC layer and a thick base layer, and Pavement 3 consists of a thick AC layer and a thick base layer. All three pavements were assumed to be supported by an unbound granular base layer and a fine-grained subgrade. For the different pavement systems, the AC layer was divided into 4 or 6 sublayers and the base layer was divided into 3 or 5 sublayers. Although the asphalt pavements usually consist of several layers with different mix designs, for simplicity the entire AC pavement was assumed to have the same material properties. The mesh for each sublayer was identical. A typical mesh along with the applied boundary conditions is shown in Figure 4.3. Pavements with a single lane (3.6 m in width) were modeled to study the worst case condition. Due to the symmetry of pavement geometry and loading condition, only a quarter of the pavement was modeled. The half-width of the pavement is 1.8 m, while the base layer and the subgrade extend to 8m from the center line. It was assumed that there is no shoulder. A rigid boundary was assumed to be at 7.5 m beneath the top of the subgrade. An 80-kN (18-kips) single-axle load, the standard axle load recommended by AASHTO (1993), was assumed to be uniformly distributed over the equivalent rectangular areas as shown in Figure 4.4.

4.3.1.2 AC Modulus

For generality, the temperature dependence of the asphalt concrete was described as (AASHTO 1993):

$$\text{Log}(E_{AC}) = 6.451235 - 0.000164671T^{1.92544} \qquad (4\text{-}1)$$

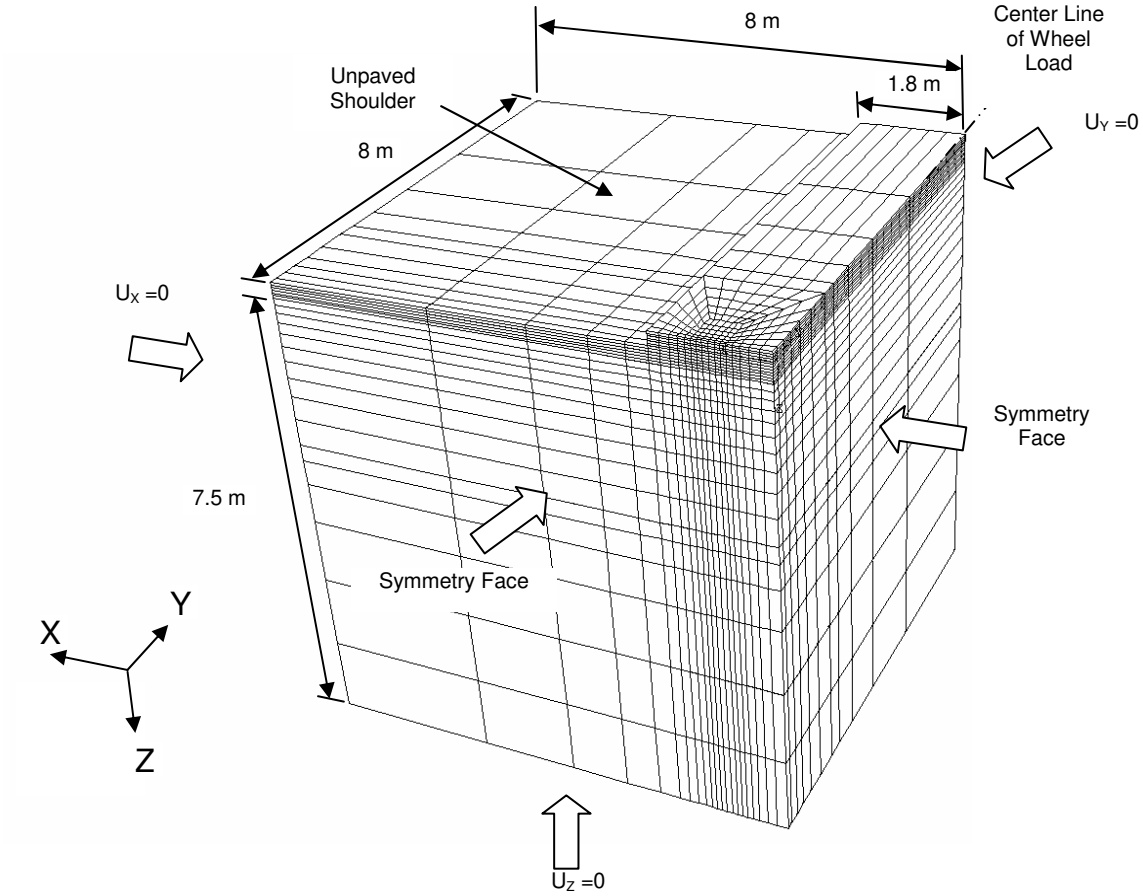

Figure 4.3 Typical Mesh and Boundary Conditions for 3D Pavement Models

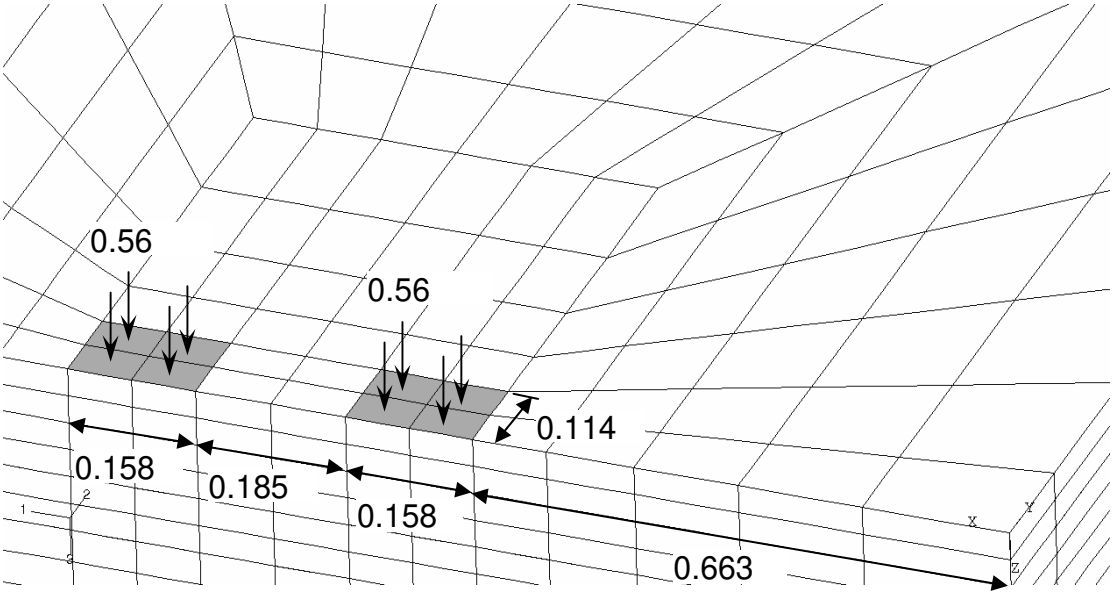

Figure 4.4 Layout of Tire Prints of a Single Axle Dual-Wheel Load

where E_{AC} = Dynamic modulus of asphalt concrete, psi;

T = Asphalt concrete temperature, ºF.

Alternatively, a site specific model (Marshall et al., 2001) could have been used.

4.3.1.3 Base Modulus

The variation in resilient modulus of the base was assumed to follow that of CR-6-Crushed Stone (Rada and Witczak, 1981). The data is from resilient modulus tests on a crushed stone with a percentage of fines (passing 200 sieve) less than 10 percent, which is similar to the crushed limestone used in Tennessee. Rada and Witczak (1981) tested the material at two different degrees of saturation (60% and 85%). Terms 'Nominal' and 'Wet' will be used to refer to these two conditions for the base material (Figure 4.5). The resilient modulus was represented by the K-θ model.

$$M_R = K\theta^n \qquad (4\text{-}2)$$

where θ = Bulk stress = Sum of principal stresses = $\sigma_1 + \sigma_2 + \sigma_3$,

K, n = Model parameters, which were assumed to vary with water content or degree of saturation, Sr, as shown in Table 4.2.

It was assumed for all three pavement models that only the modulus of the bottom 50 mm of base layer was subjected to water content variation, since only the bottom of the base layer exhibited significant water content variation at the instrumented sites in Tennessee as shown in Part I.

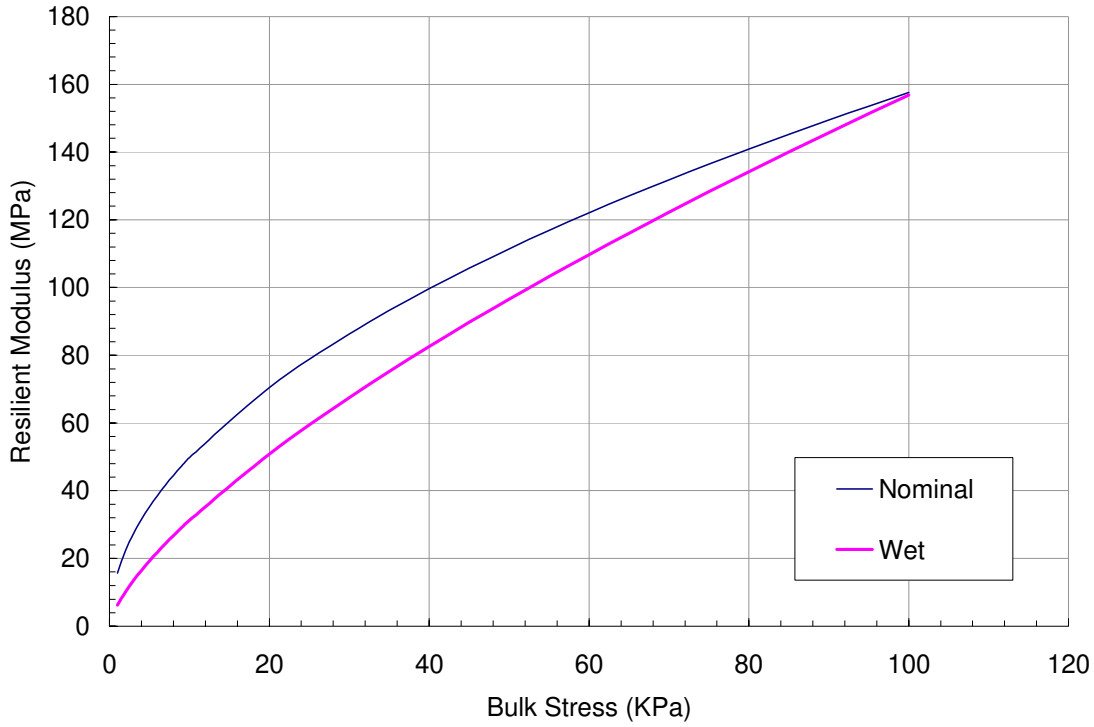

Figure 4.5 Resilient Modulus at Different Degree of Saturation (Rada and Witczak, 1981)

Table 4.2 Resilient Modulus Parameters for the Base Material (Rada and Witczak, 1981)

		Nominal (Sr=60%)	Wet (Sr=85%)
K	(psi)	6000	3500
	(Pa)	498200	49600
N		0.5	0.7

4.3.1.4 Subgrade Modulus

The resilient modulus of the fine-grained clay subgrade was characterized using Uzan (1992) model (Equation 4-3).

$$M_R = K\theta^n \tau_{oct}^{\ m} \qquad (4\text{-}3)$$

where M_R = resilient modulus

θ = Bulk stress = Sum of principal stresses = $\sigma_1 + \sigma_2 + \sigma_3$,

τ_{oct} = Octahedral shear stress = $\sqrt{\frac{1}{3}\left[(\sigma_1 - \sigma_2)^2 + (\sigma_2 - \sigma_3)^2 + (\sigma_3 - \sigma_1)^2\right]}$

K, n, m= Model parameters.

The subgrade was assumed to be fine-grained and the variation in modulus with degree of saturation was assumed to follow that for the AASHTO A-7-6(15) subgrade reported by Drumm et al., 1997). The model parameters used for the Nominal (Sr = 87%) and Wet (Sr = 92%) conditions are shown in Table 4.3.

Uzan's (1992) resilient modulus model was implemented into ABAQUS via user subroutine. Modification was made to adapt the implementation proposed by Hjelmstad and Taciroglu (2000) to account for both granular and fine materials in this analysis. Details of this implementation were described in Part III.

4.3.1.5 Total Number of Analyses

A summary of number of analyses is shown in Table 4.4. In total, 564 3-D nonlinear pavement analyses were performed using ABAQUS 6.2-1 (2001).

4.3.2 Parametric Study of Temperature and Water Content Variation

4.3.2.1 AC Temperature

In a previous parametric study in which only the mid-depth AC temperature was considered, temperature was shown to be a very important factor with respect to predicted pavement life (Zuo et al., 2002). In this study, the AC temperature profile or gradient was varied rather than just the mid-depth temperature to better simulate the actual pavement conditions.

Two years of hourly averaged AC temperature data collected at the Blount County, Tennessee site (Rainwater et al., 1999) were used in the parametric study. At the instrumented site, three thermistors were installed at different depths in the AC layer. The maximum and minimum temperature measured over this two-year period is shown in Table 4.5. In general, the AC temperature profiles defined by these three thermistors were quite linear. The two most

Table 4.3 Resilient Modulus Parameters for the Subgrade Soil

	Nominal (Sr=87.4%)	Wet (Sr=92.3%)
K (Pa)	1.58e+08	4.49E+08
N	0.26	0.24
M	-0.31	-0.50

Table 4.4 Number of Analyses in the Parametric Study

Number of Pavement Systems	3
Number of AC Temperature Profiles	47
Number of Base Types	2
Number of Subgrade Types	2
Total number of Analyses	564

Table 4.5 Maximum and Minimum Values of Temperature Data for 0.215 m Thick AC Layer (Blount County Site)

	Max. (^{o}C)	Min. (^{o}C)
Top of AC	55.94	-6.407
Mid-Depth of AC	50.96	-4.678
Bottom of AC	47.82	-2.276

nonlinear temperature profiles with assumed linear temperature profiles are shown in Figure 4.6, along with the temperature variation observed at each thermistor. Even for these two extreme temperature profiles, the differences for the mid-depth temperature between 3-point profile and the linear profile are -2.36 to 3.17 ^{o}C. Therefore, a linear temperature profile, which was determined by the top and bottom temperature, was assumed for the AC layer in the parametric study. This assumption simplified the temperature profiles from a 3D data set (top-mid-bottom) to a 2D data set (top-bottom), which greatly reduced the number of analyses without sacrificing much accuracy.

The number of hours for various temperature profiles over this two-year period is presented in Table 4.6. The 14 by 11 matrix in Table 4.6 is banded with 57 non-zero elements clustered along the diagonal, which indicates the high collinearity between the top and bottom temperatures of the AC layer. The same data are presented in Figure 4.7 in terms of a contour plot of the frequency. It should be noted that there are two high peaks in the contour plot, which is consistent with the bimodal distribution of the average mid-depth temperature (Figure 4.1).

The magnitude of the critical strains in the pavement decreases with decreasing AC temperature; the rate of decrease is small at low temperature;

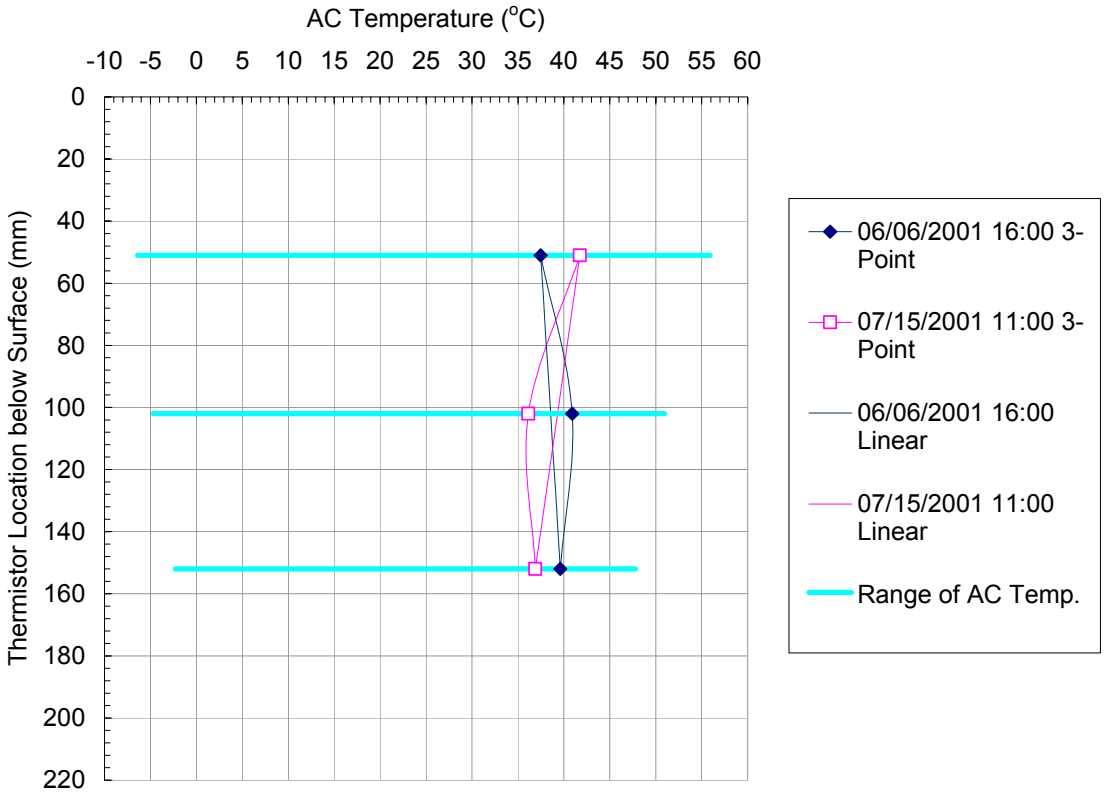

Figure 4.6 Range of Measured AC Temperature and the Temperature Profiles with Maximum Deviation from Assumed Linear Profiles

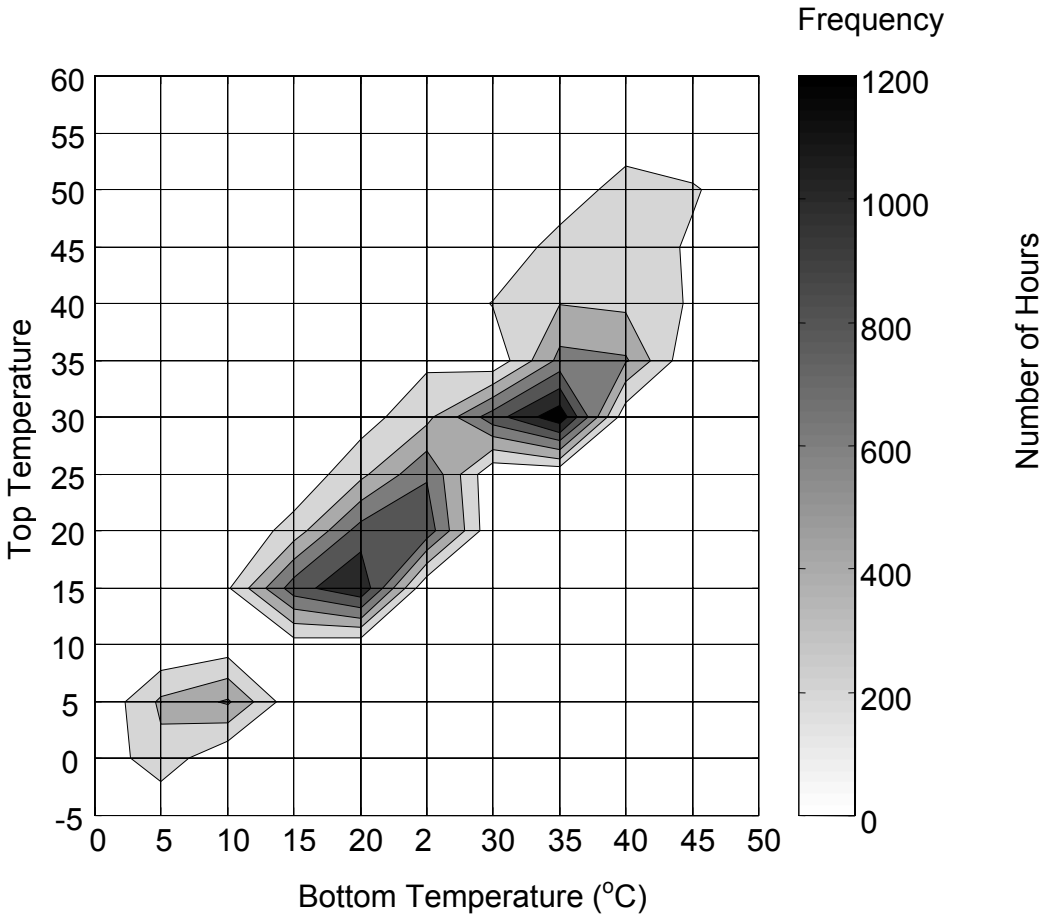

Figure 4.7 Contour of Number of Hours for Different AC Temperature Profiles in a Two-Year Period

Table 4.6 Number of Hours for Various Pavement Temperature Profiles

Temperature of AC Top (°C)	Temperature of AC Bottom (°C)										
	0	5	10	15	20	25	30	35	40	45	50
60										7	2
55									45	202	61
50								36	315	223	45
45							15	297	341	167	10
40						17	211	395	356	176	
35					7	163	404	663	623	13	
30					114	342	913	1349	45		
25				46	344	781	1008	29			
20			19	285	898	911	17				
15		4	171	911	1182	16					
10		70	750	970	66						
5	5	439	626	48							
0	36	341	7								
-5	7										

and the effect of temperature is very small when the AC temperature is lower than about 10 °C (Zuo et al., 2002). Therefore, the number of temperature profiles can be further reduced by eliminating the low temperature profiles, while assuming that the temperature profiles with temperature lower than 10 °C have the same effect as the one with a uniform temperature of 10 °C over the entire AC layer. Table 4.7 shows the temperature profiles above 10 °C, and depicts the temperature profile scheme numbering used in the FE analyses. In this way the number of temperature profiles considered in the parametric study is reduced from 57 (Table 4.6) to 47 (Table 4.7).

In each finite element analysis, the AC layer was divided into 4 or 6 sublayers 50-mm-thick (Table 4.1). Linear interpolation was used to obtain the temperature for the intermediate layers from temperatures at the top and the bottom of the AC layer. The modulus for each AC sublayers was calculated using Equation (4-1).

Table 4.7 Numbering scheme for Pavement Temperature Profiles

		Temperature of AC Bottom (°C)										
		0	5	10	15	20	25	30	35	40	45	50
Temperature of AC Top (°C)	60										46	47
	55									43	44	45
	50								39	40	41	42
	45							34	35	36	37	38
	40						29	30	31	32	33	
	35					23	24	25	26	27	28	
	30					18	19	20	21	22		
	25				13	14	15	16	17			
	20			8	9	10	11	12				
	15			4	5	6	7					
	10			1	2	3						
	5											
	0											
	-5											

4.3.2.2 Idealized Water Content Variation

The water content in the base layer and subgrade was assumed to be either the nominal water content or an elevated or wet condition, with the wet conditions in the base layer and subgrade not necessary coinciding. The timing of the different water content conditions was based on the data collected at the instrumented Blount County site. This site had the most complete data among all four instrumented sites, but, the TDR probes installed in the base layer only survived for about 500 days. The measured and idealized water content variations in the base and subgrade at the Blount County site are shown in Figure 4.8. Based on the field observations, the idealized water content condition at the bottom of the base layer was assumed to be nominal from August to November and wet for the remaining eight months. The wet period at the bottom of the base layer at the Sumner County site followed a similar pattern as the idealized Blount County variation, but with a 50 day lag period (Figure 4.9).

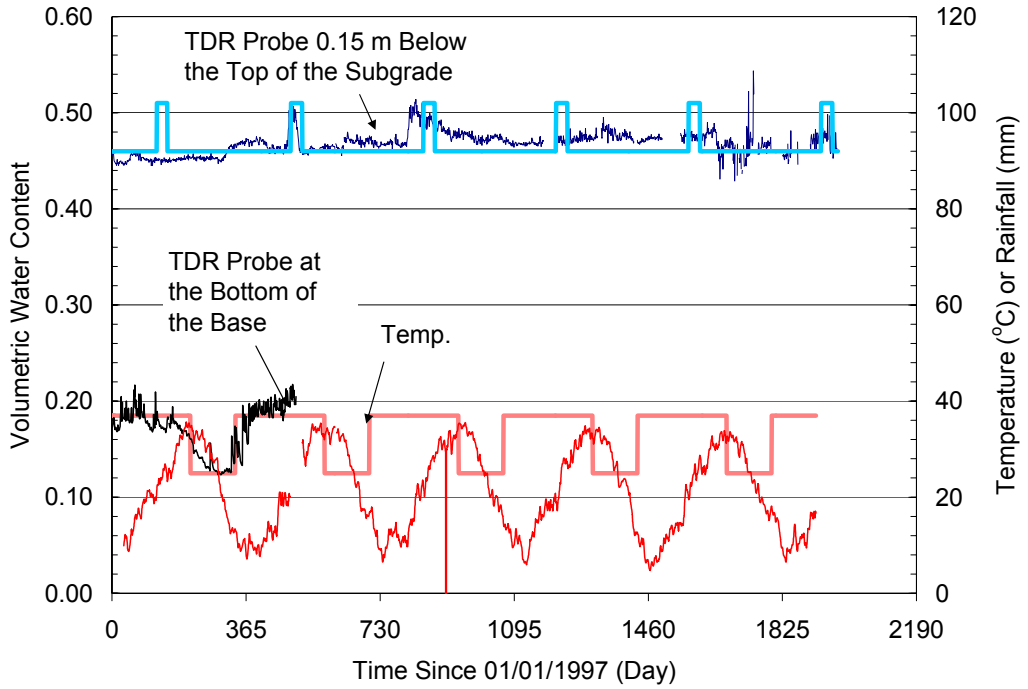

Figure 4.8 Measured and Idealized Water Content Variations at the Blount County Site

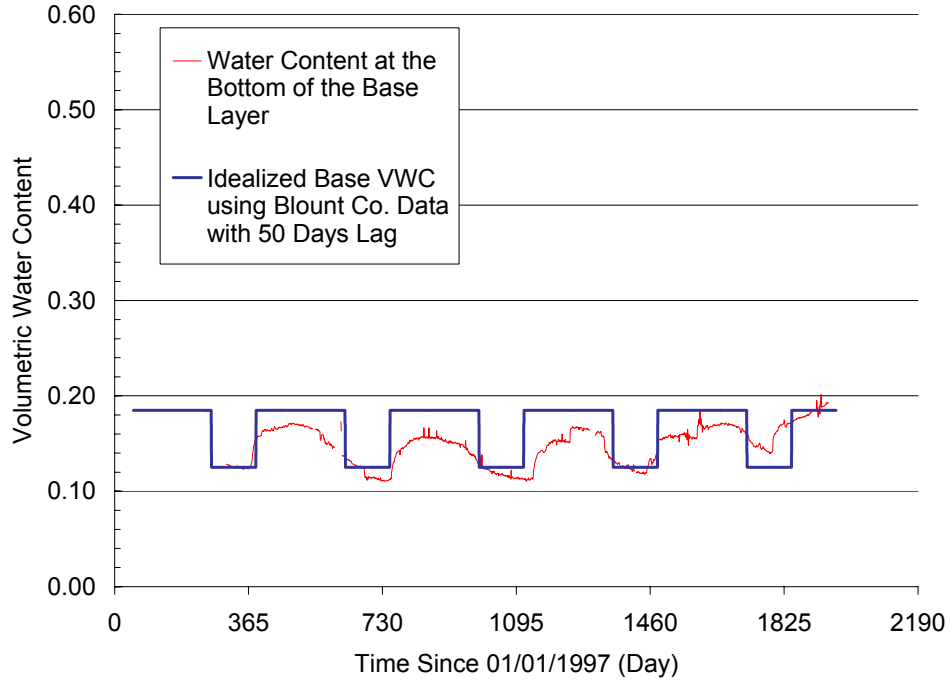

Figure 4.9 Idealized Base Course Water Content Variation Shifted in Time to Follow Sumner County Data

Also shown in Figure 4.8 is the measured water content at the top of the subgrade, which is nearly constant for the first 500 days, with the exception of a brief period of time in the spring of the second and third years. Therefore, May was assumed to be the wet condition for the subgrade and the remaining 11 months are assumed to have the nominal condition as shown in Figure 4.8. It can be noticed from Figure 4.8 that in the third year (about Day 700), the water content in the subgrade did not drop as rapidly as in the second year. However, the period of maximum water content is still about a month. The wet condition was not recorded in the fourth and the fifth years. It is possible that it occurred during periods when the instrumentation was out of service. Also shown in Figure 4.8 is the variation of subgrade temperature.

4.3.2.3 Transfer Functions

Two transfer functions were used to relate the calculated strains from the finite element analyses to pavement performance: an AC layer fatigue model and a subgrade accumulated permanent deformations model. Rutting due to the permanent deformation in the AC layer and the base layer was not considered in this study for the sake of simplicity.

The fatigue model used in this study is the one incorporated in the 9th edition of The Asphalt Institute's Thickness Design Manual (Asphalt Institute, 1982). Originally proposed by Hwang and Witczak (1979), the model equates failure to 45 percent fatigue cracking in the wheel paths and is given by

$$N_{f1} = f_0\left(10^m\right)\left(f_1\varepsilon_t^{-f_2}E^{-f_3}\right) \qquad (4\text{-}4)$$

with $m = f_4\left(\frac{V_b}{V_v + V_b} - f_5\right)$ (4-5)

where N_{f1} = Number of repetitions to failure;

f_0, f_1, f_2, f_3, f_4, and f_5 = Fitting constants;

ε_t = Tensile strain;

E = Elastic modulus of asphalt mix, psi;

V_b = Volumetric asphalt cement content of asphalt mix;

V_v = Volumetric air void content of HMA mix.

Equation (4-4) should be viewed as consisting of three distinct components. The constant f_0 is a shift factor that relates laboratory fatigue test results to field performance. The 10^m term is a mix adjustment factor that accounts for differences in fatigue behavior arising from differences in mix volumetrics, and the remaining terms are the laboratory fatigue criterion. Hwang and Witczak (1979) recommended using f_0 = 18.4, f_1 = 0.004325, f_2 = 3.291, f_3 = 0.854, f_4 = 4.84, and f_5 = 0.69, which are the values used in this study. V_b and V_v were assumed to be 13 and 5, respectively. The accumulated permanent deformations model used in this study is also the one incorporated in the 9th edition of The Asphalt Institute's Thickness Design Manual (Asphalt Institute, 1982) which is given by

$$N_{f2} = 1.365 \times 10^{-9} \varepsilon_c^{-4.477} \quad (4\text{-}6)$$

where N_{f2} = Number of repetitions to failure;

ε_c = Compressive strain at the top of the subgrade.

The lower of the number of repetitions to failure obtained from the fatigue (N_{f1}) and accumulated permanent deformations (N_{f2}) models was taken as the number of repetitions to failure of the pavement.

A different choice of parameters (or, indeed, a different choice of models) would produce different fatigue life estimates. Also, for pavements with thick AC layer, the combined effects of those two failure criteria might be used. However, those assumptions were made for simplicity, since the intention here is not to examine the influence of environmental factors on the design life of a specific pavement, but to examine the influence generally.

4.3.2.4 Incremental Damage and Pavement Life

The incremental damage caused by each application of an 80-kN (18-kip) equivalent single-axle load (ESAL) at any temperature profile *i*, bottom base water content condition *j* and subgrade water content *k* is given by

$$d_{ijk} = \frac{1}{N_{ijk}} \qquad (4\text{-}7)$$

where N_{ijk} =minimum number of repetitions needed to cause either accumulated permanent deformations failure or fatigue failure, as given by Equations 4-4 and 4-6.

The total damage done to the pavement over its lifetime is given by

$$D = \sum_{i=1}^{n}\sum_{j=1}^{m}\sum_{k=1}^{l} p_{ijk} \cdot d_{ijk} \cdot ESAL = ESAL \sum_{i=1}^{n}\sum_{j=1}^{m}\sum_{k=1}^{l} \frac{p_{ijk}}{N_{ijk}} \qquad (4\text{-}8)$$

where n = number of different temperature intervals (n= 47 for this study),

m = number of base water content conditions (m = 2 for this study),

l = number of subgrade water content conditions (l = 2 for this study),

p_{ijk} = percentage of ESALs occurring during a given temperature interval for temperature profile i, base moisture condition j and subgrade moisture condition k,

ESAL = total number of ESALs over the life of the pavement

If the total damage is set to one (lifetime), Equation 4-8 can be solved for the number of ESALs that can be accommodated before failure:

$$ESAL = \frac{1}{\sum_{i=1}^{n}\sum_{j=1}^{m}\sum_{k=1}^{l} \frac{p_{ijk}}{N_{ijk}}} \qquad (4\text{-}9)$$

The pavement life can thus be estimated for each of the pavement systems using linear AC temperature profiles and the idealized base layer and the subgrade moisture conditions.

4.4 Results and Discussion

4.4.1 Finite Element Analyses

The results of the 564 FE analyses are presented in Figure 4.10, Figure 4.11, and Figure 4.12, for the Pavement 1, 2, and 3, respectively. Each figure shows the results in terms of the computed critical strains, i.e. maximum tensile strain at the bottom of the AC layer and maximum compressive strain at the top of the

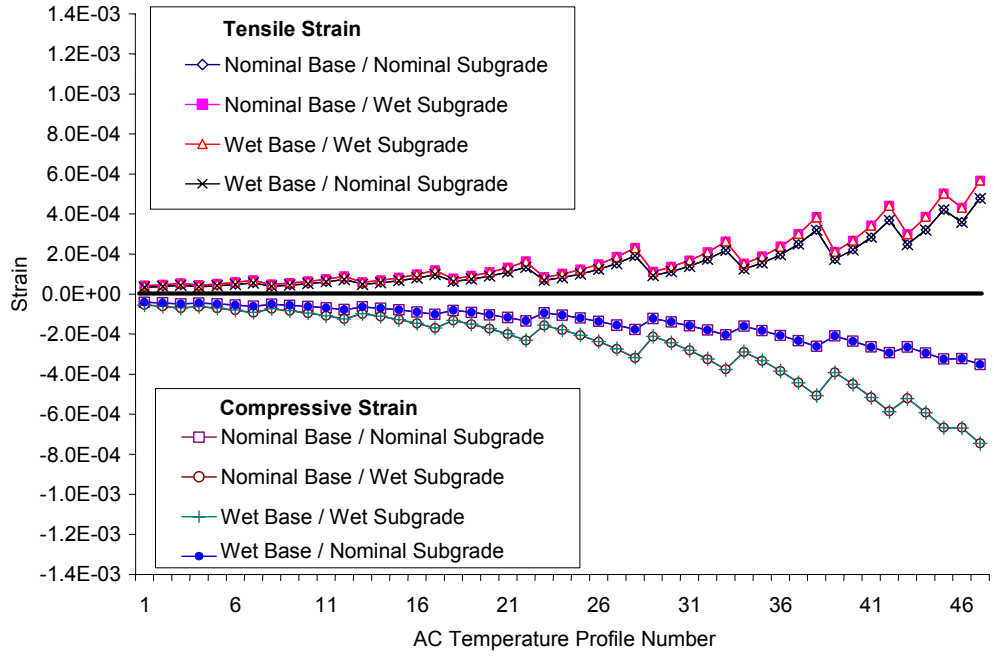

Figure 4.10 Critical Strains for Pavement 1 with Different Temperature Profiles (Table 4.7)

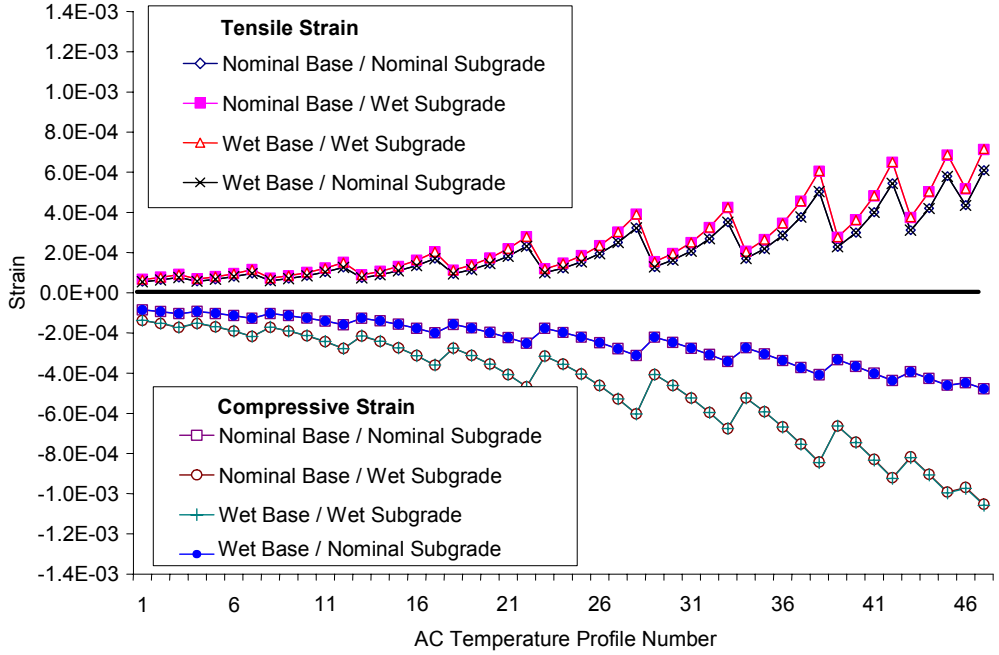

Figure 4.11 Critical Strains for Pavement 2 with Different Temperature Profiles (Table 4.7)

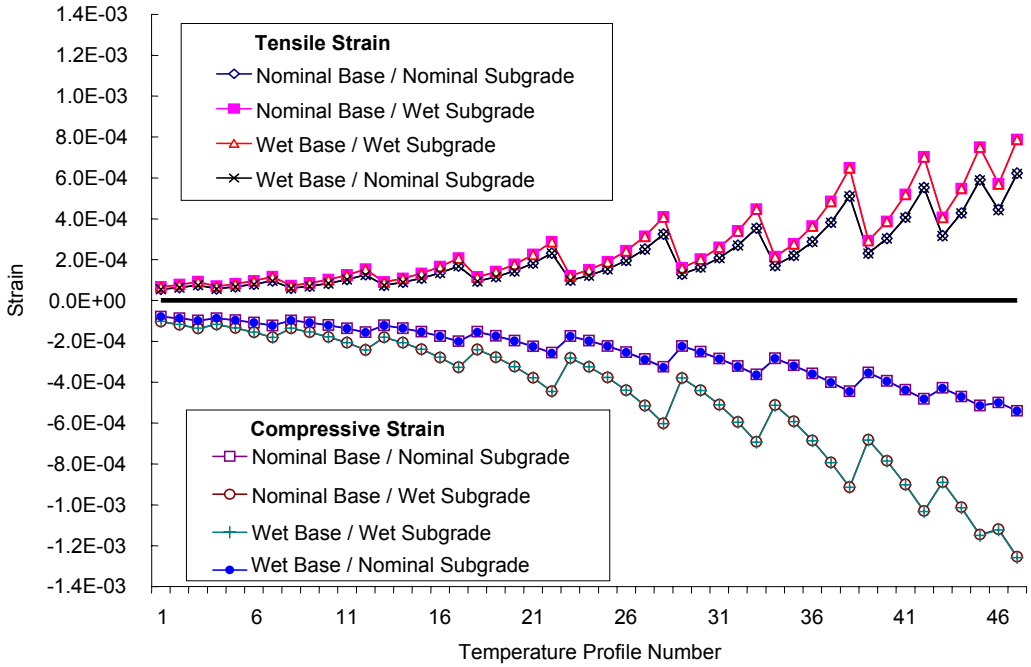

Figure 4.12 Critical Strains for Pavement 3 with Different Temperature Profiles (Table 4.7)

subgrade. The x-axis in each figure is AC temperature profile number as in Table 4.7, and the results are shown for the 4 combinations of base layer and subgrade moisture conditions. In general, an increasing temperature profile number corresponds with increasing AC temperatures. As expected, the critical strains increase with increasing temperature. This effect is more pronounced at high temperature (high AC temperature profile number), while at low temperature the critical strains change little with temperature. This validates the assumption that critical strains are almost constant for AC temperature lower than 10 ^{o}C.

From all the analyses, the critical strains in the models with wet subgrade are higher than the critical strains in the corresponding models with the nominal subgrade, and there is essentially no difference in the strains with nominal base and wet base.

One of the objectives of this parametric study is to investigate the effect of AC temperature profile rather than a single mid-depth AC temperature on computed strains in the pavement. As expected, different temperature profiles with the same mid-depth temperature yield different critical strains. The computed strains for Pavement 1 are shown in Figure 4.13. Similar results for other pavement models can be found in Appendix VIII. For the maximum compressive strain at the top of the subgrade, the difference between the uniform temperature and two temperature gradients is not discernable, but for maximum tensile strain in the AC layer, the effect of temperature profile is significant, on the order of 20%. This difference is not as significant for Pavement 2 and 3. For Pavement 3, the

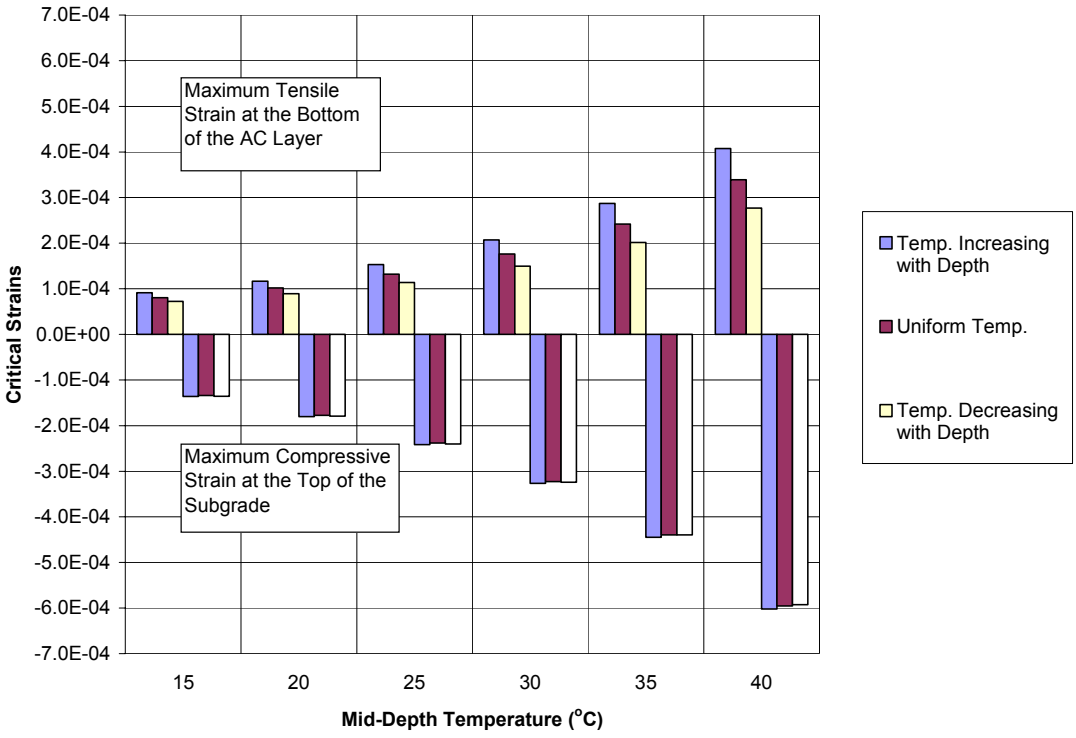

Figure 4.13 Comparison of Critical Strains for Different AC Temperature Profiles with the Same Mid-Depth AC Temperature (Pavement 1 with Wet Base and Wet Subgrade)

difference in maximum tensile strain is no more than 10% and could be neglected. As expected, the case with temperature increasing with depth, which is a condition that exists late in the afternoon, produced the largest strains and greatest pavement damage.

4.4.2 Impacts of Environmental Factors on Estimated Pavement Life

The results of the parametric study to evaluate the impacts of environmental factors on estimated pavement life will be presented in two steps: first the effects of the temperature averaging interval on pavements with uniform base and subgrade water content over the entire year, followed by the effects of the idealized seasonal variation in base and subgrade water content.

4.4.2.1 Effect of Temperature Averaging Interval on Estimated Pavement Life

The results of estimated pavement life for three pavements with different thickness are shown in Figure 4.14, demonstrating the effect of using different temperature averaging intervals. It is assumed that the specific moisture conditions for the base and subgrade exist for the entire year. One general trend in Figure 4.14 is the decrease of estimated pavement life with shorter temperature averaging interval regardless of pavement thickness. This is consistent with the conclusion of a previous parametric study using simple layered elastic theory and mid-depth temperatures (Zuo et al., 2002). It should be noted that the strains computed from the typical 2D axisymmetric analysis and used in pavement design results in underestimation in pavement life (higher critical strains) while the commonly used monthly AC temperature averages

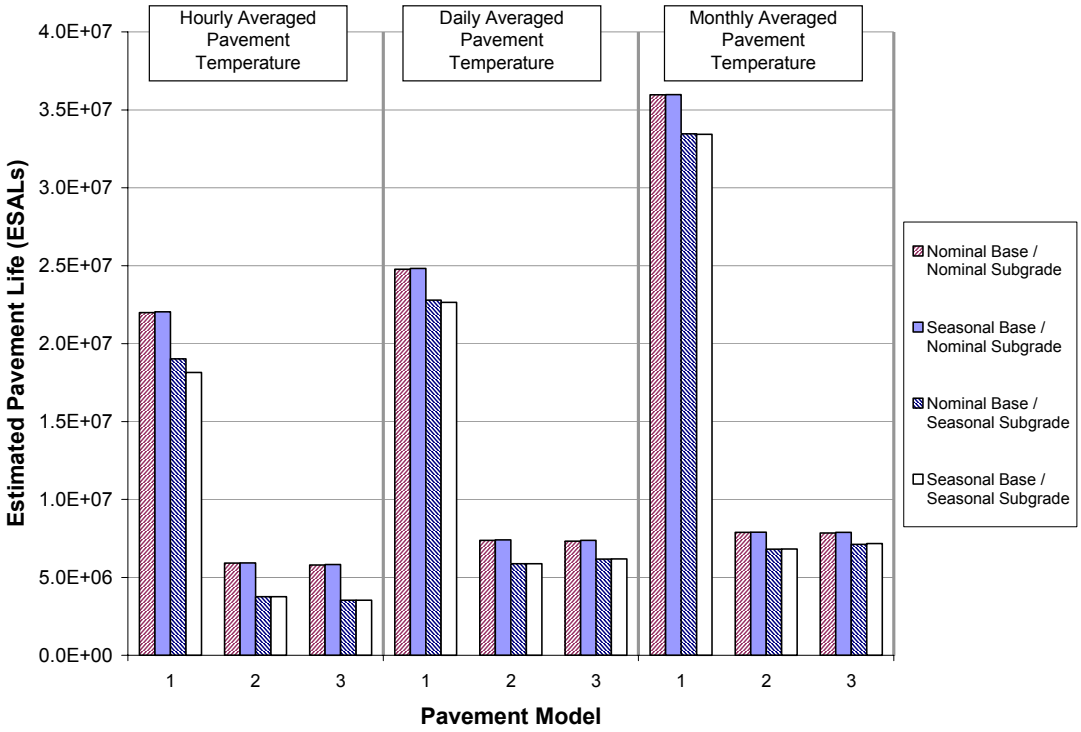

Figure 4.14 Estimated Pavement Life for Constant Water Content Conditions

result in overestimation in pavement life. These two effects may cancel each other and lead to results similar to those obtained from 3D analysis and hourly AC temperature averages. However, due to the nonlinear response of the pavement materials, the conflicting outcomes of the two analysis assumptions should be investigated for other material properties and pavement thicknesses.

For the same base water content, changing of subgrade water content from nominal to wet can reduce the estimated pavement life drastically. Base water content condition has little effect on all three pavements as discussed previously. It should be noted that the “Wet Base” condition in the figure only indicates that only the bottom 50 mm of the base is wet. Therefore, for pavements with inefficient drainage, the impact of base water content variation on estimated pavement life is expected to be much greater. It should be noted that the

subgrade was assumed to be either nominal or wet for the entire depth, but in reality, the water content of the subgrade below certain depth is constant all year long. Therefore, the assumption of the subgrade water content variations is also a worst case scenario. It is also noted that the Pavement 2 (same AC thickness as Pavement 1) has essentially the same predicted life as Pavement 1, and shows little benefit for the additional base thickness even when the base and subgrade are wet.

4.4.2.2 Effect of Subgrade Water Content and Base Variations on Estimated Pavement Life

To investigate the effects of seasonal water content variation on pavement life, it was assumed that the subgrade is only wet in May. This means that the pavement subgrade is wet only 1/12 of the pavement life, while it was assumed that the bottom 50 mm of the base was wet from November to July, or 2/3 of the pavement life. This relatively short period of wet subgrade can have large impact on pavement life. Figure 4.15 shows a comparison of estimated pavement life for pavements under different base and subgrade water contents. For Pavement 1, when hourly averaged temperature is used, pavement life can be overestimated by more than 60%, relative to the continuous nominal subgrade and base. As the temperature averaging interval increases, the differences diminish. However, for monthly averaged temperature, the overestimation is only about 10%.

These findings suggest a very important issue that could be overlooked in pavement design practice. In conventional pavement design, only monthly

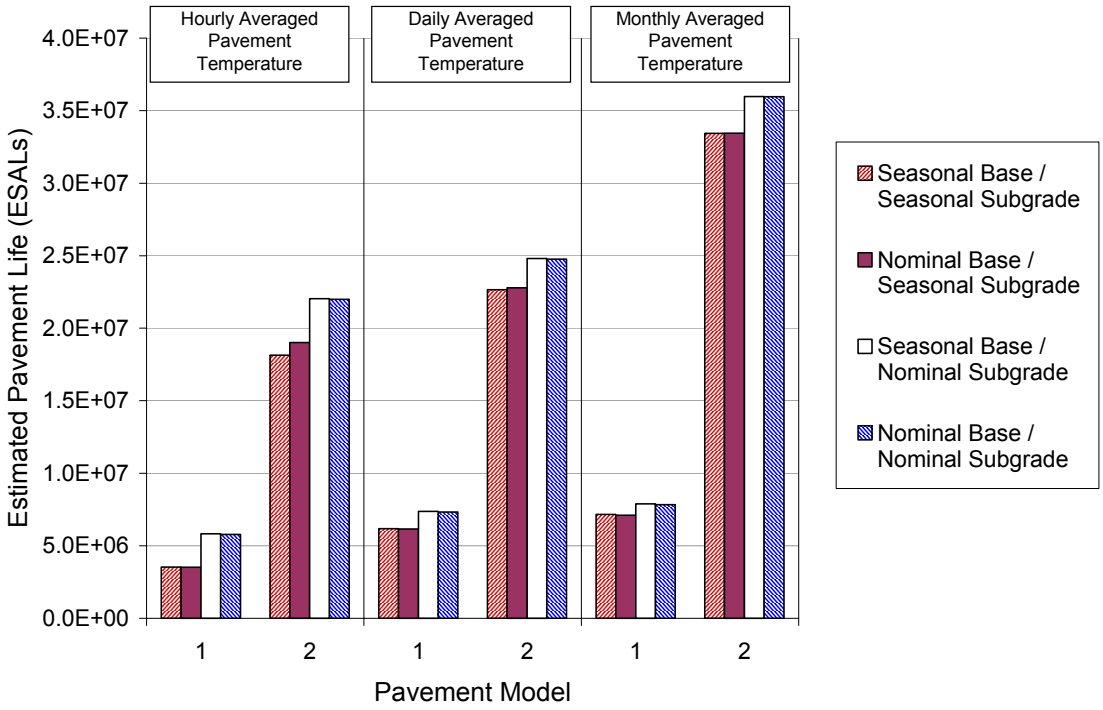

Figure 4.15 Estimated Pavement Life for Seasonal Base Water Content

averaged temperature and water content variation are usually considered. When monthly averaged temperature is used, even if the seasonal temperature and water content variation are both accounted for in the mechanistic-empirical pavement design, the results would misleadingly suggest that one month of wet subgrade is not going to significantly affect pavement life.

It should be noted all these conclusions are drawn based upon the assumption that the wet subgrade occurs in May. If it occurs in another month and/or the duration is different, the results will be different. Figure 4.16 shows the effect of the timing of the wet subgrade condition relative to the case with nominal subgrade condition existing all year long. The effect of subgrade water content on estimated pavement life is highly dependent on the temperature during the month when the subgrade is wet. If the month of wet subgrade is in March or an

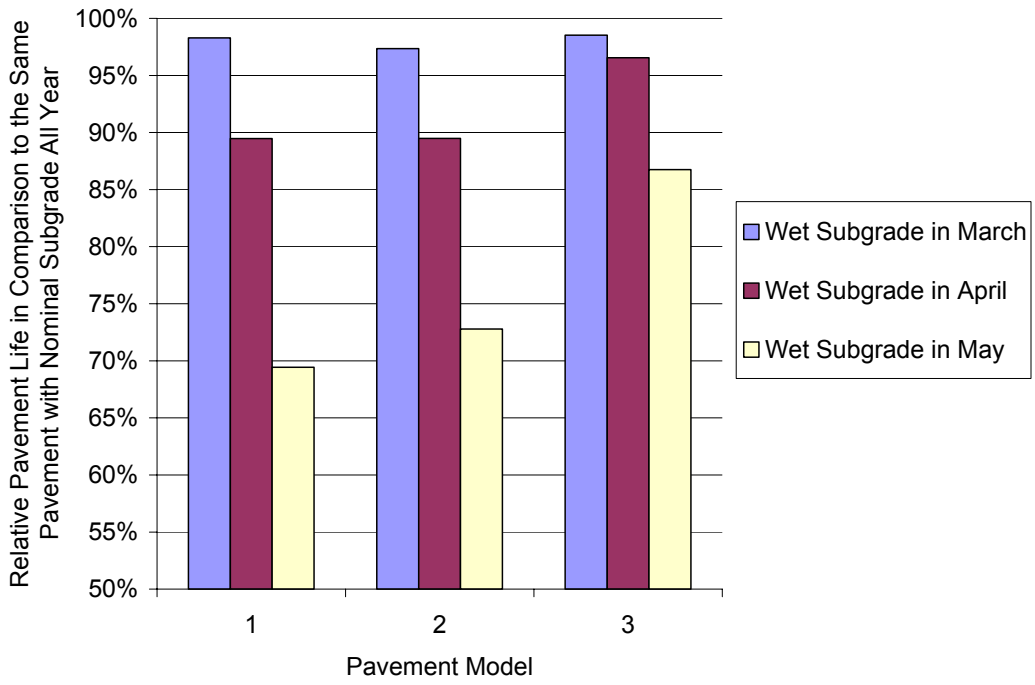

Figure 4.16 Effect of the Month for Wet Subgrade Condition (Hourly Temperature Averaging Data)

even colder month, the soft subgrade (high water content) does not significantly change the estimated pavement life relative to the nominal subgrade condition, since the stiffness of the AC layer is high and the stress transferred into the unbound layers is low. However, if the wet subgrade condition occurs in a warm month, such as May, the surface AC layer transmits stresses deeper into the wet subgrade, and the reduction in estimated pavement life is clear. Figure 4.16 suggests the importance of considering the combined effect of temperature and water content in pavement design, since the same duration of wet subgrade occurring at different times can result in different estimated pavement life.

4.5 Conclusions

The effects of pavement temperature averaging interval and seasonal water content variations in the unbound layers have been studied using the finite element method and environmental data collected from instrumented pavement sites in Tennessee. The results of the analyses showed that the effect of AC temperature gradient was significant, especially when the AC layer is thin. The length of temperature averaging interval was shown to be most critical for pavement life estimation. The results show that estimated pavement life decreases as the length of the averaging interval decreases. Pavement designs based on monthly temperature average neglect the damage that occurs during brief periods of high temperature, leading to unconservative designs. The effect of seasonal variation in water content in the base layer was not found to be significant for the pavement systems investigated. However, the estimated pavement life is susceptible to subgrade water content variation. One month of wet subgrade conditions could reduce the estimated pavement life by as much as 60%. It should be noted that this 60% in pavement life was obtained when hourly averaged AC temperature data were used. With the typical monthly averaged AC temperature, the difference in predicted pavement life would be overlooked. The effect of subgrade water content is not as critical as temperature, but it can be very significant when the periods of high subgrade water content coincide with high AC temperature, which suggests the importance of considering the combined effect of temperature and water content in pavement design. It was also suggested that the over prediction of pavement life that

accompanied the monthly temperature interval may be compensated for in practice by the more conservative estimation of life (larger strains) obtained from 2D axisymmetric analysis compared to 3D analysis. These conflicting issues are likely to be site and material property dependent, however.

It should be reiterated that the objective of this study was to assess the effect of the temperature and water content variations on pavement life. For the sake of simplicity, readily available models were used along with the parameter values suggested by the authors of those models. The use of different parameter values or different models would, of course, change the results, but the trends illustrated here would still be valid, even if the magnitude of the error changed.

References

AASHTO (1993) *AASHTO Guide for the Design of Pavement Structures*. American Association of State Highway Officials, Page 403.

ABAQUS 6.2-1 (2001) , Habbitt, Karlsson & Sorensen, Inc., Rhode Island

Asphalt Institute (1982) *Research and Development of the Asphalt Institute's Thickness Design Manual (MS-1)*. Report 82-2.

Carmichael III, R. F. and E. Stuart (1985) Predicting Resilient Modulus: A Study to Determine the Mechanical Properties of Subgrade Soils. In *Transportation Research Record 1043*, TRB, National Research Council, Washington D.C., pp. 145-148.

Cumberledge, G., G. L. Hoffman, A. C. Bhajandas, and R. J. Cominsky (1974) Moisture Variation in Highway Subgrades and the Associated Change in Surface Deflections. In *Transportation Research Record 497*, TRB, National Research Council, Washington D.C., pp. 40-49.

Drumm, E. C., J. S. Reeves, M. R. Madgett, and W. D. Trolinger (1997) Subgrade Resilient Modulus Correction for Saturation Effects. *ASCE Journal of Geotechnical Engineering* Vol. 123, No. 7, 663-670.

Hjelmstad, K. D. and E. Taciroglu (2000) Analysis and Implementation of Resilient Modulus Models for Granular Solids. *ASCE Journal of Engineering Mechanics* Vol. 126, No. 8, 821-830.

Hwang, D. and M. W. Witczak (1979) *Program DAMA (Chevron), User's Manual*. Department of Civil Engineering, University of Maryland

Jin, M. S., K. W. Lee, and W. D. Kovacs (1994) Seasonal Variation of Resilient Modulus of Subgrade Soils. *ASCE Journal of Transportation Engineering* Vol. 120, No. 4, 603-616.

Marshall, C., R. W. Meier, and M. Welsh (2001) Seasonal Temperature Effects on Flexible Pavements in Tennessee. In *Transportation Research Record 1764*, TRB, National Research Council, Washington, D.C., pp. 89-96.

Matter, N. S. and O. T. Farouki. (1994) Detailed Study on the Climatic and Seasonal Variation Effects on Pavements in Northern Ireland. *In* Proceedings of *The 4th International Conference on the Bearing Capacity of Roads and Airfields. Minneapolis, Minnesota,* pp. 721-737.

Raad, L., G. H. Minassian, and S. Gartin (1992) Characterization of Saturated Granular Base Under Repeated Loads. In *Transportation Research Record 1369*, TRB, National Research Council, Washington D.C., pp. 73-82.

Rada, G. and M. W. Witczak (1981) Comprehensive Evaluation of Laboratory Resilient Moduli Results for Granular Material. In *Transportation Research Record 810*, TRB, National Research Council, Washington D.C., pp. 23-33.

Rainwater, N. R., R. E. Yoder, E. C. Drumm, and G. V. Wilson (1999) Comprehensive Monitoring Systems for Measuring Subgrade Moisture Conditions. *ASCE Journal of Transportation Engineering* Vol. 125, No. 5, 439-448.

Tian, P., M. M. Zaman, and J. G. Laguros (1998) Gradation and Moisture Effects on Resilient Moduli of Aggregate Bases. In *Transportation Research Record 1619*, TRB, National Research Council, Washington D.C., pp. 75-84.

Uzan, J. (1992) Resilient Characterization of Pavement Materials. *International Journal for Numerical and Analytical Methods in Geomechanics* Vol. 16, 453-459.

Uzan, J., M. W. Witczak, T. Scullion, and R. L. Lytton. (1992) Development and Validation of Realistic Pavement Response Modes. *In* Proceedings of *7th International Conference on Asphalt Pavements.* International Society for Asphalt Pavements*, Austin, TX,* pp. 334-350.

Zuo, G., R. W. Meier, and E. C. Drumm (2002) The Effect of Temperature Averaging on Predicted Pavement Life. In *Transportation Research Record 1809*, National Research Council, Washington D.C., pp. 119-125.

Part V Conclusions and Recommendations

5.1 Conclusions

Data obtained from a long-term pavement monitoring program in Tennessee, USA, was used to investigate the impact of seasonal changes in base and subgrade properties on flexible pavement response. An empirical model was developed to predict the infiltration from rainfall intensity with reasonable accuracy for the pavements without a dense-graded surface layer. The longitudinal joint turned out to be a significant source of water infiltration from the pavement surface. It was determined that TDR water content measurements are susceptible to temperature changes, due to signal attenuation, and a correction scheme for temperature effects was developed. Overall, the seasonal variation of subgrade moisture content was found to be small, yet some seasonal variation in the water content at the bottom of the base course was observed.

A series of 3D finite element analyses on flexible pavements were performed. Uzan's resilient modulus model was implemented into the analysis to account for the stress-dependent behavior of the both coarse-grained and fine-grained unbound materials. In comparison to the 2D axisymmetric analysis, the application of the wheel load over dual wheels approximated by double rectangular areas in 3D analysis produced more realistic loading conditions and it lowered the computed maximum tensile strain at the bottom of the HMA layer by about 20%. While the frictional interface condition between the hot mix asphalt (HMA) layer and the base is the most realistic, the results obtained with smooth interface were within 5% of the frictional interface, and about 15% larger than what is obtained when the HMA layer is assumed to be fully tied to the base layer.

The extension of the pavement shoulder to 8 m from the center line of the wheel path only caused 5% reduction in the maximum tensile strain at the bottom of the HMA layer.

The effects of pavement temperature averaging interval and seasonal water content variations in the unbound layers were studied using the finite element method and the environmental data collected from the instrumented pavement sites. The results of the analyses showed that the effect of AC temperature gradient was significant, especially when the AC layer is thin. The length of temperature averaging interval was shown to be most critical for pavement life estimation. The results show that estimated pavement life decreases as the length of the averaging interval decreases. Pavement designs based on monthly temperature average neglect the damage that occurs during brief periods of high temperature, leading to unconservative designs. The effect of seasonal variation in the base layer was not found to be significant for the pavement systems investigated. However, the estimated pavement life is susceptible to subgrade water content variation. One month of wet subgrade conditions could reduce the estimated pavement life by as much as 60%. It should be noted that this 60% in pavement life was obtained when hourly averaged AC temperature data were used. Using the more typical monthly average for AC temperature, the difference in predicted pavement life would be overlooked. The effect of subgrade water content can be very significant when the periods of high subgrade water content coincide with high AC temperature, which suggests the importance of

considering the combined effect of temperature and water content in pavement design.

5.2 Recommendations

Additional resilient modulus data on subgrade and base at different degrees of saturation is needed. Information obtained from these tests would be valuable for the estimation of pavement life in Tennessee, and other regions where high pavement temperature and wet base and subgrade conditions occur.

Empirical models similar to the one used to predict infiltration from precipitation for the coarse-graded surface layer should be used to study the infiltration through the longitudinal joints. Probably, a similar model can also be obtained to predict base water content variation from infiltration, and consequently another model to predict subgrade water content variation from that of the base layer. In this way, rather than trying predicting subgrade water content variation directly from precipitation data, which was found not to be successful, the moisture condition at different layers of the pavement system may be predicted in steps.

The incorporation of the distribution of traffic during the day could also be included provided data on this was obtained.

Appendices

Appendix I Temperature Study on Multi-Segment TDR Probe

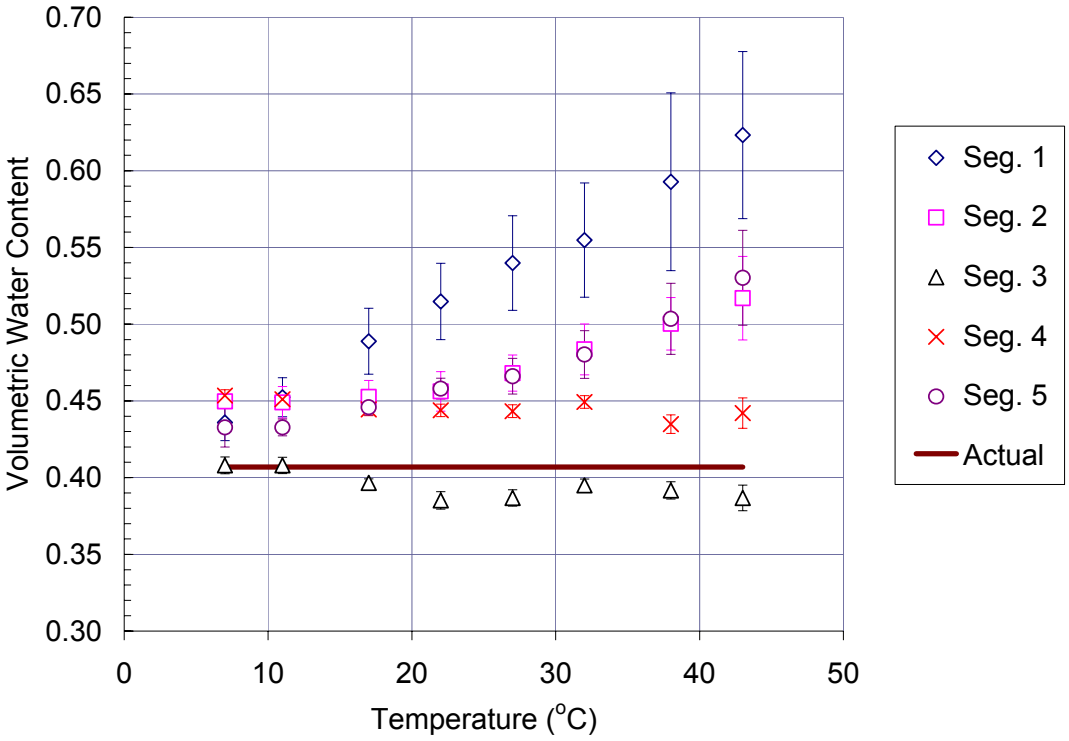

Figure A.1.1 TDR Temperature Calibration on Blount County Subgrade Repetition 1

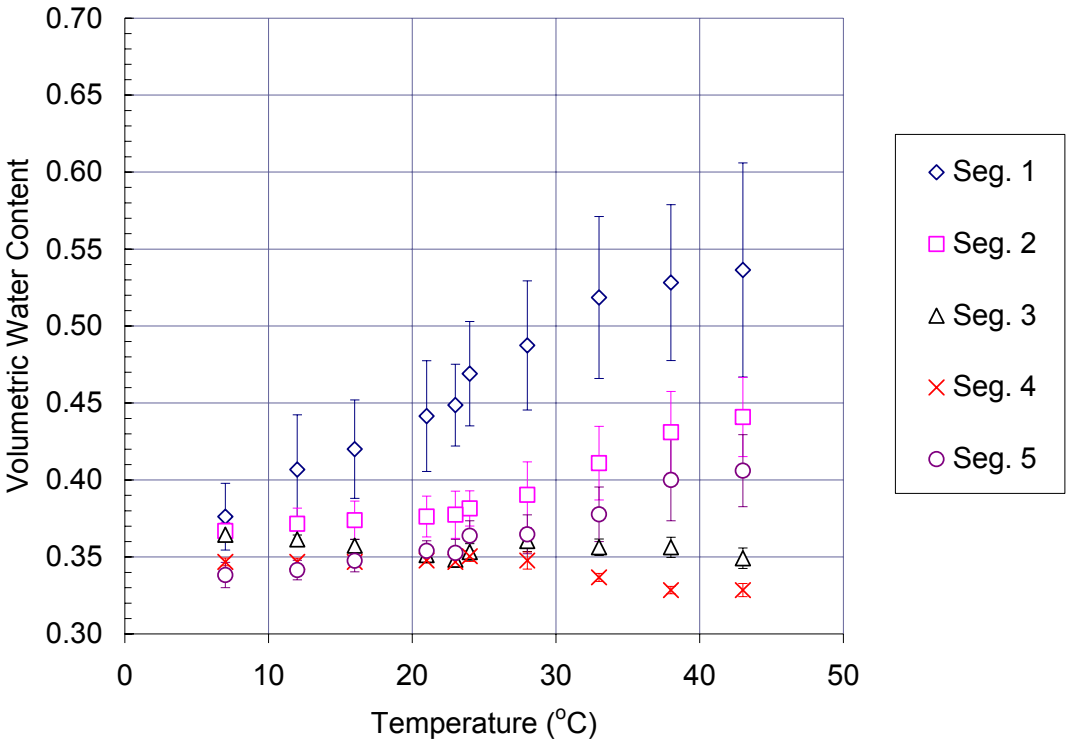

Figure A.1.2 TDR Temperature Calibration on Blount County Subgrade Repetition 2 (Primary Probe, Lab MP-917)

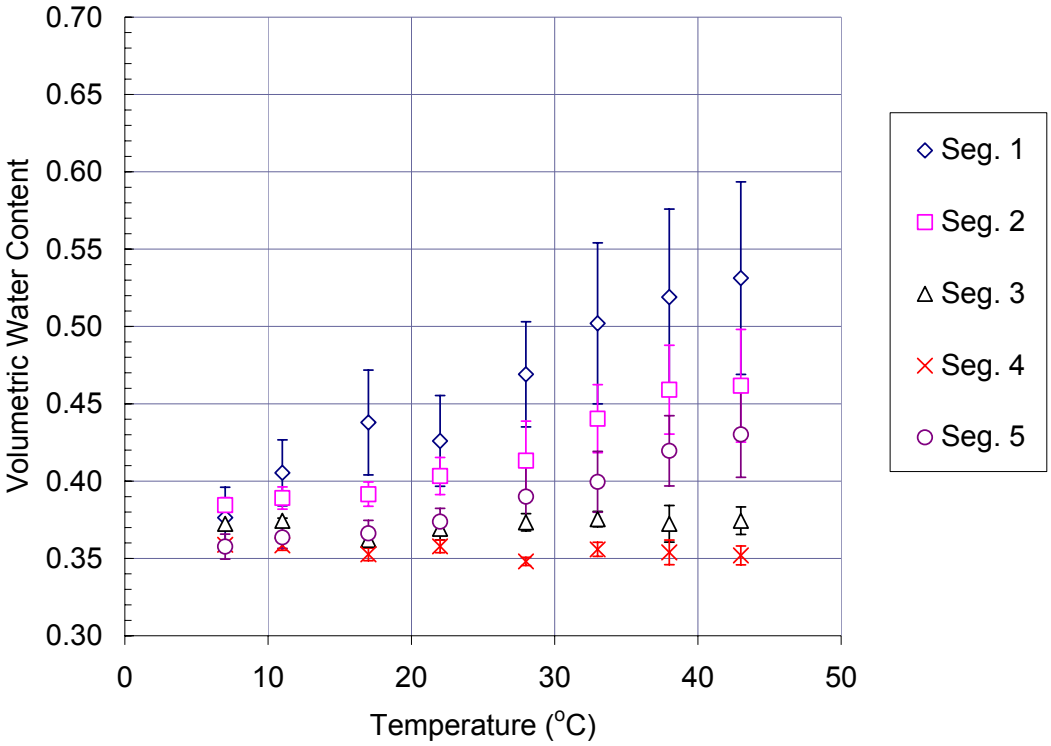

Figure A.1.3 TDR Temperature Calibration on Blount County Subgrade Repetition 3 (Primary Probe, Field MP-917)

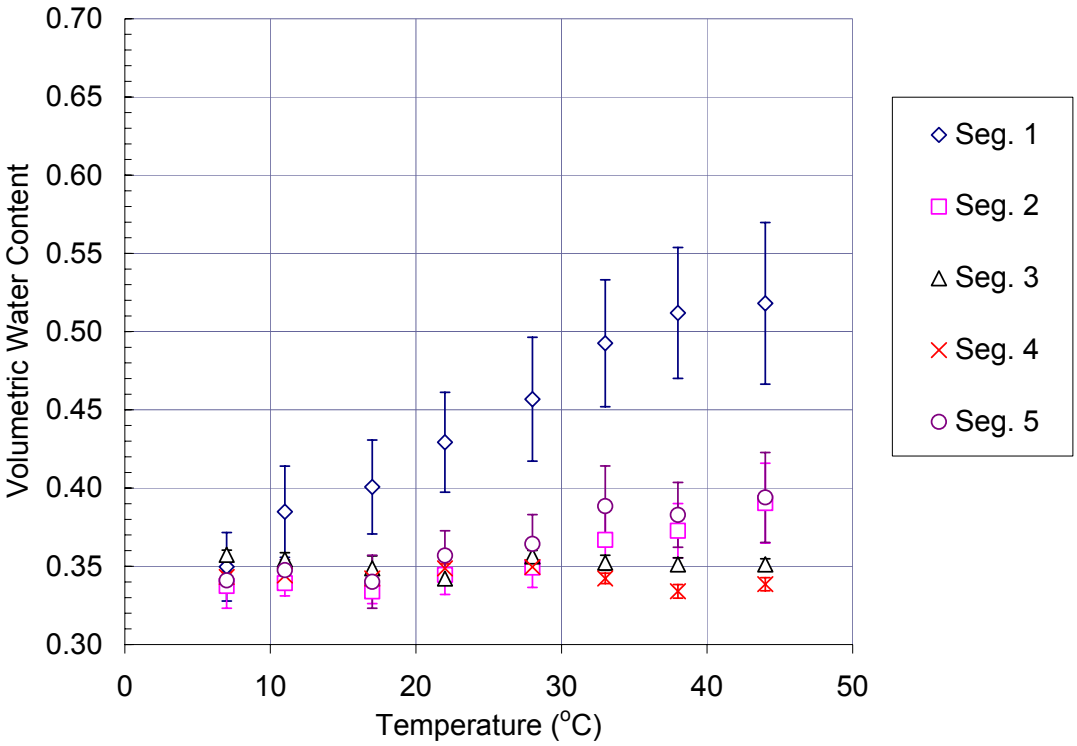

Figure A.1.4 TDR Temperature Calibration on Blount County Subgrade Repetition 4 (Secondary Probe, Lab MP-917)

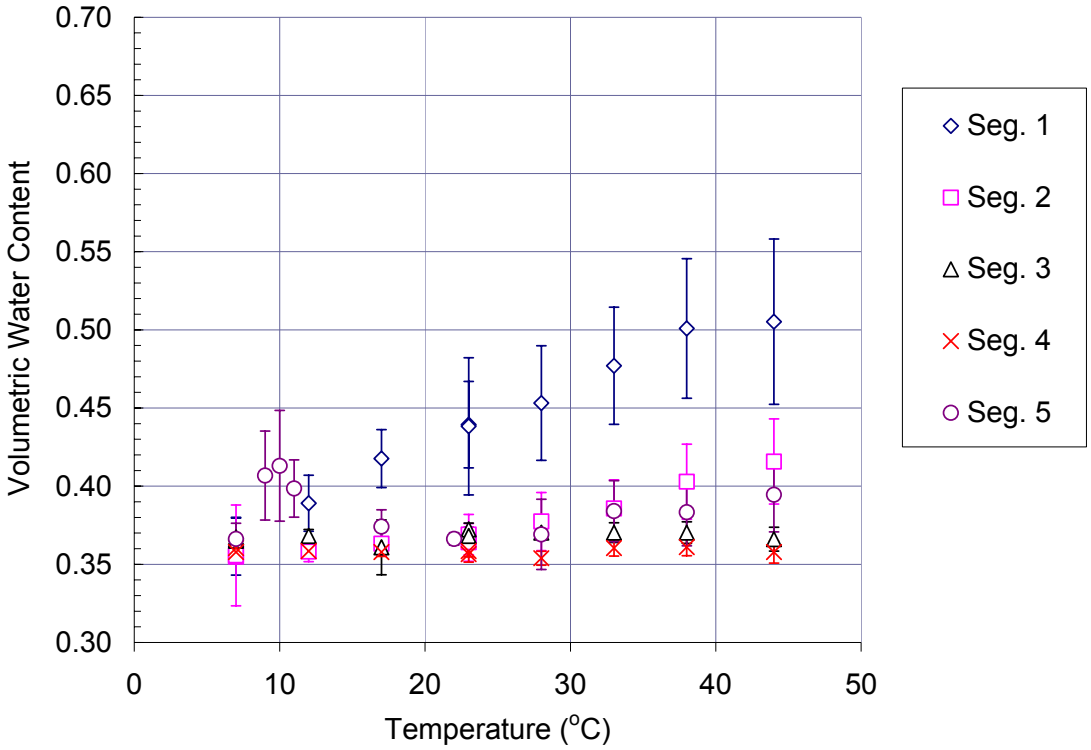

Figure A.1.5 TDR Temperature Calibration on Blount County Subgrade Repetition 5 (Secondary Probe, Field MP-917)

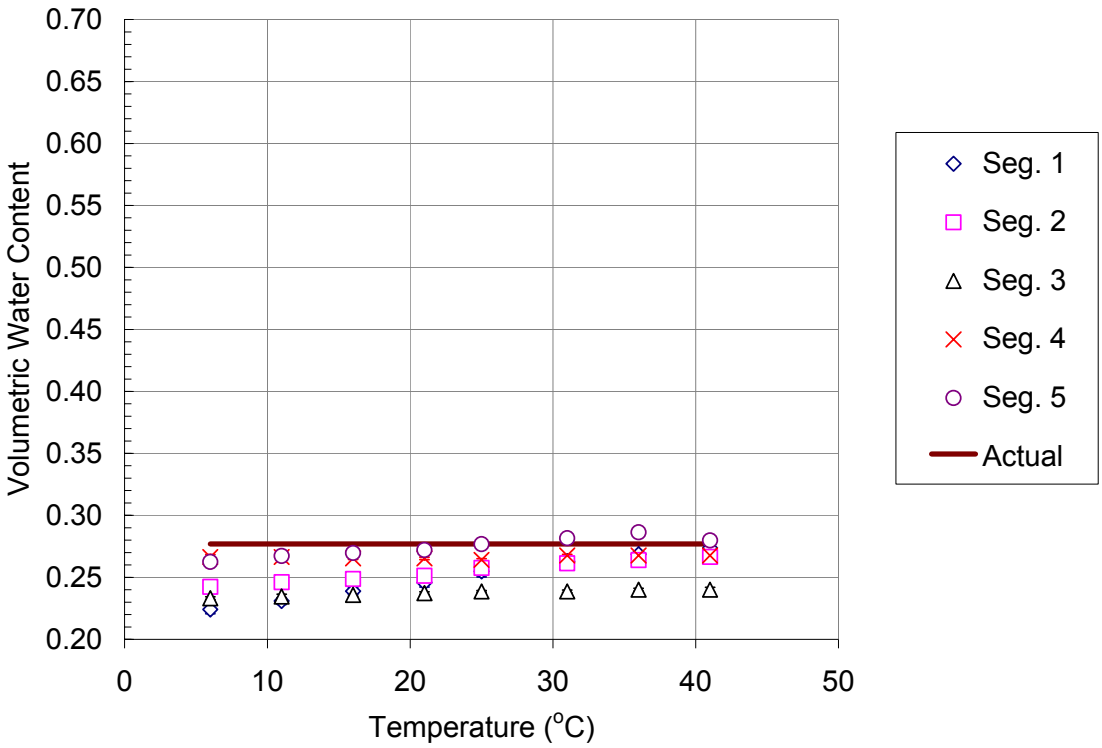

Figure A.1.6 TDR Temperature Calibration on McNairy County Subgrade Repetition 1

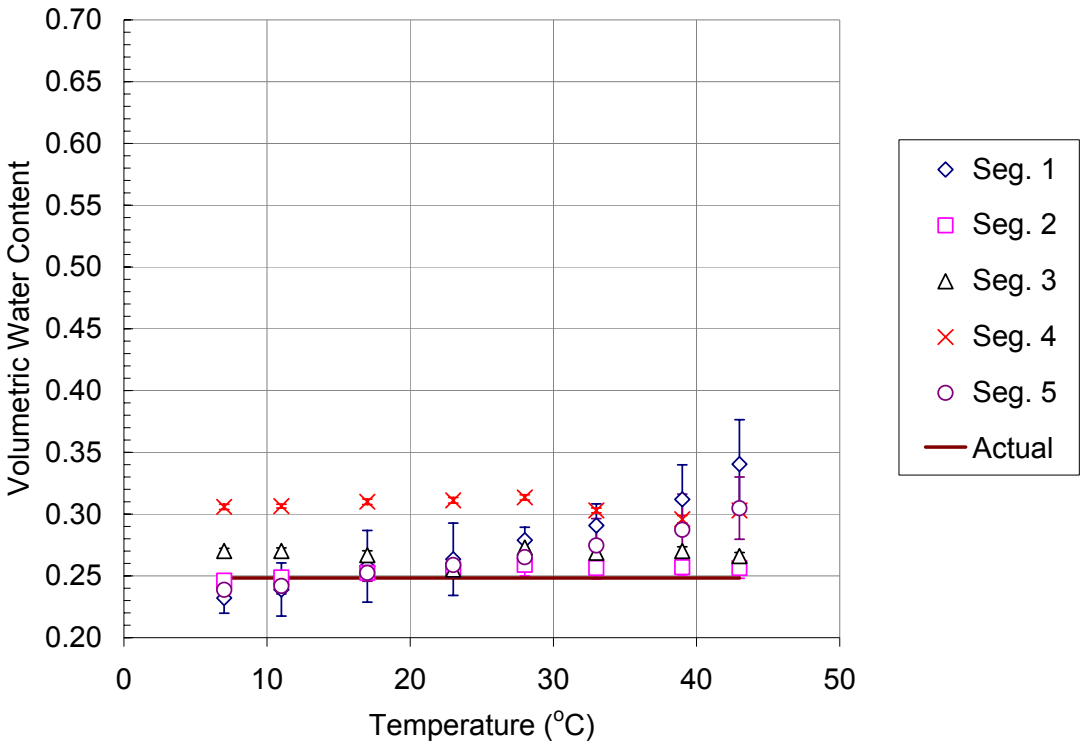

Figure A.1.7 TDR Temperature Calibration on McNairy County Subgrade Repetition 2

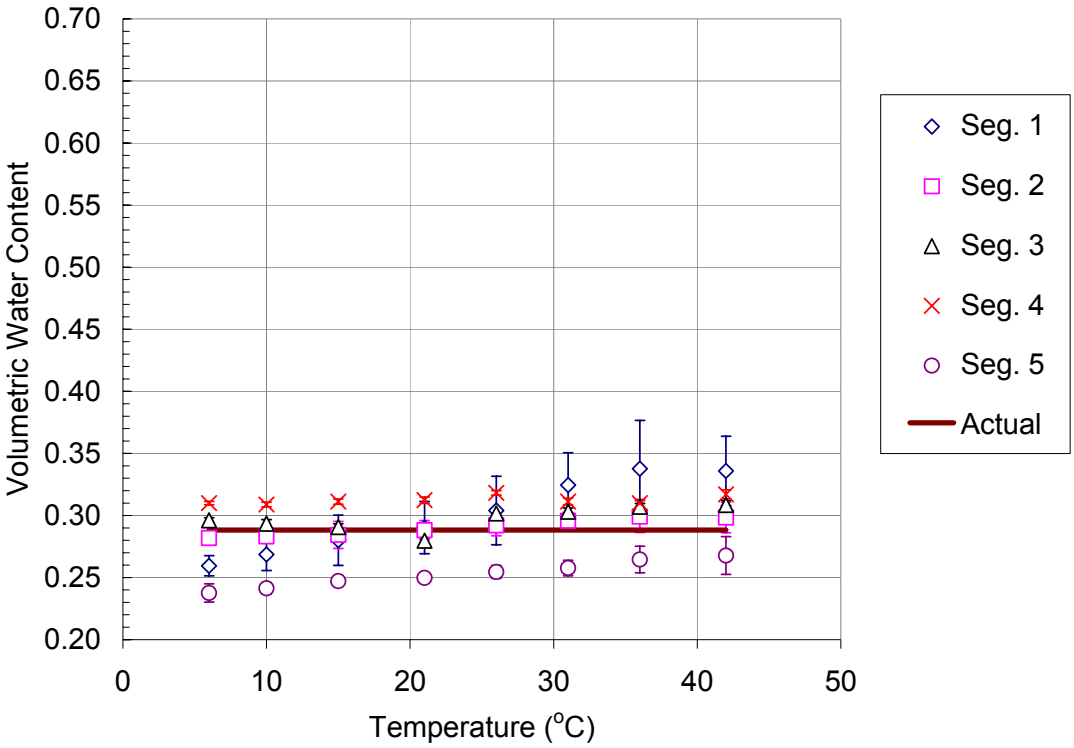

Figure A.1.8 TDR Temperature Calibration on McNairy County Subgrade Repetition 3

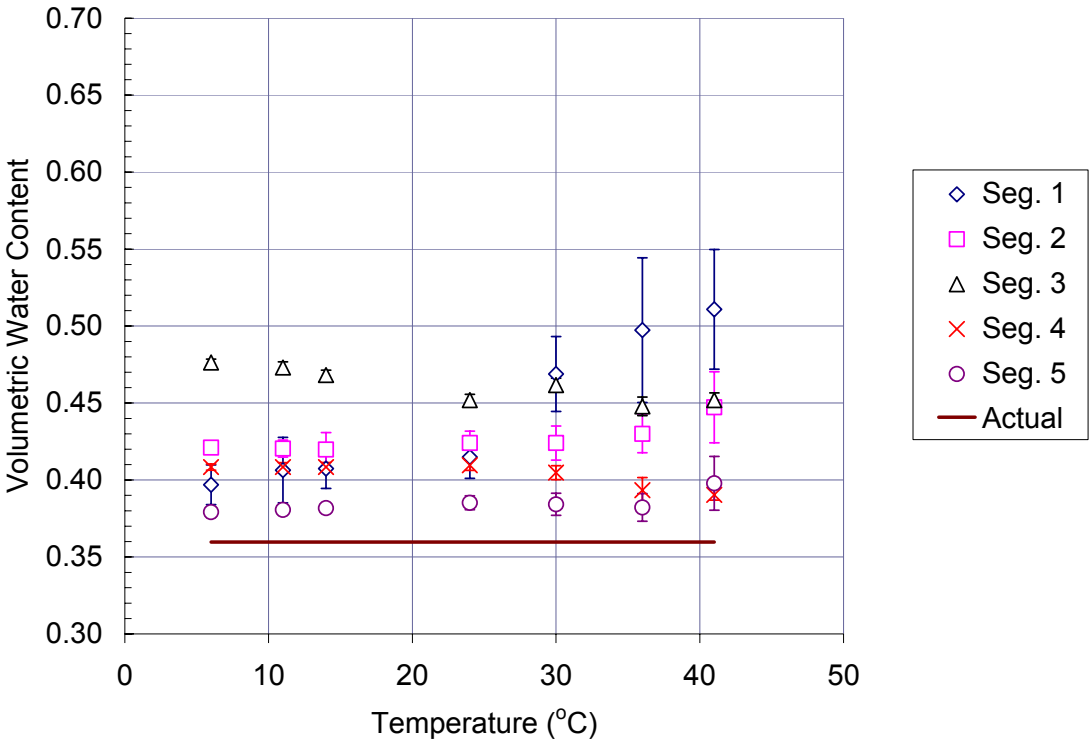

Figure A.1.9 TDR Temperature Calibration on Overton County Subgrade Repetition 1

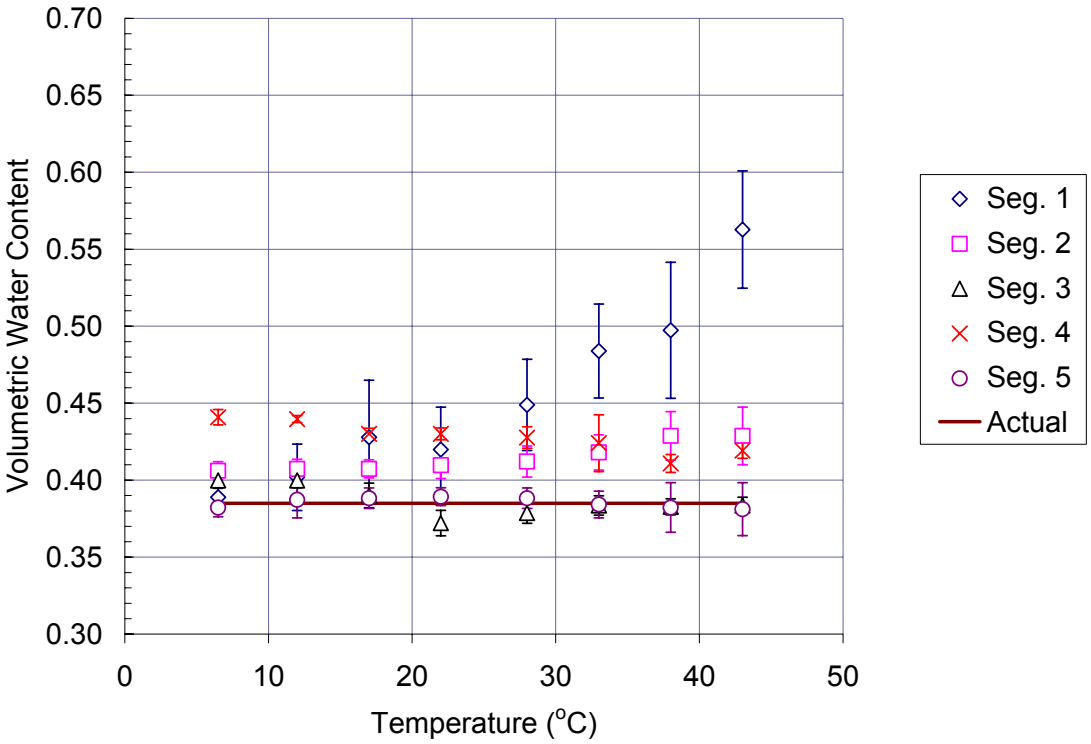

Figure A.1.10 TDR Temperature Calibration on Overton County Subgrade Repetition 2

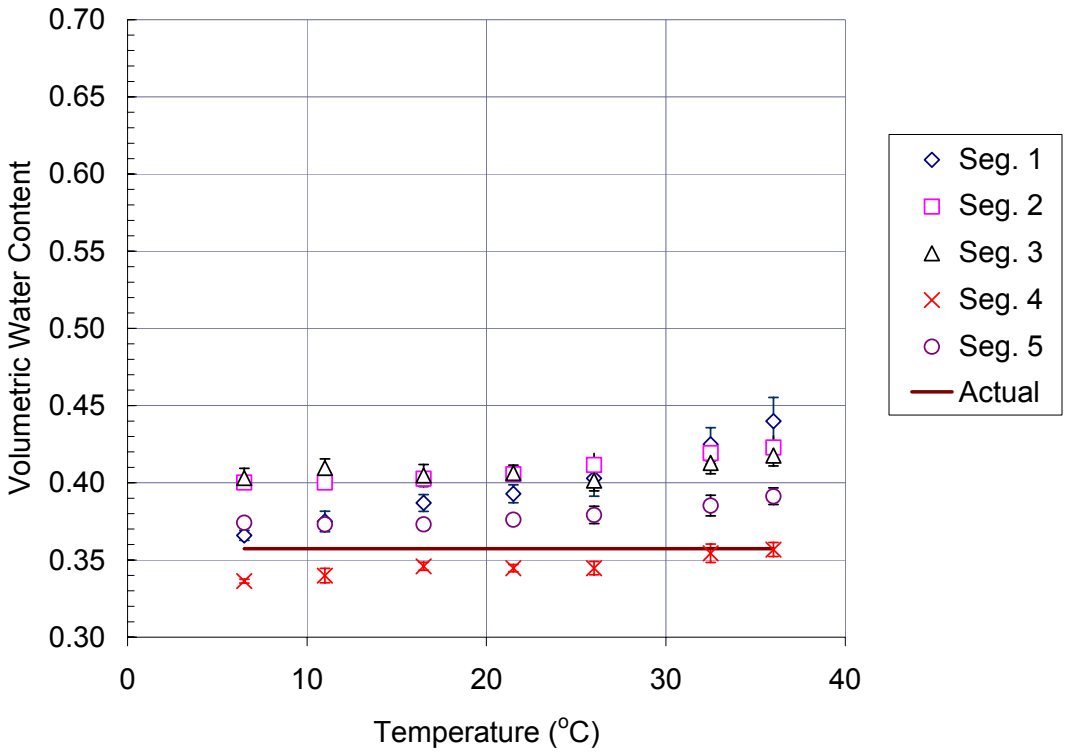

Figure A.1.11 TDR Temperature Calibration on Overton County Subgrade Repetition 3

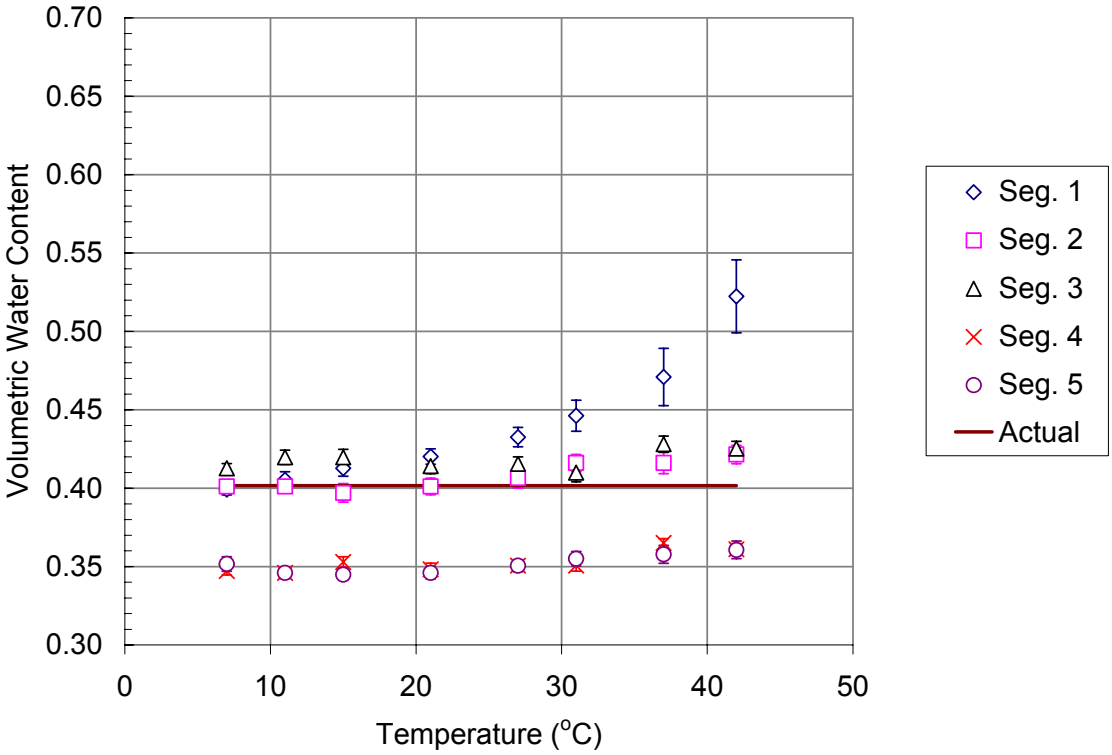

Figure A.1.12 TDR Temperature Calibration on Sumner County Subgrade Repetition 1

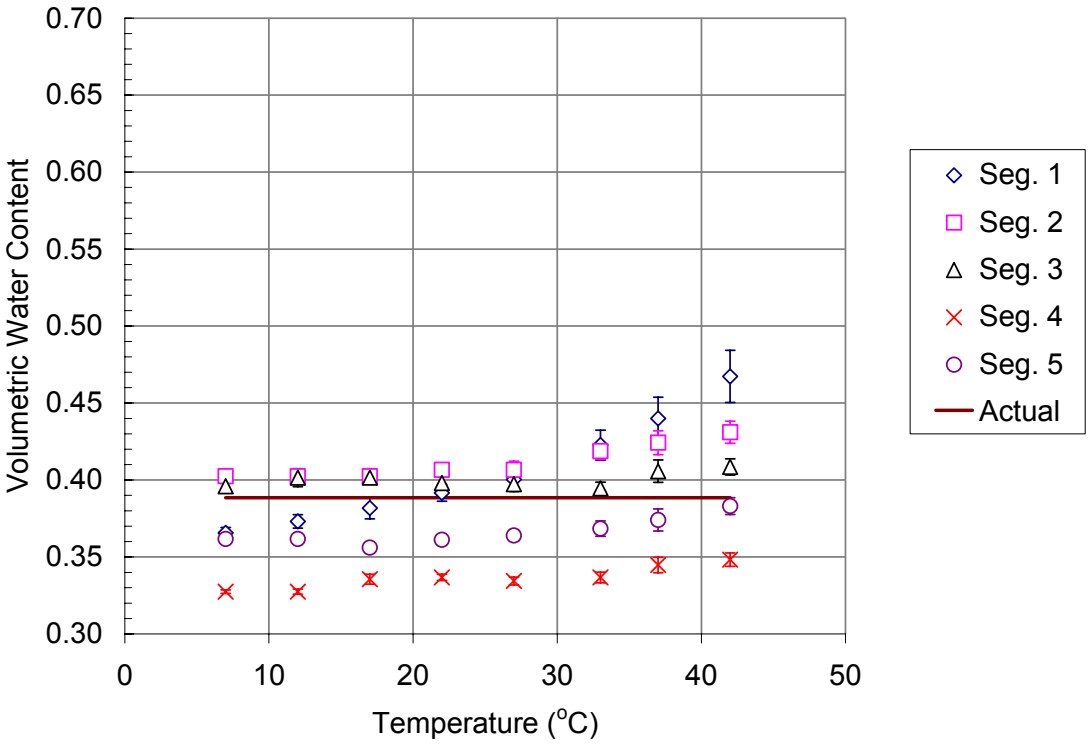

Figure A.1.13 TDR Temperature Calibration on Sumner County Subgrade Repetition 2

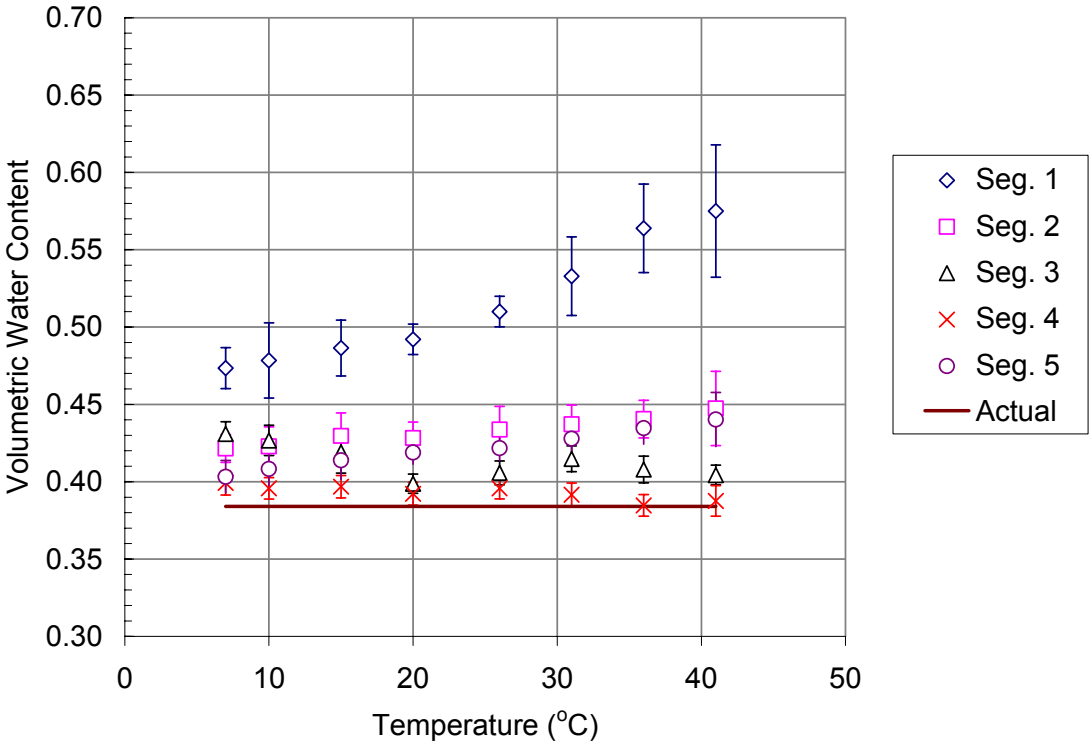

Figure A.1.14 TDR Temperature Calibration on Sumner County Subgrade Repetition 3

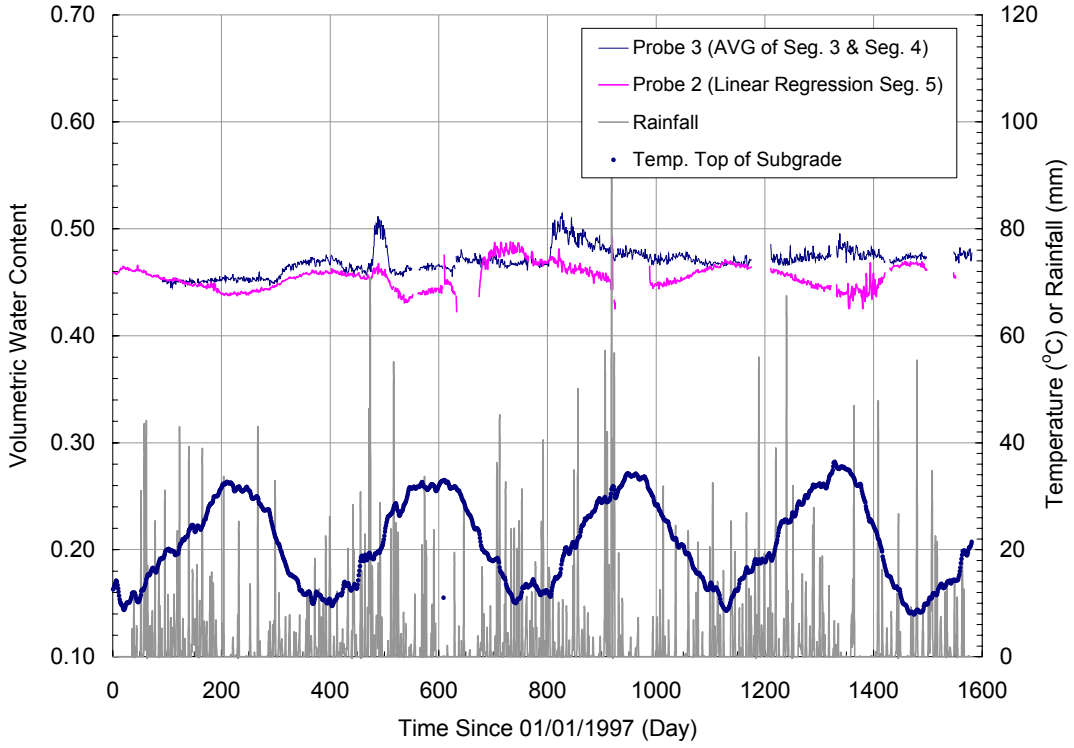

Figure A.1.15 Subgrade Water Content and Climatic Data at the Blount County Site

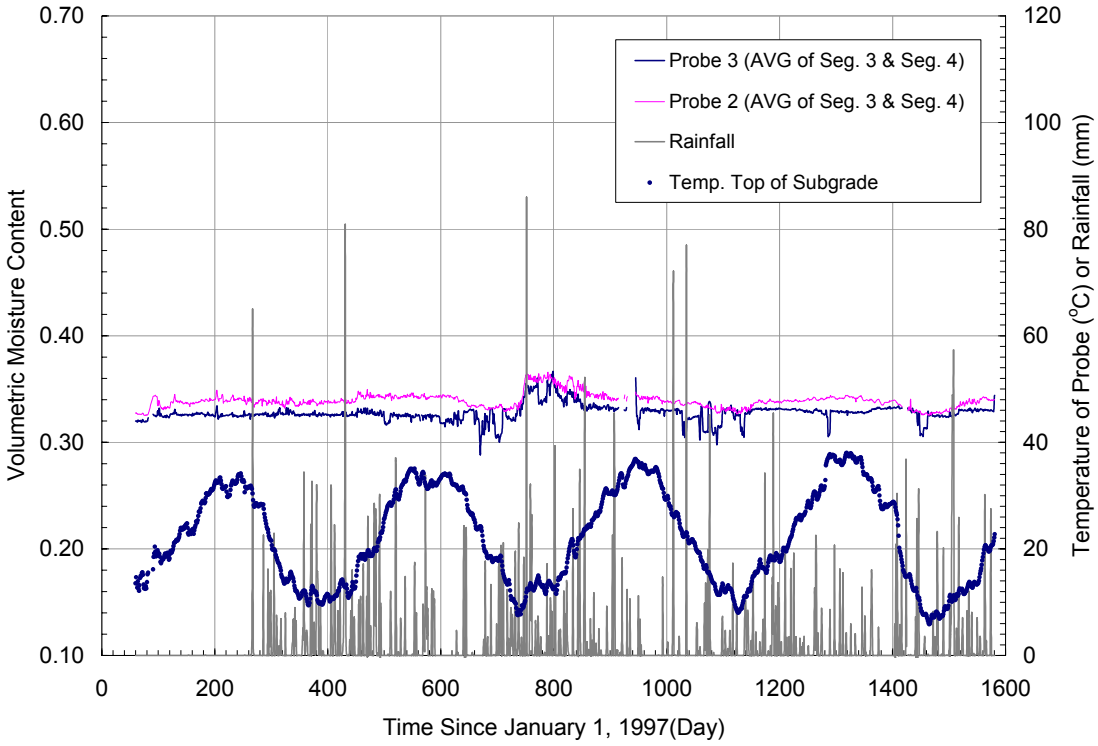

Figure A.1.16 Subgrade Water Content and Climatic Data at the McNairy County Site

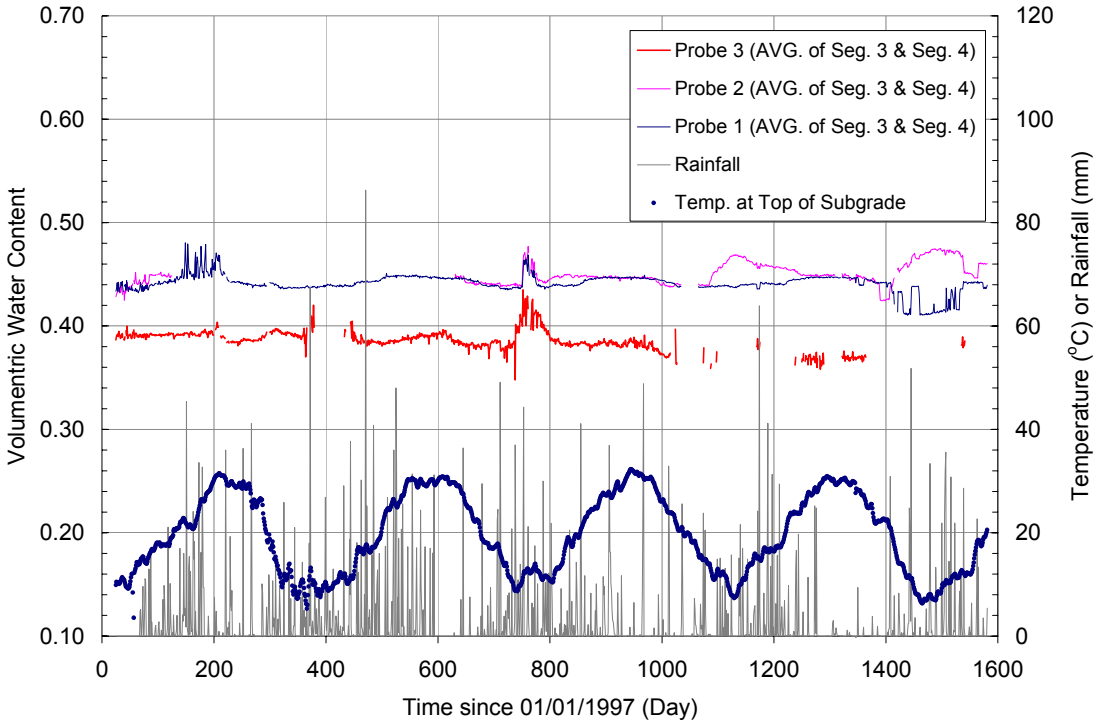

Figure A.1.17 Subgrade Water Content and Climatic Data at the Overton County Site

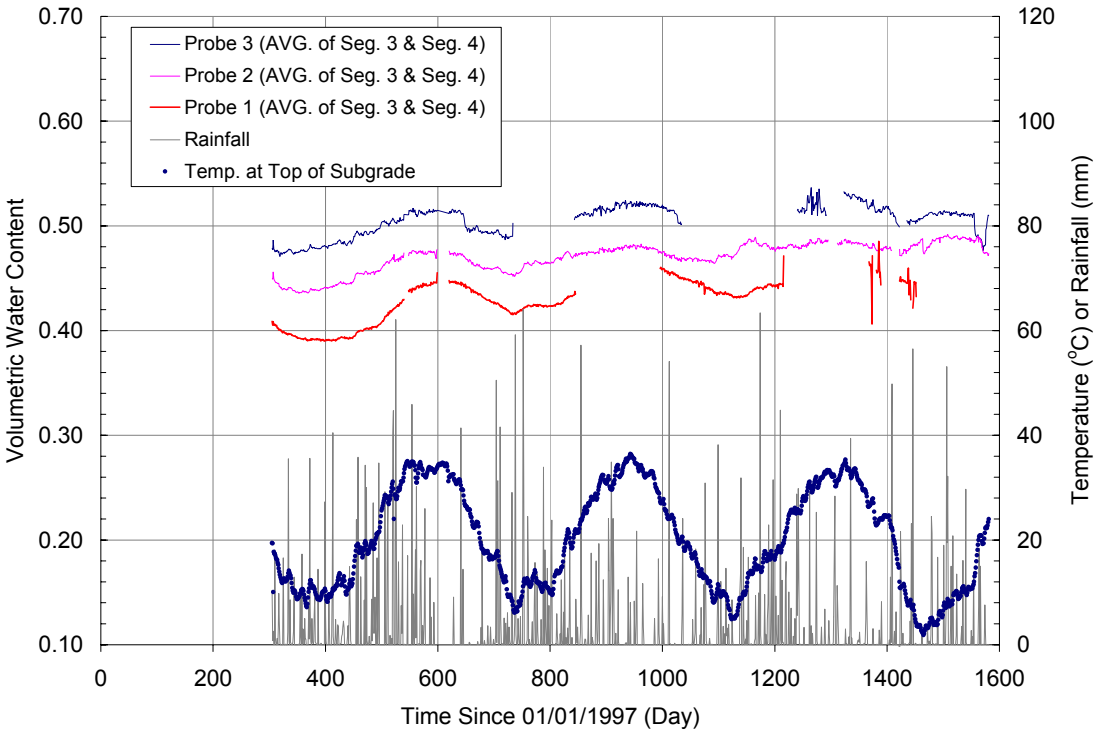

Figure A.1.18 Subgrade Water Content and Climatic Data at the Sumner County Site

Appendix II Insitu Measurement and Empirical Modeling of Base Infiltration in Highway Pavement Systems

This appendix is slightly revised from a paper with the same name published in Transportation Research Record 2001 by N. Randy Rainwater, Gang Zuo, Eric C. Drumm, Wesley C. Wright, and Ronald E. Yoder:

Rainwater, N. R., G. Zuo, E. C. Drumm, W. C. Wright, and E. J. Yoder (2001) Insitu Measurement and Empirical Modeling of Base Infiltration in Highway Pavement Systems. In *Transportation Research Record 1772*, TRB, National Research Council, Washington, D.C., pp. 143-150.

My contributions to this paper include: (1) proposal of an empirical model to predict base infiltration measured by pan lysimeter from precipitation, using Nelder-Mead Simplex method; (2) writing of that part.

ABSTRACT

Free-drainage lysimeters, commonly used in agriculture to monitor evapotranspiration and solute transport, were installed at three highway test sites in Tennessee. The lysimeters were installed below flexible pavement systems just beneath the coarse-graded asphalt stabilized base. The lysimeters collect water infiltrating the unbound aggregate (stone base) and monitor the quantity of infiltration by diverting the flow into tipping bucket rain gages. One test site indicated infiltration beneath the longitudinal joint in the first several months of monitoring. A second test site, where the dense surface layer was not in place, indicated infiltration correlating with rainfall. Data from this site was used to develop a model to predict the measured infiltration based on the recorded rainfall. The monitoring method and modeling approach may be applicable in the investigation of pavement permeability, drainage system efficiency, and the role of infiltration in the seasonal variation of water content of unbound pavement layers.

INTRODUCTION

Daily and seasonal temperature and moisture variations in pavement systems affect the material properties of the various pavement layers and can impact the structural capacity of the pavement system. High subgrade water content, with the resulting decrease in subgrade strength and stiffness, can be detrimental to roadway performance. When pavement systems are highly saturated, heavy vehicle loads cause severe damaging actions such as erosion and pumping, disintegration of cement-treated bases, stripping of asphalt coatings from bases and subbases, and overstressing of weakened subgrades. The presence of liberal amounts of water in pavements causes or increases non-load-bearing damage such as D-cracking, blow-up, frost action, expansion, shrinkage cracking, accelerated oxidation and loss of flexibility, and general deterioration of pavements and bases (Cedergren, 1998). There is increasing concern about the long term effects of open-graded Superpave mixes and methods of quantifying the permeability of pavement systems (Cedergren, 1998; Maupin, 2000; Hall and Ng, 2000; Cooley and Brown, 2000; Choubane et al., 2000). The Federal Highway Administration (FHWA) has developed d Design methods for subsurface drainage systems usually (Cooley and Brown, 2000; Choubane et al., 2000) assume that some percentage of the rainfall intensity will infiltrate the pavement surface or joints (Cedergren et al., 1973; Moulton, 1980; Cedergren, 1974). However, there is much discussion concerning the effectiveness of current subsurface drainage design (Wyatt and Macari, 2000; Birgisson and Roberson, 2000; Mallela et al., 2000; Xiao et al., 2000). There is also much

concern about cracking and raveling along longitudinal joints due to the density gradient that results from common construction practices (Kandhal and Mallick, 1997; Buchanan, 2000). This cracking can lead to a significant source of water movement into the subgrade as well as pavement deterioration. Developing methods of monitoring the sources and movement of water in pavement systems is important for the development of effective pavement performance models, which will lead to improved drainage design, improved construction methods, and reduced life-cycle costs. Existing models for the flow of water through pavement systems, such as the Infiltration-Drainage (ID) model (Liu and Lytton, 1985), usually consider only the infiltration through cracks in the pavement system, ignoring flow through the less porous intact pavement. The ID model is a module within the Enhanced Integrated Climatic Model (EICM) (Larson and Dempsey, 1997), which includes a precipitation module (Liang and Lytton, 1989) that relies on historical precipitation data to generate precipitation. Depending upon the effectiveness of the drainage layers, the water infiltrating the pavement system in the EICM can change the water content of the subgrade soils, whichshould leads to a decrease in resilient modulus. Because of difficulties in modeling infiltration through a pavement system, changes in subgrade modulus are often assumed to occur only as a result of changes in the water table elevation, ignoring infiltration. Improvements in the measurement and modeling of the infiltration process are needed.

Free-drainage lysimeters were installed at three research sites in Tennessee as part of a comprehensive monitoring system to monitor the movement of water

in the pavement. The three sites are located in different geographic regions of the state and are referred to as the Overton County Site (middle-east), Sumner County Site (middle), and McNairy County Site (west). Each test site was located in a newly constructed fill section of roadway with a grade of 1% or less and a centerline crown of 1.5% to 2.0%. Figure A.2.1 is a typical cross section of all three sites except for the McNairy County Site, which does not include the surface and binder layers. Each site includes an open graded drainage layer and edge drains. Detailed descriptions of the test sites and monitoring systems are delineated by Rainwater et al. (Rainwater et al., 1999).

Drainage lysimeters, also called zero-tension or tension-free lysimeters, are commonly used in agricultural and environmental engineering applications to monitor evapotranspiration, percolation, and solute transport (Hillel, 1998; Wilson et al., 1991; Aboukhaled et al., 1982). Their application to highway systems is very rare. Drainage lysimeters offer an economical and simple method of estimating pavement permeability and monitoring the effectiveness of pavement drainage systems. Lysimeter data, along with meteorological and water content data, can be used to develop prediction models to quantify the movement of water in pavement systems.

The objective of this study is to evaluate the effectiveness of drainage lysimeters as a monitoring technique in pavement systems and to investigate the feasibility of using lysimeter data to develop an infiltration model for pavement system.

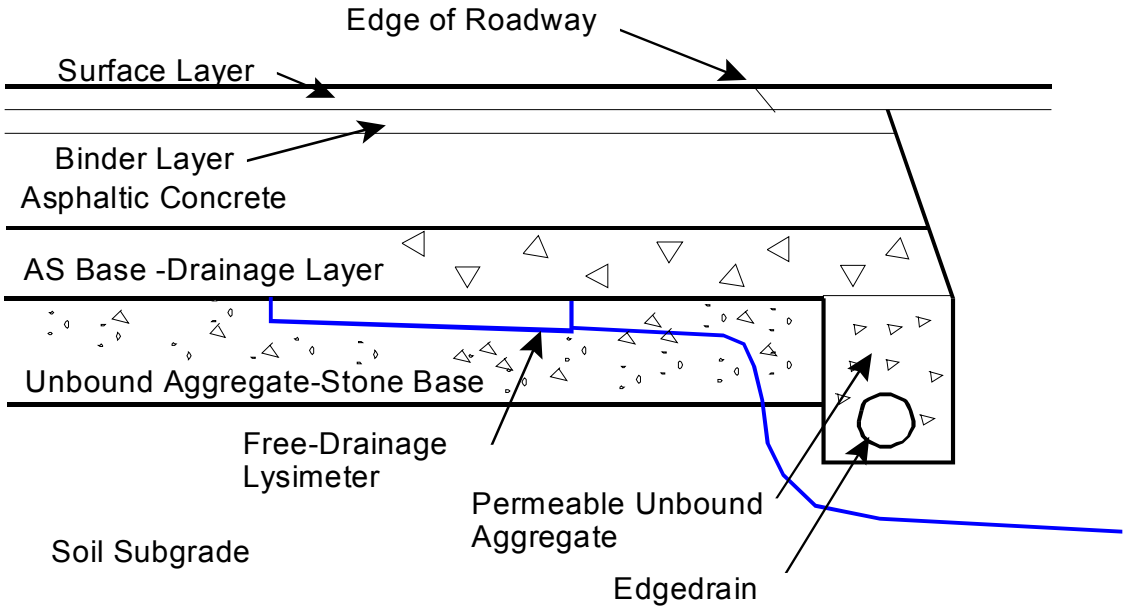

Figure A.2.1 Drainage lysimeters located in the unbound aggregate base beneath the asphalt stabilized (AS) base. Infiltration collected in the lysimeters drains to a buried vault outside the shoulder and is measured by a tipping bucket rain gage. The dense surface and binder layers were not in place at the McNairy County Site during the first 18 months of the monitoring period.

INSTRUMENTATION

Since very small infiltration amounts were expected through the new pavement, 1-m square pan lysimeters were used in this project to provide high measurement resolution, although drainage lysimeters used in agriculture are typically less than 0.5 m2. Drainage lysimeters intercept and collect free-drainage water flowing in saturated pores above the lysimeter. The lysimeters were filled and compacted with the unbound aggregate from the stone base layer to maintain hydraulic continuity with the material above the lysimeter and to be homogenous with the surrounding material. The back of each lysimeter is 76 mm deep, and the front of each lysimeter, where the outlet is located, is 102 mm

deep. The stainless steel lysimeters were fabricated and installed such that the sides are vertical, the top edge is horizontal, and the bottom slopes toward the outlet, which is covered with filter cloth to prevent fines from entering the drainage tube (Figure A.2.1). A direct measurement of infiltration is made by diverting the collected water to tipping bucket rain gages in a buried vault outside the shoulder. Two lysimeters were installed beneath the wheel path of the outside lane at each site. The Sumner County Site also includes two additional lysimeters beneath the longitudinal joint in the center of the roadway. Each pair of lysimeters was placed within 2.0 m of each other.

The lysimeters were installed in the dense layer of unbound aggregate (stone base layer) just beneath the asphalt stabilized (AS) base, drainage which is an open graded drainage layer (Figure A.2.1). Mallela et al. (2000) give three main functions of the dense graded layer of unbound aggregate: (1) to maintain separation between the permeable base and subgrade and prevent them from intermixing, (2) to form an impermeable barrier that deflects water from the permeable base horizontally toward the pavement edge, and (3) to support construction traffic and compactive effort of base and surface layers. However, at the three test sites the permeability of the stone base is greater than the soil subgrade. Although the soil subgrades at all three sites have a higher void ratio than the stone base, over 50% of the soil subgrade material passes a #200 sieve (0.075 mm)at all three sites and while only 9% to 18% of the stone base material passes a #100 sieve (0.15 mm). Therefore, the pore sizes in the soil subgrade will be much narrower and thus the hydraulic conductivity less than that of the

unbound aggregate (1998). The pavement drainage system is designed to collect any infiltrating water in the highly permeable AS base layer where it drains by gravity toward the edgedrains. As installed, the lysimeters do not directly measure vertical infiltration through the pavement, but collect water that is not successfully removed from the subgrade by the drainage system due to water that infiltrates the unbound aggregate layer. This infiltration is an indication of water that may eventually infiltrate into the soil subgrade.

Drainage lysimeters are typically less than 0.5 m2 but larger lysimeters were used in this project to improve the measurement resolution since very small infiltration amounts were expected. Tension-free lysimeters intercept and collect free-drainage water flowing in saturated pores above the lysimeter. The lysimeters were filled and compacted with the unbound aggregate to maintain hydraulic continuity with the material above the lysimeter and to be homogenous with the surrounding material. The back of each lysimeter is 76 mm deep and the front of each lysimeter, where the outlet is located, is 102 mm deep. A direct measurement of infiltration is made by diverting the collected water to tipping bucket rain gages in buried vault outside the shoulder. The Sumner County Site also includes two additional lysimeters beneath the longitudinal joint in the center of the roadway.

RESULTS AND DISCUSSION

Overton County Site

The lysimeters have not shown significant infiltration during the three-year monitoring period at the Overton County Site. The lysimeters will continue to be monitored to investigate changes in the pavement permeability with aging.

Sumner County Site

The Sumner County site includes lysimeters in the stone base layer beneath the longitudinal joint as well as the wheel path. Out of the four lysimeters at this location only one under the longitudinal joint indicates any pattern of infiltration (Figure A.2.2). This infiltration, although totaling less than 2.5 mm in five months, does correlate with rainfall events in the first few months of monitoring. The absence of infiltration after June 1998 in the same lysimeter may indicate that the joint sealed during the warm season.

McNairy County Site

At the McNairy County site, the dense surface layer and binder layer were not placed until approximately 18 months after the 0.10 m layer of asphaltic concrete. Although less permeable than the drainage layer, the asphaltic concrete layer is an asphalt treated base material using a coarser graded aggregate than the dense surface layeropen graded and is much more permeable thantypical the dense surface layer at the other two sites materials. The drainage characteristics of this site are useful for demonstrating the effectiveness of the drainage system and for modeling infiltration under pavement systems. Both

lysimeters show infiltration correlating well with rainfall until July 1999 when the surface layer was placed (Figure A.2.3). Lysimeter 1 does not show infiltration during March, April, and May of 1998 although there was substantial rainfall. This was due to a clogged rain gage funnel that was corrected in July, which resulted in the collected water being released as indicated by theexcessive infiltration reading in July datawhen the trapped water was released. The data indicate that under permeable pavement the drainage system losses efficiency.

Modeling Base Infiltration

A model was developed to predict the measured infiltration based on the recorded precipitation at the McNairy County site. The purpose of this model is to predict, on the basis of a given precipitation event, the amount of water that would infiltrate into the stone base and eventually into the soil subgrade. It

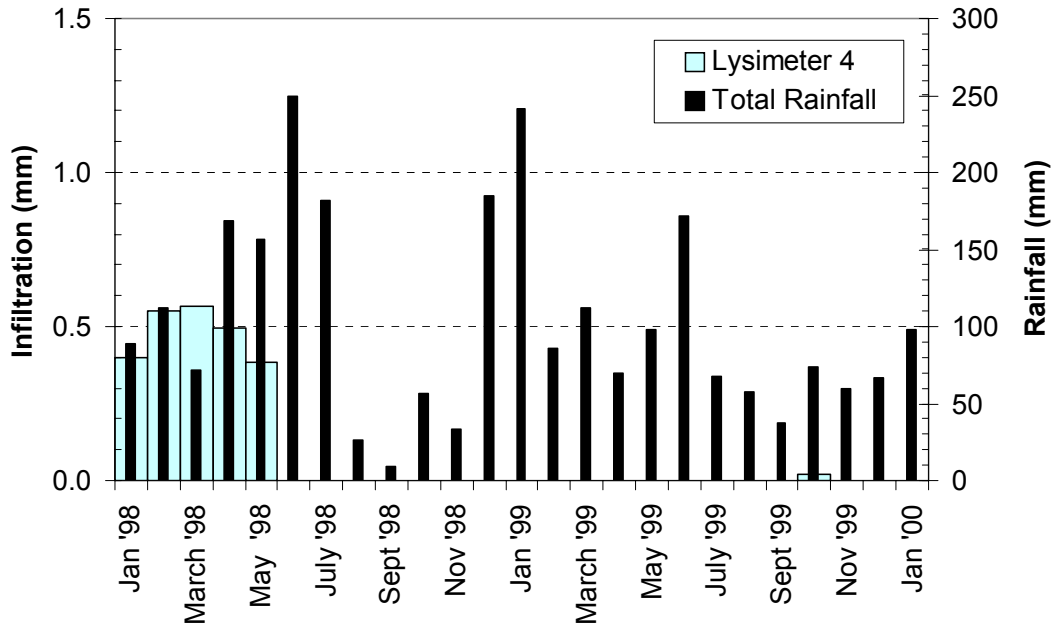

Figure A.2.2 One of the lysimeters under the longitudinal joint at the Sumner

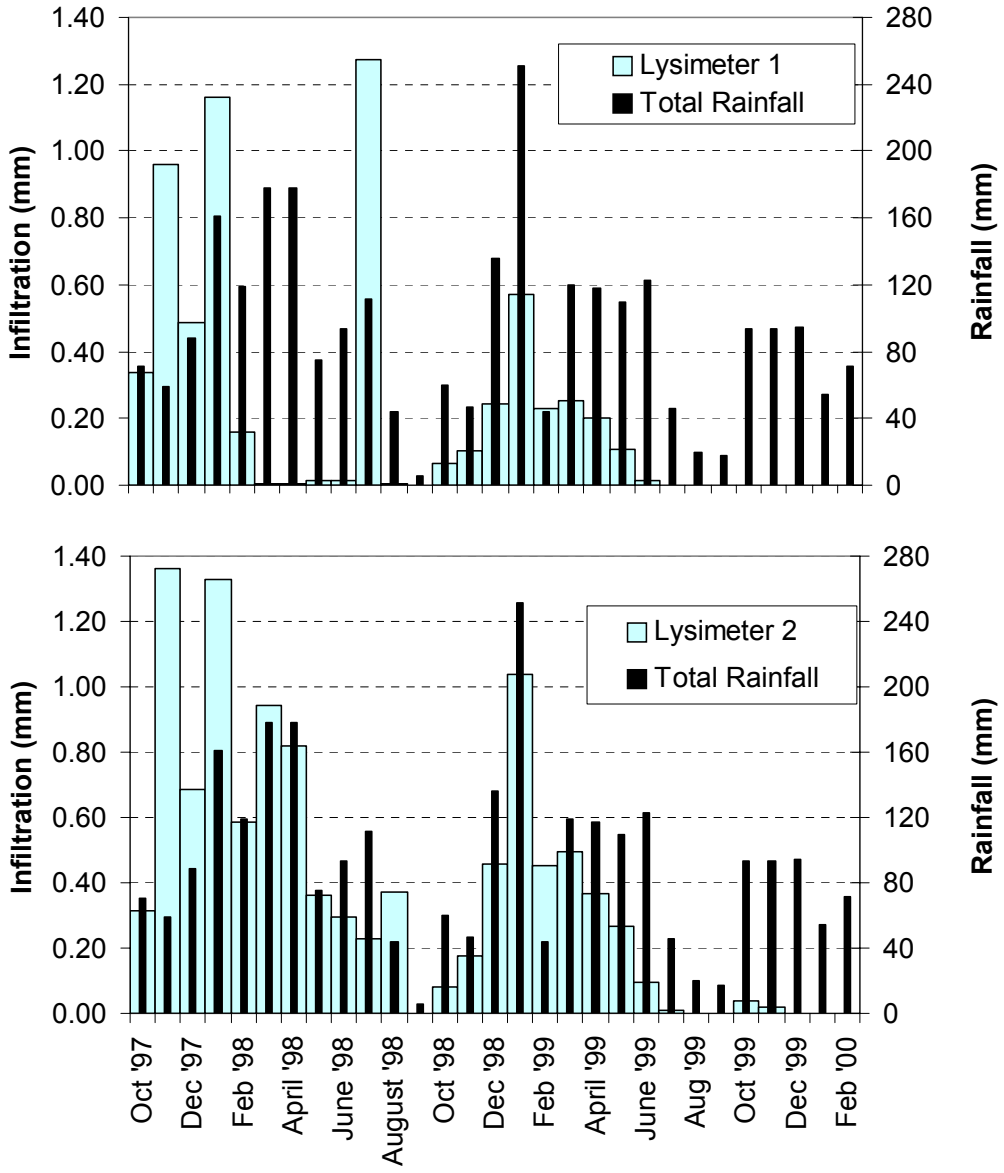

Figure A.2.3 Both lysimeters at the McNairy County Site indicated infiltration prior to placement of the surface layer July 1999.

should be noted that the pavement section did not have the final surface layer in place during the modeling period, resulting in a permeability that was greater than that typically expected for a completed pavement system. However, the somewhat enhanced permeability allows a verification of the lysimeter method for measuring infiltration through intact pavement and provides a good test case for the modeling procedure. The enhanced permeability may be more comparable to open-graded Superpave asphalt that is becoming more common in highway construction. If successful, the monitoring and modeling method may have other applications in highway engineering.

The infiltration following precipitation events was measured by the pan lysimeter several days after the rainfall ceased (Figure A.2.4). The maximum time lag between the end of the precipitation event and the measured infiltration was about 10 days and followed the rainfall on Day 495. Because of the marked difference in the duration of the precipitation and the duration of the corresponding infiltration, the linear regression method would not provide a good correlation between the infiltration and the rainfall. It is noted that the infiltration in Figure A.2.4 starts at about the same day as the rainfall, increases for a few days, then decays gradually following a bell-shaped pattern. Both the duration of the infiltration and the peak value of the infiltration appear to be related to the rainfall intensity, provided that the rainfall intensity is within a given range. A rainfall with an intensity lower than this range only wets the surface of the pavement and, due to evaporation, is not likely to result in any infiltration; a rainfall with an intensity higher than this range is not likely to increase the

infiltration, since surplus rainfall only increases the surface runoff. Because the infiltration is thought to be dependent on the rainfall intensity only with in a given range, the term total effective rainfall will be used to describe the intensity range of rainfall that is effective in infiltrating the pavement.

The following function is chosen to represent the bell-shaped intensity function, as shown in Figure A.2.5.

$$f(x) = Fy \cdot N(\frac{x - Fx}{Fx}, 1, 1) \quad (x \geq 0) \qquad \text{(A-2-1)}$$

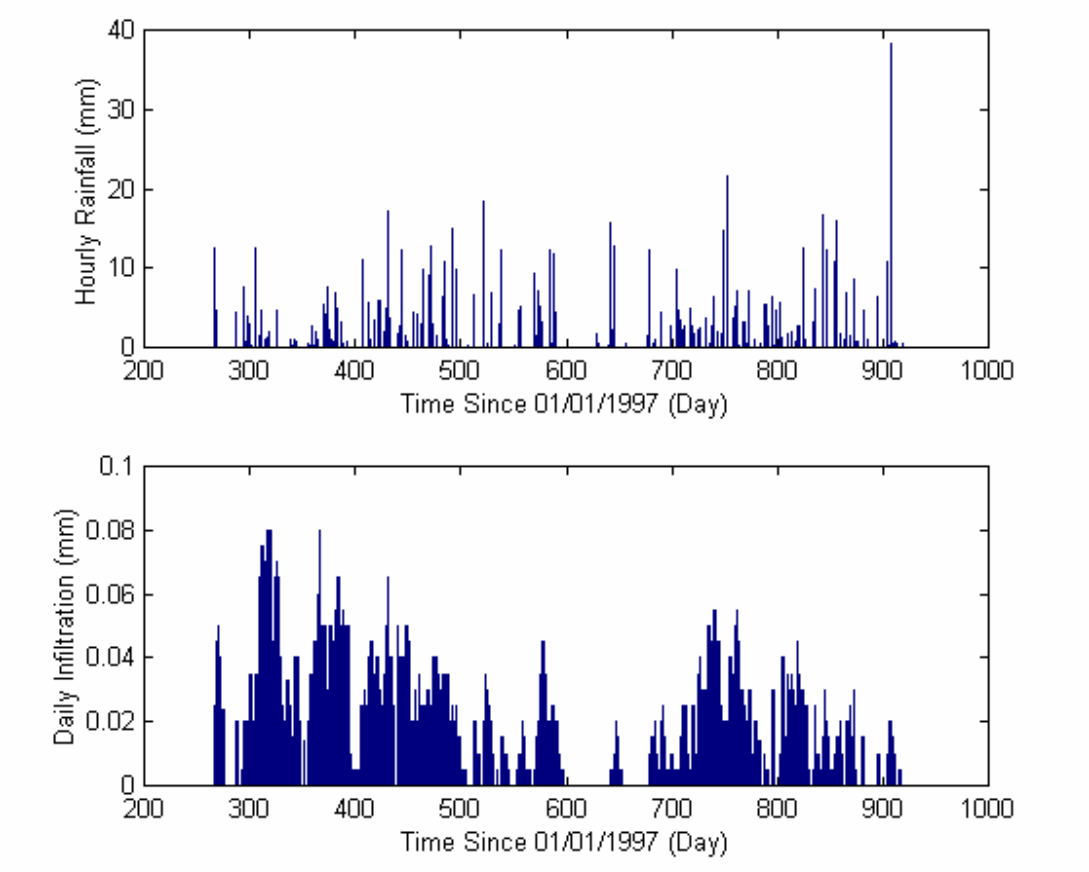

Figure A.2.4 Hourly rainfall and daily infiltration in lysimeter 2 at the McNairy County Site.

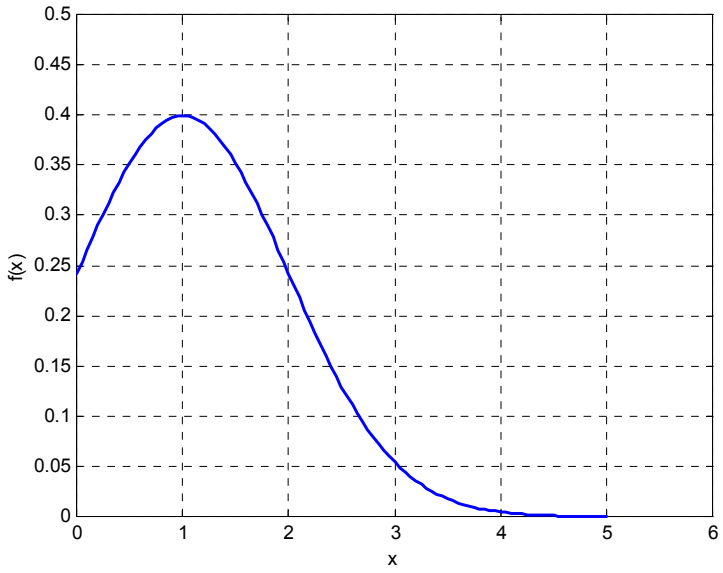

Figure A.2.5 The bell-shaped intensity function represented by equation 1.

where $N(X,1,1)$ = Probability density function (pdf) of standard normal distribution, i.e., both the mean and standard deviation equal to 1.

Fx and Fy = Constants.

Constants Fx and Fy are scaling factors applied to the probability density function for the standard normal distribution. A set of similar curves can be obtained by varying Fx and Fy as shown in Figure A.2.6, where the amount of infiltration is the area under the curve. It is assumed that the curve describing the infiltration versus time for each rainfall event is of the same functional form and aspect ratio as shown in Figure A.2.5, but the total infiltration, or area under the curve, depends upon the total effective rainfall. For example, if the total effective rainfall of a given rainfall event is doubled, both the duration and the

peak of the infiltration intensity will be increased by the same proportion, such that the area under the curve is doubled. In that case, the scale factors are assumed to be $Fx = Fy = \sqrt{2} = 1.414$. This is illustrated in Figure A.2.6. The area under the curves b, c, and d are all equal and twice as great as that under curve a, but only curve d maintains the same aspect ratio as curve a.

Total effective rainfall, $R_{h\_Eff.}$, for each hour is calculated in this way:

$$R_{h\_Eff.} = \begin{cases} 0 & , R_{h\_Measured} < R_{h\_Lower} \\ R_{h\_Measured} & , R_{h\_Lower} \le R_{h\_Measured} \le R_{h\_Upper} \\ R_{h\_Upper} & , R_{h\_Measured} > R_{h\_Upper} \end{cases} \qquad \text{(A-2-2)}$$

where $R_{h\_Measured}$ Measured hourly rainfall;

R_{h_Lower} Lower limit of rainfall intensity;

R_{h_Upper} Upper limit of rainfall intensity.

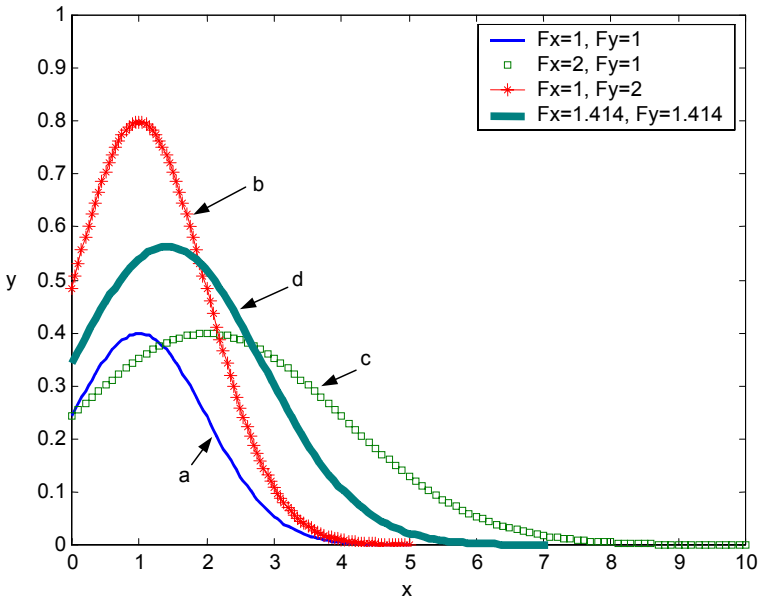

Figure A.2.6 Bell-shaped curves resulting from different duration factors (Fx) and peak factors (Fy) in equation 1.

Effective rainfalls within a 24 hour period are grouped into one rainfall event, and the total amount of rainfall for one event is considered to occur on the day this rainfall event begins. According to the assumptions above, the infiltration can be modeled by the following equation,

$$I_j = K \cdot \sum_{i=1}^{n} N\left(\frac{j - r_i}{\sqrt{R_i}} \cdot a,1,1 \right) \cdot \sqrt{R_i} \qquad \text{(A-2-3)}$$

where I_j = Infiltration measured by the pan lysimeter on day j;

K = Constant;

r_i = The ith rainfall event;

n = Number of rainfall events within 10 days before day j;

N = Probability density function of the normal distribution;

a = Constant that controls the duration of infiltration;

R_i = Total effective rainfall of the r_i th rainfall event.

The model was developed based on the data shown in Figure A.2.4. The data recorded after Day 600 were used as training data, and the data recorded before Day 600 were used as testing data. All the modeling was based on the training set, and the testing set was used to verify the model. The Nelder-Mead simplex method (MATLAB, 1999) was used to find the best solution for this problem, in which the input variables are lower and upper limits of rainfall intensity and constants a and K. The object function is the root mean square error between the predicted and measured infiltration. Although the error between the predicted

and measured infiltration was minimized, the solution frequently converged to an unreasonable result. The following procedure was found to yield a satisfactory solution:

assume values for the lower and upper limits of the rainfall intensity;

vary the initial value of the constant a such that the Nelder-Mead simplex method finds the value of constant a that maximizes the correlation coefficient between the measured and predicted infiltration, such that the predicted infiltration has a similar pattern as the measured infiltration;

constant K is solved by equating the total calculated infiltration with the total measured infiltration;

repeat with different combination of lower and upper limits of the rainfall intensity.

Different initial values of the constant a, i.e., 0, 1, 2, 5, 10, and 20 were used in the Nelder-Mead Simplex Method, together with the following lower and upper limits of rainfall intensity,

Lower limit: 0, 0.1, 0.2, ... , 1 (mm/hour);

Upper limit: 1, 2, ... , 38 (mm/hour).

This modeling process produced 2508 results of a, of which 175 turned out to be unreasonable negative values. For all other positive values of a, two consistent trends existed in the results.

1. For a fixed lower limit of rainfall intensity and as the upper limit of rainfall intensity increased, the correlation coefficient between the measured and predicted infiltration decreased, and the root mean square error between the

measured and predicted infiltration increased. This suggests that the upper limit of rainfall intensity should be as low as 1 mm/hour.

2. For a fixed upper limit of rainfall intensity, the correlation coefficient increased as the lower limit of rainfall intensity increased until the lower limit reached 0.4 mm/hour after which the correlation coefficient decreased.

Thus, the following parameters yielded results with the minimum amount of error:

Lower limit of rainfall intensity = 0.4 (mm/hour)

Upper limit of rainfall intensity = 1.0 (mm/hour)

Constant a = 1.42

Constant K = 2964.72

Further investigation showed that for a lower limit of 0.4 mm/hour, the variation of upper limit from 1 to 0.4 mm/hour only affected the RMSE and correlation coefficient by less than 1%. This indicates that the limits of rainfall intensity can be reduced to a single value, the critical rainfall intensity. Rainfall intensity lower than this value will not result in any infiltration, while rainfall intensity higher than this value does not affect the amount of water infiltrating the pavement. This critical intensity could be affected by the hydraulic conductivity of the surface layer and the roughness and slope of the pavement surface. For McNairy County site, this critical rainfall intensity is 0.4 mm/hour.

The predicted infiltration and the measured training infiltration data are shown with the rainfall data in Figure A.2.7. Figure A.2.8 is similar but is shown for the

testing data. The correlation coefficients between the measured and predicted infiltration for training data and testing data are 69% and 54%, respectively.

Although Figure A.2.7 and Figure A.2.8 suggest that the predicted infiltration over time correlate well with the measured infiltration, the actual predicted infiltration values are low. This could be related to the fact that the solution process (step 2) emphasized the pattern of infiltration, or that the lysimeter drain tube has a finite storage capacity. An obvious discrepancy exists between the predicted and measured infiltration between Day 300 and Day 350, during which, a small amount of rainfall resulted in a high infiltration measurement. This abnormally high infiltration is believed to be water released from a sag in the drain tube when the tube was straightened and secured as described earlier. If this questionable data is not included, the correlation coefficient can be increased to 67%. Although the prediction is not outstanding, the method shows promise in the correlation between rainfall and infiltration.

The lysimeters are located just beneath the drainage layer and collect water that is not removed from the subgrade but infiltrates the unbound aggregate base.

CONCLUSIONS AND RECOMMENDATIONS

Free-drainage lysimeters are an effective method of monitoring the sources and movement of water in pavement systems. Lysimeters are an inexpensive method of monitoring infiltration through permeable pavements or collecting water moving through the drainage layer. The installation of drainage lysimeters is labor intensive, especially if installed in asphalt layers.

The longitudinal joint may be a source of infiltration, and long term monitoring of water movement under the longitudinal joint will be important.

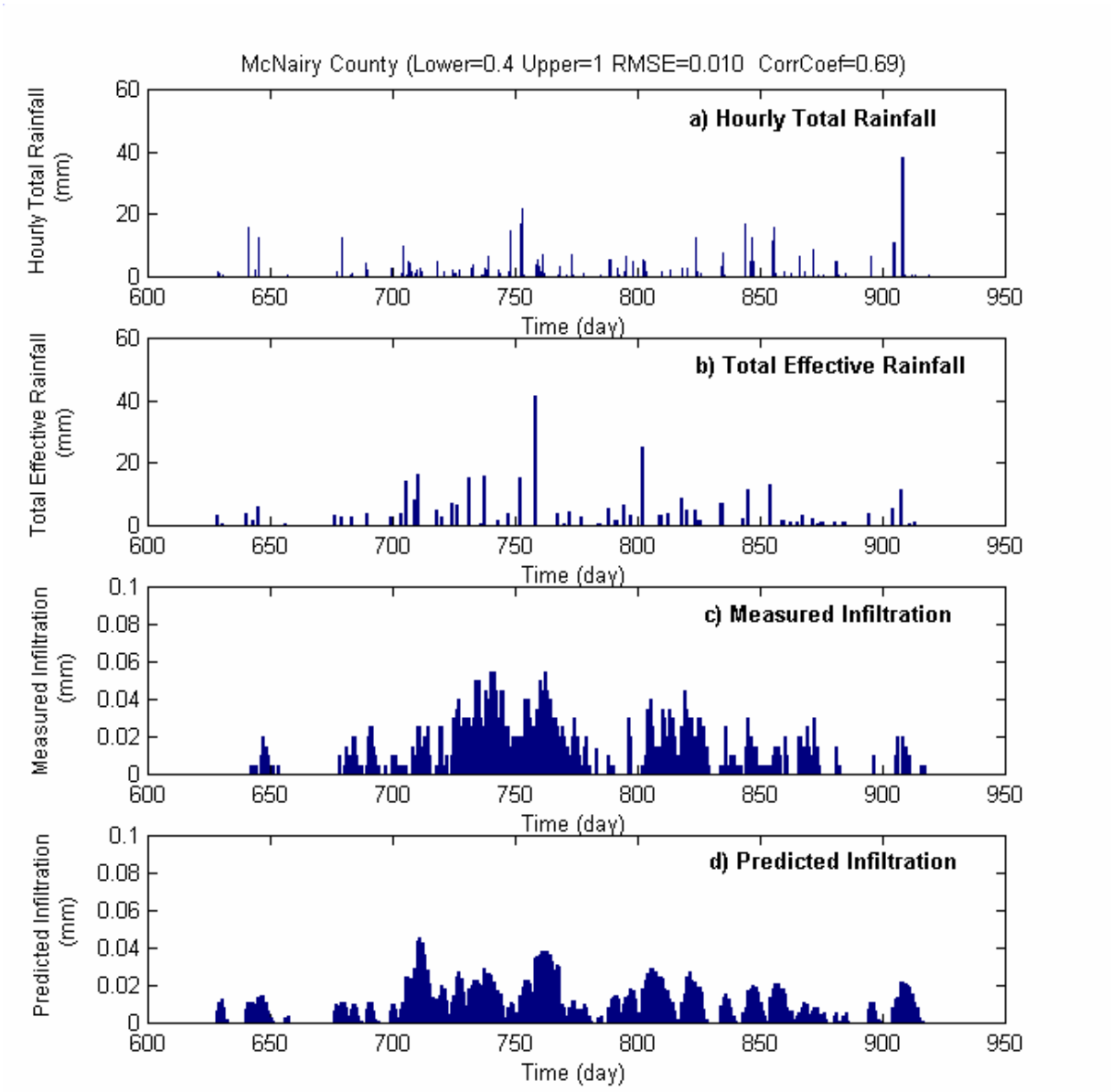

Figure A.2.7 The predicted infiltration, measured training data, and rainfall for the McNairy County Site.

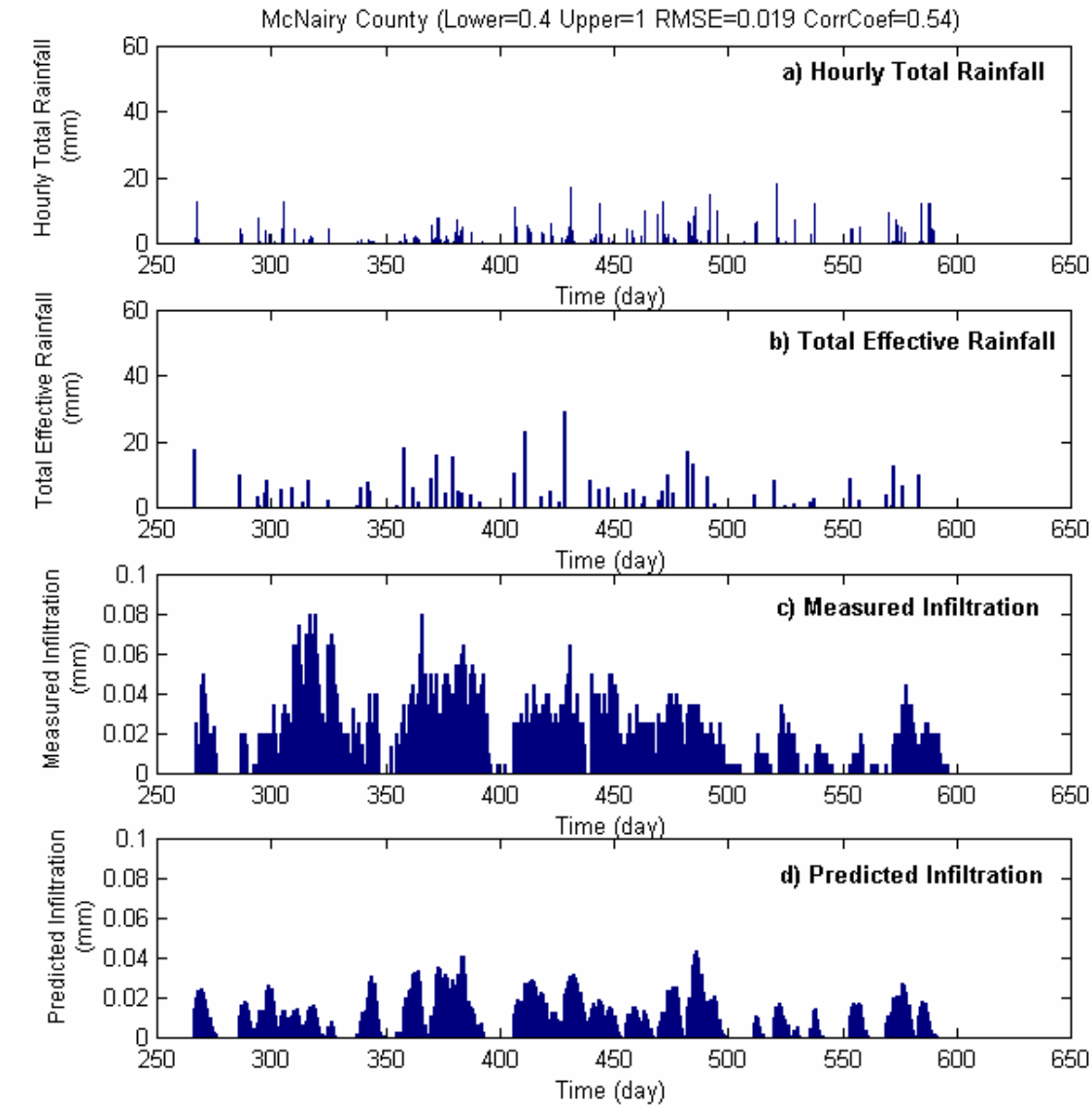

Figure A.2.8 The predicted infiltration, measured test data, and rainfall for the McNairy County Site.

The Nelder-Mead simplex method was utilized to develop a model to predict the water infiltrating the pavement system based on the measured rainfall intensity. The model parameters were developed from a set of training data and resulted in a correlation coefficient of 67% when used on an independent set of test data. Although tThe instrumentation and modeling techniques were demonstrated on a new pavement system with a permeability that was larger than that expected for most new pavements. However, the effects of discontinuities such as cracks and joints are likely to increase permeability of a pavement system with age and deterioration of the pavement.

The permeability of most pavements increases with aging and cracking. The described instrumentation system and modeling approach may be applicable for the investigation of

- the role of infiltration in the seasonal variation of the water content of unbound pavement layers.,
- the investigation of the permeability of open-graded Superpave asphalt,
- and the effectiveness of highway drainage systems.,
- the effects of pavement deterioration on the permeability of a pavement system.

ACKNOWLEDGMENT

The authors are grateful for the support provided by the Tennessee Department of Transportation-Design Division, and The Materials and Tests Division, Nashville, Tennessee.

REFERENCES

Aboukhaled, A., A. Alfaro, and M. Smith. Lysimeters. Food and Agriculture Organization of the United Nations, Rome, 1982.

Birgisson, B. and R. Roberson. Drainage of Pavement Base Material: Design and Construction Issues, Proceedings 79th Annual Meeting of the Transportation Research Board (PREPRINT CD-ROM), National Research Council, Washington D.C., January 9-13, 2000.

Buchanan, M.S. An Evaluation of Notched Wedge Longitudinal Joint Construction. Proceedings 79th Annual Meeting of the Transportation Research Board (PREPRINT CD-ROM), National Research Council, Washington D.C., January 9-13, 2000.

Cedergren, H.R., J.A. Arman, and K.H. O'Brien. Development of Guidelines for the Design of Subsurface Drainage Systems for Highway Pavement Structural Sections, Report No. FHWA-RD-73-14, Federal Highway Administration, Washington, D. C., 1973.

Cedergren, H.R. Drainage of Highway and Airfield Pavements. John Wiley & Sons, New York, 1974.

Cedergren, H.R. Why All Important Pavements Should be Well Drained. Transportation Research Record 1188, TRB, National Research Council, Washington D.C., 1988, pp. 56-72.

Choubane, B., J.A. Musselman, G.C. Page. Investigation of Water Permeability of Coarse Graded Superpave Pavements. Journal of the Association of Asphalt Paving Technologists V67, Association of Asphalt Paving Technologists, St Paul, MN, 1998, pp. 254-276

Cooley, L.A. Jr., and E.R. Brown. Selection and Evaluation of a Field Permeability Device for Asphalt Pavements. Proceedings 79th Annual Meeting of the Transportation Research Board (PREPRINT CD-ROM), National Research Council, Washington D.C., January 9-13, 2000.

Hall, K.D., J. Cruz, and Hooi Ng. Effects of Testing Time and Confining Pressure on Falling-Head Permeability Tests of Hot-Mix Asphalt Concrete. Proceedings 79th Annual Meeting of the Transportation Research Board (PREPRINT CD-ROM), National Research Council, Washington D.C., January 9-13, 2000.

Hillel, D. Environmental Soil Physics. Academic Press, San Diego, CA, 1998.

Kandhal, P.S., and R.B. Mallick. Longitudinal Joint Construction Techniques for Pavements. NCAT Report No. 97-4, National Center for Asphalt Technology of Auburn University, August 1997.

Larson, G. and B.J. Dempsey. Enhanced Integrated Climatic Model Version 2.0, Final Report Contract DTFA MN/DOT 72114, October 1997.

Liang, H.S. and R.L. Lytton. Rainfall Estimation for Pavement Analysis and Design. Transportation Research Record 1252, TRB, National Research Council, Washington D.C., 1989, pp. 42-49.

Liu, S.J. and R.L. Lytton. Environmental Effects on Pavement-Drainage, Volume IV, FHWA Report FHWA-DTFH-61-87-C-00057, Federal Highway Administration, Washington, D.C. 1985.

Mallela, J., L. Titus-Glover, and M.I. Darter. Considerations for Providing Subsurface Drainage in Jointed Concrete Pavements. Proceedings 79th Annual Meeting of the Transportation Research Board (PREPRINT CD-ROM), National Research Council, Washington D.C., January 9-13, 2000.

MATLAB® Version 5.3, The Math Works Inc., 1999.

Maupin, G.W. Jr. Asphalt Permeability Testing in Virginia. Proceedings 79th Annual Meeting of the Transportation Research Board (PREPRINT CD-ROM), National Research Council, Washington D.C., January 9-13, 2000.

Moulton, L.K. Highway Subdrainage Design, Report No. FHWA-TS-80-224, Federal Highway Administration, Washington, D. C., 1980.

Rainwater, N.R., R.E. Yoder, E.C. Drumm, and G.V. Wilson. Comprehensive Monitoring Systems for Measuring Subgrade Moisture Conditions, Journal of Transportation Engineering, Vol.125, No. 5, September/October 1999.

Wilson, G.V., P.M. Jardine, R.J. Luxmoore, L.W. Zelazny, D.A. Lietzke, and D.E. Todd. Hydrogeochemical Processes Controlling Subsurface Transport from an Upper Subcatchment of Walker Branch Watershed During Storm Events. 1. Hydrologic Transport processes. Journal of Hydrology, Vol. 123, 1991, pp. 297-316.

Wyatt, T.R., and E.J. Macari. Effective Analysis of Subsurface Drainage Features based on Design Adequacy. Proceedings 79th Annual Meeting of the Transportation Research Board (PREPRINT CD-ROM), National Research Council, Washington D.C., January 9-13, 2000.

Xiao, Ming, Lakshmi N. Reddi, and Mohan V. S. Bonala, Impact of Fine Particle Entrapment on the Performance of Subsurface Pavement Drainage Systems. Proceedings 79th Annual Meeting of the Transportation Research Board

(PREPRINT CD-ROM), National Research Council, Washington D.C., January 9-13, 2000.

Appendix III Comparison of In Situ Temperature Measurements with BELLS3 Prediction

Asphalt concrete (AC) temperatures measured by thermometers installed at different depths of the AC layer at the Blount County site were compared with the temperature predicted by BELLS3 equation (A-3-1). This comparison was performed as a simple verification of the insitu measured temperatures. BELLS3 equation was developed with data from the Long-Term Pavement Performance (LTPP) program's Seasonal Monitoring Program (Lukanen et al., 2000). The application of BELLS model to the TDOT pavement data has also been described by Marshall et al., 2001).

$$T_d = 0.95 + 0.892T_s + (\log d - 1.25)\left[1.83\sin\left(2\pi\frac{A}{18}\right) - 0.448T_s + 0.621T_{avg}\right] + 0.042T_s \sin\left(2\pi\frac{B}{18}\right) \quad \text{(A-3-1)}$$

where

T_d = pavement temperature at layer mid-depth (°C),

T_s = infrared surface temperature (°C),

T_{avg} = average of high and low air temperatures on the day before testing (°C),

d = layer mid-depth (mm)

$$A = \begin{cases} t_d + 9.5 & \text{if} \quad 0 \le t_d < 5 \\ -4.5 & \text{if} \quad 5 \le t_d < 11 \\ t_d - 15.5 & \text{if} \quad 11 \le t_d < 24 \end{cases}$$

$$B = \begin{cases} t_d + 9.5 & \text{if} \quad 0 \le t_d < 3 \\ -4.5 & \text{if} \quad 3 \le t_d < 9 \\ t_d - 13.5 & \text{if} \quad 9 \le t_d < 24 \end{cases}$$

t_d = time of day (in decimal hours).

At the Blount County site, AC temperature data were collected from three thermistors installed at 51 mm, 102 mm, and 153 mm below pavement surface, respectively. The data collected in 2000 and 2001 using new thermistors were used in the comparison. The temperature measured by the thermistor 51 mm below pavement surface was assumed to be the pavement surface temperature (T_s).The temperatures measured by the other two thermistors were predicted as mid-depth temperatures using BELLS3 equation (A-3-1). Layer mid-depths (d) used in the prediction were 51 mm and 102 mm, respectively, which were the distance between the depths of the thermistor 51 mm below pavement surface and the other two thermistors. The errors between the measured temperatures and the predicted temperatures are shown in Figure A.3.1 and Figure A.3.2. The histograms of the error follow normal distributions with non-zero means which indicate that the BELLS3 model underestimates the measured mid-depth temperature by an average of 2 and 4 $^{\circ}C$ for the temperature measured by the thermistors 102 mm and 153 mm below the pavement surface.

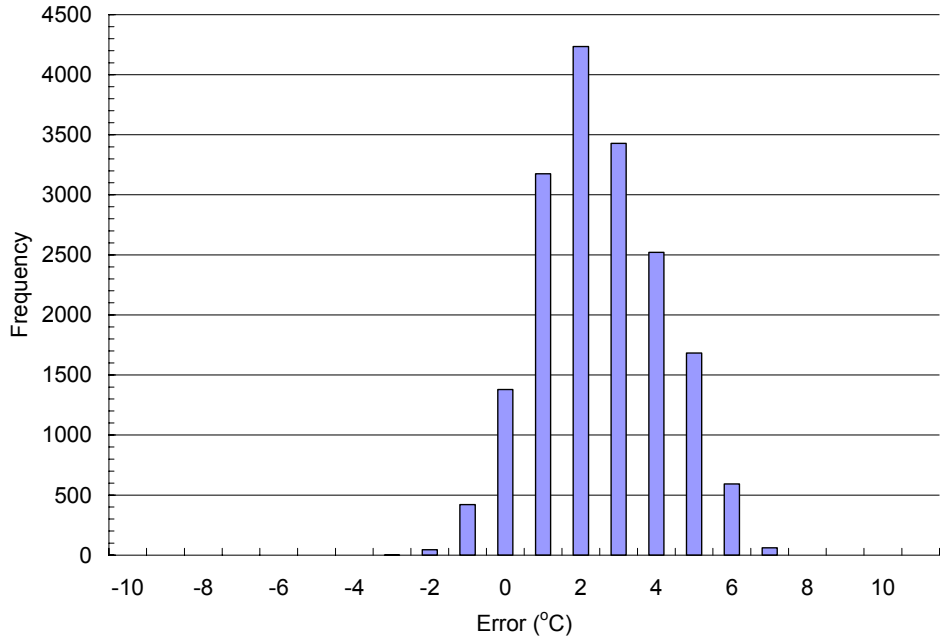

Figure A.3.1 Histogram of Error between Measured and Predicted AC Temperature 102 mm below Pavement Surface

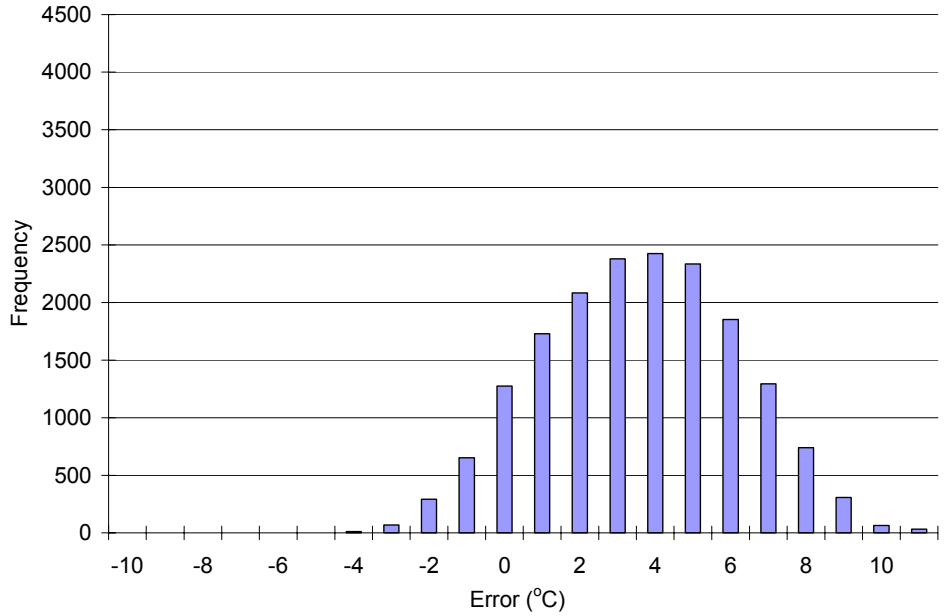

Figure A.3.2 Histogram of Error between Measured and Predicted AC Temperature 151 mm below Pavement Surface

Similar to Marshall et al. (2001), there are two possible explanations for this underestimation. 1) Difference in temperature measuring equipment: pavement surface temperature used in BELLS3 model should be measured by infrared thermometers, while in this comparison the temperatures were measured by thermistors installed 51 mm below the pavement surface, in the AC layer. 2) BELLS3 equation presumes 1 minute of shading before measurement of the surface temperature, which could lower the surface temperature by as much as 2 ^{o}C.

Furthermore, BELLS3 equations are based on daytime surface temperature data; therefore, the daytime temperature prediction is good, while the nighttime temperature prediction may be problematic. A reasonable match between measured and predicted AC temperature profiles for the highest AC temperature measured at the Blount County site is shown in Figure A.3.3. In the same graph, a comparison of measured and predicted AC temperature profiles with the largest prediction error is shown, which is from the data on a summer night while the surface of the pavement was cooled down but the AC temperature at greater depth was still high. BELLS3 equation does not predict this negative temperature profile very well.

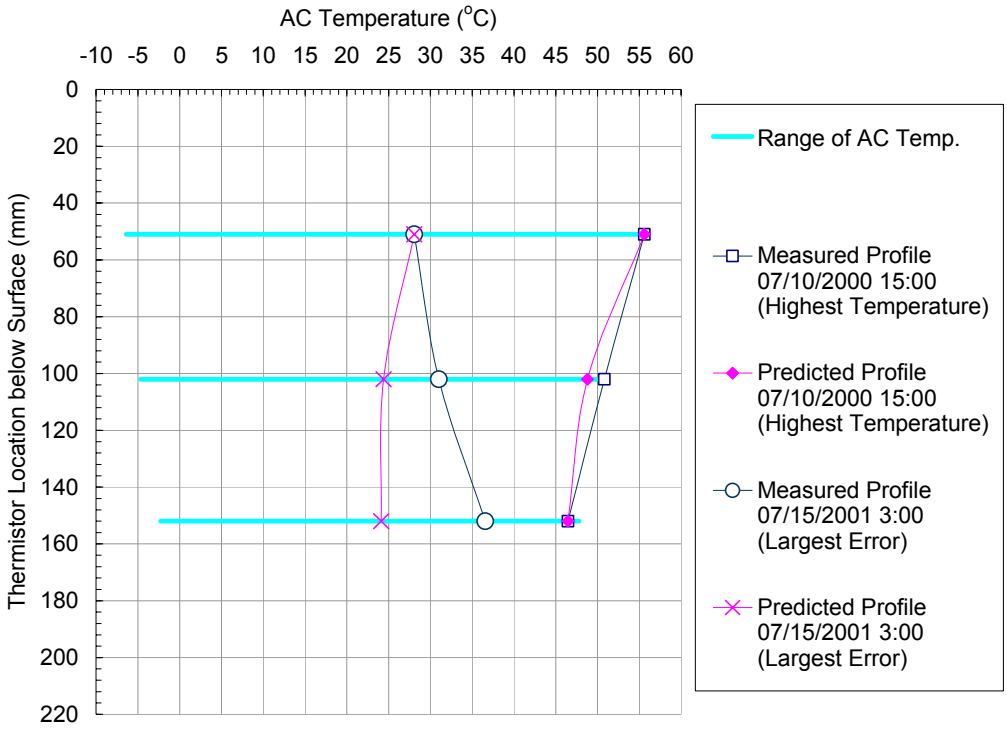

Figure A.3.3 Comparison of Measured and Predicted AC Temperature Profile

References

Lukanen, Erland O., R. Stubstad, and Robert C. Briggs (2000) *Temperature Predictions and Adjustment Factors for Asphalt Pavements*. Report FHWA-RD-98-085. Federal Highway Administration.

Marshall, C., R. W. Meier, and M. Welsh (2001) Seasonal Temperature Effects on Flexible Pavements in Tennessee. In *Transportation Research Record 1764*, TRB, National Research Council, Washington, D.C., pp. 89-96.

Appendix IV UMAT Source Code for Uzan's Resilient Modulus Model

This file was modified from the source code in the following dissertation:

Taciroglu, E. (1998) *Constitutive Modeling of the Resilient Response of Granular Solids*. A Dissertation Submitted for Fulfillment of the Degree of Doctor of Philosophy, University of Illinois, Urbana. Urbana, IL.

```
      subroutine umat (stress, statev, ddsdde,
     &           sse, spd, scd, rpl, ddsddt, drplde,
     &           drpldt, stran, dstran, time,
     &           dtime, temp, dtemp, predef, dpred,
     &           cmname, ndi, nshr, ntens, nstatv,
     &           props, nprops, coords, drot,
     &           pnewdt, celent,dfgrd0, dfgrd1, noel,
     &           npt, layer, kspt, kstep, kinc )

      include 'ABA_PARAM.INC'

c  Argument variables

      character*8 cmname
      dimension stress(ntens), statev(nstatv),
     &          ddsdde(ntens, ntens),
     &          ddsddt(ntens), drplde(ntens),
     &          stran(ntens), dstran(ntens), time(2),
     &          predef(*), dpred(*),
     &          props(nprops), coords(3), drot(3, 3),
     &          dfgrd0(3, 3), dfgrd1(3, 3)

c  Local variables

      dimension tot_stran(ntens)
      logical   singular

c  Unnamed common block for storing <c_bar> values
      dimension c_bar_old(50000,8,1)
      common c_bar_old

c  **PROLOGUE******UZAN MODEL for SOLID AXY AND PSTN LEMENTS***********
c  *                                                                  *
c  *   ABAQUS stress & strain notation:                               *
c  *                                                                  *
c  *          stress(1) = S11 = Srr   stran(1) = E11  = Err           *
c  *          stress(2) = S22 = Szz   stran(2) = E22  = Ezz           *
c  *          stress(3) = S33 = Soo   stran(3) = E23  = Eoo           *
c  *          stress(4) = S12 = Srz   stran(4) = 2 * E12 = Erz        *
c  *          stress(5) = S13 = Sro   stran(5) = 2 * E13 = Ero        *
c  *          stress(6) = S23         stran(6) = 2 * E23              *
c  *                                                                  *
c  *                                                                  *
c  *   MATERIAL MODEL DESCRIPTION:                                    *
c  *                                                                  *
c  *      Let [S] denote stress tensor   (3x3)                        *
c  *          [E] denote strain tensor   (3x3)                        *
c  *          [I] denote identity tensor (3x3)                        *
```

```
c  *                                                                     *
c  *                                                                     *
c  *------Then constitutive relationship is given by,                    *
c  *                                                                     *
c  *          [S] = c_bar * [ alpha  * tr[E] * [I] + [E] ]               *
c  *          Sij = c_bar * [ alpha  * tr[E] * dij + Eij ]               *
c  *                                                                     *
c  *      where,                                                         *
c  *         dij: Kronecker delta ( 1 if i=j , 0 if i/=j )               *
c  *                                                                     *
c  *          Mr: Resilient Modulus => <res_mod>                         *
c  *                                                                     *
c  *       c_bar = res_mod / (1 + dnu)                                   *
c  *                                                                     *
c  *              Mr =  dk * abs(theta)^dn  * (TAUoct)^dm                *
c  *                                                                     *
c  *      NOTE!!! : in this version the resilient modulus                *
c  *                is given by the above equation, where                *
c  *                <theta> is the volumetric stress i.e.                *
c  *                 theta = S11 + S22 + S33, not(!) the                 *
c  *                mean volumetric stress, i.e. <theta/3>               *
c  *                given in the reference paper.                        *
c  *                                                                     *
c  *           c_bar = {dk_bar * alpha_bar^dn * (abs(tr[E]))^dn          *
c  *                                    *  (gamma_oct)^dm }^ dmu         *
c  *                                                                     *
c  *             dk_bar = dk / (1 +dnu)                                  *
c  *                                                                     *
c  *         dnu: Poisson's Ratio => <props(1)>                          *
c  *                                                                     *
c  *          dk: Material param. => <props(2)>                          *
c  *                                                                     *
c  *          dn: Material param. => <props(3)>                          *
c  *                                                                     *
c  *          dm: Material param. => <props(4)>                          *
c  *                                                                     *
c  *           E: Young's Modulus => <props(5)>                          *
c  *                                                                     *
c  *        damp: Damping factor  => <props(6)>                          *
c  *                                                                     *
c  *      switch: Secant Switch   => <props(7)>                          *
c  *                                                                     *
c  *               switch =  0. => use secant matrix                     *
c  *               switch =/ 0. => use tangent matrix                    *
c  *                                                                     *
c  *       alpha: dnu / (1 - 2dnu)                                       *
c  *                                                                     *
c  *   alpha_bar: (1 + dnu) / (1 - 2dnu)                                 *
c  *                                                                     *
c  *         dmu: 1 / (1 - dn - dm)                                      *
c  *                                                                     *
c  *    singular: a logical flag to mark singularity                     *
c  *                                                                     *
c  *       tr[E]: 1st invariant of E => <treps>                          *
c  *              tr[E] = Err + Ezz + Eoo                                *
```

```
c  *                                                                     *
c  *       theta: 1st invariant of stress tensor                         *
c  *              theta = Srr + Szz + Soo                                *
c  *                                                                     *
c  *      TAUoct: Octahedral shear stress (also an invariant)            *
c  *              TAUoct = {(1/3) * tr[Sd*Sd]} ^ 0.5                     *
c  *                                                                     *
c  *   gamma_oct: Octahedral shear strain                                *
c  *              (also an invariant)   => <gamma_oct>                   *
c  *              gamma_oct = {(1/3) * tr[Ed*Ed]} ^ 0.5                  *
c  *                                                                     *
c  *        [Sd]: Deviatoric stress tensor                               *
c  *              [Sd] = [S] - 1/3 theta [I]                             *
c  *                                                                     *
c  *        [Ed]: Deviatoric strain tensor                               *
c  *              [Ed] = [E] - 1/3 tr[E] [I]                             *
c  *                                                                     *
c  *                                                                     *
c  *------Material tangent stiffness [C]                                *
c  *                                                                     *
c  *            C     = d([S]) / d([E])                                  *
c  *            Cijkl = d([Sij]) / d([Ekl])                            *
c  *                                                                     *
c  *      thus, with summation implied over repeated                     *
c  *            indices, i;j;k;l = {1,2,3}                             *
c  *                                                                     *
c  *            Sij = Cijkl Ekl                                        *
c  *                                                                     *
c  *            Cijkl =  c_bar { dik * djl                             *
c  *                     +  A dij * dkl                                 *
c  *                     +  B Eij * dkl                                 *
c  *                     +  C dij * Ekl                                 *
c  *                     +  D Eij * Ekl }                               *
c  *                                                                     *
c  *      where,                                                         *
c  *            A = alpha * ( dmu * x + 1)                             *
c  *            C = D * alpha * (tr[E])                                *
c  *            D = dmu * dm / (3*gamma_oct^2)                         *
c  *            B = dmu * x / (tr[E])                                  *
c  *            x = dn - dm * ( tr[E]/ 3gamma_oct) ^2                  *
c  *                                                                     *
c  *      Or in matrix notation,                                         *
c  *                                                                     *
c  *            vec(S) = mat(C) * vec(E)                               *
c  *                                                                     *
c  *      where,                                                         *
c  *            vec(S): Stress vector => <stress>                      *
c  *            vec(E): Strain vector => <tot_stran>                   *
c  *            mat(C): Material tnagent dtiffness matrix => <ddsdde>  *
c  *                                                                     *
c  *                                                                     *
c  *                              1   1   1    0   0   0                *
c  *                              1   1   1    0   0   0                *
c  *                              1   1   1    0   0   0                *
c  *            mat(dijdkl) =                                          *
```

```
c  *                            0   0   0    0   0   0                *
c  *                            0   0   0    0   0   0                *
c  *                            0   0   0    0   0   0                *
c  *                                                                  *
c  *                                                                  *
c  *                            1   0   0    0   0   0                *
c  *                            0   1   0    0   0   0                *
c  *                            0   0   1    0   0   0                *
c  *              mat(dikdjl) =                                       *
c  *                            0   0   0    .5  0   0                *
c  *                            0   0   0    0   .5  0                *
c  *                            0   0   0    0   0   .5               *
c  *                                                                  *
c  *                                                                  *
c  *                            E11 E11 E11  0   0   0                *
c  *                            E22 E22 E22  0   0   0                *
c  *                            E33 E33 E33  0   0   0                *
c  *              mat(Eijdkl) =                                       *
c  *                            E12 E12 E12  0   0   0                *
c  *                            E13 E13 E13  0   0   0                *
c  *                            E23 E23 E23  0   0   0                *
c  *                                                                  *
c  *                                                                  *
c  *                            E11 E22 E33  E12 E13 E23              *
c  *                            E11 E22 E33  E12 E13 E23              *
c  *                            E11 E22 E33  E12 E13 E23              *
c  *              mat(dijEkl) =                                       *
c  *                            0   0   0    0   0   0                *
c  *                            0   0   0    0   0   0                *
c  *                            0   0   0    0   0   0                *
c  *                                                                  *
c  *                                                                  *
c  *                          | E11 |                                 *
c  *                          | E22 |                                 *
c  *                          | E33 |                                 *
c  *              mat(EijEkl) = |     | * [E11 E22 E33 E12 E13 E23]     *
c  *                          | E12 |                                 *
c  *                          | E13 |                                 *
c  *                          | E23 |                                 *
c  *                                                                  *
c  *-------NOTES:                                                     *
c  *                                                                  *
c  *          1- Modifications made for improving convergence         *
c  *             characteristics of model are as follows.             *
c  *             if stran = dstran = 0, instead of returning          *
c  *             the material stiffness, we shall return              *
c  *             a material secant stiffness, based on the            *
c  *             user supplied property <e> (<props(5)>). This        *
c  *             is achieved by setting A = alpha B=C=D=0 and         *
c  *             c_bar = e / ( 1 + dnu ).                             *
c  *                                                                  *
c  *             This is done to avoid the singularity of the         *
c  *             global stiffness matrix. The singularity is          *
c  *             due to the fact that,                                *
c  *                                                                  *
```

```
c  *             when  tr(E)=0 or gamma_oct=0                          *
c  *                                                                   *
c  *                Mr = (Mr)' = (Mr)'' = 0                            *
c  *                                                                   *
c  *             This causes problems usually at the first iteration   *
c  *             for equilibrium, since the material stiffness         *
c  *             matrix may have zero eigenvalues, and thus may        *
c  *             become singular. The method described above is        *
c  *             essentialy the folloeing,                             *
c  *                                                                   *
c  *                       | E   FOR 1st iteration                     *
c  *                  Mr =|                                           *
c  *                       | Mr  FOR subsequent iters.                 *
c  *                                                                   *
c  *          2- Another way of improving convergence is to use        *
c  *             a damping factor for the resilient modulus. To        *
c  *             wit, resilient modulus (or c_bar) is updated          *
c  *             as the following,                                     *
c  *                                                                   *
c  *              Mr[E(i)] = damp * Mr[E(i-1)] + (1-damp) * Mr[E(i)]   *
c  *                                                                   *
c  *             or equivalently,                                      *
c  *                                                                   *
c  *              c_bar[E(i)] = damp * c_bar[E(i-1)]                   *
c  *                          + (1-damp) * c_bar[E(i)]                 *
c  *                                                                   *
c  *             where i denotes the i-th iteration.                   *
c  *             Note that damp = 1. defaults to the undamped          *
c  *             implementation.                                       *
c  *                                                                   *
c  *             This option is allowed only with the secant           *
c  *             formulation. If the user request tangent              *
c  *             formulation the damping will be ignored.              *
c  *                                                                   *
c  *          3- Syntax for the input file is,                         *
c  *                                                                   *
c  *            *MATERIAL, NAME = <a name>                             *
c  *            *USER MATERIAL, (UN)SYMMETRIC, CONSTANTS = 7           *
c  *               <nu>, <k>, <n>, <m>, <E>, <damp>, <switch>          *
c  *            *DEPVAR                                                *
c  *               1                                                   *
c  *                                                                   *
c  *           4- Mr value can be output for each element via card     *
c  *              in input file,                                       *
c  *                                                                   *
c  *             *EL FILE, POSITION=CENTROIDAL                         *
c  *               SDV1                                                *
c  *                                                                   *
c  *              or,                                                  *
c  *                                                                   *
c  *             *EL PRINT, POSITION=CENTROIDAL                        *
c  *               SDV1                                                *
c  *                                                                   *
c  *              Resilient modulus (Mr) will be computed at the       *
c  *              end of each load increment and stored in             *
```

```
c  *                                                                   *
c  *                  <statev(1)> : current resilient modulus value    *
c  *                                                                   *
c  *              To make statev operational include in input file     *
c  *             **DEPVAR                                              *
c  *                1                                                  *
c  *                                                                   *
c  *              Also, note that the resilient modulus that is        *
c  *              computed and output is the actual resilient          *
c  *              modulus (i.e. the one used in updating the           *
c  *              stress) , but NOT the damped one which               *
c  *              might have been used in the secant material          *
c  *              matrix, if damping was requested by the user.        *
c  *                                                                   *
c ***************************************************END*PROLOGUE*****
c ********************************************************************
c  * This source code is modified from the source code in Taciroglu's *
c  * dissertation:                                                     *
c  * Taciroglu, E., Constitutive Modeling of the Resilient Response of*
c  * Granular Solids.  A Dissertation Submitted for Fulfillment of the*
c  * Degree of Doctor of Philosophy, University of Illinois, Urbana.  *
c  * Urbana, IL, 1998.                                                 *
c  *                                                                   *
c  * A lower limit of octahedral strain has been added to the model to*
c  * account for the overflow error as a result of the negative power *
c  * for fine materials in Uzan's model.                               *
c  *                                                                   *
c ********************************************************************


c  Initialize Material Properties
      dnu    = props(1)
      dk     = props(2)
      dn     = props(3)
      dm     = props(4)
      e      = props(5)
      damp   = props(6)
      switch = props(7)

      alpha     = dnu / (1. - 2.*dnu)
      alpha_bar = (1. + dnu)/ (1. - 2. * dnu)
      dmu       = 1. / (1. - dn - dm)
      dk_bar    = dk / (1. + dnu)

c  Get total strain vector and strain invariants tr(E), gamma_oct

      do i=1,ndi
       tot_stran(i)  = stran(i) + dstran(i)
      end do
      do i=ndi+1,ntens
         tot_stran(i) = (stran(i) + dstran(i)) / 2.
      end do
      treps = tot_stran(1) + tot_stran(2) + tot_stran(3)

      gamma_oct = 0.
```

```
      do i=1,ndi
         gamma_oct = gamma_oct + tot_stran(i)**2.
      end do
      do i=ndi+1,ntens
         gamma_oct = gamma_oct + 2.*tot_stran(i)**2.
      end do
      gamma_oct = gamma_oct - treps**2. / 3.
c  Positive check to assure that it will not cause an error in sqrt()
      if (gamma_oct.gt.0) then
       gamma_oct = sqrt(gamma_oct/3.)
      endif
c  Select appropriate modulus value <c_bar> for <ddsdde> and <stress>

      singular = .true.
c  A lower limit of 1e-6 is set for the octahedral shear strain to
avoid c  overflow
      if(gamma_oct.gt.1e-6) then
       do i=1,ntens
            if(tot_stran(i).ne.0) singular = .false.
         end do
      end if

      if(singular) then

         c_bar = e / ( 1. + dnu)
      else
         c_bar = dk_bar * alpha_bar**dn * abs(treps)**dn *
gamma_oct**dm
         c_bar = c_bar ** dmu
         if (damp.ne.0.AND.switch.eq.0.) then
                       ! damping is not allowed with tangent
formulation

            c_bar = damp * c_bar_old(noel,npt,1) + (1. - damp) * c_bar
         end if

      end if
      res_mod = c_bar * (1. +dnu)

c  Update <stress> vector

      do i=1,ndi
      stress(i) = c_bar * ( alpha * treps + tot_stran(i))
      end do
      do i=ndi+1,ntens
        stress(i) = c_bar * tot_stran(i)
      end do


c  Update tangent stiffnes matrix <ddsdde>

      if(switch.eq.0..OR.singular) then
         a = alpha              ! either actual secant was singular
         b = 0.                 ! or user wants secant
```

```
      c = 0.
      d = 0.
   else
      x = dn - dm * (treps/(3.*gamma_oct))**2.
      d = dmu * dm /(3.*gamma_oct**2.)
      a = alpha * (dmu * x + 1.)
      b = dmu * x / treps
      c = d * alpha * treps
   end if

   do i=1,ntens
     do j=1,ntens
       ddsdde(i,j)=0.
     end do
   end do

   do i=1, ndi
      ddsdde (i,i) = 1.
   end do
   do i=ndi+1 , ntens
      ddsdde (i,i) = 0.5
   end do

   do i=1, ndi
      do j=1,ndi
         ddsdde(i,j) = ddsdde(i,j)
  &                  + a + b * tot_stran(i)
  &                  + c * tot_stran(j)
  &                  + d * tot_stran(i) * tot_stran(j)
      end do
   end do


   do i=1, ndi
      do j=ndi+1,ntens
         ddsdde(i,j) = ddsdde(i,j)
  &                  + c * tot_stran(j)
  &                  + d * tot_stran(i) * tot_stran(j)
         ddsdde(j,i) = ddsdde(j,i)
  &                  + b * tot_stran(j)
  &                  + d * tot_stran(j) * tot_stran(i)
      end do
   end do

   do i=ndi+1, ntens
      do j=ndi+1, ntens
         ddsdde(i,j) = ddsdde(i,j) + d * tot_stran(i) * tot_stran(j)
      end do
   end do

   do i=1,ntens
     do j=1,ntens
       ddsdde(i,j)=c_bar*ddsdde(i,j)
     end do
   end do
```

```
c  Store current resilient modulus

      statev(1) = res_mod
c  Store <c_bar> value to <c_bar_old>

      c_bar_old(noel,npt,1) = c_bar
c      write(7,888) tot_stran(1),
tot_stran(2),tot_stran(3),tot_stran(4)
c      write(7,889) stress(1), stress(2), stress(3), stress(4)
c      write(7,890) res_mod

      return
 100  format(' stran(',i1,') =', e12.4)
 200  format(20x,' dstran(',i1,') =', e12.4)
 300  format(20x,' tot_stran(',i1,') =', e12.4)
 400  format(20x,' stress(',i1,') =', e12.4)
 500  format(10x,6(x,f10.1))
 888  format(2x, 'strain = ', 4e11.3)
 889  format(2x, 'stress = ', 4e11.3)
 890  format(2x, 'res_mod= ', 1e11.3)
      end
```

Appendix V A Brief Overview of Parametric Study in ABAQUS Using Python Script

With the parametric study feature of ABAQUS, it is possible to generate, execute, and gather the results of multiple analyses that differ only in the values of some of the parameters used in the input file. For the pavement analyses, once the geometry of a model is defined, required critical strains for different combinations of parameters, such as HMA stiffness and constants in resilient modulus model of unbound materials, can be gathered automatically.

The procedures of a parametric study will be given with an example. The objective of the parametric study is to investigate the relationship between critical strains and unbound material moduli. A 2-D axisymmetric linear elastic model will be used, in which the pavement consists of three layers, the HMA layer, base course, and subgrade. Gravitational load is first applied at Step 1. Circular wheel load is then applied at Step 2.

Generate an input file using ABAQUS CAE, (2d.inp).

Change the input file into a parametrized input file template.

In the input file, define the parameters. In this example, Eb and Es will be used to define the elastic moduli of base course and subgrade, respectively. While defining parameters, they should be assigned to initial values.

```
** Parametric study
*PARAMETER
Eb=2.4E+08
Es=4.0E+07
```

Defined parameters should then be used to replace the values in the input file. In this example the following will be updated in the input file.

```
**
** MATERIALS
**
```

```
*Material, name=Base
*Density
2200.,
*Elastic
 <Eb>, 0.32
*Material, name=HMA
*Density
2400.,
*Elastic
 1.38e+09, 0.35
*Material, name=Soil
*Density
1700.,
*Elastic
 <Es>, 0.45
**
```

Create the Python script file (2dstudy1.psf)

The following is the Python script file to perform a parametric study using three different base moduli and one subgrade modulus. The results at the end of the first step (gravitational load) are gathered.

```
#
# This is the first trial of parametric study using Python Programming
#
# 2D Pavement analysis, with various base and subgrade moduli
#
# Execute parametric study and gather results at Step 1
#
# Create a parametric study
unbound2d=ParStudy(par=('Eb','Es'),name='unbound2d')
# Parameter Definition
unbound2d.define(CONTINUOUS,par='Eb',domain=(1.2E+08,3.6E+08))
# Parameter sampling for Eb
unbound2d.sample(NUMBER,par='Eb',number=3)      # Eb = 1.2E+08,
2.4E+08, 3.6E+08
# Parameter Definition
unbound2d.define(DISCRETE,par='Es',domain=(1.0E+07,2.0E+07,4.0E+07))
# Parameter sampling for Es
unbound2d.sample(NUMBER,par='Es',number=3)      # Es= 2.0E+07
# Combination of parameter samples
unbound2d.combine(MESH,name='Set1') # Mesh combination
# Generate input files (3 x 1 = 3 input files in total)
unbound2d.generate(template='2d') # use 2d.inp input file
# Execute ABAQUS analyses
unbound2d.execute(ALL)
# Specify the source of the results to be gathered
unbound2d.output(file=ODB,step=1,frameValue=LAST)
# Gather results (strain at all four integration points
```

```
unbound2d.gather(results='e43_strain1',variable='E',element=43,int=1)
unbound2d.gather(results='e43_strain2',variable='E',element=43,int=2)
unbound2d.gather(results='e43_strain3',variable='E',element=43,int=3)
unbound2d.gather(results='e43_strain4',variable='E',element=43,int=4)
unbound2d.gather(results='e282_strain1',variable='E',element=282,int=1)
unbound2d.gather(results='e282_strain2',variable='E',element=282,int=2)
unbound2d.gather(results='e282_strain3',variable='E',element=282,int=3)
unbound2d.gather(results='e282_strain4',variable='E',element=282,int=4)
# Save the gathered results to a file
# E11 of element 43 (bottom of HMA layer)
# and E22 of element 282 (top of # subgrade)
unbound2d.report(FILE,
results=('e43_strain1.1','e43_strain2.1','e43_strain3.1',
      'e43_strain4.1',
      'e282_strain1.2','e282_strain2.2','e282_strain3.2',
      'e282_strain4.2'),
                  variation=ON,file='2dstudy01')
```

It should be noted that different parameters should be defined and sampled separately (define Eb, sample Eb, define Es, sample Es). Otherwise, it will result in errors (define Eb, define Es, sample Eb, sample Es).

Run Python script file

Use the following command to run the script file.

```
Abaqus script=2dstudy1.psf
```

Execution in more than one session

Results can be gathered and reported multiple times, after the parametric variations of the study have been executed. It is possible to define, generate, and execute a parametric study in one session and gather and report results in a separate session.

The following Python script (2dstudy2.psf) gather results at Step 2 from the result files generated by 2dstudy1.psf.

```
#
# This is the first trial of parametric study using Python Programming
#
```

```
# 2D Pavement analysis, with various base and subgrade moduli
#
# Gathering results at Step 2 Only
#
unbound2d=ParStudy(par=('Eb','Es'),name='unbound2d')
unbound2d.define(CONTINUOUS,par='Eb',domain=(1.2E+08,3.6E+08))
unbound2d.sample(NUMBER,par='Eb',number=3)
unbound2d.define(DISCRETE,par='Es',domain=(1.0E+07,2.0E+07,4.0E+07))
unbound2d.sample(NUMBER,par='Es',number=3)
unbound2d.combine(MESH,name='Set1')
unbound2d.output(file=ODB,step=2,frameValue=LAST)
unbound2d.gather(results='e43_strain1',variable='E',element=43,int=1)
unbound2d.gather(results='e43_strain2',variable='E',element=43,int=2)
unbound2d.gather(results='e43_strain3',variable='E',element=43,int=3)
unbound2d.gather(results='e43_strain4',variable='E',element=43,int=4)
unbound2d.gather(results='e282_strain1',variable='E',element=282,int=1)
unbound2d.gather(results='e282_strain2',variable='E',element=282,int=2)
unbound2d.gather(results='e282_strain3',variable='E',element=282,int=3)
unbound2d.gather(results='e282_strain4',variable='E',element=282,int=4)
# Save the gathered results to a file
# E11 of element 43 (bottom of HMA layer)
# and E22 of element 282 (top of # subgrade)
unbound2d.report(FILE,
results=('e43_strain1.1','e43_strain2.1','e43_strain3.1',
            'e43_strain4.1','e282_strain1.2','e282_strain2.2',
            'e282_strain3.2','e282_strain4.2'),
            variation=ON,file='2dstudy02')
```

The script is similar to the previous one, except that the execute command (`unbound2d.execute(ALL)`) is not necessary, since the result files are already there after the 2dstudy1.psf was completed.

The results of the parametric study are show in Table A.5.1 and Table A.5.2. The differences of the strains between those two tables are the strains caused by wheel loading.

Table A.5.1 Output File 2dstudy01

Parametric study: unbound2d

Variation,	Eb,	Es,e43_strain,e43_strain,e43_strain,e43_strain,e282_strai,e282_strai,e282_strai,e282_strai,							
Set1_c1,	1.2e+08,	1e+07,	-4.3e-10,	-2.3e-10,	-4.9e-10,	-2.2e-10,	-0.00075,	-0.00075,	-0.00076,	-0.00076,
Set1_c2,	2.4e+08,	1e+07,	-4.9e-11,	8e-11,	-9.4e-11,	8.7e-11,	-0.00075,	-0.00075,	-0.00076,	-0.00076,
Set1_c3,	3.6e+08,	1e+07,	8.5e-11,	1.8e-10,	5.3e-11,	1.9e-10,	-0.00075,	-0.00075,	-0.00076,	-0.00076,
Set1_c4,	1.2e+08,	2e+07,	-4e-10,	-2.2e-10,	-4.6e-10,	-2.1e-10,	-0.00038,	-0.00038,	-0.00038,	-0.00038,
Set1_c5,	2.4e+08,	2e+07,	-5.6e-11,	6.3e-11,	-9.8e-11,	7e-11,	-0.00038,	-0.00038,	-0.00038,	-0.00038,
Set1_c6,	3.6e+08,	2e+07,	7.4e-11,	1.7e-10,	4.3e-11,	1.7e-10,	-0.00038,	-0.00038,	-0.00038,	-0.00038,
Set1_c7,	1.2e+08,	4e+07,	-3.5e-10,	-2e-10,	-3.9e-10,	-2e-10,	-0.00019,	-0.00019,	-0.00019,	-0.00019,
Set1_c8,	2.4e+08,	4e+07,	-6.4e-11,	4.1e-11,	-1e-10,	4.7e-11,	-0.00019,	-0.00019,	-0.00019,	-0.00019,
Set1_c9,	3.6e+08,	4e+07,	5.8e-11,	1.4e-10,	3e-11,	1.5e-10,	-0.00019,	-0.00019,	-0.00019,	-0.00019,

Table A.5.2 Output File 2dstudy02

Parametric study: unbound2d

Variation,	Eb,	Es,e43_strain,e43_strain,e43_strain,e43_strain,e282_strai,e282_strai,e282_strai,e282_strai,							
Set1_c1,	1.2e+08,	1e+07,	0.00026,	0.0002,	0.00027,	0.00021,	-0.00098,	-0.00098,	-0.00098,	-0.00098,
Set1_c2,	2.4e+08,	1e+07,	0.00019,	0.00015,	0.00019,	0.00015,	-0.0009,	-0.0009,	-0.0009,	-0.0009,
Set1_c3,	3.6e+08,	1e+07,	0.00015,	0.00012,	0.00015,	0.00012,	-0.00086,	-0.00086,	-0.00087,	-0.00087,
Set1_c4,	1.2e+08,	2e+07,	0.00027,	0.0002,	0.00027,	0.00021,	-0.00056,	-0.00056,	-0.00056,	-0.00056,
Set1_c5,	2.4e+08,	2e+07,	0.00019,	0.00015,	0.00019,	0.00015,	-0.0005,	-0.0005,	-0.0005,	-0.0005,
Set1_c6,	3.6e+08,	2e+07,	0.00015,	0.00012,	0.00015,	0.00012,	-0.00047,	-0.00047,	-0.00047,	-0.00047,
Set1_c7,	1.2e+08,	4e+07,	0.00027,	0.00021,	0.00027,	0.00021,	-0.00032,	-0.00032,	-0.00032,	-0.00032,
Set1_c8,	2.4e+08,	4e+07,	0.00019,	0.00015,	0.00019,	0.00015,	-0.00029,	-0.00029,	-0.00029,	-0.00029,
Set1_c9,	3.6e+08,	4e+07,	0.00015,	0.00012,	0.00015,	0.00012,	-0.00027,	-0.00027,	-0.00027,	-0.00027,

Appendix VI Validation of Uzan's Resilient Modulus Model Implementation into Finite Element Analysis

Single Element Study

A single element study using the Uzan's (1985) resilient modulus model implementation in ABAQUS 6.2-1 (2001) was performed to check whether this implementation worked properly. In the single element study, a 1m x 1m x 1m cube of the material with the properties as listed in Table A.6.1 was subjected to pressure in all three orthogonal directions, with σ_1 = 100 kPa, σ_2 = 60 kPa, and σ_3 = 40 kPa. According to the Uzan model, the resilient modulus of this material under this stress state should be 164 MPa. The resilient modulus obtained from finite element analysis is 164 MPa. This suggests that the implementation of Uzan's resilient modulus model into ABAQUS was successful.

Comparison Study

A validation of the Uzan's (1985) resilient modulus model implementation into finite element analysis was performed by comparing the results from a finite element analysis (ABAQUS 6.2-1, 2001) with KENLAYER (Huang, 1993). Kenlayer is an elastic layered system model for flexible pavement analysis.
A simple 2D plate loading problem was used in the comparison. A granular material with the material properties listed in Table A.6.2 was subjected to 552 kPa of pressure over a circular area with a diameter of 0.304 m. The mesh of the

Table A.6.1 Material Properties Used in Single Element Study

Poisson's Ratio	υ	0.45
Parameters in Uzan's Model	K (Pa)	1.58e+08
	n	0.26
	m	-0.31

Table A.6.2 Material Properties Used in Comparison Study

Density	ρ (Mg/m^3)	2200
Poisson's Ratio	υ	0.35
Parameters in Uzan's Model	K (Pa)	5.87E+05
	n	0.45
	m	0.00

model used in finite element analysis is shown in Figure A.6.1.

Figure A.6.2 compares the distribution of vertical stress directly under the center of the circular loading plate from the finite element (FE) and KENLAYER analyses. The vertical stress obtained from FE analysis (561 kPa) is very close to the applied load, while that of the KENLAYER (862 kPa) is much higher than the applied load (552 kPa). This is due to the fact that KENLAYER (Huang, 1993) is based on the elastic layered system solution, in which the uniformly distributed load is approximated by a Bessel function for an equivalent load. However, this difference exists only at the very top part of the model, and it diminishes quickly with increasing depth.

References

ABAQUS 6.2-1 (2001), Habbitt, Karlsson & Sorensen, Inc., Rhode Island

Huang, Y. H. (1993) *Pavement Analysis and Design*. Prentice Hall, Page 31.

Uzan, J. (1985) Characterization of Granular Material. In *Transportation Research Record 1022*, TRB, National Research Council, Washington D. C., pp. 52-59.

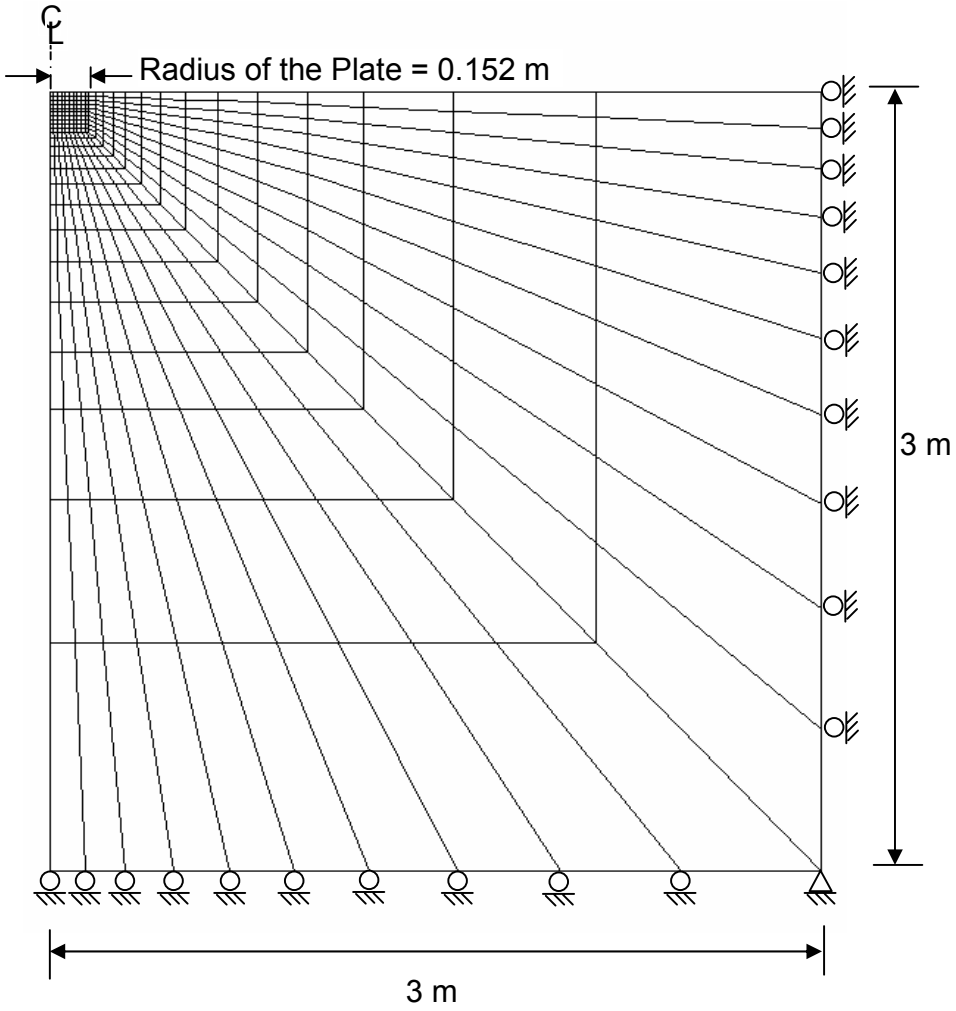

Figure A.6.1 Mesh of the 2D Axisymmetric Model Used in Finite Element Analysis

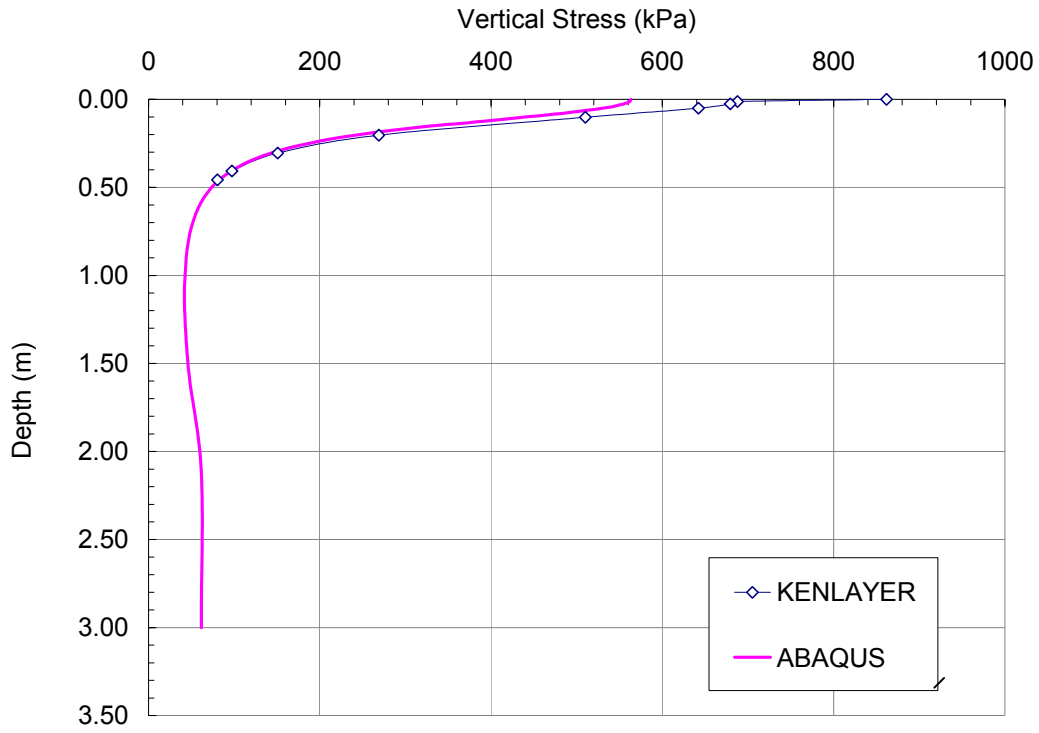

Figure A.6.2 Comparison of Vertical Stress along the Center Line

Appendix VII Study on Distance to Boundary for a 3D Pavement Model

In finite element analysis, it is important to verify the effect of the selected domain and size boundary conditions. A boundary condition set too close would impair the accuracy of the results, while a boundary condition set too far is not efficient for the analysis, since more computation time is needed for a larger model with similar element size.

The Thin pavement model with smooth AC-Base interface condition as described in Part III (Original) was used in this study. Another model, identical to the first but extended 2 m in all three directions (Extended) was used for comparison as shown in Figure A.7.1, in which the extended parts are shaded. It was found that the extension of boundaries in all three directions for 2 m had no effect on the computed critical strains (Table A.7.1). Therefore, the distances to boundaries used in Part III and IV are sufficient to have no impact on the computed results.

Table A.7.1 Comparison of Critical Strains for Different Boundary Conditions

		Original	Extended
Max. Tensile Strain at the Bottom of AC Layer	Longitudinal	2.20E-04	2.20E-04
	Transverse	1.34E-04	1.34E-04
Max. Compressive Strain at the Top of Subgrade		2.07E-04	2.07E-04

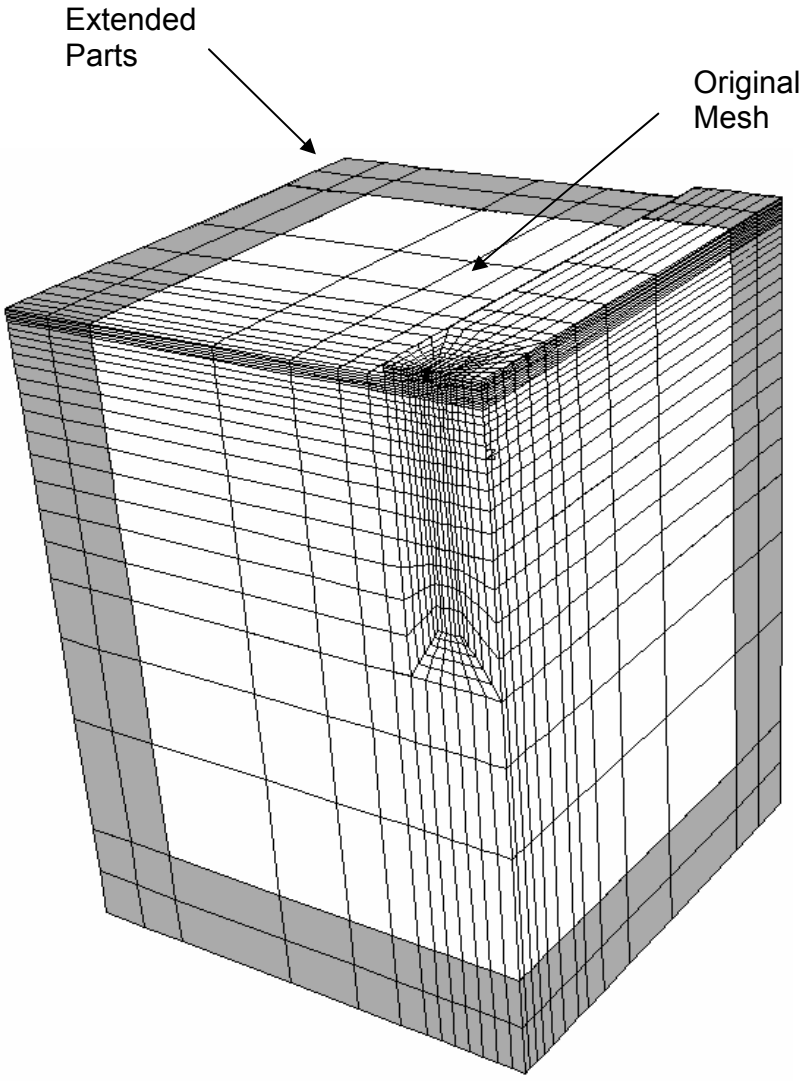

Figure A.7.1 Mesh of the Extended Model

Appendix VIII Results of Parametric Study

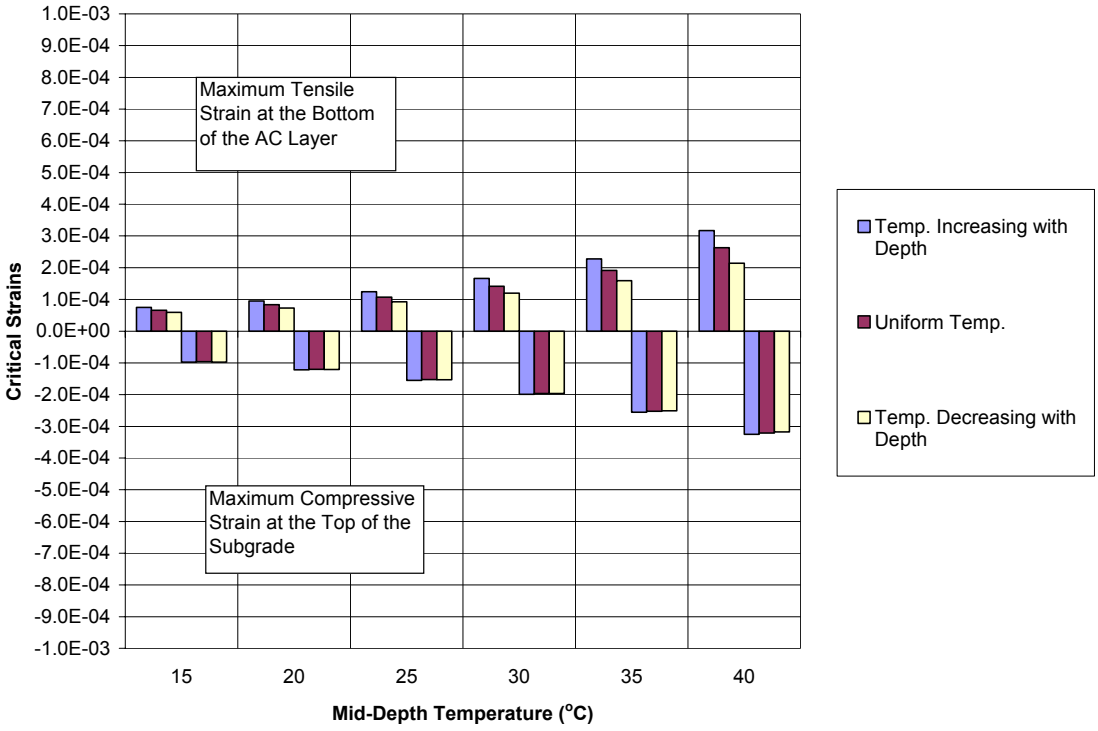

Figure A.8.1 Comparison of Critical Strains for Different AC Temperature Profiles with the Same Mid-Depth AC Temperature (Pavement 1 with Dry Base and Dry Subgrade)

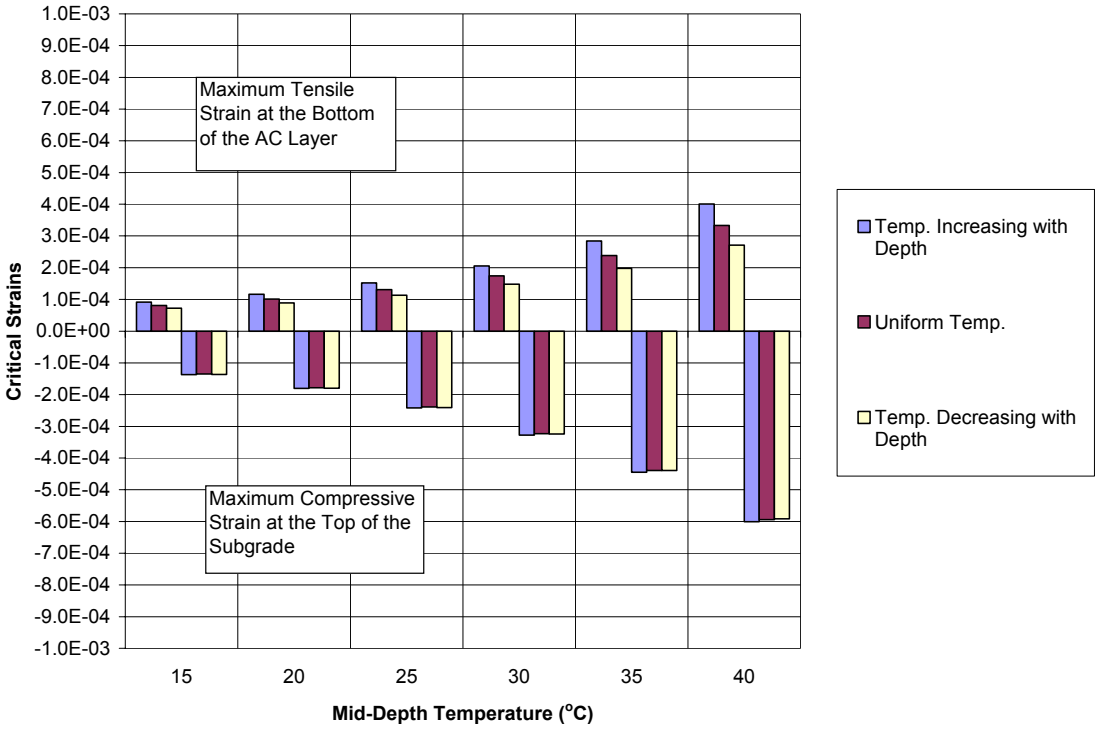

Figure A.8.2 Comparison of Critical Strains for Different AC Temperature Profiles with the Same Mid-Depth AC Temperature (Pavement 1 with Dry Base and Wet Subgrade)

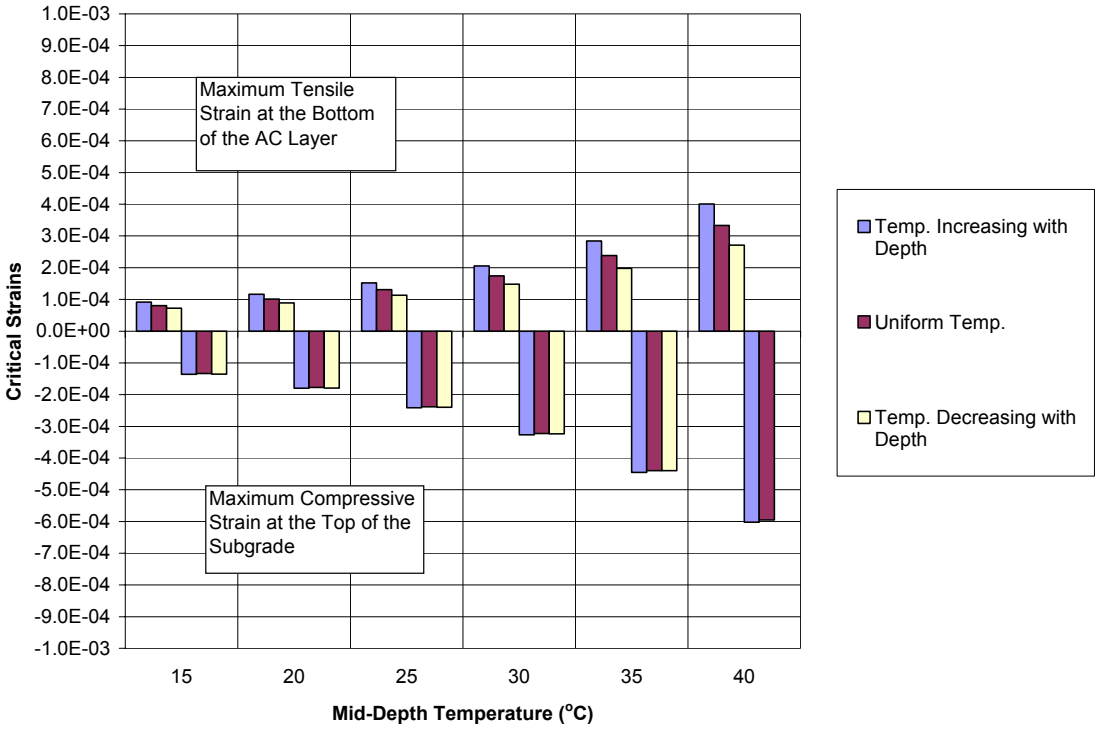

Figure A.8.3 Comparison of Critical Strains for Different AC Temperature Profiles with the Same Mid-Depth AC Temperature (Pavement 1 with Wet Base and Wet Subgrade)

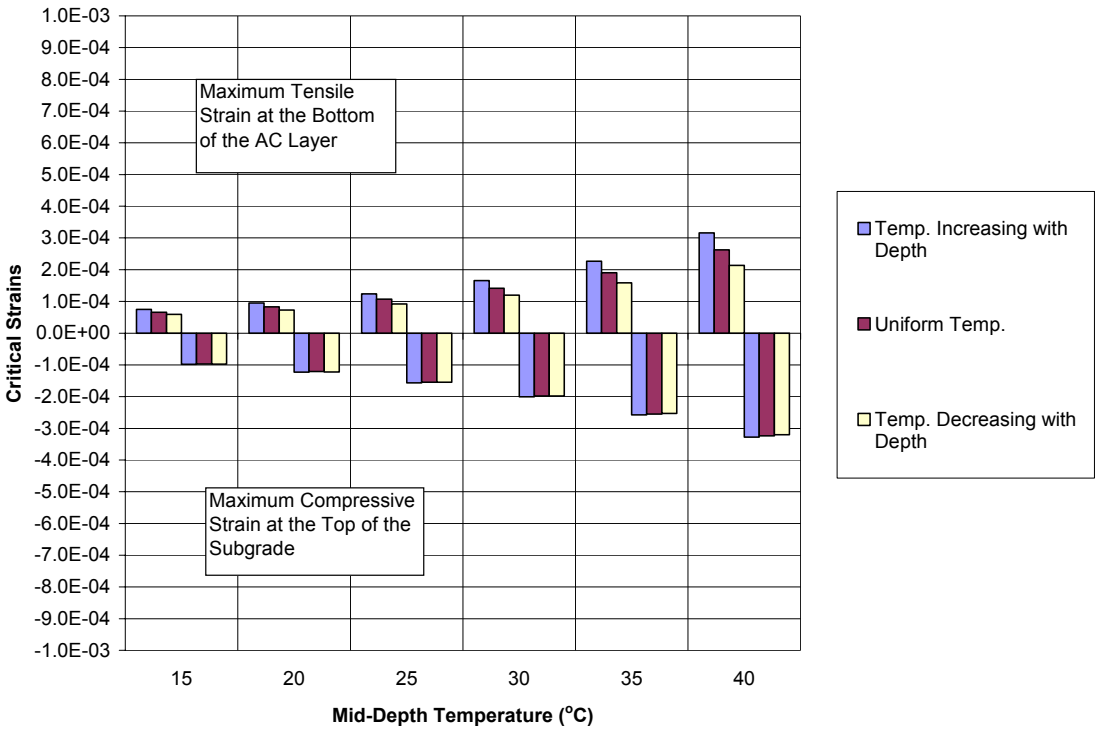

Figure A.8.4 Comparison of Critical Strains for Different AC Temperature Profiles with the Same Mid-Depth AC Temperature (Pavement 1 with Wet Base and Dry Subgrade)

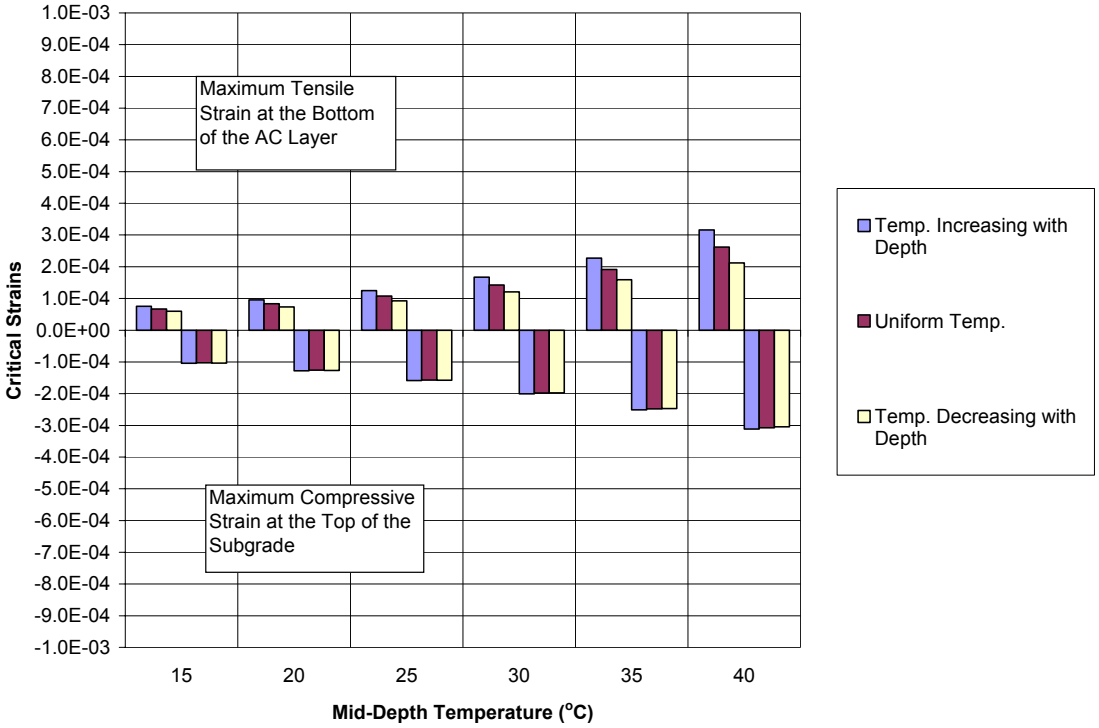

Figure A.8.5 Comparison of Critical Strains for Different AC Temperature Profiles with the Same Mid-Depth AC Temperature (Pavement 2 with Dry Base and Dry Subgrade)

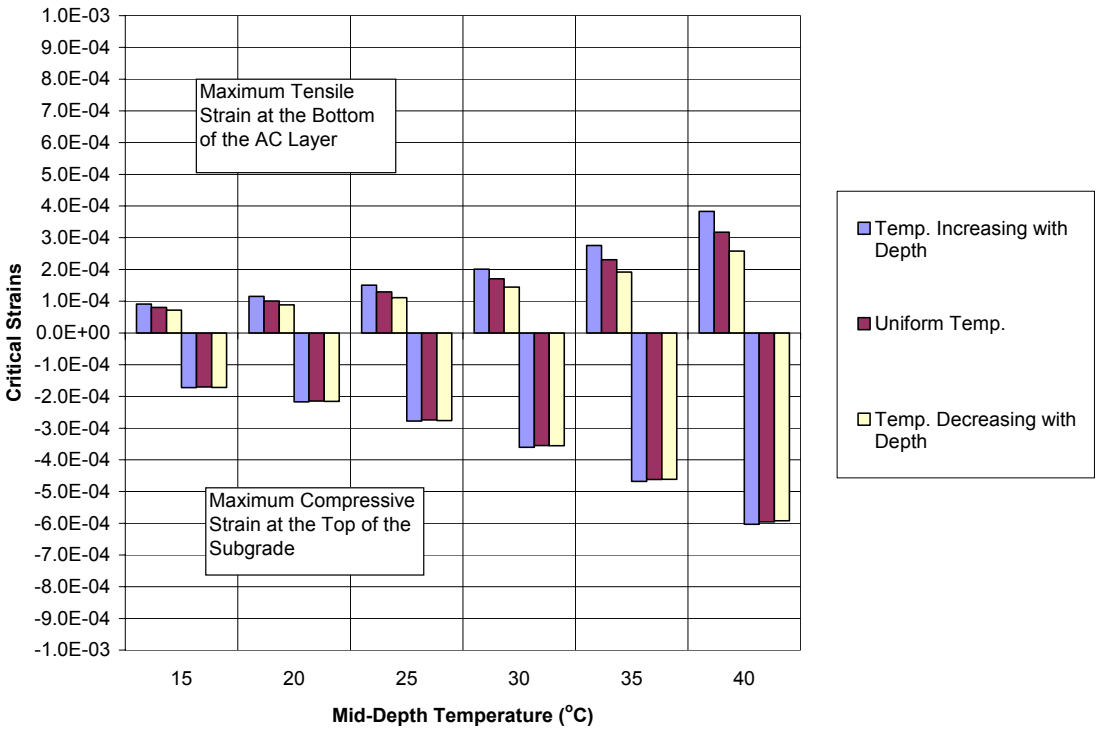

Figure A.8.6 Comparison of Critical Strains for Different AC Temperature Profiles with the Same Mid-Depth AC Temperature (Pavement 2 with Dry Base and Wet Subgrade)

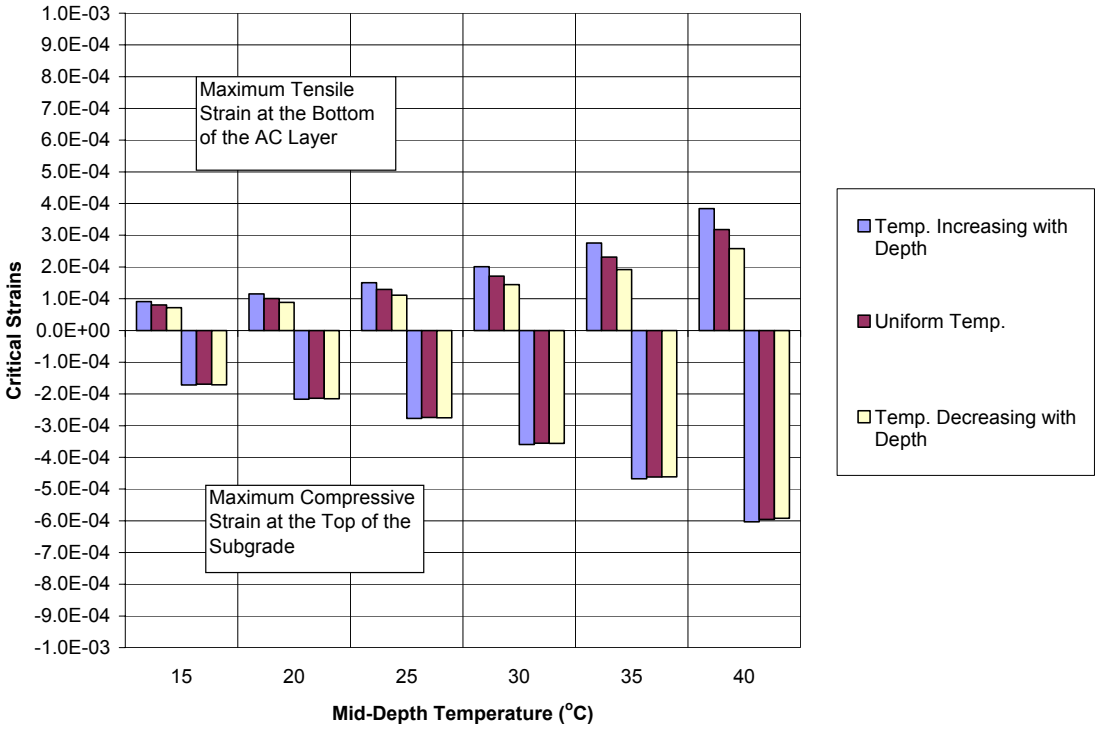

Figure A.8.7 Comparison of Critical Strains for Different AC Temperature Profiles with the Same Mid-Depth AC Temperature (Pavement 2 with Wet Base and Wet Subgrade)

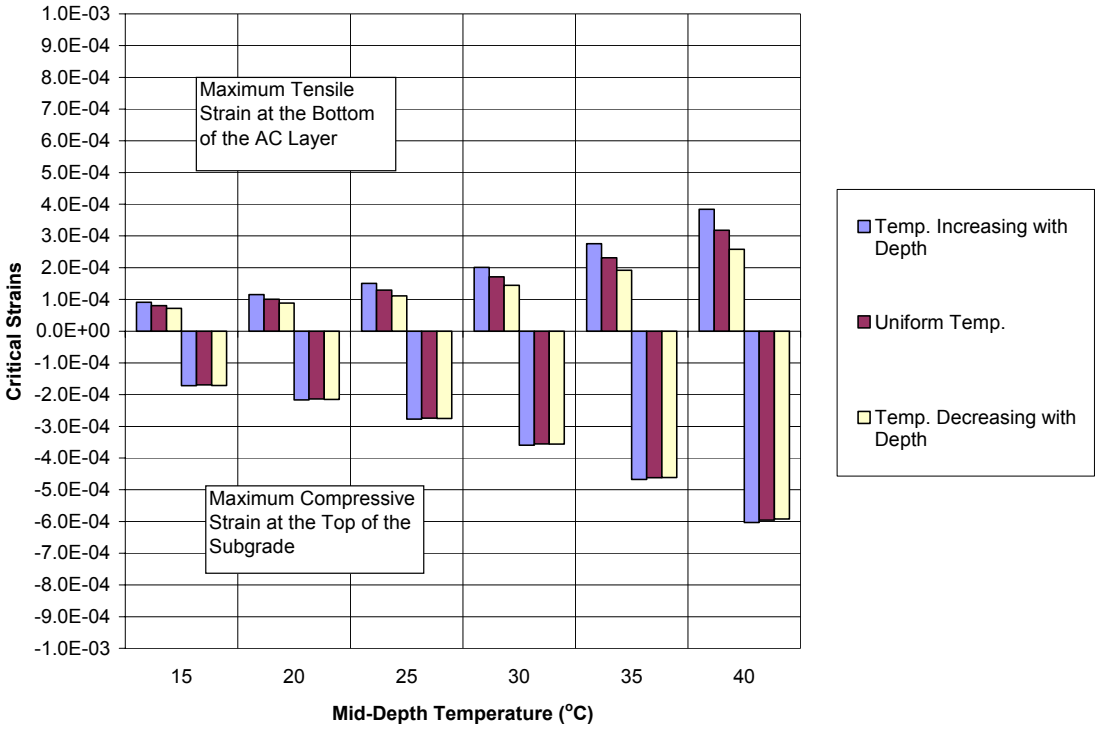

Figure A.8.8 Comparison of Critical Strains for Different AC Temperature Profiles with the Same Mid-Depth AC Temperature (Pavement 2 with Wet Base and Dry Subgrade)

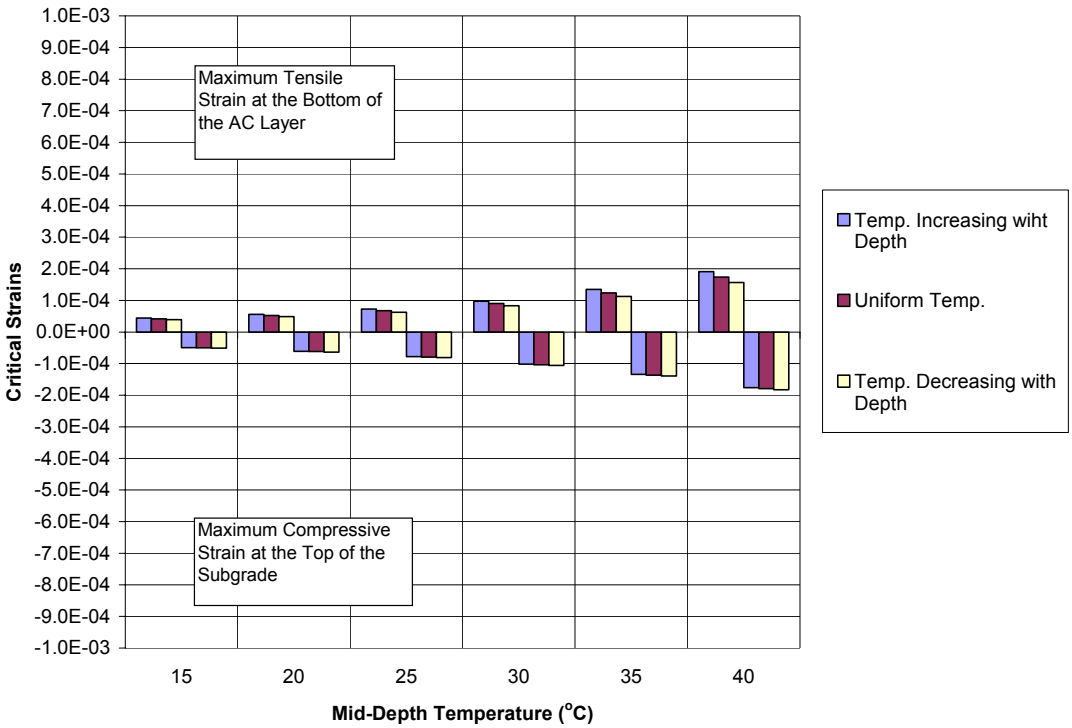

Figure A.8.9 Comparison of Critical Strains for Different AC Temperature Profiles with the Same Mid-Depth AC Temperature (Pavement 3 with Dry Base and Dry Subgrade)

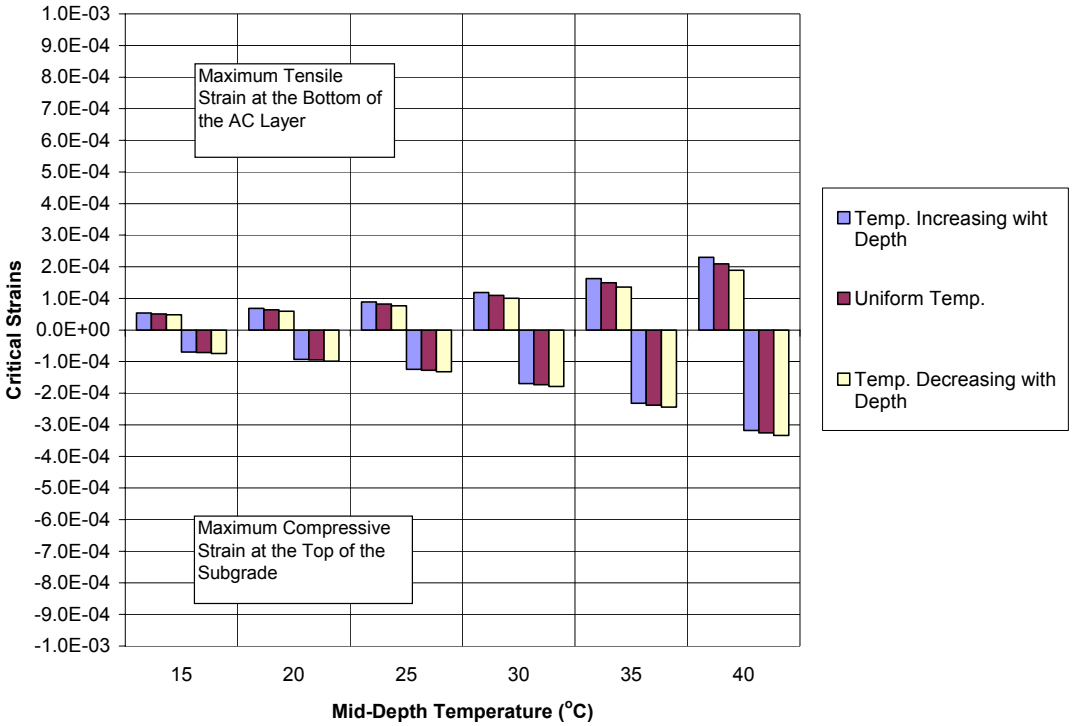

Figure A.8.10 Comparison of Critical Strains for Different AC Temperature Profiles with the Same Mid-Depth AC Temperature (Pavement 3 with Dry Base and Wet Subgrade)

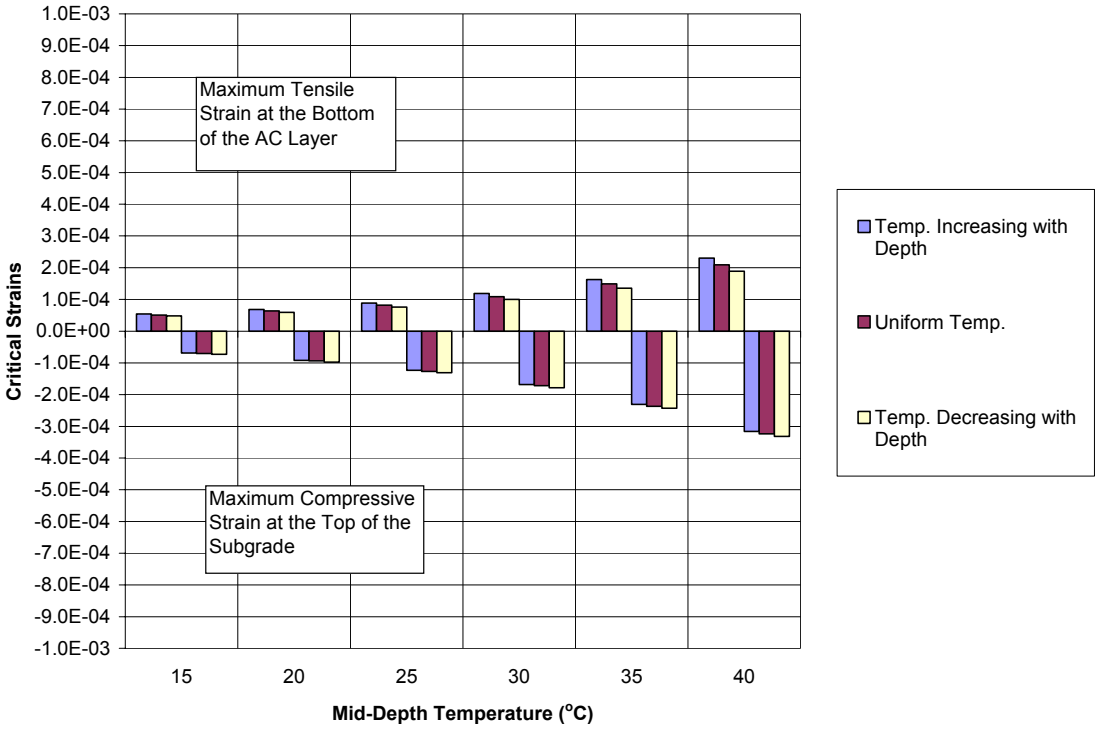

Figure A.8.11 Comparison of Critical Strains for Different AC Temperature Profiles with the Same Mid-Depth AC Temperature (Pavement 3 with Wet Base and Wet Subgrade)

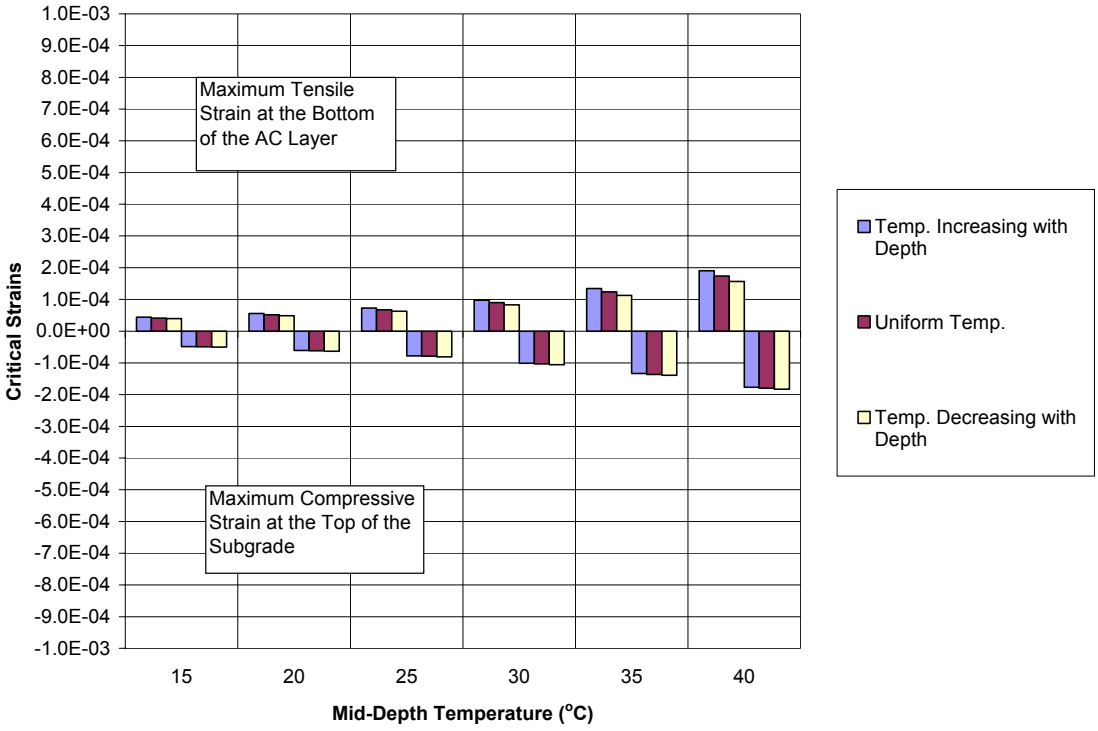

Figure A.8.12 Comparison of Critical Strains for Different AC Temperature Profiles with the Same Mid-Depth AC Temperature (Pavement 3 with Wet Base and Dry Subgrade)

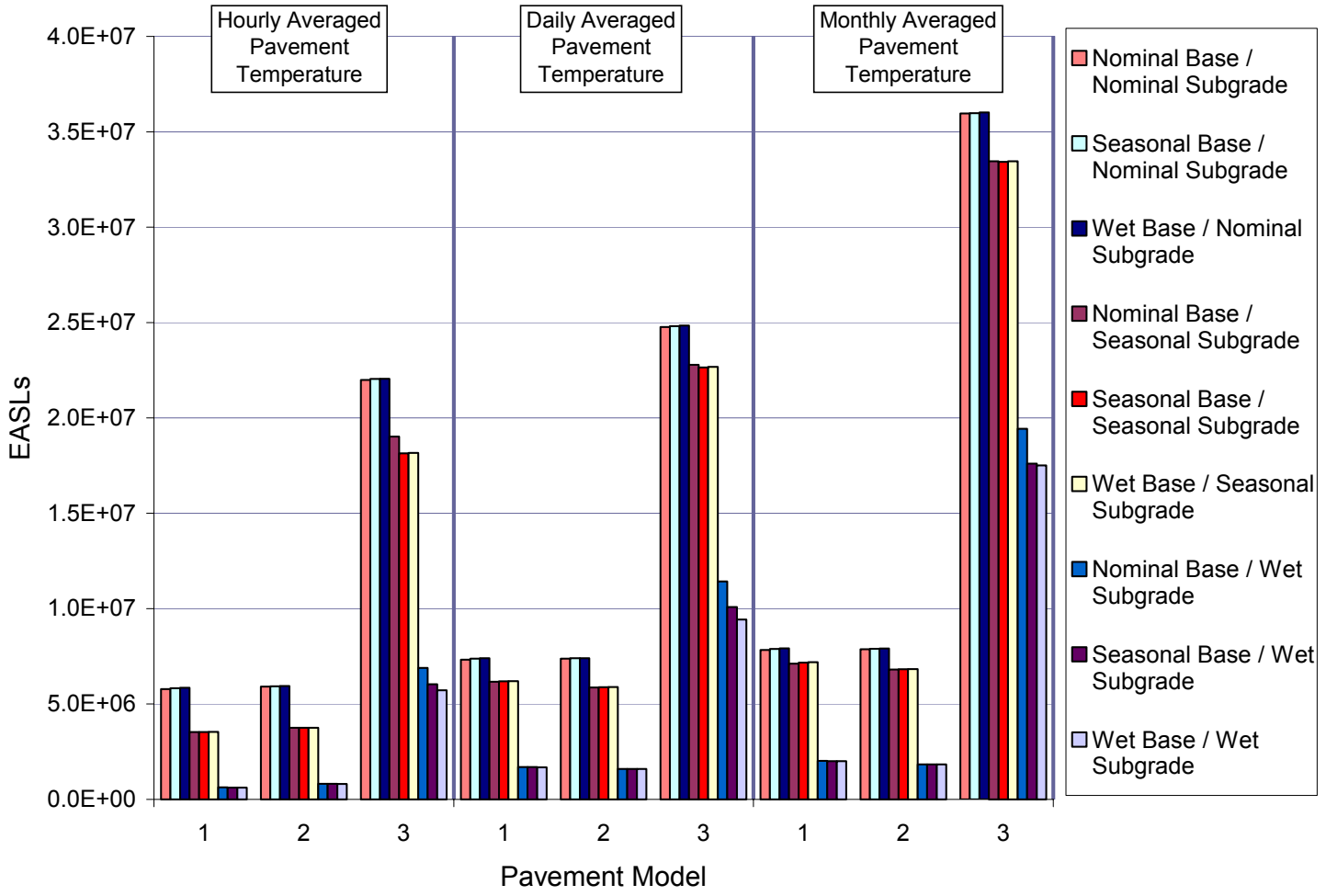

Figure A.8.13 Predicted Pavement Lives for Different Base and Subgrade Water Contents

Appendix IX Literature Review on Effects of Moisture Content Variation on Unbound Materials

Introduction

Temporal changes in environmental factors such as temperature and moisture content can cause significant variations in the properties of pavement materials, thus affecting the response and performance of the pavement system. In many areas, freezing and thawing of the pavement layers can result in abrupt changes in the properties of the pavement layers, and the loss of capacity during spring thaw often leads to premature pavement failure. The back-calculated layer moduli determined from Falling Weight Deflectometer testing of flexible pavements can be highly dependent upon the temperature and/or temperature gradient at the time of the test. The following review summarizes recent research findings relative to the daily and seasonal variations in temperature and moisture conditions and their effects on material properties and pavement structural capacity.

The pavement design procedures presented in the American Association of State Highway Officials (AASHTO) Guide for Design of Pavement Structures (AASHTO, 1993) require the use of mechanical properties for the asphalt concrete, base course, and soil subgrade. The stiffness of the soil subgrade and base materials are represented by the resilient modulus, M_R which replaces the empirical "soil support value" used in the earlier design guides. A sensitivity analysis of the AASHTO's design equation showed that the resilient modulus of the unbound materials has the most pronounced effect on the structural number (SN) of flexible pavements (Baus and Fogg, 1989). Since the behavior of unbound base materials is similar to that of coarse-grained subgrade materials, the effects of

moisture content changes are similar. Typically, the resilient modulus of unbound materials is determined in the laboratory in accordance with AASHTO T294 under conditions of maximum dry density and optimum water content. Although pavement subgrades are usually compacted close to optimum water content and maximum dry density during construction, seasonal variations in water content or degree of saturation occur. Most fine-grained soils exhibit a decrease in modulus as the water content is increased, leading to increased deflections in the pavement subgrade. Coarse-grained materials may experience this change, depending upon the amount of fine grained particles present. In general, an increased deflection in the subgrade leads to a decrease in pavement design life (Thompson and Elliot, 1985; Elliot and Thornton, 1988; Monismith, 1992).

Seasonal variations in soil moisture content

The variation of soil moisture is complicated, because of the influenced of a number of factors, such as soil type, precipitation, location of the groundwater table, solar radiation, and the topography. Different models have been developed to simulate the process of wetting and drying of soil.

The variation of soil moisture in the subgrade soil is important to the pavement design process, because change in the soil stiffness or modulus due to moisture variation is the direct cause of the distress in pavements. For most cases, it is not appropriate to predict the variation of soil moisture with an analytical model, which can include all the processes like infiltration, drainage, evaporation and heat transfer. Instead, the variation of soil moisture is obtained from in situ

measurements, and then regression methods are used to find the correlation between the soil moisture variation and environmental factors.

Subgrade Soil Moisture and Hydrologic cycle

The variation in soil moisture with time is part of the earth's hydrologic cycle. Water reaches the surface of the ground in the forms of condensation and precipitation. It then runs from the slopes in thin sheets into streams and rivers and eventually arriving at the ocean, or infiltrates into the soil and is transmitted to groundwater or is stored in the soil near surface where it comes back to the sky by evaporation or transpiration of plants. A schematic (Guymon, 1994) of hydrologic cycle is depicted in Figure A.9.1.

As shown in Figure A.9.1, soil moisture domain or region can be divided into two major zones, separated by the groundwater table, i.e., unsaturated zone and saturated zone. The boundary of these two zones, the groundwater table, varies seasonally. A localized saturated zone or a perched saturated zone may exist as a result of the underlying semipervious soils. Generally, such zones are much thinner than the two major zones. The unsaturated zone is the part of soil moisture domain most commonly involved with pavement engineering. The interaction of soil moisture changes between the unsaturated zone and the saturated zone, together with precipitation and evaporation, makes the properties of the unsaturated zone very complicated.

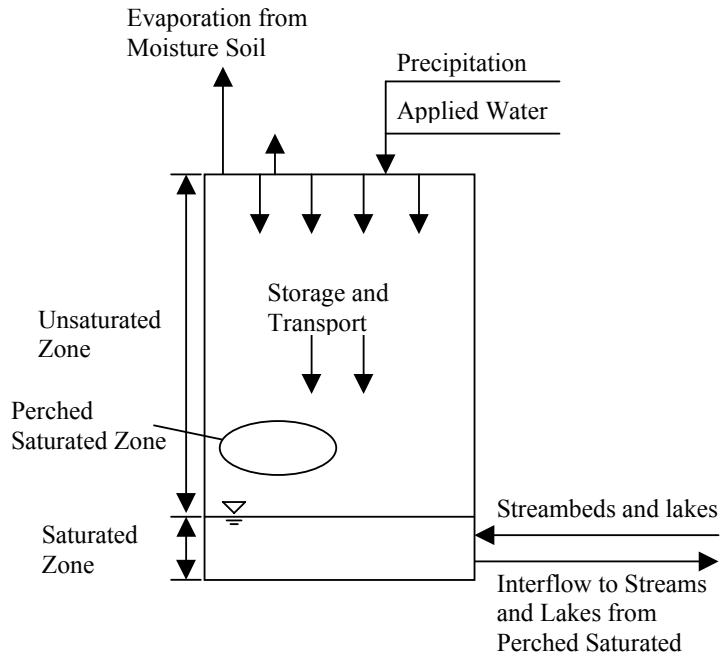

Figure A.9.1 Schematic of the Hydrologic Cycle (Guymon, 1994)

Enhanced Integrated Climatic Model (EICM)

Enhanced Integrated Climatic Model (Lytton et al., 1990; Larson and Dempsey, 1997) is a one-dimensional coupled heat and moisture flow program for the analysis of pavement systems due to climatic factors such as temperature, rainfall, wind speed and solar radiation. A schematic of the entire model (Birgisson et al., 2000) is shown in Figure A.9.2. It consists of four independently developed models which have been integrated into the EICM:

Precipitation model (Liang and Lytton, 1989) is used to generate precipitation patterns from historical climatic data available from National Oceanic and Atmospheric Administration (NOAA). Based on the statistical information calculated from 30 years of precipitation data, the number of wet days of each

month and the intensity of rainfall can be generated using congruential algebra and number theory. It is recommended that if an extreme rainfall event is to be modeled, actual rainfall data should be used instead of generated data.

Infiltration-Drainage Model (ID Model) (Liu and Lytton, 1985) models the water infiltration through the cracks in the pavement surface and subsequent flow in the drainage layer. This model can also perform a pavement design evaluation. The wetting front penetrating into the subgrade at a given time is calculated. The modulus of the base course is assumed to be constant for a degree of saturation lower than 60 percent. For a degree of saturation higher than 60 percent, the reduction of base course modulus is assumed to be proportional to the increase of surface deflection due to the increase in degree of saturation. Subgrade modulus can be determined as a function of the degree of saturation, which is correlated with the wetting front, from a linear regression equation.

The CRREL model (Guymon et al., 1986) developed at the U. S. Army Cold Regions Research and Engineering Laboratory (CRREL), is used to compute the one-dimensional coupled heat and moisture flow in the subgrade soil at temperatures that are above, below, and at the freezing temperature of water. This model provides reasonably accurate predictions of frost and thaw penetration, heave, and settlement. Darcy's law is used in the moisture flow model. The unfrozen unsaturated water content is related to the negative pore water pressure through the Soil-Water Characteristic Curves (SWCC). The SWCC can be expressed by the Gardner function as shown in Equation (A-9-1),

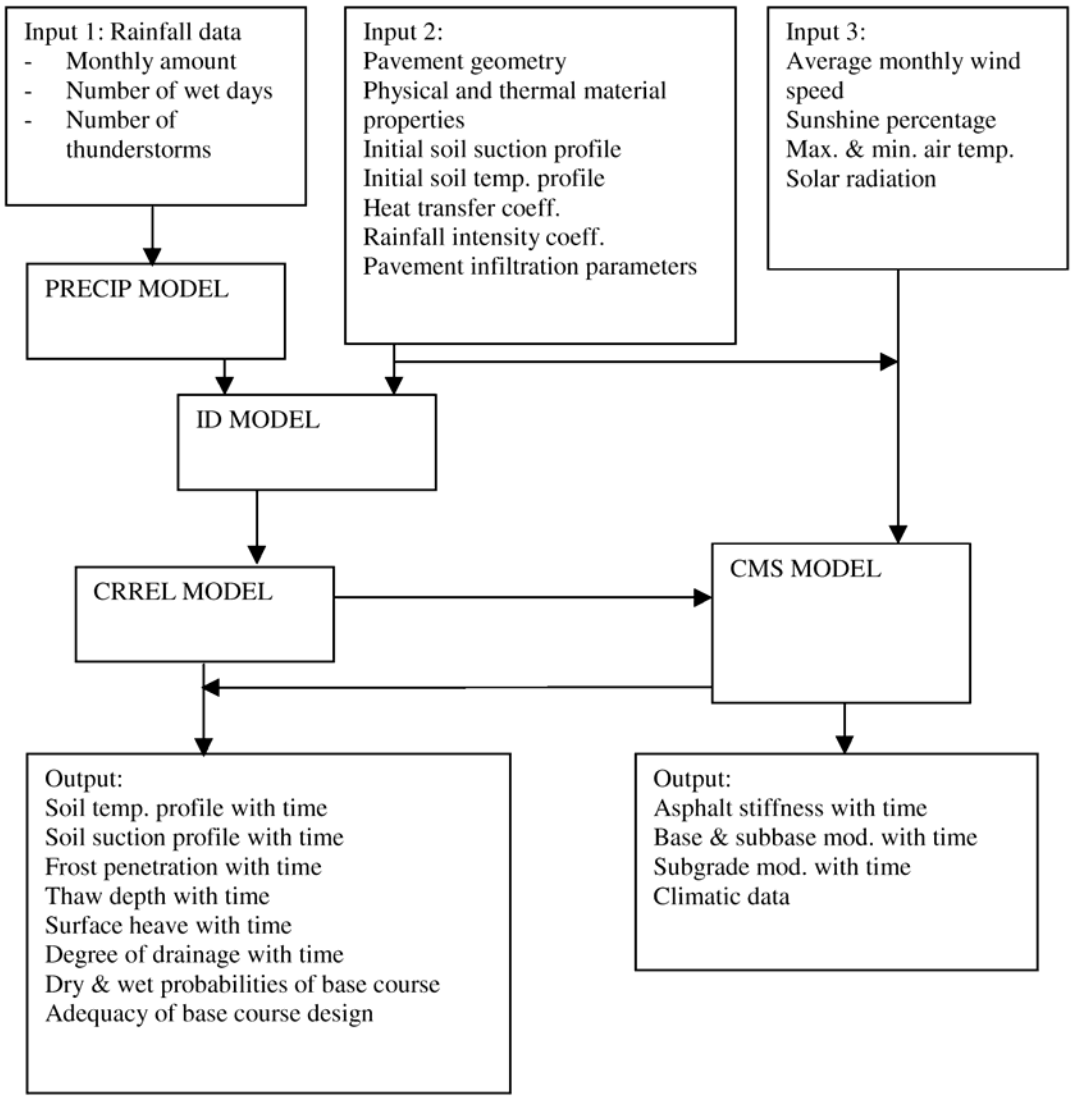

Figure A.9.2 Schematic of the Enhanced Integrated Climatic Model (Birgisson et al., 2000)

$$\theta_u = \frac{n}{1 + A_w |h|^a} \qquad \text{(A-9-1)}$$

where n = the porosity of the soil,

A_w, a = constants describing the soil-water characteristic curve,

$|h|$ = the absolute value of the negative pore water pressure (suction),

usually expressed in centimeters of water head.

The Climate-Materials-Structural Model (CMS Model) (Dempsey et al., 1985) is used to simulate climatic conditions that control temperature and moisture conditions in the pavement layers and in the subgrade. A one-dimensional, forward finite difference, heat transfer model is used to determine frost penetration and temperature distribution in the pavement system. Base and subbase moduli are calculated from unfrozen and frozen moduli and temperature. Unfrozen subgrade modulus is a regression function of water content, which is obtained from the CRREL model.

A schematic of the EICM calculation procedure of subgrade resilient modulus is depicted in Figure A.9.3.

The ID model, which accounts for the precipitation and infiltration, is not used in the direct calculation of the subgrade modulus. The subgrade modulus is determined only as a function of the distance above the water table. Thus, the ID model only applies to sites with a high water table. For sites with a low water table, this model would result in an unreasonably low and relatively constant moisture content, even if the subgrade is subjected to climatic variations. In addition, for pavement sites with a shallow water table, soil suction may not vary

linearly with distance from the water table as calculated from hydrostatic pressure (Croney et al., 1958). For example, the existence of a coarse gravel layer right above the water table would provide a capillary break. Nevertheless, for many conditions the combination of water table position and SWCC still serve as a reasonable approach to estimate moisture content which can be correlated to the subgrade resilient modulus.

Birgisson et al. (2000) used the EICM to compare field and model predictions of seasonal variations in flexible pavements at the Minnesota Road Research Project (Mn/ROAD). The results indicated that the EICM can provide reasonable prediction of seasonal variations in temperature, layer modulus, and volumetric moisture content, except during the spring thaw period. Two flexible pavement test sites were studied in this research, both with shallow water tables (<20 ft.). Therefore, the moisture content of the subgrade was mainly influenced by the ground water table location. For sites with a deeper ground water table, the results might not be as good.

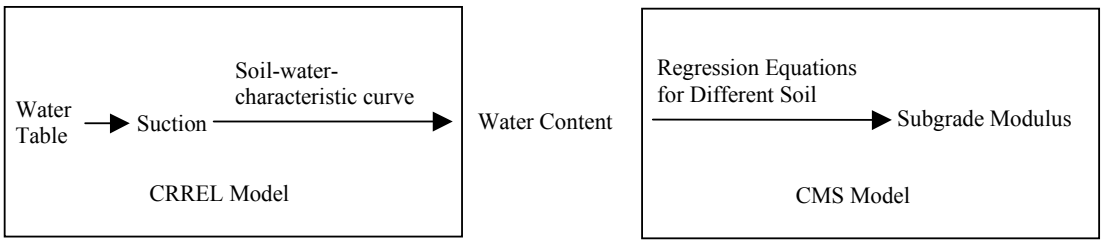

Figure A.9.3 Procedures for the Subgrade Resilient Modulus Calculation in EICM

Soil Moisture in Cuts, fills, and Uncovered/Covered Ground

Soil Moisture in Cuts and Fills

Khogali and Anderson (1996) reported the significant differences between subgrade stiffness in cut sections and fill sections. Moduli backcalculated from FWD in the cut section experience large seasonal fluctuations than their counterparts in the fill section, and the subgrade moduli of fill areas were 65% greater than their counterparts in cut areas. These differences were believed to be caused by superior compaction and drainage in fill areas.

Soil Moisture in Uncovered Ground

Croney et al. (1958) pointed out that "to establish moisture equilibrium, water may flow from a granular soil of low moisture content into an adjacent clay soil of initially much higher moisture content. Even in a mass of uniform soil, moisture migration may take place from areas of low moisture content to areas of higher moisture content, depending on the previous moisture history of the soil." It is the potential that controls the movement of moisture. This potential may be mechanical potential, thermal potential, chemical potential and electrical potential. Chemical and electrical potential usually have little effect on soils with low ion content.

The flow of moisture under mechanical potential in saturated or unsaturated soil can both be approximated by Darcy's Law. The difference is that the hydraulic conductivity in saturated flow is a constant while it is a function of moisture content in unsaturated flow (Guymon, 1994).

Topsoil usually shows a quick response to rainfall and sharp increase of suction during continuously rainless days. Moisture variation occurs in uncovered ground primarily above a soil depth of 2 m, particularly in the upper 100 cm of soil. The rate at which the suction increases has been found to decrease with the elapsed time from the rain cessation (Musiake et al., 1988).

The flow of moisture under a thermal gradient is complex. Generally, moisture (both in liquid phase and vapor phase) tends to move opposite the temperature gradient, i.e., towards low temperature zone. However, the phenomenon of moisture in the liquid phase flowing in the opposite direction as the vapor phase was reported by Gurr et al. (1952). In the experiment the effect of a temperature gradient on the movement and distribution of the water in soil was examined in closed columns of soil for a wide range of initial water content. Small amounts of salts acting as a tracer served to distinguish between liquid and vapor movement. The result showed higher water content toward the colder end, but a high concentration of salt toward the hot end. This indicates a net transfer of water from hot to cold, in which water evaporating from the hotter end moves to the colder end, where it condenses and returns as a liquid when a favorable gradient of pressure potential has been established.

Soil Moisture in Covered Ground

Soil Moisture Movement and Distribution in Covered Ground

When the ground surface is covered by pavement, infiltration of water from precipitation is reduced significantly. If the surface shielding of pavement is

completely impermeable, on a wet day the moisture content under the center of the pavement will be much lower than that under the edge. On a dry day, the opposite will be true, with the moisture content under the center of the pavement higher than that under the edge. There will be a lag between the moisture change in the soil under the central part and under the edge of the pavement. The length of the lag depends on the hydraulic conductivity of soil. This effect was reported during a study of seasonal variation in soil moisture in Britain (Russam, 1970). A finite element simulation of moisture distribution under surface shielding was also consistent with this phenomenon (Ter-Martirosyan et al., 1986).

Roadside vegetation is believed to play an important role in the process of subgrade moisture removal. Plant root systems can remove moisture from the subgrade soil at great depth by transpiration, although a dry soil crust at the soil surface can prevent evaporation from taking place (Rahim and Picornell, 1989; van Gurp, 1994). Moisture removal ability of the roadside vegetation varies with both the type of plant and the season. Week of the year in was recommended as a good indicator of the approximate stage of vegetal development, which reflects typical evapotranspiration conditions (Linsley et al., 1992).

The phenomenon of the subgrade moisture accumulation during and after construction has been reported by a number of researchers. Seasonal variation of moisture content was found to be superimposed on a trend of increasing moisture over time (Haliburton, 1971). Vaswani (1975) observed that the rate of increase is dependent on soil density, compaction and soil gradation. It was

observed that one or two years after construction, the rate of moisture content increase slowed down, and the fluctuation due to temperature gradient became noticeable. After about 10 years, there was practically no change in subgrade moisture and temperature gradient had no effect. Maree et al. (1982) explained this accumulation of subgrade moisture by the compaction of traffic.

Russam (1970) proposed a classification of subgrades based on the water table depth and annual rainfall. Similar classifications were adopted by Yoder and Witczak (1975). The description of the three main categories of subgrade is as follows:

Category 1 – Subgrades where a water table is close to the surface, at a depth less than 20 ft in clays, 10 ft in sandy clays or silts, and 3 ft in sands. The depth to the water table is the main factor of the variation of moisture content of subgrades. Under a relatively impermeable surface, the soil water will tend toward equilibrium with the water table. The moisture content is governed by the fluctuation of water table.

Category 2 – Subgrades where the water table is deeper than that described in category 1 and the rainfall is more than 10 in. per year. The moisture content in this category will be governed by seasonal changes in the rainfall.

Category 3 – Subgrades where the water table is deep and the rainfall is less than 10 in. per year. In this category the moisture content of subgrade will differ little from the uncovered soil at the same depth.

A reasonably precise estimation can be made for the subgrade moisture content of category 1 from the depth of the water table and SWCC, but the fluctuation of

the water table is also related to rainfall. An important assumption in the category 1 subgrades is that the surface of the pavement is impermeable, and the variation of soil moisture is related only to the fluctuation of water table. In fact, the surface layer of most pavements is never completely impermeable. Longitudinal joints in flexible pavements (Rainwater et al., 1999) and expansion joints in rigid pavements (Guinnee, 1958) provide paths for infiltration. Cracks that develop as a result of inevitable distress of the pavement will increase the permeability of the surface layer.

The infiltration of precipitation through these joints and cracks will make any theoretical model more complicated. Rahim and Picornell (1989) proposed a computer program to model the moisture movement under the pavement. In the program, the expansive subsurface soil was simulated by rectangular blocks separated by parallel cracks. When all the cracks in the subgrade are filled with water during a rainfall event, all the remaining rainfall was assigned to run off. Cracks tend to close after the absorption of water and re-open when water is depleted. The volume change of each soil block is assumed to be equal to the volume of water absorbed or lost by the block. The rate of water movement in each block is controlled by master block curves derived by modeling the one-dimensional unsaturated water flow within the soil block subjected to zero suction for the wetting phase or 15 bars suction for the drying phase. The only form of moisture removal was assumed to be the plant transpiration of roadside vegetation. The cross-section of the pavement was divided into three regions, i.e. pavement, edge, and uncovered. In the ‘uncovered’ region, moisture can be

removed by plant transpiration. Roots of the vegetation are assumed to extend under the pavement and form the 'edge' region. In the 'pavement' region, water can only infiltrate through the cracks of the pavement surface, through which no moisture will be removed. This model explains the accumulation of moisture after construction and the phenomenon that subgrade moisture close to the edge exhibits more variation. However, according to this model, water will never be removed from the subgrade soil which is out of reach of the of the roadside vegetation root system. The infiltration of water is through vertical cracks only. Lateral moisture movement never takes place. No theoretical models exist to simulate the moisture movement and distribution properly. Even the Enhanced Integrated Climatic Model (Lytton et al., 1990; Larson and Dempsey, 1997) does not account for the infiltration of water from the surface and the lateral movement of moisture from uncovered soil to the subgrade.

Statistical Analysis of Subgrade Moisture Based on Precipitation

Since the theoretical models have a number of limitations, statistical analysis of data from field instrumentation is often used.

Several researchers have tried to find the correlation between rainfall and variation of moisture content by observing the precipitation data and moisture data (Cumberledge et al., 1974), or calculating the correlation coefficient directly (Valdez, 1991; Hossain et al., 1997). Almost all these researchers ended up with the same conclusion that there is no relationship between rainfall and subgrade moisture variation. Some attribute this result to insufficient instrumentation, for

instance, rainfall data was not collected at the testing site, but obtained from a nearby weather station, and rainfall at these two different locations could be different (Valdez, 1991). Some researchers found a lag between rainfall and subgrade moisture variation by eyeballing the precipitation vs. soil moisture data (Marks and Haliburton, 1969; Hall and Rao, 1999). The lag of response could vary from 3 weeks to 2 months. A rational statistical method capable of finding the lag between two time series, the Cross-Correlation Method, was first used in this kind of analysis by Bandyopadhyay and Frantzen (1983). The lag obtained using Cross-Correlation Method is up to 3 weeks. Several factors could affect this lag, some major factors are listed as following:

- Distress of the surface layer
- The Intensity of cracks on the pavement surface, the aperture of the cracks and the permeability of the filling material govern the infiltration rate during rainfall.
- Thickness of the HMA layer
- Thickness of the HMA layer will affect the properties of the subgrade. It is found that for HMA layer thickness < 6 in, spring is the most critical season. When the HMA layer thickness > 6 in, summer is the most critical season (Elliott and Thompson, 1985).
- Effective drainage of the base course
- Effective drainage of the base course controls how fast the water that infiltrates through the cracks and joints of the surface layer can be drained. An effective drainage layer can prevent the water from perching at the

interface between the base course and the subgrade, and consequently reduces the amount of water that reaches the subgrade.

- Slope of the shoulder
- Slope of the shoulder is another important factor of the pavement structure that affects the variation of subgrade moisture content. A properly designed shoulder can remove the runoff caused by rainfall rapidly. For the same rainfall event, a properly designed shoulder will produce less infiltration of water through the pavement surface and more infiltration of water into the soil off the shoulder. This may result in the relatively low moisture content in the subgrade and a longer lag between the rainfall event and the increase in subgrade moisture content.
- Topography of the site location
- Surface runoff always tends to flow to the lower position due to the gravity, so higher moisture content is always found in the low-lying areas.
- Intensity and duration of the rainfall
- Intensity and duration of the rainfall also affect subgrade moisture variation. During a rainfall event, less water infiltrates through the pavement surface layer and base course into the subgrade than infiltrates into the uncovered ground, because of the relatively low permeability of the surface layer. The higher the rainfall intensity, the more significant the differences between the moisture content under the pavement and the nearby uncovered ground. This difference in moisture content will affect the time needed for the moisture to come to equilibrium.

As mentioned before, the hydraulic conductivity of the unsaturated soil is governed by the moisture content. If the intensity of rainfall is low and at the same time the duration is short, not enough water will be able to infiltrate into both the pavement surface and the topsoil of the uncovered ground. Thus the conductivity is not high enough to let the water reach the subgrade or deep into the uncovered ground. The small amount of moisture will soon be evaporated after the rainfall, and will have very little effect on increasing the moisture content of the subgrade. There must be a threshold of rainfall below which the moisture content of the subgrade will not be affected.

Thom (1970) proposed a correlation between the thresholded rainfall and the variation of subgrade moisture content. Monthly total rainfall less than 0.1 inch was assumed to have no effect on the variation of moisture content. This threshold value seems to be quite arbitrary, but according to Thom (1970), a somewhat arbitrarily selected threshold may yield good results, because if there is a correlation between the variation of subgrade moisture and a true threshold value, there will also be correlations with thresholds near the true value. Unfortunately, Thom (1970) only found good correlation between the thresholded rainfall and moisture content in the natural soil. The same correlation for pavement subgrades was very poor. It should be noted that Thom did not notice the lag between rainfall and the change in subgrade moisture content. If cross-correlation method were used, better results would probably have been obtained.

van Gurp (1992) noticed the subgrade moisture content is predominantly affected by the precipitation surplus, which is defined as the precipitation minus the

evapotranspiration. The increase in moisture content from its mean annual base level were reported to be paired to positive values of 30-day prior precipitation surplus, although no definite relationship were found.

Moisture Movement due to Temperature Gradient

Russam (1970), Vaswani (1975), and Hall and Rao (1999) have reported the phenomenon of moisture movement due to temperature gradient in pavement subgrade. This movement of water in the vapor phase might be significant only where a sharp seasonal fall in temperature occurs, and a zone of wet soil exists not far below the surface of sandy or silty clay soils (Russam, 1970).

The relationship between the variation of the subgrade moisture content and precipitation is not simply a time lag. The subgrade moisture content on the n th day is not only influenced by the precipitation which occurred on the $(n-lag)$ th day, but is also affected by the precipitation which occurred before the $(n-lag)$ th day as well. Hinshaw and Northrup (1991) used the antecedent-precipitation index (API) to predict the degree of saturation of the shallow subgrade soil under aggregate surfacing. When good weather station data close to the site were available, this prediction yielded a R^2 value of 0.78. The antecedent-precipitation index (API) is an index that accounts for the time effect of rainfall using weighting factor, defined by equation (A-9-A-9-2) (Linsley et al., 1992),

$$\mathrm{P}_{\mathrm{a}_{\mathrm{N}}} = \mathrm{b}\mathrm{P}_{\mathrm{a}_{\mathrm{N-1}}} + \mathrm{P}_{\mathrm{N}} \qquad \text{(A-9-2)}$$

where $\mathrm{P}_{\mathrm{a}_{\mathrm{N}}}$ is the precipitation index value at the end of the N th day

$\mathrm{P}_{\mathrm{a}_{\mathrm{N-1}}}$ is the precipitation index value on the previous day

P_N is the precipitation recorded on the Nth day

b is a coefficient.

It is reasonable to use API directly to predict the subgrade moisture under aggregate surfacing, but if the subgrade moisture under a surface layer with low permeability is to be predicted, the combination of a cross-correlation analysis and API might be more favorable. In short, the use of a threshold rainfall, cross-correlation, and antecedent precipitation index may provide a better way to predict the subgrade moisture content from precipitation.

Models for Resilient Modulus

Fine-grained materials

Generally, the resilient modulus of fine-grained soil is believed to be a function of deviator stress. Different models have been proposed to simulate this function.

Bilinear Model (Thompson and Robnett, 1979)

$$M_R = K_1 + K_2\sigma_d \text{ when } \sigma_d < \sigma_{di} \quad \text{(A-9-3)}$$

$$M_R = K_3 + K_4\sigma_d \text{ when } \sigma_d > \sigma_{di} \quad \text{(A-9-4)}$$

where M_R = Resilient modulus,

σ_d = Deviator stress,

σ_{di} = Deviator stress at which the slope of M_R changes,

K_1, K_2, K_3, and K_4 = Model parameters.

A breakpoint resilient modulus, M_R at σ_{di} was often used to characterize the resilient properties of subgrade soils.

Two-Parameter Power Model (Moossazadeh and Witczak, 1981)

$$\mathrm{M_R} = \mathrm{k}\sigma_{\mathrm{d}}^{\mathrm{n}} \qquad \text{(A-9-5)}$$

where k, n = Model parameters.

Semilog Model (Fredlund et al., 1977)

$$\log M_R = c_{1d} - m_{1d}(\sigma_1 - \sigma_3) \qquad \text{(A-9-6)}$$

where c_{1d}, m_{1d} = Model parameters.

Hyperbolic Model (Drumm et al., 1990)

$$M_R = \frac{k + n\sigma_d}{\sigma_d} \qquad \text{(A-9-7)}$$

where k, n = Model parameters.

Octahedral Model (Shackel, 1973)

$$M_R = k\frac{\sigma_{oct}^n}{\tau_{oct}^m} \qquad \text{(A-9-8)}$$

where σ_{oct}, τ_{oct} = Octahedral stresses,

m, n = Model parameters.

Suction plays an important part in the model of resilient modulus. Generally, the lower the moisture content, the higher the suction, and consequently the higher the modulus. It was reported that for the range of water content form -0.5% to +3.2% above optimum, and confining pressure of 14 kPa, the resilient modulus of a clayey sand can be changed (from 70 Mp to 10 MPa) (Khogali and Anderson, 1997). However, a critical suction, beyond which resilient modulus will drop with

increasing suction, was reported by Edil and Motan (1979) based on a series of resilient modulus tests on a silty loam and a sandy mix. The critical value is approximately 2% dry of optimum. Similar result was obtained by Gehling et al., (1998). Effects of confining pressure on the relation between suction and resilient modulus was reported by Phillip and Cameron (1995). For suction < 3.8 pF (620 kPa), confining pressure was found to have little effect on resilient modulus. When suction >3.8 pF (620 kPa), for stiff clay, Resilient modulus was found to increase with confining pressure; for soft clay, resilient modulus was found to decrease with confining pressure.

Coarse-grained materials

The resilient modulus of coarse-grained soil is believed to be a function of bulk stress, given in equation (A-9-9), a two-parameter power model in the same form as the one used for fine-grained soil Hicks and Monismith, 1971. Although this has been questioned by a number of researchers (Brown and Pappin, 1981; Nataatmadja and Parkin, 1989), it is still the most widely used model.

$$M_R = K_1\theta^{K_2} \qquad \text{(A-9-9)}$$

where θ = Bulk stress = Sum of principal stresses = $\sigma_1 + \sigma_2 + \sigma_3$,

K_1, K_2 = Model parameters.

Gradation of granular material and the drainage condition in laboratory cyclic test are both considered to have effect on resilient modulus.

A study conducted by Raad et al. (1992) demonstrated the significant effect of gradation on resilient behavior of unbound material. Crushed sedimentary river

deposits of igneous origin were tested under saturated undrained loading conditions. The resilient modulus for all aggregate gradations was observed to decrease as a result of the increase in pore water pressure and corresponding decrease in effective stress. Resilient moduli of dense-graded aggregates were high, while open-graded aggregates exhibited low resilient modulus. Open-graded aggregates were more resistant to pore water pressure buildup than the dense-graded aggregates. For aggregates with the same gradation, the increase of fine content can make the material more susceptible to pore water pressure buildup.

Pappin et al. (1992) performed a series of repeated triaxial tests on well-graded limestone in both saturated and partially saturated conditions to determine the effect of pore water pressure on resilient behavior of the material. It was found that the resilient stress-strain behavior of saturated granular materials is identical to that of dry material, provided that full drainage is allowed. For the undrained tests, both the saturated and partially saturated specimens behave in accordance with the predictions of the dry model provided that an effective stress analysis is performed.

Heydinger et al. (1996) performed an analysis of resilient modulus for different aggregate materials with different gradations and different moisture content. It was indicated from this test that the effect of gradation is different for different aggregate materials. For limestone aggregate, the open-graded specifications had higher moduli than the dense-graded specifications. For gravel aggregate, no obvious trend in the variation of resilient modulus with respect to gradation

could be found. For slag aggregate, the denser gradation tended to have high moduli but there was no consistent trend for the variation of modulus with moisture condition.

The research of Tian et al. (1998) also concluded that among three different gradations varying from finer to coarser limit, an open-graded aggregate (coarser limit gradation) produces higher resilient modulus, because of faster drainage. A Multiple Linear Regression (MLR) model was developed, in which both gradation and moisture content were taken into account. The regression model is a function of bulk stress, deviator stress, moisture content, c, tan(ϕ), and unconfined compressive strength. The last three variables were considered to be dominated by gradation.

Thom and Brown (1987) argued that the effect of moisture on resilient behavior of aggregates is not the pore water pressure, but lubrication. The conclusion was drawn after a series of repeated load drained triaxial tests on a crushed-rock aggregate with variations in grading and degree of compaction. During testing, moisture content varied and no noticeable pore pressure were developed, although a trend of decreasing stiffness with increasing moisture content is apparent.

Elliott and David (1989) investigated the behavior of k-theta model at the stress beyond static failure. It was found that the k-theta model failed to predict the decrease in resilient modulus with increasing bulk stress. Stress-ratio was then incorporated into the k-theta model to account for this post-failure behavior.

Extended Bulk Modulus Model

The k-Theta model has been widely used, but it does have some deficiencies. Also, it was reported that the relationship between resilient modulus and bulk stress also varies deviator stress. May and Witczak (1981) suggested that for granular material, the in-situ resilient modulus is not only affected by the stress state of bulk stress, but also the shear strain induced mainly by shear and deviator stress. Cole et al. (1981) showed that the relationship is dependent on stress ratio. Uzan (1985) reported the reversed trends of resilient modulus of a dense graded aggregate and suggested a general model for the resilient modulus as shown in equation (9). This equation can be used to model both fine-grained soils and coarse-grained soil. When K_2 = 0, this equation is equivalent to the two-parameter model of fine-grained soils; when K_3 = 0, this equation is equivalent to the two-parameter model of coarse-grained soils. Both the bulk stress and deviator stress are considered in this model, so it is believed to give more reasonable values of resilient modulus. This relationship is still dimensionally unsatisfactory. A later version of the formula which is called the extended bulk modulus model gives the same relationship but in normalized form (Uzan et al., 1992), just like Hicks and Monismith (1971) recommended for the k-Theta model. The inclusion of p_a not only makes the solution dimensionless, but also eliminates the error induced by collinearity in the regression analysis to determine model parameters (Puppala and Mohammad, 1997).

$$M_R = K_1 \theta^{K_2} \sigma_d^{K_3} \qquad \text{(A-9-10)}$$

$$M_R = (K_1 p_a)\left(\frac{\theta}{p_a}\right)^{K_2}\left(\frac{\tau_{oct}}{p_a}\right)^{K_3} \quad \text{(A-9-11)}$$

where τ_{oct} = Octahedral shear stress,

p_a = Atmospheric pressure,

K_1, K_2, K_3 = Model parameters.

Hyperelastic (Taciroglu, 1998) and hypoelastic (uzan, 1999) models have also been successfully used to characterize granular materials. These models were claimed to achieve better fitting of the test data. However, the idea is still new and there are very few applications.

Micro-mechanics Model

Theoretical models based on micro-mechanics have been used to account for the change in response due to water content variations. Chandra et al. (1989) and Jin et al. (1994) proposed a model in which soil particles were simulated by idealized spheres of the same size. The packing configuration of spheres was assumed to be somewhere between face-centered cubic (fcc), which is the densest arrangement, and simple cubic (cs), which is the loosest arrangement. Both temperature and suction variations will result in a change in the bulk stress, and consequently result in a change in the modulus,

$$\Delta M_R = K_1 K_2 \theta^{K_2 - 1}(\Delta\theta_T + \Delta\theta_S) \quad \text{(A-9-12)}$$

where M_R = Resilient modulus

ΔM_R = Change in resilient modulus,

K_1, K_2 = Constants,

θ = Bulk stress = $\sigma_1 + \sigma_2 + \sigma_3$,

$\Delta\theta_T$ = Change in bulk stress due to the change in temperature, and

$\Delta\theta_S$ = Change in bulk stress due to the change in suction.

The bulk stress change due to the temperature variation $\Delta\theta_T$ for an assembly of randomly packed spherical particles was described as follows:

$$\Delta\theta_T = \left[\frac{X}{\sqrt{2}\omega} + \frac{(1-X)}{4\omega}\right]\left(\frac{1}{3}\alpha_v \Delta T\right)^{3/2} \quad \text{(A-9-13)}$$

where X = The volumetric fraction of face-centered cubic (fcc) grains,

$\omega = \frac{3(1-\nu^2)}{4E}$, a property of the material,

α_v = Cubical thermal coefficient,

ν = Poisson's ratio of the material,

E = Young's modulus of elasticity of the material, and

ΔT = Change in temperature.

The bulk stress change due to the suction variation $\Delta\theta_S$ is

$$\Delta\theta_S = -\Delta(\text{suction})\frac{V_W}{V_T} \quad \text{(A-9-14)}$$

where $\Delta(\text{suction})$ = Change in suction,

V_W = Volume of water, and

V_T = Total volume.

According to this model, after running the resilient test on the material at certain temperature and suction level, the resilient modulus of a material at any

temperature and suction can be obtained. However, in natural soils, the estimation of volumetric fraction of fcc grains is difficult.

Regression Method

The most common way to correlate moisture content with resilient modulus is through the use of regression method. Factors besides moisture content are also found to affect the resilient modulus. These factors are 1) stress state, which includes the magnitude of deviator stress and confining stress, and the number of repetitive loading and their sequence; 2) soil strength, such as unconfined compressive strength and California Bearing Ratio (CBR); 3) other soil properties, such as plasticity index, liquid index, plastic limit, soil classification, percentage of fine; 4) test condition, such as whether specimen is grouted to the base plate, sample age, etc. A number of regression equations have been developed (Cumberledge et al., 1974; Thompson and Robnett, 1976; Jones and Witczak, 1977; Visser et al., 1983; Carmichael III and Stuart, 1985Killingsworth et al., 1994; Hudson et al., 1994; Pezo and Hudson, 1994; Drumm et al., 1997). Another interesting study performed by Lee et al. Lee et al., 1997 found that the relationship between the stress at 1% strain in the unconfined compression test and the moisture content coincides with the relationship between resilient modulus and moisture content. This correlation was observed for both disturbed and undisturbed samples.

Moisture Content and Resilient Modulus

Laboratory Data

Cumberledge et al. (1974) concluded from a study of pavement surface deflection associated with moisture variation that the percentage change in deflection depends significantly upon the moisture variation in the subgrade. An equation was developed through stepwise multi-linear regression analysis to predict pavement deflection from moisture content, percentage of fine passing #200 sieve, liquid limit, and dry density of the subgrade, and the thickness of the pavement system.

Carmichael III and Stuart (1985) developed a regression model based on extensive literature review. The database contained more than 3,300 records of resilient modulus test results for more than 250 different soils at specific confining pressures and deviator stresses. Two regression equations were given for cohesive soil and granular soil.

For cohesive soil:

$$\begin{aligned} M_R &= 37.431 - 0.4566(PI) - 0.6179(\%w) \\ &\quad - 0.1424(S200) + 0.1791(CS) - 0.3248(DS) \\ &\quad + 36.422(CH) + 17.097(MH) \end{aligned} \qquad \text{(A-9-15)}$$

where M_R = resilient modulus (ksi),

PI = plasticity index,

%w = percentage water,

S200 = percentage passing #200 sieve, and

CS = confining stress (psi),

DS = deviator stress (psi),

CH = 1 for CH soil,

= 0 otherwise (for MH, ML, or CL soil)

MH = 1 for MH soil

= 0 otherwise (for CH, ML, or CL soil).

For granular soil:

$$M_R = 0.523 - 0.0225(\%w) + 0.544(\log T) + 0.173(SM) + 0.197(GR) \quad \text{(A-9-16)}$$

where T = bulk stress (psi) (DS + 3CS),

SM = 1 for SM soil,

= 0 otherwise;

GR = 1 for GR soil

= 0 otherwise.

This model was verified by another 300 resilient modulus testing results. The scatter in the results was attributed to the fact that before AASHTO T274-82, no standard resilient modulus test procedure existed. It was suggested that the relationships was useful as a preliminary estimation of resilient modulus and its seasonal variation, provided that the input variables are within the range from which the equations were developed.

Dividing the subgrade into different types before carrying out the regression analysis seemed to be a fairly efficient procedure. In a similar analysis of the data from North Atlantic and Southern SHRP Regions of the Strategic Highway Research Program Long-Term Pavement Performance (SHRP – LTPP) study

(Killingsworth et al., 1994), it was found that R^2 = 0.56, when all the data were used to develop a single regression model. After the subgrade was divided into clay, silt and sand, R^2 = 0.8886, 0.7809, and 0.8371, respectively. It should be noted that the combination of input variables in this regression model is quite complicated, and moisture content is only considered in the clay model.

Hudson et al. (1994) proposed a regression equation to estimate resilient modulus from soil properties including liquid index, degree of saturation, AASHTO soil classification, deviator water content, and plastic limit. A complete design handbook based on the resilient response of Tennessee subgrades was developed. This handbook allows the resilient modulus to be estimated with a minimum of laboratory testing.

May and Witczak (1981) evaluated the 101 nonlinear relationship of resilient modulus developed from six typical Maryland State highway materials. The parameters in the K-theta model were found to vary with different saturation and compactive effort.

Moisture adjustment factors were introduced by Thompson and LaGrow (1988), as reported by Hall and Thompson (1994), to account for the decrease of breaking point resilient modulus (Thompson and Robnett, 1976) with increasing water content. The moisture adjustment factors were developed based on the U.S. Department of Agriculture (USDA) textural classification of the soil, and each factor represents the decrease in breaking point resilient modulus (in kips per square inch) for each 1 percent increase in moisture content above the optimum moisture content.

USDA Textural Class	Moisture Sensitivity (ksi/%)
Clay, Silty Clay, Silty Clay Loam	0.7
Silt Loam	1.5
Loam	2.1

Drumm et al. (1997) proposed a method to correct the resilient modulus for the effect of saturation based on the testing result of 11 soils in Tennessee. The gradient of resilient modulus with respect to saturation, obtained from laboratory resilient moisture test, was used predict resilient modulus wet of optimum water content.

Field Data

The Seasonal Monitoring Program (SMP) sites, which form a part of the Long-Term Pavement Performance Program (LTPP) provide an opportunity to investigate relationship between resilient modulus and environmental effects. Resilient moduli of different layers are determined by back-calculation from the results Nondestructive Testing (NDT), such as FWD. Because the moduli of the surface layers of both flexible pavements and the rigid pavements are affected by temperature, the FWD measurements must be correct for temperature. Although the modulus of asphalt concrete decreases with elevated temperature in the summer and increases in the winter, the behavior of Portland cement concrete layers is opposite, because the shrinkage of concrete increases the width of the cracks (McCullough and Taute, 1982).

Ali and Lopez (1996) performed a statistical analysis in which different analysis methods, such as multiple linear regression, principal component analysis, and

stepwise regression analysis, were used. The resilient modulus was predicted based on the temperature in the base, the temperature gradient, and the moisture contents measured at different depths. Unfortunately, only about 30 percent of the modulus variation could be explained by the regression model.

It should be noted that the temperature effects more than just the modulus of the surface layers. The stress state of the subgrade is also affected by temperature, both directly and indirectly. The change in the stress state, in turn, affects the subgrade modulus, since subgrade modulus is stress-dependent. Four reasons that can lead to the change in the subgrade stress state with temperature are listed below.

Change in the stiffness of the asphalt surface layers – The temperature-induced changes in the modulus of the asphalt layers affects the level of stresses transferred to the underlying subgrade. (van Gurp, 1994; Matter and Farouki, 1994; Long et al., 1997; Andrew et al., 1998).

Measurement induced variation – The stiffness of the buffers or pads on the FWD deveice are also affected by temperature. At the same drop height, the duration of impact increases with temperature. As a result, the stress state within the subgrade is also changed. (Matter and Farouki, 1994van Gurp, 1994)

Thermally induced Stress – According to the previously mentioned micro-mechanics model (Chandra et al., 1989; Jin et al., 1994), in granular subgrade, a rise in temperature causes an increase in the contact forces between particles, consequently increases the bulk stress. van Gurp (1994) indicated that the lower

the initial bulk stress and the more closely packed the subgrade is, the more the subgrade stiffness is affected by the increase in soil temperature.

Change in the suction – An increase of temperature will decrease the surface tension in the pore water, decreasing the suction in the subgrade. This will result in a decrease in the effective stresses (Cheung et al., 1991) and a decrease in the subgrade resilient modulus.

Although temperature effects on unbound materials are often neglected, the above aspects may be evident in the back-calculated moduli of unbound materials determined from FWD testing. Matter and Farouki (1994) indicated that the moisture content and temperature effects might reach their peak impacts at different times or seasons. Thus, the effects of one factor may be offset by the effects of the other, making it hard to separate them.

Fine-grained subgrade soils were observed to exhibit larger variations in the resilient modulus throughout the year than the more granular subgrade soils (Lary and Mahoney, 1984; van Gurp, 1992) same study, it was also reported that "when frost penetration into the pavement structure is minimal, variation in modulus is primarily a function of rainfall and the minimum modulus for the year does not necessarily occur during the spring."

Moisture Content and Parameters in the Resilient Modulus Model

A total of 271 test results were evaluated by Rada and Witczak (1981). It was found that for crushed, angular materials, when the two-parameter power model is used, an increase in moisture leads to a small to moderate decrease in the K_1 value and relatively minor changes in the K_2 magnitude. But, sand gravels

showed a marked decrease in K_1 and increase in K_2 with increasing moisture, and an increase of fine material (percent passing #200 sieve) will make sand gravel material more susceptible to moisture variation.

A regression equation can be used to predict resilient modulus from bulk stress, %200, compactive effort, and degree of saturation. Similar to Killingsworth et al. (1994), in comparison to the general model, higher values were also obtained for all the other aggregates but the slag, when aggregates are divided into silty sands, sand gravels, sand-aggregate blends, crushed stones, limerocks, and slags.

Jin et al. (1994) observed that regression coefficient K_1 decreases and K_2 increases, as moisture content increases from the testing of two glacial deposit soils. Tian et al. (1998) also reported an increase in moisture content leads to a decrease in K_1 and an insignificant increase in K_2 for aggregate base. Tian et al. (1998) considered that K_2 could be assumed to be 0.5.

Mohammad et al. (1999) performed a multiple linear regression based on the laboratory repeated load triaxial test on eight subgrade soils commonly found in Louisiana. Soil classifications of these soils vary from sand to clay. The normalized octahedral stress model, which was considered to be more practical and realistic in the material characterization, was used in the multiple linear regression. Multiple linear regression to predict resilient modulus constants K_1, K_2 and K_3. Among the three different sets of input variables, as listed following,

best result was obtained while only basic soil properties are used as input variables.

Basic soil properties such as moisture content, dry density, degree of compaction, liquid limit, plastic limit, percentage of sand and percentage of silt,

Basic soil properties and CBR,

Basic soil properties with UCS.

Incorporation of Seasonal moisture variations into Pavement Design

To account for the seasonal variation in moisture content, the AASHTO Guide for Design of Pavement Structures (AASHTO, 1993) describes a procedure for the identification of a single subgrade resilient modulus value for flexible pavement design. The year is divided into intervals or seasons, with each interval assigned a resilient modulus. Based on the anticipated pavement damage for that modulus value, a single value of M_R known as the "effective roadbed soil resilient modulus," is obtained for design.

The AASHTO procedure (AASHTO, 1993) is a rational means for the incorporation of seasonal variations of subgrade moisture content into the flexible pavement design process. However, a procedure for the determination of the seasonally adjusted resilient modulus is not described.

Guan et al. (1998) proposed a weighted average method to determine the effective subgrade resilient modulus. The approach developed by Guan et al. (1998), follows the seasonal weighting factor approach of Gomez-Achezar and

Thompson (1984). The seasonal effect of environmental conditions on M_R can be represented using the following equation:

$$WF_i = \frac{nM_{R_i}^{-2.32}}{\sum_{i=1}^{n} M_{R_i}^{-2.32}} \qquad \text{(A-9-17)}$$

where WF_i = Weighting Factor for i-th Month,

M_{R_i} = Resilient Modulus of Subgrade for i-th Month,

n = Number of months used.

The Weighting Factor equation assigns relative damage to the calculated subgrade modulus for each month, and can be used to determine an effective M_R. The weighted mean value of subgrade modulus for any set of values is at a point where WF_i is equal to 1. The effective annual subgrade modulus is determined by solving the Weighting Factor equation for M_{R_i} with WF_i equal to 1. The effective modulus corresponds to a unique value of modulus that results in the same annual pavement damage expected from the seasonal modulus values. Additionally, the Weighting Factor approach can be used to discern the most important seasons for evaluating pavement performance. In both approaches to determining the weighted average of seasonal values, it is important to give careful consideration to selecting the seasons with the most pronounced environmental effect upon M_R.

Before resilient modulus is used as an input variable of pavement design, Bhajandas et al. (1977) tried to account for seasonal variation by using deflection adjustment factors. Uhlmeyer et al. (1995a), Uhlmeyer et al. (1995b), Mahoney

et al. (1996) tried to provide guidance for the selection of seasonal adjustment factors for layer moduli, based on both lab and NDT results. The adjustment factor is the ratio of measured modulus of a given month to the modulus measured in a dry season (the maximum measured modulus). Aggregate is found to be more susceptible to seasonal variation than subgrade, especially in freezing and thawing environments. Adjustment factors were used as following Drainage factors (m) are related to these adjustment factors for the design of base.

Adjustment factors when multiplied by the subgrade resilient modulus can be used to calculate equivalent resilient modulus.

References

AASHTO (1993) *AASHTO Guide for the Design of Pavement Structures*. American Association of State Highway Officials.

Ali, H. A. and A. Lopez (1996) Statistical Analysis of Temperature and Moisture Effects on Pavement Structural Properties Based on Seasonal Monitoring Data. In *Transportation Research Record 1540*, TRB, National Research Council, Washington D.C., pp. 48-55.

Andrew, J. W., N. M. Jackson, and E. C. Drumm. (1998) Measurement of Seasonal Variation in Subgrade Properties, Geotechnical Special Publication No. 85, Application of Geotechnical Principles in Pavement Engineering. *In* Proceedings of *Sessions of Geo-Congress 98. Boston, Massachusetts,* pp. 13-38.

Bandyopadhyay, S. S. and J. A. Frantzen (1983) Investigation of Moisture-Induced Variation in Subgrade Modulus By Cross-Correlation Method. In *Transportation Research Record 945*, TRB, National Research Council, Washington D.C., pp. 10-15.

Baus, R. L. and J. A. Fogg (1989) AASHTO Flexible Pavement Design Equation Study. *Journal of Transportation Engineering* Vol. 115, No. 5, 559-564.

Bhajandas, A. C., G. Cumberledge, and G. L. Hoffman (1977) Flexible Pavement Evaluation and Rehabilitation Transportation Engineering. *Journal of ASCE* Vol. 103, No. TE1, 75-85.

Birgisson, B., J. Ovik, and D. E. Newcomb. (2000) Analytical Predictions of Seasonal Variations in Flexible Pavements at the Mn/Road Site. *In* Proceedings of *the 79th Annual Meeting in January 2000 of the Transportation Research Board. Washington, D. C.,*

Brown, S. F. and J. W. Pappin (1981) Analysis of Pavements with Granular Bases. In *Transportation Research Record 810*, TRB, National Research Council, Washington D.C., pp. 17-23.

Carmichael III, R. F. and E. Stuart (1985) Predicting Resilient Modulus: A Study to Determine the Mechanical Properties of Subgrade Soils. In *Transportation Research Record 1043*, TRB, National Research Council, Washington D.C., pp. 145-148.

Chandra, D., K. M. Chua, and R. L. Lytton (1989) Effects of Temperature and Moisture on the Load Response of Granular Base Course Material in Thin Pavements. In *Transportation Research Record 1252*, TRB, National Research Council, Washington D.C., pp. 33-41.

Cheung, S. C. H., M. N. Gray, R. N. Yong, and A. M. O. Mohamed. (1991) The Effects of Moisture Content, Salinity and Temperature on the Load-Bearing Capacity of a Dense Clay-Based Backfill. Material Research Society Symposium*,* pp. 491-498.

Cole, D. M., L. H. Irwin, and T. C. Johnson (1981) Effect of Freezaing and Thawing on Resilient Modulus of a Granular Soil Exhibiting Nonlinear Behavior. In *Transportation Research Record 809*, TRB, National Research Council, Washington D.C., pp. 19-26.

Croney, D., J. P. Coleman, and W. P. Black (1958) *Movement and Distribution of Water in Soil in Relation to Highway Design and Performance*. Report 40. Highway Research Board.

Cumberledge, G., G. L. Hoffman, A. C. Bhajandas, and R. J. Cominsky (1974) Moisture Variation in Highway Subgrades and the Associated Change in Surface Deflections. In *Transportation Research Record 497*, TRB, National Research Council, Washington D.C., pp. 40-49.

Dempsey, B. J., W. A. Herlach, and A. J. Patel (1985) *The Climatic-Material-Structural Pavement Analysis Program*. Report FHWA/RD-84/115. Federal Highway Administration.

Drumm, E. C., Y. Boateng-Poku, and T. Johnson Pierce (1990) Estimation of Subgrade Resilient Modulus from Standard Tests. *Journal of the Geotechnical Engineering Division* Vol. 116, No. 5, 774-789.

Drumm, E. C., J. S. Reeves, M. R. Madgett, and W. D. Trolinger (1997) Subgrade Resilient Modulus Correction for Saturation Effects. *Journal of Geotechnical Engineering* Vol. 123, No. 7, 663-670.

Edil, T. B. and S. E. Motan (1979) Soil-Water Potential and Resilient Behavior of Subgrade Soils. In *Transportation Research Record 705*, TRB, National Research Council, Washington D.C., pp. 54-63.

Elliot, R. P. and S. I. Thornton (1988) Resilient Modulus and AASHTO Pavement Design. In *Transportation Research Record 1196*, TRB, National Research Council, Washington D.C., pp. 116-124.

Elliott, R. P. and L. David (1989) Improved Characterization Model for Granular Bases. In *Transportation Research Record 1227*, TRB, National Research Council, Washington D.C., pp. 128-133.

Elliott, R. P. and M. R. Thompson (1985) ILLI-PAVE Mechanistic Analysis of AASHO Road Test Flexible Pavements. In *Transportation Research Record 1043*, TRB, National Research Council, Washington D.C., pp. 39-49.

Fredlund, D. G., A. T. Bergan, and P. K. Wong (1977) Relation Between Resilient Modulus and Stress Conditions for Cohesive Subgrade Soils. In *Transportation Research Record 642*, TRB, National Research Council, Washington D.C., pp. 73-81.

Gehling, W. Y. Y., J. A. Ceratti, W. P. Nunez, and M. R. Rodrigues. (1998) A Study of the Influence of Suction on the Resilient Behaviour of soils from Southern Brazil. *In* Proceedings of *Second International Conference on Unsaturated Soils. Beijiing, China,* pp. 47-53.

Gomez-Achezar, M. and M. R. Thompson (1984) *Mechanistic Design Concepts for Full-Depth Asphalt Concrete Pavements*. Report 41. University of Illinois.

Guan, Y., E. C. Drumm, and N. M. Jackson (1998) Weighting Factors for Seasonal Subgrade Resilient Modulus. In *Transportation Research Record 1619*, TRB, National Research Council, Washington D.C., pp. 94-100.

Guinnee, J. W. (1958) Field Studies on Subgrade Moisture Conditions. In *HRB Special Report 40*, Highway Research Board, Washington D. C., pp. 253-267.

Gurr, C. G., T. J. Marshall, and J. T. Hutton (1952) Movement of Water in Soil due to a Temperature Gradient. *Soil Science* Vol. 74, No. 5,

Guymon, G. L. (1994) *Unsaturated Zone Hydrology* . PRENTICE HALL.

Guymon, G. L., R. L. Berg, and T. C. Johnston (1986) *Mathematical Model of Frost Heave and Thaw Settlement in Pavements*. U.S. Army Cold Regions Research and Engineering Laboratory.

Haliburton, T. A. (1971) Highway Designs to Resist Subgrade Moisture Variations. In *Highway Research Record 360*, Highway Research Board, Washington D.C., pp. 45-56.

Hall, D. K. and S. Rao (1999) Predicting Subgrade Moisture Content for Low-Volume Pavement Design Using In Situ Moisture Content Data. In *Transportation Research Record 1652*, TRB, National Research Council, Washington D.C., pp. 98-107.

Hall, K. D. and M. R. Thompson (1994) Soil-Property-Based Subgrade Resilient Modulus Estimation for Flexible Pavement Design. In *Transportation Research Record 1449*, TRB, National Council, Washington D.C., pp. 30-38.

Heydinger, A. G., Q. Xie, B. W. Randolph, and J. D. Gupta (1996) Analysis of Resilient Moulus of Dense- and Open-Graded Aggregates. In *Transportation Research Record 1547*, TRB, National Research Council, Washington D.C., pp. 1-6.

Hicks, R. G. and C. L. Monismith (1971) Factors Influencing the Resilient Response of granular Materials. In *Highway Research Record 345*, HRB, National Research Council, Washington D.C., pp. 15-13.

Hinshaw, R. F. and J. L. Northrup (1991) Predicting Subgrade Moisture Under Aggregate Surfacing. In *Transportation Research Record 1291*, TRB, National Research Council, Washington D.C., pp. 193-203.

Hossain, M., S. J. Kotdwala, B. Long, and A. J. Gisi. (1997) Subgrade Moisture Monitoring Using Time Domain Reflectometry. *In* Proceedings of *Transportation Research Board 76th Annual Meeting. Washington, D.C.,*

Hudson, J., E. C. Drumm, and M. Madgett. (1994) Design Handbook for the Estimation of Resilient Response of Fine-grained Subgrades. *In* Proceedings of *4th International Conference on the Bearing Capacity of Roads and Airfields. Minneapolis,* pp. 917-931.

Jin, M. S., K. W. Lee, and W. D. Kovacs (1994) Seasonal Variation of Resilient Modulus of Subgrade Soils. *Journal of Transportation Engineering* Vol. 120, No. 4, 603-616.

Jones, M. P. and M. W. Witczak (1977) Subgrade Modulus on the San Diego Test Road. In *Transportation Research Record 641*, TRB, National Research Council, Washington D.C., pp. 1-6.

Khogali, W. E. I. and K. O. Anderson (1996) Evaluation of Seasonal Variability in Cohesive Subgrades Using Backcalculation. In *Transportation Research Record 1546*, TRB, National Research Council, Washington D.C., pp. 140-150.

Khogali, W. E. I. and K. O. Anderson. (1997) Assessing Seasonal Variations in Cohesive Subgrade Soils. *In* Proceedings of *Eighth International Conference on Asphalt Pavements.* University of Washington*, Seattle, Washington,* pp. 803-822.

Killingsworth, B. M., J. F. Daleiden, A. L. Simpson, and R. Zamora (1994) Analysis of Procedures for Establishing In-situ Subgrade Moduli. In *Transportation Research Record 1462*, TRB, National Research Council, Washington D.C., pp. 102-107.

Larson, G. and B. J. Dempsey (1997) *Enhanced Integrated Climatic Model Version 2.0*. Report Contract DTFA MN/DOT 72114.

Lary, JO. A. and Joe P. Mahoney (1984) Seasonal Effects on the Strength of Pavement Structures. In *Transportation Research Record 954*, TRB, National Research Council, Washington, D. C., pp. 88-94.

Lee, W., N. Bohra, A. G. Altschaeffl, and T. D. White (1997) Resilient Modulus of Cohesive Soils. *Journal of Geotechnical and Geoenvironmental Engineering* Vol. 123, No. 2, 131-136.

Liang, H. S. and R. L. Lytton (1989) Rainfall Estimation for Pavement Analysis and Design. In *Transportation Research Record 1252*, TRB, National Research Council, Washington D.C., pp. 42-49.

Linsley, R. K., J. B. Franzini, D. L. Freyberg, and G. Tchobanoglous (1992) *Water-Resources Engineering*. McGraw-Hill, Inc.

Liu, S. J. and R. L. Lytton (1985) *Environmental Effects on Pavement-Drainage*. Report FHWA-DTFH-61-87-C-00057. Federal Highway Administration.

Long, B., M. Hossain, and A. J. Gisi (1997) Seasonal Variation of Backcalculated Subgrade Moduli. In *Transportation Research Record 1577*, TRB, National Research Council, Washington D.C., pp. 70-80.

Lytton, R. L., D. E. Pufahl, C. H. Michalak, H. S. Liang, and B. J. Dempsey (1990) *An Integrated Model of the Climatic Effects on Pavements*. Report FHWA-RD-90-033.

Mahoney, J. P., L. M. Pierce, and R. L Costead (1996) *Estimation of Seasonal Effects for Pavement Design and Performance - Volume III*. Report FHWA-FLP-95-008. USDA-Forest Service.

Maree, J. H., N. J. W. Van Zyl, and C. R. Freeme (1982) Effective Moduli and Stress Dependence of Pavement Materials as Measured in Some Heavy-Vehicle Simulator Tests. *Transportation Research Record 852* , 52-60.

Marks, B. D. III and A. Haliburton (1969) Subgrade Moisture Variations Studied with Nuclear Depth Gages. In *Highway Research Record 276*, Highway Research Board, Washington D.C., pp. 14-24.

Matter, N. S. and O. T. Farouki. (1994) Detailed Study on the Climatic and Seasonal Variation Effects on Pavements in Northern Ireland. *In* Proceedings of *The 4th International Conference on the Bearing Capacity of Roads and Airfields. Minneapolis, Minnesota,* pp. 721-737.

May, Richard W. and Matthew W. Witczak (1981) Effective Granular Modulus to Model Pavement Responses. In *Transportation Research Record 810*, TRB, National Research Council, Washington, D. C., pp. 1-9.

McCullough, B. F. and A. Taute (1982) Use of Deflection Measurements for Determining Pavement Material Properties. In *Transportation Research Record 852*, TRB, National Research Council, Washington D.C., pp. 8-14.

Mohammad, L. N., B. Huang, A. J. Puppala, and A. Allen (1999) Regression Model for Resilient Modulus of Subgrade Soils. In *Transportation Research Record 1687*, TRB, National Research Council, Washington D.C., pp. 47-54.

Monismith, C. L. (1992) Analytically-Based Asphalt Pavement Design and Rehabilitation-Theory to Practice (1962-1992), TRB Distinguished Lecture. In *Transportation Research Record 1354*, TRB, National Research Council, Washington D.C., pp. 5-25.

Moossazadeh, J. and M. W. Witczak (1981) Prediction of Subgrade Moduli for Soil that Exhibits Nonlinear Behavior. In *Transportation Research Record 810*, TRB, National Research Council, Washington D.C., pp. 9-17.

Musiake, K., Y. Oka, and M. Koike (1988) Unsaturated Zone Soil Moisture Behavior Under Temperate Humid Conditions -- Tensiometric Observations and Numerical Simulations. *Journal of Hydrology* No. 102, 179-200.

Nataatmadja, A. and A. K. Parkin (1989) Characterization of Granular Materials for Pavements. *Canadian Geotechnical Journal* Vol. 26, 725-730.

Pappin, J. W., S. F. Brown, and M. P. O'Reilly (1992) Effective Stress Behaviour of Saturated and Partially Saturated Granular Material Subjected to Repeated Loading. *Geotechnique* Vol. 42, No. 3, 485-497.

Pezo, R. and W. R. Hudson (1994) Prediction Models of Resilient Modulus for Nongranular Materials. *Geotechnical Testing Journal* Vol. 17, No. 3, 349-355.

Phillip, A. W. and D. A. Cameron (1995) The influence of soil suction on the resilient modulus of expansive soil subgrades. Balkema Publishers, Paris, pp. 171-176.

Puppala, A. J. and L. N. Mohammad. (1997) A Regression Model for Better Characterization of Resilient Properties of Subgrade Soils. *In* Proceedings of *Eighth International Conference on Asphalt Pavements.* University of Washington, Seattle, Washington *, Seattle, Washington,* pp. 859-866.

Raad, L., G. H. Minassian, and S. Gartin (1992) Characterization of Saturated Granular Base Under Repeated Loads. In *Transportation Research Record 1369*, TRB, National Research Council, Washington D.C., pp. 73-82.

Rada, G. and M. W. Witczak (1981) Comprehensive Evaluation of Laboratory Resilient Moduli Results for Granular Material. In *Transportation Research Record 810*, TRB, National Research Council, Washington D.C., pp. 23-33.

Rahim, M. A. B. A. and M. Picornell (1989) *Moisture Movement Under the Pavement Structure*. Report Research Report 1165-1, Research Study 10-8-88-1165. The Texas State Department of Highways and Public Transportation with The U.S. Department of Transportation Federal Highway Administration, Center for Geotechnical & Highway Materials Research.

Rainwater, N. R., R. E. Yoder, E. C. Drumm, and G. V. Wilson (1999) Comprehensive Monitoring Systems for Measuring Subgrade Moisture Conditions. *Journal of Transportation Engineering* Vol. 125, No. 5, 439-448.

Russam, K. (1970) Subgrade Moisture Studies by the British Road Research Laboratory. In *Highway Research Record 301*, Highway Research Board, Washington D.C., pp. 5-17.

Shackel, B. (1973) The Derivation of Complex Stress-strain Relations. *In* Proceedings of *8th Int. Conf. on Soil Mech. and Found. Engng. Moscow,* pp. 353-359.

Taciroglu, E. (1998) *Constitutive Modeling of the Resilient Response of Granular Solids*. A Thesis/Dissertation Submitted for Fulfillment of the Degree of Doctor of Philosophy, University of Illinois, Urbana. Urbana, IL.

Ter-Martirosyan, Z. G., I. I. Demin, and E. A. Demina (1986) Effect of Surface Shielding on Modification of Moisture Regime and Displacements of Swelling Soil. *Soil Mechanics and Foundation Engineering* Vol. 23, No. 4, 158-161.

Thom, H. C. S. (1970) Quantitative Evaluation of climatic Factors in Relation to Soil Moisture Regime. In *Highway Research Record 301*, Highway Research Board, Washington D.C., pp. 1-4.

Thom, N. H. and S. F. Brown (1987) Effect of Moisture on the Structural Performance of a Crushed-Limestone Road Base. In *Transportation Research Record 1121*, TRB, National Research Council, Washington D.C., pp. 50-56.

Thompson, M. R. and R. P. Elliot (1985) ILLI-PAVE - Based Response Algorithms for Design of Conventional Flexible Pavements. In *Transportation Research Record 1043*, TRB, National Research Council, Washington, D.C., pp. 50-57.

Thompson, M. R. and T. LaGrow (1988) A Proposed Conventional Flexible Pavement Thickness Design Procedure. In *Civil Engineering Studies Transporation Engineering Series No. 55*University of Illinois,

Thompson, M. R. and Q. L. Robnett (1976) *Resilient Properties of Subgrade Soils*.

Thompson, M. R. and Q. L. Robnett (1979) Resilient Properties of Subgrade Soils. *Journal of Transportation Engineering* Vol. 105, No. TE1, 71-89.

Tian, P., M. M. Zaman, and J. G. Laguros (1998) Gradation and Moisture Effects on Resilient Moduli of Aggregate Bases. In *Transportation Research Record 1619*, TRB, National Research Council, Washington D.C., pp. 75-84.

Uhlmeyer, J. S., J. P. Mahoney, G. Hanek, G. Wang, R. L. Copstead, and D. J Jassen (1995a) *Estimation of Seasonal Effects for Pavement Design and Performance - Volume I*. Report FHWA-FLP-95-006. USDA-Forest Service.

Uhlmeyer, J. S., J. P. Mahoney, G. Hanek, G. Wang, R. L. Copstead, and D. J Jassen (1995b) *Estimation of Seasonal Effects for Pavement Design and Performance - Volume II*. Report FHWA-FLP-95-007. USDA-Forest Service.

uzan, J (1999) Granular Material Characterization for Mechanistic Pavement Design. *Journal of Transportation Engineering* Vol. 125, No. 2, 108-113.

Uzan, J. (1985) Characterization of Granular Material. In *Transportation Research Record 1022*, TRB, National Research Council, Washington D. C., pp. 52-59.

Uzan, J., M. W. Witczak, T. Scullion, and R. L. Lytton. (1992) Development and Validation of Realistic Pavement Response Modes. *In* Proceedings of *7th International Conference on Asphalt Pavements.* International Society for Asphalt Pavements*, Austin, TX,* pp. 334-350.

Valdez, S. F. (1991) *Subgrade Resilient Modulus Evaluation*. Report FHWA-GA-91-8801.

van Gurp, C. (1992) Impact of Season on the Structural Condition of Asphalt Pavements. *In* Proceedings of *7th International Conference on Asphalt Pavements.* University of Michigan*,* pp. 372-385.

van Gurp, C. (1994) Effect of Temperature Gradients and Season on Deflection Data. *In* Proceedings of *The 4th International Conference on the Bearing Capacity of Roads and Airfields. Minneapolis, Minnesota,* pp. 199-214.

Vaswani, N. K. (1975) Case Studies of Variations in Subgrade Moisture and Temperature under Road Pavements in Virginia. In *Transportation Research Record 532*, TRB, National Research Council, Washington, D. C., pp. 30-42.

Visser, A. T., Queiroz C., and W. R. Hudson (1983) Study of Resilient Characteristics of Tropical Soils for Use in Low-Volume Pavement Design. In *Transportation Research Record 898*, TRB, National Research Council, Washington D.C., pp. 133-140.

Yoder, E. J. and M. W. Witczak (1975) *Principles of Pavement Design*. John Wiley & Sons.

Vita

Gang Zuo was born in China in 1973. He attended Tongji University, Shanghai, China in 1991, where he received his Bachelor's degree in Civil Engineering (Geotechnical Engineering) in 1995 and his Master's degree in Geotechnical Engineering in 1998. In 1999, he then went to the University of Tennessee, Knoxville, to pursue his Ph.D. in Civil and Environmental Engineering. He received his doctor of Philosophy Degree in Civil Engineering with concentration in Geotechnical Engineering in August, 2003.